

MICROENCAPSULATED PHASE CHANGE MATERIALS FOR THERMAL ENERGY STORAGE IN BUILDINGS: DESIGN, CHARACTERIZATION AND MODELLING

Paroutoglou, Evdoxia

DOI (link to publication from Publisher):
[10.54337/aau620099832](https://doi.org/10.54337/aau620099832)

Publication date:
2023

Document Version
Publisher's PDF, also known as Version of record

[Link to publication from Aalborg University](#)

Citation for published version (APA):
Paroutoglou, E. (2023). *MICROENCAPSULATED PHASE CHANGE MATERIALS FOR THERMAL ENERGY STORAGE IN BUILDINGS: DESIGN, CHARACTERIZATION AND MODELLING*. Aalborg Universitetsforlag. <https://doi.org/10.54337/aau620099832>

General rights

Copyright and moral rights for the publications made accessible in the public portal are retained by the authors and/or other copyright owners and it is a condition of accessing publications that users recognise and abide by the legal requirements associated with these rights.

- Users may download and print one copy of any publication from the public portal for the purpose of private study or research.
- You may not further distribute the material or use it for any profit-making activity or commercial gain
- You may freely distribute the URL identifying the publication in the public portal -

Take down policy

If you believe that this document breaches copyright please contact us at vbn@aub.aau.dk providing details, and we will remove access to the work immediately and investigate your claim.

**MICROENCAPSULATED PHASE CHANGE
MATERIALS FOR THERMAL ENERGY
STORAGE IN BUILDINGS:
DESIGN, CHARACTERIZATION
AND MODELLING**

**BY
EVDOXIA PAROUTOGLOU**

DISSERTATION SUBMITTED 2023



AALBORG UNIVERSITY
DENMARK

MICROENCAPSULATED PHASE CHANGE MATERIALS FOR THERMAL ENERGY STORAGE IN BUILDINGS: DESIGN, CHARACTERIZATION AND MODELLING

Evdoxia Paroutoglou

Ph.D. Dissertation



AALBORG UNIVERSITY
DENMARK

Dissertation submitted: July 2023

PhD supervisor: Professor Alireza Afshari,
Aalborg University

Assistant PhD supervisors: Associate Prof. Peter Fojan,
Aalborg University
Associate Prof. Leonid Gurevich
Aalborg University
Associate Prof. Göran Hultmark,
Aalborg University

PhD committee: Senior Researcher Ernst Jan de Place Hansen (chair)
Aalborg University, Denmark
Associate Professor Stefania Doppiu
CIC energiGUNE, Spain
Professor Ioannis S. Chronakis
Technical University of Denmark, Denmark

PhD Series: Faculty of Engineering and Science, Aalborg University

Department: Department of the Build Environment

ISSN (online): 2446-1636

ISBN (online): 978-87-7573-773-4

Published by:
Aalborg University Press
Kroghstræde 3
DK – 9220 Aalborg Ø
Phone: +45 99407140
aauf@forlag.aau.dk
forlag.aau.dk

© Copyright: Evdoxia Paroutoglou

Printed in Denmark by Stibo Complete, 2023

ABSTRACT

Thermal energy storage (TES) has a significant role in saving thermal energy and improving indoor climate. Latent heat thermal energy storage (LHTES) using Phase Change Materials (PCM) in heating, ventilation, and air-conditioning (HVAC) building applications allows storage of a substantial amount of energy in a relatively small volume and absorbs/releases it in a narrow temperature range.

The main objective of the current study was to develop and thermally characterize microencapsulated PCM for LHTES in building applications. The microencapsulated PCM stores substantial energy, and leakage or phase separation is avoided compared to PCM in bulk and PCM emulsions.

In the current thesis, seven PCM belonging to the categories of organic paraffins, organic non-paraffins, and inorganic salts were thermally characterized. Additionally, this study presents the development of PCM emulsions, PCM polymers, and PCM electrospun fiber matrices. All variations of PCM emulsions, polymer, and electrospun fibers were characterized thermally and morphologically. Commercial organic paraffin RT18™ with a melting temperature of 18°C in bulk, emulsion, and electrospun fiber forms was found suitable for application in LHTES systems in HVAC building applications. Bulk RT18™ showed latent heats of melting/solidification of 137-139 kJ/kg, while RT18™ water emulsion possessed latent heats of about 180 kJ/kg. PCM core-PCL shell electrospun fibers of organic paraffin RT18™ showed latent heats of melting solidification of 102.1/82.21 kJ/kg.

Additionally, after conducting experimental studies on PCM, a numerical analysis of LHTES systems of different geometries was carried out using Comsol Multiphysics 6.0 FEM software. The effect of internal and external fins in a double tube encapsulating bulk PCM in the annular space was studied. Additionally, a single-tube LHTES using PCM electrospun fiber matrix in direct contact with water was analyzed. The phase change processes were accelerated with an increase in the length of fins.

DANSK RESUME

Termisk energilagring (TES) har en væsentlig rolle i at spare termisk energi og forbedre indeklimaet. Latent varme, termisk energilagring (LHTES) ved hjælp af faseskiftende materiale (PCM) i bygningsapplikationer til opvarmning, ventilation og aircondition (HVAC) gør det muligt at lagre en betydelig mængde energi i et relativt lille volumen og absorbere/frigive det i et snævert temperaturområde.

Hovedformålet med den nuværende undersøgelse var at udvikle og termisk karakterisere mikroindkapslet PCM til LHTES i bygningsapplikationer. Den mikroindkapslede PCM lagrer væsentlig energi, og lækage eller faseadskillelse undgås sammenlignet med PCM i bulk og PCM-emulsioner.

I den aktuelle afhandling blev syv PCM omfattende klasserne af organiske paraffiner, organiske ikke-paraffiner og uorganiske salte termisk karakteriseret. Derudover præsenterer denne undersøgelse udviklingen af PCM-emulsioner, PCM-polymerer og PCM elektrospundne fibermatricer. Alle variationer af PCM-emulsioner, polymer og elektrospundne fibre blev karakteriseret termisk og morfologisk. Kommerciel organisk paraffin RT18™ med en smeltetemperatur på 18°C i bulk-, emulsions- og elektrospundne fiberformer blev fundet egnet til anvendelse i LHTES-systemer. Bulk RT18™ udviste latent smelte-/størkningsvarme på 137-139 kJ/kg, mens RT18™-vandemulsion havde latent varme på ca. 180 kJ/kg. PCM-kerne-PCL-skal elektrospundne fibre af organisk paraffin RT18™ viste latente smeltestørkningsvarme på 102,1/82,21 kJ/kg.

I forlængelse af de eksperimentelle undersøgelser af PCM blev en numerisk analyse af LHTES-systemer med forskellige geometrier udført ved hjælp af Comsol Multiphysics 6.0 FEM-software. Effekten af interne og eksterne finner i et dobbeltrør, der indkapsler bulk PCM i det ringformede rum, blev undersøgt. Derudover blev en enkeltrørs LHTES med PCM elektrospundet fibermatrix i direkte kontakt med vand analyseret. Faseændringsprocesserne blev accelereret med en stigning i længden af finnerne.

PREFACE

Thesis Title: Microencapsulated phase change materials for thermal energy storage in buildings: design, characterization and modelling

Ph.D. Student: Evdoxia Paroutoglou

Supervisors: Professor Alireza Afshari, Aalborg University
Associate Professor Peter Fojan, Aalborg University
Associate Professor Leonid Gurevich, Aalborg University
Associate Professor Göran Hultmark, Aalborg University

This thesis is submitted to the Ph.D. school of engineering as partial fulfillment of the Ph.D. degree. The current study was conducted in both Department of the Built Environment and Department of Materials and Production of Aalborg University from June 2018 to July 2023. The experiments related to this study were conducted in the department of Materials and Production from October 2018 to January 2020. The author deeply appreciated the financial support provided by Danish Energy and Aalborg University. The dissertation is based on published research papers; and the published scientific papers listed below are the main body of the thesis. Co-authors statements are available to the Ph.D. school and assessment committee. The current dissertation is available for limited and closed circulation as copyrights may not be ensured.

The Ph.D. thesis main body is constituted by the following scientific papers:

[1] E. Paroutoglou, A. Afshari, N. C. Bergsøe, P. Fojan, and G. Hultmark, “A PCM based cooling system for office buildings: a state of the art review,” E3S Web Conf., vol. 111, no. 201 9, p. 01026, 2019.

[2] E. Paroutoglou, A. Afshari, P. Fojan, and G. Hultmark, “Investigation of Thermal Behavior of Paraffins, Fatty Acids, Salt Hydrates and Renewable Based Oils as PCM,” Proc. 14th Int. Renew. Energy Storage Conf. 2020 (IRES 2020), vol. 6, 2021, doi: 10.2991/ahe.k.210202.006.

[3] E. Paroutoglou, P. Fojan, L. Gurevich, G. Hultmark, and A. Afshari, “Thermal Analysis of Organic and Nanoencapsulated Electrospun Phase Change Materials,” Energies, vol. 14, no. 4, p. 995, 2021, doi: 10.3390/en14040995.

[4] E. Paroutoglou, P. Fojan, L. Gurevich and A. Afshari, “Thermal properties of novel phase-change materials based on tamanu and coconut oil encapsulated in electrospun fiber matrices”, Sustainability, vol. 14, no. 12, p. 7432, Jun. 2022, doi: 10.3390/su14127432.

[5] E. Paroutoglou, P. Fojan, L. Gurevich, S. Furbo, J. Fan, M. Medrano and A. Afshari, "A Numerical Parametric Study of a Double-Pipe LHTES Unit with PCM Encapsulated in the Annular Space", *Sustainability*, vol. 14, no. 20, p. 13317, Oct. 2022, doi: 10.3390/su142013317.

ACKNOWLEDGEMENTS

This is the final page of my Ph.D. journey. I would have never made it to the end without the help of many people in my personal and professional environment.

At first, I would like to thank prof. Alireza Afshari the main supervisor in this project who guided me through the whole Ph.D. process and helped me to go through such a complex and interesting project. Special thanks to Associate Prof. Peter Fojan my co-supervisor in this project who helped me a lot to get deeper insight and guided me in the experimental part of the project. Special thanks to my co-supervisor Associate Prof. Leonid Gurevich, who helped me a lot with his thoughtful advice and guidance. I would like to thank Associate Professor Göran Hultmark and Senior Researcher Niels Christian Bergsøe who have been involved in the Ph.D. project and of course all my colleagues in the department of the Built Environment.

I would also like to thank my mother and father and especially my husband Antonis who has been patient with me when my focus was on my Ph.D. project.

Lastly a big thank you note to my daughter Irene who was born during the Ph.D. project period and has been my motivation and my driving force to finish this Ph.D.

This project has been financially supported by International Energy Agency and Aalborg University.

To Irene who taught me how to love unconditionally and gave me strength in the good and bad periods, in my ups and downs without even knowing it.

TABLE OF CONTENTS

I INTRODUCTION

1. Introduction.....	2
1.1. Background.....	2
1.1.1. Energy use in Heating Ventilation and Air Conditioning (HVAC) systems in buildings	2
1.1.2. Thermal energy storage	3
1.1.3. Latent heat thermal energy storage.....	4
1.2. Objective, scope and research questions	5
1.3. Outline of the thesis.....	6
2. Phase Change Materials.....	8
2.1. Solid-liquid PCM.....	8
2.1.1. Organic PCM.....	9
2.1.2. Inorganic PCM	10
2.1.3. Eutectic PCM.....	11
2.1.4. Selection of PCM candidates.....	13
2.2. PCM encapsulation.....	14
2.2.1 PCM emulsions	16
2.2.2. PCM polymers.....	20
3. Electrospinning and PCM electrospun fiber matrices.....	22
3.1. Electrospinning fundamentals	22
3.2. Electrospun fiber matrices with solid-liquid PCM	26
3.2.1. Single fluid electrospinning encapsulating solid-liquid PCM	26
3.2.2. Co-axial electrospinning encapsulating solid-liquid PCM	27
3.2.3. Solid-liquid PCM encapsulated in fiber matrices through other spinning methods.....	28
4. Heat transfer in LHTES.....	30
4.1.Heat transfer in PCM.....	30
4.2. Thermal Testing Methods.....	31

4.2.1. Differential Scanning Calorimetry	31
4.2.2. Differential Scanning Calorimetry testing on PCM	33
4.2.3. Differential Scanning Calorimetry in experimental studies	34
4.3. Heat transfer in LHTES systems.	34
4.3.1. Heat transfer mechanisms.....	34
4.3.2. Heat exchangers classification.....	35
4.3.3. Governing equations.....	36
4.4. Numerical and experimental studies of double-pipe LHTES systems ..	37
5. General outline of research study	40
5.1. Research process	40
II RESEARCH PAPERS	
Introduction to research papers.....	44
6. PAPER I: A PCM based cooling system for office buildings: a state of the art review	46
7. PAPER II: Investigation of thermal behavior of paraffins, fatty acids, salt hydrates, and renewable based oils as PCM	56
8. PAPER III: Thermal Analysis of Organic and Nanoencapsulated Electrospun Phase Change Materials.....	64
9. PAPER IV: Thermal properties of novel phase-change materials based on tamanu and coconut oil encapsulated in electrospun fiber matrices	80
10. PAPER V: A Numerical Parametric Study of a Double-Pipe LHTES Unit with PCM Encapsulated in the Annular Space.....	102
11. Thermal tests of bulk PCM and PCM formulations	120
11.1. Introduction	120
11.2. Methods and Materials	121
11.2.1. PCM emulsions and polymers.....	121
11.2.2. PCM fiber matrices.....	121
11.3. Results and Discussion	122
11.3.1. PCM emulsions and polymers.....	122
11.3.2. PCM fiber matrices.....	127
11.4. Conclusion.....	129

III DISCUSSION, CONCLUSION AND FUTURE RESEARCH

12. Discussion	132
12.1 Thermal performance of PCM.....	132
12.1.1 Long-Term Stability of PCM in pure form	132
12.1.2 Formulation and Thermal identification of PCM composites	134
12.1.3 Formulation and Thermal identification of PCM fiber matrices.....	136
12.2 Numerical analysis of a LHTES system.....	138
13. Conclusion	140
14. Future research.....	142
Literature list	144

LIST OF FIGURES

Figure 1: Basic PCM applications in buildings.....	4
Figure 2: Classification of solid-liquid PCM (adapted from [21]).....	8
Figure 3: PCM with a melting temperature in the range of 15-20°C. Data combined from [13]	13
Figure 4: Classification of encapsulation methods.....	15
Figure 5: Encapsulated PCM.....	15
Figure 6: Emulsion instability mechanisms (adapted from [63])	17
Figure 7: Spinneret configurations of electrospinning	23
Figure 8: Single-fluid, co-axial, and tri-axial electrospinning spinneret configurations.....	23
Figure 9: Solution needle-based electrospinning setup	24
Figure 10: Y-flow electrospinner and Taylor cone	25
Figure 11: Set up for single fiber construction (left) and fiber in fiber construction (right)	25
Figure 12: Phase transition of PCM	30
Figure 13: Time-temperature profile and supercooling process.....	31
Figure 14: DSC curve profile	32
Figure 15: Double pipe LHTES	36
Figure 16: Flow chart of the research process.....	41
Figure 17: Flow chart of the research process.....	120
Figure 18: Water bath set up	121
Figure 19: SEM figures of Pure Temp-18™ (left) and Pure Temp-15™ (right) fiber matrices	128
Figure 20: SEM figures of RT15™ (left) and RT18™ (right) fiber matrices	128
Figure 21: RT18 and RT18 composites in melting/solidification temperature range 15-20°C	137
Figure 22: RT15 and RT15 composites in melting/solidification temperature range 15-20°C	137
Figure 23: Charging and Discharging time (case 1-3: double-pipe LHTES without fins, case 4-6: double-pipe LHTES with internal fins, case 7-9: double-pipe LHTES with external fins, case 10: double-pipe LHTES with internal and external fins and case 11: LHTES unit with PCM fiber matrix [17])	138
Figure 24: Experimental setup of the charging phase for the LHTES.....	142
Figure 25: Experimental setup of the discharging phase for the LHTES	143

LIST OF TABLES

Table 1: Organic PCM with melting temperature 15-20°C.....	10
Table 2: Inorganic PCM with melting temperature 15-20°C	11
Table 3: Eutectic PCM with a melting temperature of 15-20°C	12
Table 4: Selected PCM.....	14
Table 5: PCM emulsions with melting temperature 15-20°C	19
Table 6: Advantages and disadvantages of thermal testing methods	32
Table 7: Water bath test of organic paraffins and non-paraffins in water emulsions	122
Table 8: Water bath test of coconut oil in water emulsions	123
Table 9: Water bath test of tamanu oil in water emulsions with tween 80 emulsifier	123
Table 10: PCM-PVP-APS polymers testing conditions and thermal analysis results	124
Table 11: PCM emulsion-PVP-APS polymers testing conditions and thermal analysis results	125
Table 12: PCM -PEGDa-BPO polymers testing conditions and thermal analysis results	126
Table 13: PCM-PEGDa-BPO polymers testing conditions and thermal analysis results	126
Table 14: Testing conditions and thermal properties of single PCM-PVA fiber	127
Table 15: Testing conditions and thermal properties of PCM emulsion encapsulated in PVA shell	128

NOMENCLATURE

The nomenclature list includes the abbreviations and symbols used in the current Ph.D. thesis.

HVAC	Heating ventilation and air conditioning
MEPS	Minimum energy performance standards
IEA	International Energy Agency
TES	Thermal Energy Storage
SHTES	Sensible heat thermal energy storage
LHTES	Latent heat thermal energy storage
PCM	Phase Change Material
TGA	Thermogravimetric analysis
DTA	Differential thermal analysis
DSC	Differential scanning calorimetry
T-history	Thermal history
Q	Thermal energy stored (kJ)
m	Mass (kg)
C_p	Specific heat capacity (kJ/(kg K))
ΔT	Temperature change (K)
ΔH	Enthalpy (J/(kg))
$\Delta_r G$	Gibbs free energy (J/kg)
$\Delta_r S$	Entropy change of the reaction (J/K kg)
$\frac{dQ}{dt}$	Heat flow (W/g)
$\frac{dT}{dt}$	Heating rate (°C)/min
$f(t, T)$	Time dependent kinetic components
k	Thermal conductivity constant (W/mK)
∇T	Temperature gradient (K/m)
σ	Stefan–Boltzmann constant W / (m ² K ⁴)
h	Heat transfer coefficient W/(m ² K)
a_m	Mass fraction
θ	Fraction/Indicator of phase transition
P	Pressure (Pa)
ρ	Density (kg/m ³)
p_{ph}	Phase indicator
u	Velocity (m/s)
L(1→2)	Latent heat of fusion (kJ/kg)

PART I.

INTRODUCTION

Chapter 1

INTRODUCTION

1.1 Background

1.1.1 Energy use in Heating Ventilation and Air Conditioning (HVAC) systems in buildings

The significance of reducing the energy use in the building sector became obvious in mid-1970s, when oil prices increased and the energy crisis started. To address this challenge, in the late 1970s, European Union established the first standards addressing heat transfer, hygrometric performance, and building envelope permeability. Still, even nowadays, buildings are responsible for 40% of the energy use in the European Union. Additionally, around 35% of the housing stock in the European Union is over 50 years old and requires higher energy input. The current energy crisis has led to new challenges since the energy demand is growing faster than the available renewable resources.

Overall, EU has committed to improving energy efficiency by 32.5% by 2030 [1]. The energy efficiency goal focuses on the building sector, including reduced energy footprint, cutting off reliance on external oil and gas suppliers, and improved indoor environment thermal comfort. To achieve this, heating and cooling strategies should be applied to the building envelope energy efficiency. Heating, ventilation, and air conditioning (HVAC) make up 40% of total building energy use. HVAC systems improvement of design and installations is of utmost importance for energy conservation. HVAC systems designers have been using renewable energy sources lately, aiming to improve energy efficiency and reduce CO₂ emissions. Minimum energy performance standards (MEPS) for final energy use are introduced in ca. one hundred countries, and in twenty countries, MEPS are being developed [1]. Rapid transition to energy-efficient technologies in all markets by 2030 is a prerequisite for reaching the milestone of net zero emissions by 2050 [1].

Passive systems designed for heating and cooling is promising approach to achieving energy savings in an environmentally friendly way. It should be noted that since global temperatures are rising, the need for cooling in building envelopes keeps increasing in both developed and developing countries [1]. According to International Energy Agency (IEA), sales of ACs from 1990-2016 more than tripled by 135 million units [1], which are responsible for 1/5 of all the electricity used. In 2020, the covid pandemic and heatwaves contributed to a growing global energy demand for cooling; as a consequence of lockdown, space cooling made up around 16% of final electricity consumption in 2020 [2].

From this perspective, it is important that the building envelope and HVAC system are optimized to minimize energy use for cooling. Towards this direction, proper building design measures shall be applied, e.g., utilization of higher performance active cooling systems, thermal insulation, and improved passive building components design. As analyzed in [2], the AC energy performance has to be boosted by 50% by 2030 to achieve the new energy efficiency standards. MEPS for ACs have already been implemented in around 80 countries and are under development in more than 20 countries. However, uniform policies are urgently needed to minimize upfront costs due to the looming energy crisis.

1.1.2 Thermal Energy Storage (TES)

In energy-saving technologies, thermal energy storage (TES) is an important way for renewable energy optimization. TES systems can be active or passive according to the TES concept. Some typical applications for TES are solar thermal power plants and TES for heating and cooling in the building HVAC systems [3].

The main advantages for TES systems implementation connected to HVAC are presented below [4],[5]:

- Reduction of energy generation costs
- Improved system's efficiency and reliability
- Increased energy efficiency
- Minimization of CO₂ emissions

TES systems operate in a sequence of three basic steps: charging, storing, and discharging [4]. TES systems, e.g., sensible heat storage, latent heat storage, and thermochemical heat storage, can store thermal energy to be used later.

In the case of sensible heat thermal energy storage (SHTES), the storage of thermal energy is associated with an increase or decrease of the storage medium temperature. SHTES systems are characterized by low cost, stable thermal performance, and reduced CO₂ emissions. The thermal energy stored in SHTES systems is expressed in equation 1.

$$Q = m C_p \Delta T \quad (1)$$

$m = \text{mass (kg)}, C_p = \text{specific heat capacity } \left(\frac{\text{kJ}}{\text{kg K}} \right), \Delta T = \text{raise in temperature}$

On the other hand, in the latent heat thermal energy storage (LHTES) systems, the enthalpy of a phase transition (solid to liquid, solid to solid, liquid to gas, etc.) is used. The thermal energy stored in LHTES systems can be expressed as in equation 2.

$$Q = m \Delta H \quad (2)$$

$m = \text{mass (kg)}$, $\Delta H = \text{enthalpy } \left(\frac{\text{J}}{\text{kg}}\right)$ in the phase change process

In thermochemical heat storage, heat is absorbed or released through a chemical reaction or sorption mechanism [6]. The heat of reaction is given by equation 3.

$$Q = \Delta_R H = \Delta_R G + T \Delta_R S \quad (3)$$

$\Delta_R G = \text{Gibbs free energy (J/kg)}$, $T = \text{Temperature (K)}$,
 $\Delta_R S = \text{entropy change of the reaction } \left(\frac{\text{J}}{\text{K} \cdot \text{kg}}\right)$

1.1.3 Latent heat thermal energy storage (LHTES)

LHTES systems with Phase Change Materials (PCM) can potentially store a substantial amount of heat in a relatively small volume and temperature range. PCMs store latent heat upon a phase transition of the medium and can store this thermal energy for later use [7]. The main advantages of LHTES systems over SHTES are their higher energy storage capacity and the ability to maintain a nearly constant temperature throughout charging and discharging thermal cycles. The most popular thermal management applications with PCM are solar and building applications. Some common LHTES applications in solar systems are solar water and air heating systems, solar cookers, solar greenhouses, etc. [8]. PCM in building applications enhances thermal comfort and promotes energy conservation. In Figure 1, the primary applications of PCM in buildings are depicted. In passive system design, PCM can be incorporated in wallboards, Trombe walls, window shutters, and building materials. On the other side, active systems, e.g., floor heating, air, and water-based heating and cooling systems, ceiling boards, and heat exchangers, were reviewed by many researchers for PCM application [9]–[11].

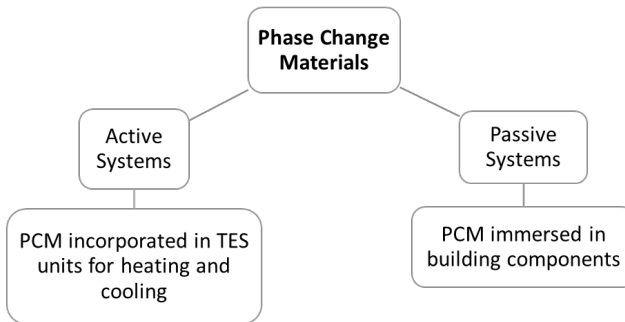


Figure 1: Basic PCM applications in buildings

LHTES incorporated in cooling systems is widely used in HVAC technologies. Cold storage devices with water as heat transfer fluid (HTF) have been studied extensively by many researchers [12],[13]. Fin and tube, shell and tube, flat plate, double tube, and triple tube are some commonly employed configurations of LHTES systems with PCM. The current study analyzes PCM thermal properties and the design optimization for a double tube LHTES.

1.2 OBJECTIVE, SCOPE AND RESEARCH QUESTIONS

The main idea of the project is the microencapsulation of phase change materials for future use in energy storage systems for building applications. The developed PCM layer is prepared to absorb the excessive heat from the building during occupied hours and release it to the environment at night [13].

The Ph.D. project is divided into three parts.

The first part of the thesis consists of a literature review on PCM. The primary research question addressed in this part is to identify PCM and PCM composites with a phase change temperature range of 15-20°C and determine which PCM and PCM composites reported in the literature demonstrate the highest latent heat under repeated thermal cycles within the desired temperature range? The answers to the research questions posed in the first part of the thesis are addressed in Chapter 6: Paper I [13].

The second part of the thesis focuses on the thermal identification of the selected PCM candidates, designing PCM composites, and conducting thermal testing on them. The primary research question of this part is: What is the behavior of the PCM's latent heat and phase change temperature in its pure form upon thermal cycling? Is it possible to formulate PCM composites in a way that preserves the highest degree of latent heat in pure PCM and maintains its melting/solidification temperatures? The answers to the research questions in the second part of the thesis are addressed in Chapter 7: Paper II [14], Chapter 8: Paper III [15], Chapter 9: Paper IV [16] and Chapter 11: Thermal tests of bulk PCM and PCM formulations.

The final part of the thesis focuses on the numerical analysis of an LHTES system. The main research questions for this part are; How does an LHTES system, encapsulating PCM, perform? What is the optimal geometry for the system? Does the addition of fins enhance the thermal performance of the LHTES system? The answers to these research questions are addressed in Chapter 10: Paper V [17].

1.3 OUTLINE OF THE THESIS

The thesis is divided into three parts: Part I: Introduction, Part II: Research papers and Part III: Discussion and Conclusion.

Part I Introduction includes the first four chapters of the Ph.D. project. Chapter 1 Introduction presents the motivation, objective, scope, and an outline of the thesis. Chapters 2, 3, and 4 analyze the state-of-the-art literature on Phase Change Materials, Electrospinning, and Latent Heat Thermal Energy Storage technologies. Chapter 5 presents the general overview of research process. The research approach, which combines the testing methods in the experimental part and the design methodology of the LHTES are described in Chapters 2,3, 4 and 5.

Five Research papers were published during the Ph.D. period. Part II, Research Papers, is split into Chapters 6–11. Chapter 6 is dedicated to a review of the state-of-the-art, focusing on PCM-based cooling systems. The methods and materials used in the Ph.D. project were determined based on the research conducted presented in this chapter. Chapter 7 provides a preliminary presentation of the experimental results obtained for all selected PCM in pure, emulsion, and polymeric structures. Chapter 8 examines and analyzes the thermal properties of various PCM, including organic paraffins and organic fatty acids in pure form, emulsion form, and electrospun fiber matrices. In Chapter 9, the methods described in Chapter 8 are applied to tamanu oil and coconut oil, which are potential sustainable PCM candidates. Chapter 10 provides a description of the numerical parametric analysis conducted on an LHTES system. The final chapter of Part II, Chapter 11, presents additional experimental data that was not covered in Chapters 6–10.

Part III Discussion and Conclusion provides a summary of the results of the Ph.D. Chapter 12 discusses the analysis results in Chapters 6-11. Chapter 13 outlines the conclusions drawn from the research study, while Chapter 14 explores future research opportunities.

Chapter 2

PHASE CHANGE MATERIALS

Alan Tower Waterman of Yale University first observed some peculiarities in the conductivity of molybdenite (MoS_2) as Phase Change Material in the early 1900s [18]. Water, which is a common coolant material with a specific heat of 4.18 (J/g/K) , is also a common example of a Phase Change Material (PCM) with a latent heat of the solid-liquid transition of 334 kJ/kg . Generally, PCMs can be classified into three basic categories: solid-solid, solid-liquid, liquid-gas, and solid-gas [13]. Solid-solid PCM absorbs or releases thermal energy at a given temperature through a crystalline or semi-crystalline phase to a crystalline or semi-crystalline phase transition [19]. Solid-liquid PCMs undergo a solid-liquid phase transition and absorb energy from the surroundings while remaining at a stable temperature [20]. The liquid-to-gas phase change occurs when the liquid reaches the boiling point, which requires an energy equal to the heat of vaporization. This chapter focusses on solid-liquid PCM.

2.1 Solid-liquid PCM

Solid-liquid PCM are classified as organic (paraffin and nonparaffin), inorganic (salt hydrates and metallic), and eutectic (mixture of two or more PCM). The classification of PCM is presented in Figure 2. The focus of the thesis was on solid-liquid PCM with a melting temperature range of $15\text{-}20^\circ\text{C}$, making them applicable for LHTES.

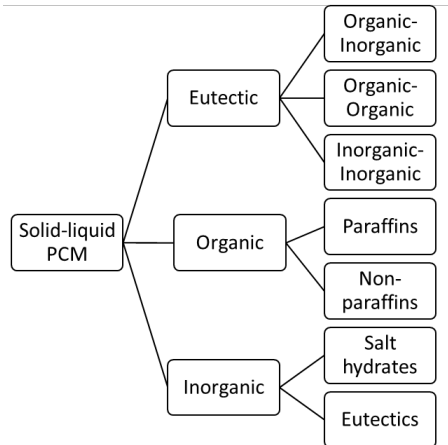


Figure 2: Classification of solid-liquid PCM (adapted from [21])

2.1.1 Organic PCM

Organic PCM are suitable for building applications since they are abundantly available, inexpensive, physically and chemically stable, possess high latent heat, do not phase segregate, and exhibit only minor supercooling [7], [22]. Organic PCM are commonly used in building energy systems, low-temperature thermal energy storage, solar heating, air-conditioning, and smart textile materials [8],[23]. A common disadvantage of organic PCMs is their low thermal conductivity, which can be offset by introducing fins in PCM storage systems, microencapsulation of PCM, or use of metal composites [24].

The main categories of organic PCM are paraffins and non-paraffins. Organic paraffins (C_nH_{2n+2}) have exceptional chemical and thermal stability during repeated thermal cycles [25], displaying high latent heats (200-300 kJ/kg) with a density of around 900 kg/m³ [22] and have a low vapor pressure [22]. Their phase change temperature is also found in a wide range, making them suitable for hot and cold storage [26]. Nonetheless, organic paraffins have low thermal conductivity (≈ 0.2 W/mK), are incompatible with plastic containers, are relatively inexpensive, and are flammable.

A number of experimental and analytical studies have been performed on organic paraffins, e.g. [27]–[29]. For instance, the incorporation of a 5 cm layer of Hexadecane $CH_3-(CH_2)_{14}-CH_3$ in a thermally active building system to improve thermal comfort in office buildings has been investigated numerically and experimentally in [27]. Paraffin RT20 [28] from Rubitherm Technologies was encapsulated in structure spheres size in a LHTES, enabling free cooling techniques with fresh air recirculation, and the numerical model was experimentally validated. A CFD numerical model has been developed for a PCM heat exchanger with organic paraffin type A16 with a melting temperature of 16 °C [29].

Organic non-paraffins are classified as fatty acids, fatty acid esters, glycols, and alcohols. Organic fatty acids ($CH_3(CH_2)_{2n}COOH$) exhibit melting temperatures in a range suitable for thermal comfort applications (5 to 70 °C) and latent heat in the range of (45 to 210 kJ/kg). Some additional advantages of fatty acids are non-toxicity, biodegradability, long-term stability during operation, and a low degree of supercooling. Nonetheless, the thermal conductivity of fatty acids is low in the range of 0.15-0.17 W/mK.

Several studies [30]–[34] have focused on organic non-paraffins in a temperature range of 15-20°C. Butyl stearate and Propyl palmitate are two commonly studied fatty acids which exhibit a melting temperature of 19°C [30]. Isopropyl stearate ($C_{21}H_{42}O_2$) [31] has been studied experimentally, and their melting temperatures were found at 14–18°C. Caprylic acid ($C_8H_{16}O_2$) [31], [32] exhibits a melting temperature of 16.3-16.5°C. Dimethyl sulfoxide with a melting point of 16.5°C [33] was proved suitable for application in cold storage. Palm oil [34] has been identified

suitable for LHTES applications in the range of 15-20°C with a melting point of 17.26°C and latent heat of 127.3 kJ/kg. Table 1 depicts the organic paraffins, non-paraffins and fatty acids with melting temperature 15-20°C.

Table 1: Organic PCM with melting temperature 15-20°C

PCM	Classification	Melting temperature (°C)	Latent heat of fusion (kJ/kg)	Reference
Hexadecane	Organic paraffin	18	236	[27]
RT20	Organic paraffin	20	-	[28]
A16	Organic paraffin	15-17	213	[29]
Butyl stearate	Organic fatty acid ester	19	140	[30]
Propyl palmitate	Organic fatty acid	19	186	[30]
Isopropyl stearate	Organic fatty acid ester	14-18	142	[31]
Caprylic acid	Organic fatty acid	16.3-16.5	148.5	[31],[32]
Dimethyl sulfoxide	Organic non-paraffin	16.5	85.7	[33]
Palm oil	Organic fatty acid	17.26	127.3	[34]

2.1.2 Inorganic PCM

Inorganic PCMs are divided into salt, salt hydrates, and metallics and are commonly used in solar energy applications. Salt hydrates and salts demonstrate similar properties and are characterized by their distinct crystalline structure. The phase change temperature of salt hydrates is found in the wide range of 10-900°C [7]. Salts and salt hydrates of higher melting temperatures are commonly used, whereas organic paraffins and non-paraffins are the principal choices in the low melting temperature range. Salt hydrates are characterized by relatively low cost and high thermal conductivity (≈ 0.5 W/mK). Additionally, some favorable properties of salt hydrates are their inflammability, high latent heat, and slight variation in density during transition [7].

The main drawbacks of salt hydrates as PCM is their phase segregation, corrosiveness, thermal instability, and supercooling [26]. When the salt hydrate is phase segregated, the dense salt sediments on the container bottom.

Metallic PCM are not commonly used, mainly because of their low heat of fusion. However, the wide range of melting temperatures in this category makes metallic PCM suitable for both low and high-temperature applications. Other advantages of metallic PCM include their high thermal conductivity and their physical and chemical stability at higher temperatures. Aluminum (Al) is a characteristic example of metallic PCM with very high thermal conductivity (237 W/mK) and high latent heat (388 kJ/kg) [7]. Despite the beneficial thermal properties of metallic PCM, their applications are limited.

Very few inorganic PCM [35], [36] in the existing literature were found in a melting temperature range of 15-20°C. Potassium fluoride tetrahydrate ($\text{KF} \cdot 4\text{H}_2\text{O}$) is a salt hydrate suitable for cooling applications in buildings [35] with a melting temperature of 18.5°C and latent heat of 231 kJ/kg. Inorganic salt hydrate Sodium hydroxide trihemihydrate ($\text{NaOH} \cdot 3.5\text{H}_2\text{O}$) [36] displayed a melting temperature of 15.4°C and energy storage density of 284.4 MJ/m³. Table 2 encloses inorganic PCM with melting temperature 15-20°C.

Table 2: Inorganic PCM with melting temperature 15-20°C

PCM	Melting temperature (°C)	Latent heat of fusion (kJ/kg)	Reference
Potassium fluoride tetrahydrate	18.5	231	[35]
Sodium hydroxide trihemihydrate	15.4	284.4	[36]

2.1.3 Eutectic PCM

Eutectic PCMs are classified as organic-organic, organic-inorganic, and inorganic-inorganic. The eutectic PCM are the melting composition of different PCM melting and solidifying congruently [4]. Most common eutectic mixtures are constituted by fatty acid mixtures such as capric acid, lauric acid, stearic acid, and palmitic acid [8],[37],[38]. In the solidification process, the two components, when frozen, form a single component and, when melted, are not phase separated. Combining two different components leads to the formation of novel PCM with tailored melting/solidification points and latent heat of melting/solidification.

Several studies [39]–[43] focused on organic eutectics in a melting temperature range of 15-20°C. Capric-lauric acid (fatty acid eutectic mixture) with mole composition of 65-35% was examined and exhibited a melting point of 18°C and heat of fusion of 148 kJ/kg [39]. E19 [40] is an eutectic material with a melting temperature of 19°C and latent heat of 146 kJ/kg. An eutectic mixture of 40% organic paraffin with a melting point of 18°C, 40% organic paraffin with a melting

point of 28°C, and 20% stearic acid was investigated [41]. The eutectic material MT17 [41] exhibited peak melting/solidification temperatures of 17.5°C/18.5 °C and latent heats of melting/solidification of 77/86 kJ/kg. An air-conditioning system for office building applications was investigated in [42] and stored 89% of the cooling load daily. The PCM [42] used in their air-conditioning system was an eutectic mixture of organic PCM hexadecane-octadecane in a weight ratio of three to seven with melting/solidification temperatures of 18.5/20.2°C and latent heat of 121 kJ/kg. In [43] stearic, palmitic, and oleic acid eutectic mixtures' melting points were investigated. Methyl Oleate- Methyl Stearate and Methyl Oleate- Methyl Palmitate [43] exhibited melting temperatures of 20°C and 19°C.

Table 3: Eutectic PCM with a melting temperature of 15-20°C

PCM	Classification	Melting temperature (°C)	Latent heat of fusion (kJ/kg)	Reference
Capric-lauric acid	Organic eutectic	18	148	[39]
E19	Organic eutectic	19	146	[40]
MT17	Organic eutectic	17.5	77	[41]
Hexadecane-octadecane	Organic eutectic	18.5	121	[42]
Methyl Oleate-Methyl Stearate	Organic eutectic	20	93	[43]
Methyl Oleate-Methyl Palmitate	Organic eutectic	19	174	[43]
Calcium chloride hexahydrate- calcium bromide hexahydrate	Inorganic eutectic	14.7	140	[8]
Manganese nitrate hexahydrate- Manganese chloride tetrahydrate	Inorganic eutectic	15–25	125.9	[44]

Few studies [8], [44] presented inorganic eutectics in a melting temperature range of 15-20°C. An inorganic eutectic mixture of 45% calcium chloride hexahydrate ($\text{CaCl}_2 \cdot 6\text{H}_2\text{O}$) with 55% calcium Bromide Hexahydrate ($\text{CaBr}_2 \cdot 6\text{H}_2\text{O}$) exhibited a

melting point of 14.7°C and latent heat of 140 kJ/kg [8]. An inorganic mixture of Manganese nitrate hexahydrate ($\text{Mn}(\text{NO}_3)_2 \cdot 6\text{H}_2\text{O}$) with Manganese chloride tetrahydrate ($\text{MnCl}_2 \cdot 4\text{H}_2\text{O}$) [44] showed a melting temperature range of 15–25°C and latent heat of 125.9 kJ/kg. Table 3 includes eutectic PCM with melting temperature 15–20°C.

2.1.4 Selection of PCM candidates

Initially, it was intended to select PCM candidates PCM from all classes. To summarize, which of all PCM examined in the literature possess melting/solidification temperatures of 15–20°C; all data presented in [13] was shown in Figure 3.

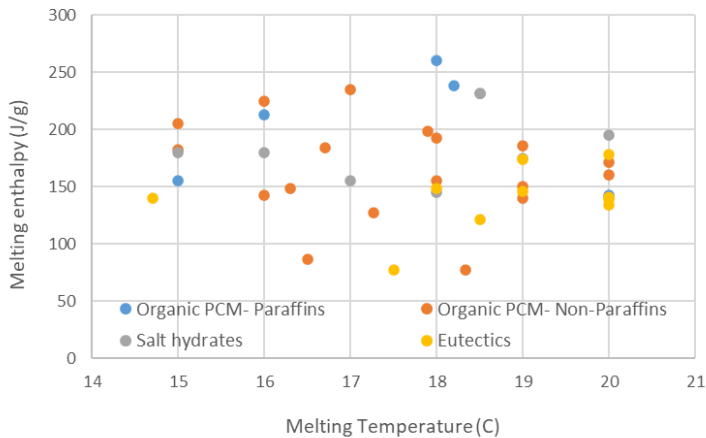


Figure 3: PCM with a melting temperature in the range of 15–20°C. Data combined from [13]

In this study, we selected seven PCM candidates for experimental identification for a low-temperature LHTES application (15–20°C). Five PCM constitute the classes of inorganic salt hydrates, organic paraffins: and organic non-paraffins. Two renewable-based oils (coconut oil and tamanu oil) have also been selected. Table 4 depicts the selected PCM analyzed in the current study. It was intended in the present work to examine PCM deriving from different classes. All PCM were commercially available, and purchasing and using them was easy. The experimental work on PCM candidates in pure form is presented in Chapter 7: Paper II, Chapter 8: Paper III, Chapter 9: Paper IV, and Chapter 11: Thermal tests of bulk PCM and PCM formulations.

Table 4: Selected PCM

PCM	PCM class	Melting Temperature (°C)	Latent Heat (J/g)	Reference
SP15	Salt hydrate	15-17	180	[45]
RT15	Organic paraffin	10-17	155	[45]
RT18	Organic paraffin	17-19	260	[45]
Pure Temp 15	Organic non-paraffin	15	182	[46]
Pure Temp 18	Organic non-paraffin	18	192	[46]
Tamanu oil	Organic non-paraffin	23-26	-	[47]
Coconut oil	Organic non-paraffin	25	-	[48]

2.2 PCM encapsulation

Research on nanoencapsulation and microencapsulation was initiated in the 1950s and overgrew in the 1970s [49]. The classification of encapsulation methods is presented in Figure 4. Encapsulated solid-liquid PCM sustain their shape during melting, and the PCM resists the leakage during phase change by being isolated by the surrounding coating. The encapsulation process improves the thermal and mechanical stability and the heat transfer rate, isolates the PCM and avoids the reaction of PCM from environmental factors, controls the volume change, facilitates transportation, and limits the leakage of PCM [50], [51].

Many researchers have studied Encapsulated PCM in a wide range of applications [52],[53], such as heating and cooling, agricultural, industrial textiles, food storage, pharmaceutical, construction materials, and medical applications. Encapsulation can be achieved with physical, chemical, and physicochemical methods [54]. Encapsulated PCM are classified according to their size in nano encapsulated (1-1000 nm), microencapsulated (1-1000 μm), and macro encapsulated (>1000 μm) [50], [51]. Microcapsules are distinguished based on core-shell structure in mononuclear capsules, polynuclear capsules, multi-wall, and matrices [50], [55]. Figure 5 depicts a typical example of mononuclear (core-shell) PCM encapsulation. The encapsulated PCM is composed of the core and shell material with various shapes: spherical, irregular, oval, etc. [56]. Different emulsification methods used are high shear mixers, ultrasound homogenizers, high pressure homogenizers, microfluidizers, colloid mills and membrane emulsification [57].

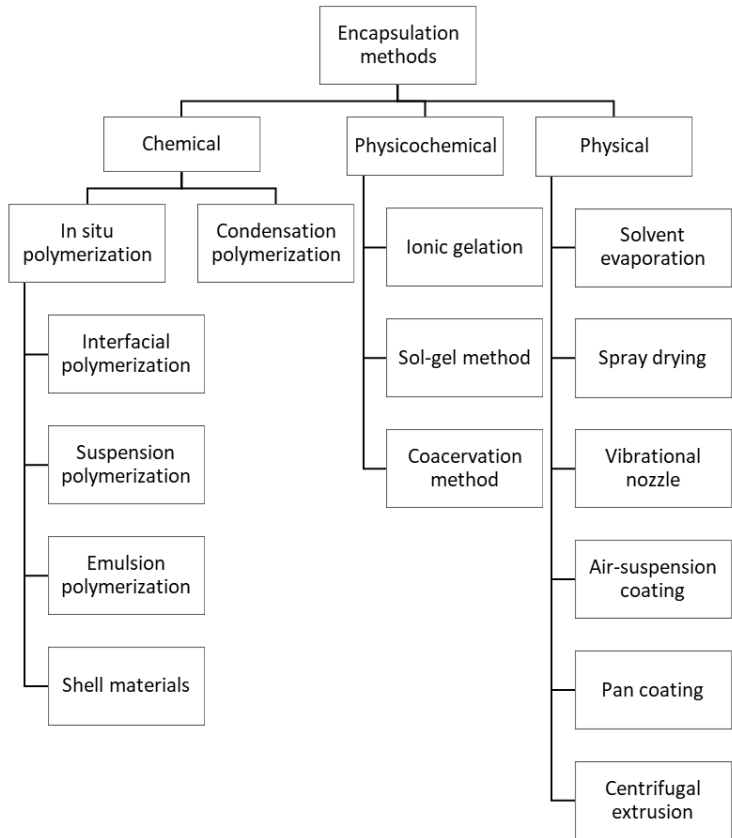


Figure 4: Classification of encapsulation methods

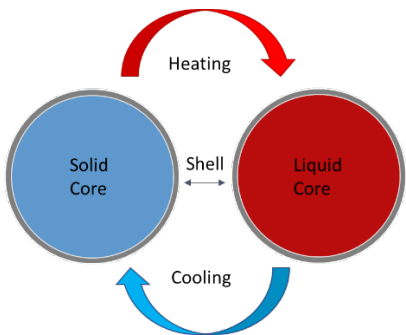


Figure 5: Encapsulated PCM

2.2.1 PCM emulsions

In oil-in-water emulsions, the oil is dispersed in the water, which is the dispersion medium, and the opposite process occurs in water-in-oil emulsions [58]. Emulsions are distinguished according to droplet size into microemulsions (~10 nm), nanoemulsions (~100 nm), and macroemulsions (>1 μm) [59]. A significant challenge often met in emulsion formation is maintaining the emulsion stability. The emulsion stability is improved with surfactants, which enhance the emulsion's interfacial viscosity and decrease the tension [58]. The most influential parameters to the emulsion's stability are [58],[60]:

- The amount of surfactant
- The emulsion's mixing speed
- The ratio of oil to water concentration
- The temperature

The emulsion droplet size characterizes the emulsion stability and instability [60],[61]. The instability mechanisms, e.g., creaming, sedimentation, flocculation, coalescence, and ostwald ripening, leading to phase separation. Creaming is observed when the lighter emulsion droplets separate and rise to the surface [62]. In sedimentation, denser droplets are separated and found in the emulsion's bottom [62]. Creaming of emulsions is often met in oil-in-water emulsions, whereas sedimentation is a more common phenomenon in a water-in-oil emulsion. Flocculation occurs when droplets aggregate and larger units are created. Coalescence happens after flocculation and is observed when small droplets merge, and larger droplets are formed [58]. In ostwald ripening, the particles of emulsion redeposit [58], [60]–[62]. In phase inversion, the dispersed phase converts to a dispersion medium and the opposite [62]. Figure 6 depicts the emulsion instability mechanisms.

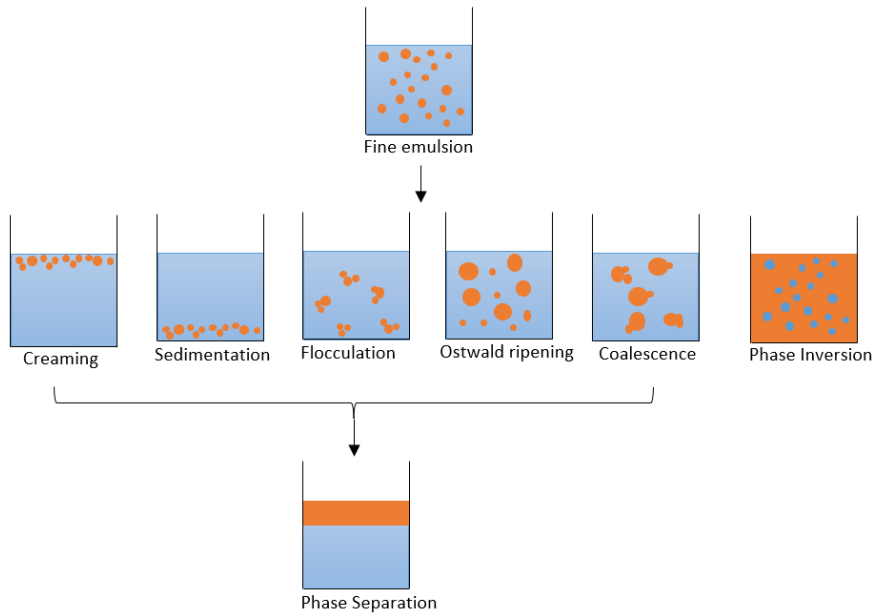


Figure 6: Emulsion instability mechanisms (adapted from [63])

LHTES uses PCM for absorbing and releasing energy in the phase change process at a relatively constant temperature. However, PCM disadvantages are low thermal conductivity, high supercooling degree, thermal instability, leakage, and corrosion. PCM emulsions are composed by mixing PCM with heat transfer fluids and represent a common HTF solution for TES systems. PCM in water emulsions are formed when PCM are dispersed in water using emulsifiers [63]. PCM emulsions exhibit high energy storage density, improved heat transfer, enhanced thermal conductivity, and decreased supercooling degree of PCM [64]. Various studies [65] have focused on cooling system applications in which PCM emulsions were inserted. Such systems are heat sinks [65],[66], coiled tanks [67], cooling panels [68].

Many studies [63], [68]–[77] in the existing literature are focused on the formation of PCM in water emulsions. However, only a few studies [63], [70], [73], [74] refer to PCM emulsions in a PCM temperature range of 15–20°C. Hexadecane in water emulsions have been used in many studies [63], [68], [70], [73]–[76], [78]–[80]. A 30 wt% n-hexadecane in water nanoemulsion with Tween 80/Span 80 (1/1) as emulsifiers was formed and acquired a solidification temperature of 17 °C latent heat of 62.23 kJ/kg [63]. Hexadecane in water emulsion was formed using multi-wall carbon nano-tube particles as nucleating agents [70]. In the cases of hexadecane in water emulsion with the addition of 0.4 wt%, 0.6 wt%, and 0.8 wt% nucleating agents, the supercooling degree was reduced, and both melting and solidification

peak temperatures were found in the range 15-20°C [70]. N-hexadecane nano-emulsions were prepared with phase inversion temperature and emulsion inversion point emulsification methods by using Brij L4 as an emulsifier [73]. N-hexadecane in water nanoemulsion was used in a TES system for a cooling application [68] characterized by high energy efficiency. PCM paraffins emulsions were studied in [80], and all paraffin emulsions showed lower enthalpies than paraffins in pure form (75–77%).

The supercooling effect in PCM emulsions has been investigated in [76],[78],[79]. The size of hexadecane droplets in emulsions was found in the range of 0.2-20µm, and a subcooling of 10K was observed for smaller droplets in the emulsion [76]. The average droplet size of 0.2-12.5 µm for hexadecane in water emulsions formed with sodium dodecyl sulfate and tween 40 as surfactants [78], [79], and the investigated emulsions exhibited subcooling of up to 15K. Table 5 includes the PCM emulsions in a melting temperature range 15-20°C.

Table 5: PCM emulsions with melting temperature 15-20°C

PCM	Emulsifier	Melting temperature (°C)	Latent heat of fusion (kJ/kg)	Average emulsion size (nm)	Ref.
n-Hexadecane (1.5 wt% SiO ₂)	Tween 80 / Span 80	18.3	60.7	N/A	[54]
n-Hexadecane (2 wt% SiO ₂)	Tween 80 / Span 80	18.3	62.9	N/A	[54]
Hexadecane (0.4 wt% MWCNT)	SDS/Tween20 / Tween 80	19.49	72.53	N/A	[70]
Hexadecane (0.6 wt% MWCNT)	SDS/Tween20 / Tween 80	19.69	80.56	N/A	[70]
Hexadecane (0.8 wt% MWCNT)	SDS/Tween20 / Tween 80	19.37	80.51	N/A	[70]
n-Hexadecane	Brij L4	16	N/A	59.8-126.5	[73]
n-Hexadecane	Brij L4 and polyethylene-block-(ethylene glycol)	12–15	43.0	N/A	[68]
n-Hexadecane	SDS/ Tween 40	N/A	N/A	100-20000	[76]
Hexadecane	SDS	17.4	N/A	20-12500	[78]
Hexadecane	Tween 40	17.3	N/A	20-12500	[78]
Hexadecane	SDS/Tween 40	17.3	N/A	20-12500	[78]
P16-97	linear alcohol ethoxylates	16.2	55.6	<1000	[80]
P16-97/P18-97	linear alcohol ethoxylates	18.4	57.9	<1000	[80]
L17	linear alcohol ethoxylates	19.6	60.6	<1000	[80]

2.2.2 PCM polymers

Polymerization is a chemical reaction where smaller molecules called monomers form larger molecules (macromolecules) [81]. In situ polymerization is one of the most efficient encapsulation approaches [82]. The presence of two immiscible liquids (water and oil) helps to confine the chemical reaction to the surface of the droplet which is a basic of the *in situ* polymerization process [53].

Some common polymeric shell materials for in situ polymerization are: melamine-formaldehyde [83], [84], polystyrene [85], [86] styrene [87], silica, polyurethane, polymethyl acrylate, polymethylmethacrylate [49], styrene-methyl methacrylate [88], styrene-butyl acrylate [89]. N-hexadecane[49], [84], n-octadecane [86], polyethylene glycol [90], [91], paraffin waxes [85], [87]–[89] and fatty acids [83], [92], [93] are PCMs commonly studied as encapsulated by many researchers.

In-situ miniemulsion polymerization was used to encapsulate n-hexadecane in a polymethyl methacrylate shell [49]. The cross-linked nanocapsules nPCM13 and nPCM14 of N-hexadecane had a shell thickness of 12nm and exhibited enthalpies of 95-98 kJ/kg and 122-130 kJ/kg correspondingly [49]. Hexadecane in melamine formaldehyde microcapsules achieved the highest thermal stability at a size of 6.8 μm and enthalpy of 150 kJ/kg which was achieved mechanically at a homogenization speed of 6,000 rpm [84]. N-octadecane was encapsulated in a polystyrene shell with an ultrasonic method and miniemulsion in situ polymerization with an average nanocapsule size of 124 nm and latent heat of 124.4 kJ/kg [86].

Srinivasaraonaik et al. [83] encapsulated an eutectic mixture of 75% of Stearic acid and 25% of Capric acid in the core of a melamine formaldehyde shell. The MPCMs with a spherical shape size of 10.41 μm showed thermal stability within 2000 thermal cycles and latent heat of fusion of 103.9 kJ/kg [83]. A suspension polymerization technique was used to encapsulate PRS paraffin wax in a polystyrene shell microcapsule acquiring an energy storage capacity of 153.5 kJ/kg [85]. Microcapsules constructed by suspension polymerization by varying core (paraffin wax) to coating (styrene monomer) mass ratio [87] showed that a mass ratio of 1.5 (paraffin wax RT27 to styrene monomer) resulted in the highest energy storage density. Carboxyl, amine, amide, and hydroxy emulsifiers were used for encapsulating with one-step polymerization a heptane core in high porous and rough MPCMs [94]. Methyl methacrylate and styrene polymer shells were used to microencapsulate paraffin wax [88]. A Pickering emulsion was formed with paraffin wax and silicon carbide (SiC) in water [95]. RT80 was encapsulated with efficiency close to 80 wt% in a nanoshell of styrene-butyl acrylate copolymer with miniemulsion polymerization [89]. The latent heats of melting and crystallization were 5-25 kJ/kg, and the melting temperatures were 1-7°C lower than the temperature of RT80 and showed stable performance after 200 thermal cycles [89]. Capric, lauric, palmitic, and stearic acid were absorbed by four diatomites and

formed shape-stabilized PCM [92]. Capric-lauric acid shape stabilized in diatomite showed a phase change temperature of 16.74°C and a decrease of 57% for the heat of fusion [92]. Shape stabilized EMA- g-C_nH_{2n+1}OH polymeric PCMs were synthesized with esterification reaction and were tested with DSC showing stable performance after 300 cycles [96]. With the side-chain length increasing the phase change temperature of EMA- g-C_nH_{2n+1}OH was shifted from 36.4 to 67.1°C, and the enthalpy was raised from 125.7 to 146.2 kJ/kg [96].

Polyethylene glycol diatomite form-stable phase change composites with additives of single wall carbon nanotubes at the inner diatomite surface exhibited an increased thermal conductivity compared to pure polyethylene glycol [90]. In another study, PEG was stabilized with graphene oxide sheets showing 93.9% of the enthalpy of pure PEG [91].

Chapter 3

ELECTROSPINNING AND PCM ELECTROSPUN FIBER MATRICES

3.1 Electrospinning fundamentals

Nano and microfiber technology is a scientific area engaging matters in 60 nm to a few micrometers. Such fibers and composites are typically produced with a method referred to as electrospinning. The favorable properties of nano and microfibers, such as large surface area and directional strength, make them suitable for a wide range of applications [97].

Polymer fiber production is based on two different methods: melt spinning and solution spinning. Melt spinning is an effective, ecological, and economical method for fiber manufacturing of polymers where the fiber is melted in the spinneret and then solidified by cold air [97], [98]. In the melt spinning process, no additional solvent is required, unlike in the solution spinning method [97], [98]. The most significant spinning processes in solution spinning are wet, dry spinning, and electrospinning [98]. In wet spinning, polymer in organic or inorganic solvent is extruded in a coagulant solution [99]. In dry spinning, volatile organic solvents are used, so the polymer solution is transformed into a fiber upon rapid solvent evaporation [100].

Electrospinning is a straightforward and cost-effective method for the manufacturing of fibers with the use of electrostatic forces. Physicist William Gilbert was the first to observe the electrostatic attraction of liquids back in 1600, which was the crux of the electrospinning technology [101]. The first electrospinning patent was filed by John Francis Cooley in 1900 [101]. Electrospinning has become a popular manufacturing process due to its potential for producing fibers in micrometer and nanometer ranges for various applications. Some typical applications of electrospinning in the fields of science and technology are biomedical, electrical, and industrial textiles, filters, sensors, energy storage devices, etc. [102], [103]. Electrospinning technology can be applied to various materials such as polymers, composites, semiconductors, and ceramics [103].

Polymers are most used materials in electrospinning applications. Polymers are popular due to their relatively low cost, accessibility, and physicochemical properties [104]. Both natural and synthetic polymers are widely used in electrospinning research [105].

There are two main approaches in electrospinning: needle-based and needleless, which can involve different spinneret configurations, as shown in Figure 7.

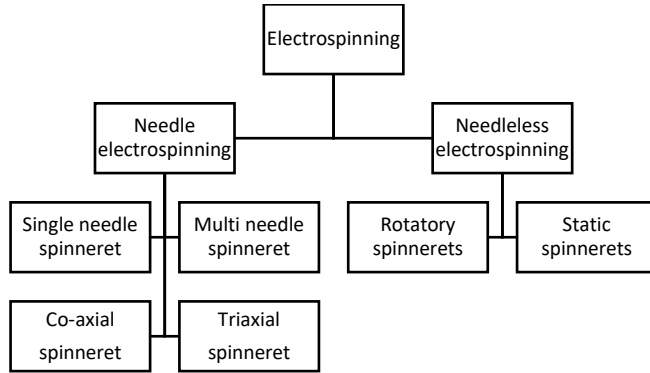


Figure 7: Spinneret configurations of electrospinning

Various electrospinning spinneret configurations in needle electrospinning, such as single needle, multi-needle, co-axial, and tri-axial have been studied by researchers [103],[106]. Figure 8 depicts a schematic graph of single-fluid, co-axial, and tri-axial electrospinning.

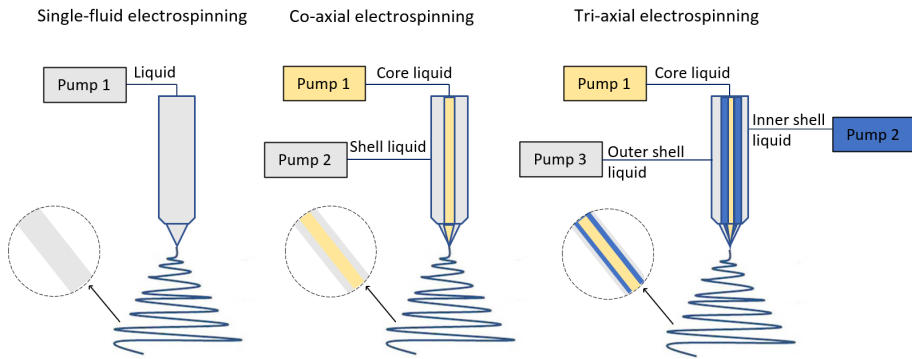


Figure 8: Single-fluid, co-axial, and tri-axial electrospinning spinneret configurations

A single polymer solution is spun through the capillary tip in single fluid electrospinning. Single fluid or single needle electrospinning is considered a traditional electrospinning method with low efficiency in industrial applications [107]. Multi-needle electrospinning follows the same idea as single-needle electrospinning but is more suitable for mass production [108]. In co-axial electrospinning, a modified spinneret design is used where one solution is extruded, constituting the shell material, and another solution makes up the core material through two different capillary tubes. In the co-axial electrospinning method, low conductivity and high surface tension polymer solutions can be electrospun in the fiber's core. Some researchers [109],[110] have focused on isolating the internal

fiber and fabricating hollow fibers. Triaxial electrospinning involves the production of triple-layer fiber, including core, intermediate layer, and sheath [111]. Needleless electrospinning involves the fabrication of nanofibers through electrospinning the solution from an open reservoir instead of a syringe [112]. Some rotating spinnerets reported in the literature are cylinder, spiral coil, disc, and ball spinneret [112]. Static spinnerets in the needleless electrospinning method can use magnet liquids, solution bubbles, and ultrasound transducer electrospinning [112].

In the current study, we have focused on solution needle-based electrospinning with single fluid and co-axial spinneret configurations. In the solution electrospinning process, electrospinning forces allow the formation of uniaxial fibers from viscoelastic solutions. The electrospinning setup comprises a capillary tip and a grounded collector, between which an electric field is applied and a pump to transport the solution. A high-voltage source is used to create the electric field. Polymer solutions are fed to the capillary tip by the pump, and under the action of electric field, a polymer droplet at the end of the tip is transformed first into a hemisphere and then into a cone. The conical shape known as the Taylor cone [113] is created after induced charges from the high-voltage electrostatic field cause jet initiation. Electrospun fibers are formed by jets emerging from the Taylor cone in several paths, e.g., bend, spiral, and loop. Nanofibers can be collected on aluminum foil and metal surfaces. A schematic graph of the jet motion is presented in Figure 9.

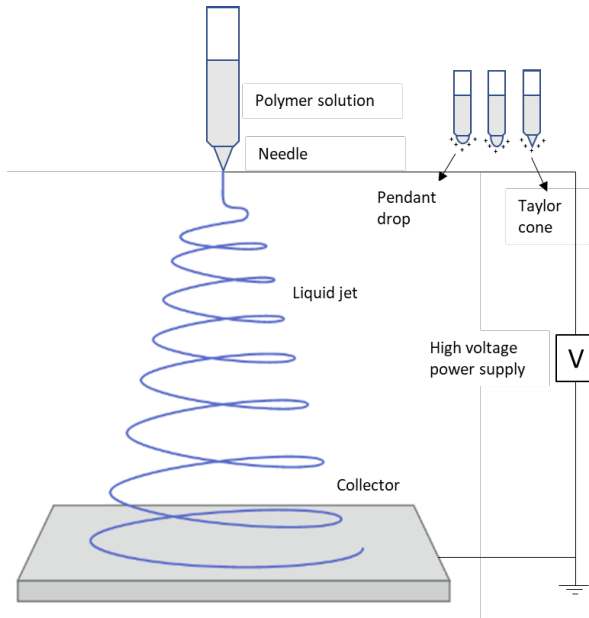


Figure 9: Solution needle-based electrospinning setup

The Y-flow electrospinner used in the experimental process and the Taylor cone appearing in the electrospinning process are presented in Figure 10.



Figure 10: Y-flow electrospinner and Taylor cone

Figure 11 depicts two electrospinning variations: single fluid (left) and coaxial electrospinning (right) used in the experimental part of this Ph.D. project.



Figure 11: Set up for single fiber construction (left) and fiber in fiber construction (right)

Several parameters during the electrospinning process play a significant role in the stability and successful manufacturing of electrospun fibers and can be used to tune the fiber diameter. The most significant parameters of electrospinning are [98]:

- The distance between the tip and the collector
- The applied voltage in the electrospinner
- The hydrostatic pressure in the needle
- The humidity and temperature in the electrospinning setup
- Viscosity, molecular weight, and vapor pressure of the solvent

Form stable PCM in the form of electrospun fiber matrices have a great potential for heat storage while PCM leakage is prevented. Several studies focus on the

encapsulation of PCM in electrospun fiber matrices. The current thesis analyzes studies examining PCM encapsulated in fiber matrices through single fluid electrospinning, co-axial electrospinning, and other electrospinning methods.

3.2 Electrospun fiber matrices with solid-liquid PCM

3.2.1 Single fluid electrospinning encapsulating solid-liquid PCM

Many researchers [114]–[120] focused on fabricating PCM fibers encapsulating Polyethylene glycol with a single fluid electrospinning setup. Polyethylene glycol cellulose acetate fibers showed good thermal stability after 100 thermal cycles with melting and solidification temperatures and latent heats of 58.47 C, 86.03 kJ/kg, and 38.96 C and 65.15 kJ/kg, respectively [114]. In another study, polyethylene glycol/cellulose acetate fibers were crosslinked with toluene-2, 4-diisocyanate [115], and the crosslinked ultrafine fibers presented decreased enthalpies compared to polyethylene glycol/cellulose acetate fibers presented in [114]. Fibers based on polyvinylpyrrolidone, earth Eu³⁺ ions, and polyethylene glycol were fabricated with single fluid electrospinning and tested with field emission SEM and DSC [116]. The average diameters (796–1190 nm) and enthalpies (116–141 kJ/kg) of electrospun PVP/Eu-PEG fiber were increased gradually with an increase in the molecular weight of PEG [116]. Polyethylene glycol polydl-lactide (PEG/PLA) electrospun fibers tested under DSC showed enthalpies of 54.8 to 74.7 kJ/kg [117]. Polyethylene glycol polyvinylalcohol crosslinked electrospun fibers (PEG/PVA) showed good thermal stability under 1000 thermal cycles and presented latent heats of 72.3 kJ/kg [118]. The fibers' diameter and enthalpies were increased with an increased content of DADOE ranging from 375 nm – 1 μ m and 10.8–66.5 kJ/kg. An emulsion of PCM in polyvinylalcohol was electrospun with a single fluid spinneret and a rotating drum collector [119]. A higher amount of PCM led to increased fiber diameters and the PCM fibers had a stable thermal performance after 100 thermal cycles [119]. Diacid dioctadecyl esters/polyethylene terephthalate fibers were synthesized with electrospinning [120].

Few studies focused on encapsulating organic paraffins [121], [122] in single-fiber electrospinning. Dodecane [121] was successfully encapsulated in a polycaprolactone and polylactide matrix with 37wt% of heat storage capacity, similar melting behavior but a higher supercooling degree than the PCM in pure form. N-octadecane silk emulsion electrospun fibers were fabricated through single fluid electrospinning, and the DSC results indicated enthalpies ranging from 7.92 - 37.58 kJ/kg and good thermal stability after 100 thermal cycles [122].

Numerous studies [123]–[132] address the encapsulation of organic non-paraffins and fatty acids in single electrospun fibers. Lauric acid/polyethylene terephthalate

(LA/PET) at a rate of 1:1 w/w composite electrospun fibers were examined in [123]. Several testing methods (FE-SEM, DSC, tensile test) characterized the ultrafine fibers with high heat of fusion of 70.76 kJ/kg, average diameter of 710 nm, and competent tensile strength [123]. Electrospun fibers from lauric acid, polyethylene terephthalate, and silica nanoparticles (LA/PET/SiO₂) showed reduced fiber diameter compared to lauric acid, polyethylene terephthalate fibers (LA/PET) [124]. Binary fatty acid mixtures of lauric-myristic acid, lauric-palmitic acid, lauric-stearic acid, myristic-palmitic, myristic-stearic acid, and palmitic-stearic acid were encapsulated with electrospinning in polyethylene terephthalate matrices [125]. The SEM and DSC analysis results exhibited average diameters of 1-2 μm and lower phase change temperatures and enthalpies compared to pure fatty acids [125]. Lauric acid (LA), myristic acid (MA), palmitic acid (PA), and stearic acid with polyethylene terephthalate (PET) were electrospun, and the LA/PET fibers exhibited average diameters of 454-800 nm and enthalpies of melting and solidification of 169.41 and 165.12 kJ/kg [126]. Lauric acid polyamide 6 (LA/PA6) electrospun fibers in several mass ratios were examined, and the amount of LA significantly affected the fibers' latent heat [127]. When the electrospun fibers underwent thermal treatment possessed lower enthalpies of melting and crystallization in the ranges 56-70 kJ/kg and 57-48 kJ/kg, respectively [127]. Lauric acid and polyamide 6 carbon nanofibers showed heat enthalpies lower than the enthalpy of lauric acid [128]. The mixture of capric, lauric, palmitic, and myristic acids with Ag-coated polyurethane was electrospun, and the fibers showed melting enthalpy and temperature of 110 kJ/kg and 17°C [129]. Phase Change composite fibers of ionic liquid aluminum nitride and copolyimide were tested with DSC and SEM, and the fibers exhibited 86.4 kJ/kg and 0.92–1.07 μm average fiber diameter [130]. Stearyl stearate/polyethylene terephthalate (SS/PET) form-stable ultrafine fibers indicated higher average diameter (989-1021 nm) and enthalpies (14.25-53.77 kJ/kg) with a higher percentage of SS in the fiber content [131]. Coconut oil was encapsulated in polycaprolactone gelatin nanofibers in 5-10% concentrations, and the results of several tests displayed 300-370 nm average diameter [132].

3.2.2 Co-axial electrospinning encapsulating solid-liquid PCM

Co-axial electrospinning is a popular method for encapsulating PCM in the core of fibers [133]–[139]. The melt co-axial electrospinning method was used to fabricate nanofibers with encapsulated 45 wt% of octadecane, and the resultant fiber matrices were thermally stable under DSC testing [133]. Bio-based soy wax was encapsulated in Polyurethane (PU) shell with co-axial electrospinning and tested with several methods (ESEM, TEM, DSC, XRD) [134]. The results indicated good thermal stability under 100 thermal cycles and higher enthalpy with higher soy-wax content

[134]. A phase-change thermochromic material CVL–bisphenol A–1-tetradecanol was encapsulated in the core of polymethyl methacrylate nanofiber through melt co-axial electrospinning technique, and the fibers showed an average diameter of 0.5-2 μm and good thermochromic performance [135]. An emulsion of organic paraffin RT5-polyvinyl alcohol and surfactant polyoxyethylene sorbitan monolaureate was encapsulated in a Polycaprolactone matrix with co-axial electrospinning [136]. An addition of 0.32% in weight of the surfactant improved the heat storage capacity, and 82% of the PCM was successfully encapsulated in the fiber matrices [136]. Coconut oil was encapsulated in a cellulose shell [137]. The specific heat capacity and specific heat of melting of electrospun fiber were increased by 98% and 41%, respectively, compared to coconut oil in pure form [137]. Fibers with polytetradecyl acrylate and carbon nanotube in the core of a polyethylene terephthalate shell were fabricated with co-axial electrospinning and indicated stable shell core structure in temperatures below 300°C [138]. Polyacrylonitrile shell, isopropyl palmitate, and paraffin oil core co-axial electrospun fiber matrices possessed fiber diameters in the range of 0.6-0.72 μm [139].

3.2.3 Solid-liquid PCM encapsulated in fiber matrices through other spinning methods

Multi-needle electrospinning [140],[141], electrospraying [142], [143], co-electrospinning [142], [144] needless electrospinning [145] and centrifugal spinning [146], [147], [148] are other methods met in literature for the encapsulation of PCM. Organic paraffin RT5 was encapsulated in polycaprolactone and polystyrene matrices through multi-needle electrospinning [140],[141]. In [140], Paraffin RT5 (44 wt %) was encapsulated in a polycaprolactone shell. In [141], 34 wt.% of RT5 was encapsulated in a polystyrene matrix, and the encapsulation efficiency reached 78%. Co-electrospun electrosprayed fatty acids: capric acid, lauric acid, and their ternary eutectic mixtures in carbon fiber powder with graphene were fabricated [142]. The graphene and carbon fiber powder fiber matrices exhibited melting temperatures of 14.5°C and 16.9°C. Co-axial electrospraying with a PCM made of lauric and stearic acid with a melting temperature of 39°C was used to fabricate microparticles controlling NGF (nerve growth factor) for biomedical applications [143]. Co-electrospinning of capric-lauric acid and capric-palmitic acid in polyethylene terephthalate showed that the fiber diameter increased with higher PCM content [144]. Additionally, the co-electrospinning method exhibited higher enthalpies of melting and solidification (54.74 and 46.62 kJ/kg) at an increased PCM content [144].

A needleless electrospinning method with a static drum collector was used to encapsulate virgin coconut oil in a polyurethane shell, and the resulting fiber showed

reduced diameter (886 ± 207 nm) and better thermal stability compared to pure PU composite [145].

Centrifugal spinning was applied for the fabrication of polyacrylonitrile polyethylene glycol PCM fiber with 4 wt% nanoscale silicon carbide showed a melting point at 51.31°C and latent heat of 69.91 kJ/kg [146]. Polyvinylpyrrolidone and polyethylene glycol fibers were formed with centrifugal electrospinning and high-speed rotary spinneret [147]. The PVP/PEG fibers exhibited latent heats of melting and crystallization of 79-127 kJ/kg after being subjected to 100 thermal cycles [147]. Polyacrylonitrile polyethylene glycol (PAN/PEG) fibers, formed via centrifugal spinning, possessed enthalpies of melting and crystallization of 82.97 and 75.47 kJ/kg [148].

Chapter 4

HEAT TRANSFER IN LHTES

4.1 Heat transfer in PCM

Heat transfer at the PCM interface relies on the melting-solidification mechanism. In the melting process, the PCM absorbs energy. In this way, the atomic bonds are loosened, and the PCM reaches the solid-liquid mixture state and undergoes the phase transition from solid to liquid [7]. In the endothermal process of solid-liquid phase transition, PCM store thermal energy in the form of latent heat (kJ/kg). Then, when PCM temperature is decreased to solidification temperature, the molecules' chemical bonds become stronger. In an exothermal process, heat will be released as PCM returns to a solid state. The phase transition of solid-liquid PCM is presented in Figure 12.

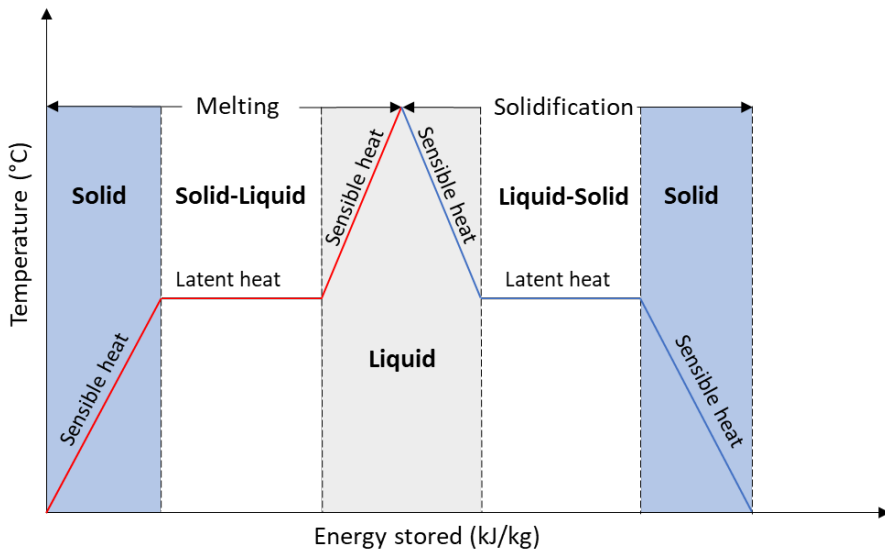


Figure 12: Phase transition of PCM

Supercooling (sometimes also referred to as subcooling in the literature) occurs during cooling when the PCM stays liquid at a temperature below its melting temperature without solidifying. Substantial supercooling/superheating generally occurs due to a delay in the nucleation process. The supercooling degree is defined as the temperature difference between the nucleation temperature and the melting

temperature T_m . Supercooling can result in a sudden temperature increase after the onset of nucleation due to the release of latent heat. (Figure 13).

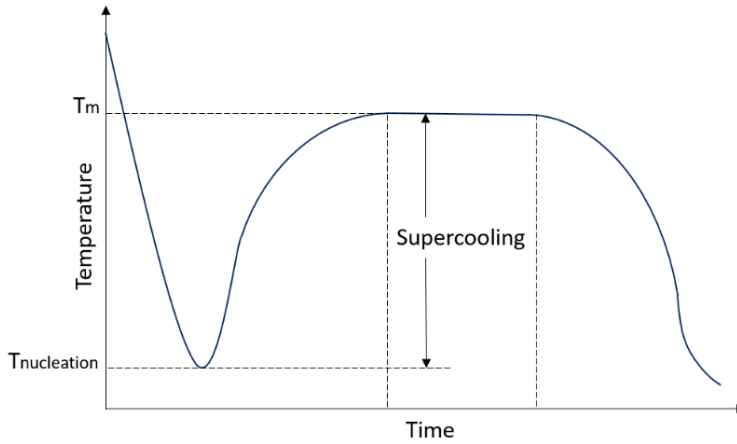


Figure 13: Time-temperature profile and supercooling process

The supercooling degree shall be minimized in order to have charging and discharging thermal cycles in a consistent temperature range [7]. When a PCM reaches its phase change temperature and remains liquid, additional energy is needed to maintain in thermal equilibrium. For this reason, supercooled PCMs are not desirable for applications involving day/night thermal cycles, and several methods [149] (e.g., use of nucleation agents) have been developed by researchers to minimize the supercooling degree. For long-term thermal energy storage applications (e.g., summer/winter), supercooled PCM are attractive due to their ability to store energy for a longer time period. Among the different classes of PCM, many researchers have analyzed salt hydrates [150], [151] and found that most salt hydrates are thermally unstable over repeated thermal cycles.

4.2 Thermal Testing Methods

4.2.1 Differential Scanning Calorimetry

The most common thermal analysis methods met in the literature are thermogravimetric analysis (TGA), differential thermal analysis (DTA), differential scanning calorimetry (DSC) and thermal history (T-history) method. A material's thermal stability is monitored with the analysis of weight change in a sample when being heated at a constant rate with TGA method [152]. In DTA the temperature difference between sample and reference is monitored for heating cooling cycles and the heat flow is calculated [153]. With T-history method the thermophysical parameters of several samples can be tested simultaneously [154]. The transition in

heat released or absorbed under physical or chemical changes is measured with calorimetry [155]. Differential Scanning Calorimetry (DSC) is a simple and fast thermal testing method in quantitative analysis. DSC measures the temperatures and heat flow through time affiliated with the transition in the material in a controlled environment [150]. Table 6 presents some key characteristics of thermal testing methods.

Table 6: Advantages and disadvantages of thermal testing methods

Thermal testing method	Measured property	Advantage	Disadvantage	Reference
DSC	Heat flow	Rapid procedure, relatively inexpensive	Reduced sample size	[156]
DTA	Temperature	High sensitivity	Uncertainty in heat of fusion	[157]
TGA	Mass	Convenient and rapid procedure	Only homogeneous materials	[158]
T-history	Temperature	Large sample size and wide variety of PCM	Not available for commercial use	[159]

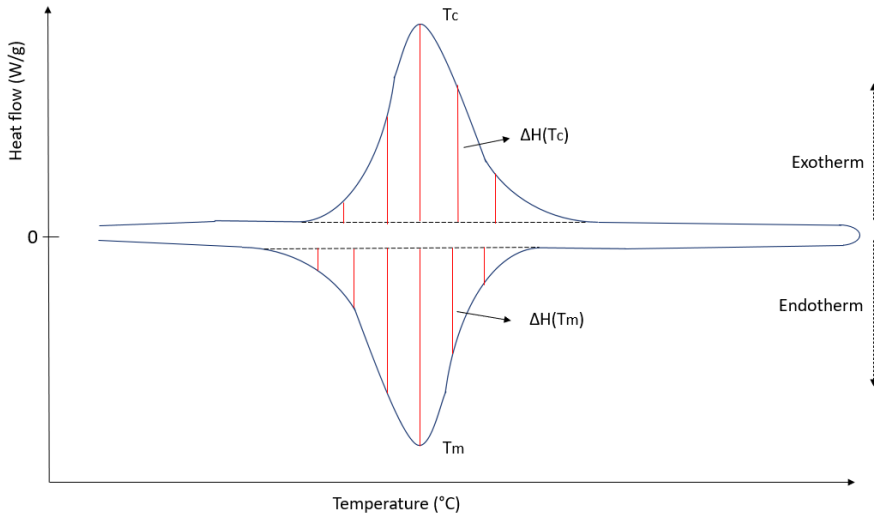


Figure 14: DSC curve profile

The DSC method identifies physical and chemical changes in the material transition for endothermic and exothermic processes [150]. In DSC few mg of the examined materials are required. Two different modes are met in the DSC method the

isothermal mode and the dynamic mode. The DSC in isothermal temperature condition is not affected by the changes in heat capacity. In dynamic DSC, the samples are tested under a controlled temperature range, and the temperature increases linearly as a time function [160]. The DSC graph depicted in Figure 14 is a plot of the heat flow (W/g) in relation to temperature (°C). The two peaks for exothermic and endothermic processes at the highest deviation of heat flow represent the solidification and melting point, respectively. The change in enthalpy in the DSC curve equals to the latent heat. The change in enthalpy is calculated from the integral of heat flow in the DSC curve [161]. The heat flow in isothermal DSC mode is calculated via equation (4), and the heat flow in dynamic DSC mode is calculated by equation (5).

$$\frac{dQ}{dt} = f(t, T) \quad (4)$$

$$\frac{dQ}{dt} = C_p \frac{dT}{dt} + f(t, T) \quad (5)$$

$$\begin{aligned} \frac{dQ}{dt} &= \text{heat flow} \left(\frac{W}{g} \right), \quad C_p = \text{specific heat capacity} \left(\frac{J}{g \cdot ^\circ C} \right) \\ \frac{dT}{dt} &= \text{heating rate} \left(\frac{^\circ C}{min} \right), f(t, T) = \text{time dependent kinetic components} \end{aligned}$$

4.2.2 Differential Scanning Calorimetry testing on PCM

DSC is one of the most commonly used techniques for identifying PCM thermophysical properties [162]–[171]. The dynamic and step mode differences of DSC for thermal characterization of paraffins and salt hydrates were studied in [162]. Salt hydrates shall be analyzed in a slower dynamic mode, but there was negligible change when examining paraffins in step and dynamic mode [162]. In [164] it was showed that an increased sample mass and heating rate during DSC testing led to an increase in phase change temperature range and a decrease in specific heat. In [165] the T-history method was compared with DSC for PCM with a phase change temperature below 100°C, and the two techniques differed by 2.1% and showed good agreement with the literature. 3D printed specimens of polylactic acid containing two different organic PCM have been tested with DSC and showed that polylactic acid is a suitable solution for PCM encapsulation [166]. DSC proved to be an accurate method for indicating the performance of a full-scale TES system; thus, large-scale tests can be set in a later stage of development [168]. DSC proved to be compatible with the thermodynamic behavior of PCM, and a new method for determining specific enthalpy with model coupling of heat transfer was proposed in

[167]. The effect of the heating/cooling rate on the kinetics of allotropic PCM was studied in [169] and the results indicated that phase change finish temperatures show a great degree of sensitivity to heating/cooling rates. The importance of DSC calibration was underlined in [170] and proved that higher-order reference material could improve the calibration process. A polymeric material was studied in [171] and developed a new experimental methodology for DSC testing where they replaced an empty crucible with a crucible composed of a polymeric matrix to obtain better signal and accuracy.

4.2.3 Differential Scanning Calorimetry in experimental studies

DSC method was adopted in the experimental study in order to identify thermally the properties of PCM in different forms [14],[15],[16]. Different scanning rates, temperature ranges and mass of samples were used during testing.

However, the repeatability of results were observed in the temperature range -30 to $+80^{\circ}\text{C}$ with a scanning rate of $1.5^{\circ}\text{C}/\text{min}$. The mass of samples was found in the range 3-8 mg

4.3 Heat transfer in LHTES systems

4.3.1 Heat transfer mechanisms

Heat is transferred in three ways: conduction, convection, and radiation. Conduction is the transfer of energy between particles of bodies without any macroscopic motion of materials in direct contact [172],[173]. The thermal conductivity constant k is the capability of a material to conduct heat and expresses the heat flowing per time [173]. The equation for conduction heat flux density is shown in equation (6).

$$q = -k\nabla T \quad (6)$$

q is the heat flux density (W/m^2)

k is the thermal conductivity constant (W/mK)

∇T is the temperature gradient (K/m)

Convection is the transfer of energy due to the macroscopic motion of the materials, which can be either natural (due to e.g. buoyancy) or forced [172]. In natural convection, the buoyancy forces driving the flow are induced by the difference in the density of hot and cold fluids [172]. For forced convection, external forces (e.g. mechanical) are used to induce the flow [173]. The heat transfer rate in convection is expressed by equation (7).

$$q = h A \Delta T \quad (7)$$

ΔT is the temperature difference between the fluid and the surface

A is the contact area (m^2)

h is the heat transfer coefficient, which depends on the interface and fluid properties, flow regimes, and other thermohydraulic conditions $\text{W}/(\text{m}^2\text{K})$.

Thermal radiation is the energy transferred by emission of electromagnetic waves from a surface with a certain temperature T [172]. Equation (8) expresses heat by radiation.

$$q = \sigma A T^4 \quad (8)$$

q is heat by radiation (W)

σ is the Stefan–Boltzmann constant ($\text{W} / (\text{m}^2 \text{K}^4)$)

A = Surface of body (m^2)

T = Temperature (K)

4.3.2 Heat exchangers classification

Heat exchangers are engineered devices designed to carry out heat transfer in the most efficient way. Heat exchanger fluids can be gas to gas, liquid to gas, and liquid to liquid. Additionally, heat exchangers are classified according to flow configuration:

- Co-current (parallel) flow
- Counter-current flow
- Crossflow

In co-current flow, hot and cold fluids flow in the same direction, and the streams are parallel [174]. In counter-current flow, the fluids are antiparallel, and the streams start at the opposite end [174]. Crossflow heat exchangers include fluids that flow perpendicularly. Additionally heat exchangers are classified as direct and indirect contact heat exchangers [175]. Direct transfer type heat exchangers include fluid streams that transfer heat by coming into direct contact and then the streams are separated [175]. Indirect transfer type heat exchangers include separate flow paths, and heat is transferred continuously from the hot to the cold fluid across a separating wall [174]. Tubular, plate type and extended surface heat exchangers belong to indirect transfer type heat exchangers [175]. Tubular heat exchangers are shell and tube, double pipe, and spiral tube [175]. Shell and tube heat exchangers consist of a cylindrical shell including a bundle of tubes while spiral tube heat exchangers are made of spirally wound coils included in a shell [175]. Double-pipe heat exchangers consist of two concentric pipes with one fluid flowing through the inner pipe and another one flowing in the annular space between inner and outer pipe [175].

4.3.3 Governing equations

In the current Ph.D. thesis, there is a focus on double-pipe heat exchangers. In the double pipe heat exchanger design, PCM is encapsulated in the annular space and water as heat transfer fluid (HTF) flows through the inner tube. Figure 15 depicts the design of a double pipe LHTES.

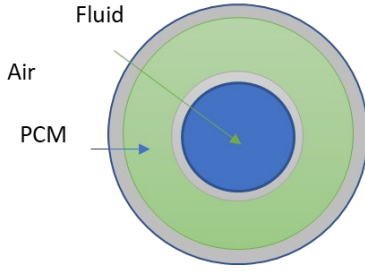


Figure 15: Double pipe LHTES

The Navier Stokes equation and the fluid flow continuity equation are given in (9) and (10).

$$\rho \left(\frac{\partial u}{\partial t} + u \nabla u \right) = -\nabla p + \nabla [\mu (\nabla u + (\nabla u)^T)] + \nabla [\lambda (\nabla u)I] + \rho g \quad (9)$$

$$\frac{\partial \rho}{\partial t} + \nabla(\rho u) = 0 \quad (10)$$

The energy equation for calculating heat transfer in solids and liquids in the LHTES system is expressed by equation (11) [17]. The apparent heat capacity is expressed by equation (12) [17].

$$\rho C_p \frac{\partial T}{\partial t} + \rho C_p u \nabla T = \nabla (k \nabla T) \quad (11)$$

$$C_p = \frac{1}{\rho} (\vartheta \rho_{phase,1} C_{p,phase,1} + (1 - \vartheta) \rho_{phase,2} C_{p,phase,2}) + L_{1 \rightarrow 2} \frac{\partial a_m}{\partial T} \quad (12)$$

$L_{1 \rightarrow 2}$ = Latent heat of fusion (kJ/kg) in phase transition 1 \rightarrow 2

The mass fraction and the heat conductivity equations are presented in equations (13) and (14). The density equation of the PCM is presented in equation (15) [17].

$$a_m = \frac{1}{2} \frac{(1 - \vartheta)\rho_{phase,2} - \vartheta\rho_{phase,1}}{\rho} \quad (13)$$

$$k = \vartheta k_{phase,1} - (1 - \vartheta)k_{phase,2} \quad (14)$$

$$\rho = (1 - \vartheta)\rho_{phase,2} + \vartheta\rho_{phase,1} \quad (15)$$

4.4 Numerical and experimental studies of double-pipe LHTES systems

Several researchers [176]–[185],[186]–[189] have tested numerically and experimentally double-pipe LHTES systems. A double tube LHTES with RT82 as PCM with the dispersion of graphene quantum dot and single-walled carbon nanotubes were studied numerically with Ansys Fluent [176]. The results indicated that reducing pipe and fin thickness by 0.5mm (from 1.5 mm to 1mm) reduced the melting rate by 31% [176]. A concentric double tube containing Al₂O₃ nanofluid and n-eicosane was studied experimentally, and the results indicated that the average heat transfer effectiveness was increased with an increased flow ratio [177]. A vertical double u-tube ground LHTES with RT18™ as backfill material is tested numerically [178]. The energy storage presents an improved performance in the case of borehole thermal heat exchanger (BTES) with PCM against BTES with mortar backfill material [178]. A numerical model of a double-pipe LHTES with a helical shape using RT50 was studied and validated through experiments [179]. The helical coil double pipe melting phase was compared with a horizontal and a vertical double pipe and exhibited 25.7% and 60% savings, respectively [179]. A horizontal double pipe LHTES with RT50 as PCM and water as heat transfer fluid flowing through the inner tube [180]. Downward movement of the inner pipe caused a significant reduction of melting time by up to 64% [180]. A numerical CFD model of a horizontal double tube with an eccentrically placed inner tube and N-eicosane as PCM was studied in [181]. The optimal Fourier number (dimensionless number that expresses transient heat conduction [190]) is 0.99 for achieving the shortest discharging time [181]. An experimental study of a concentric double tube LHTES with PCM as RT52 in the inner tube was conducted in [182]. The results indicated that with an increase of 5°C in the heat transfer fluid temperature the duration of the melting process was reduced by 34% [182]. A finned double tube LHTES with RT35 as PCM was investigated numerically with COMSOL Multiphysics software [183]. The investigation of the mushy zone constant has shown that larger values of mushy zone constant reduced the effects of natural convection in melting and solidification processes [183]. A double-pipe configuration LHTES was studied under partial load in melting and solidification processes [184]. The melting and

solidification time duration was decreased by 50% with a stored energy of 30% in a melting fraction equal to 0.75 [184]. The effect of fins arrangement in a double tube LHTES was investigated in [185]–[189]. Wavy fins of 2mm amplitude and 1mm wavelength lead to a reduction of 43.49% and 17.81% for charging and discharging processes [185], [186]. Longitudinal fins in six configurations (different fin number and orientation) were studied and the results indicated that 2 vertical fins instead of 8 led to charging process reduction [187]. The effect of fin type and orientation was analyzed in a CFD simulation study and the transversal corrugated fin arrangement resulted in shorter melting/solidification times [188]. A double tube LHTES with paraffin wax as PCM with different fins arrangements (no fins, longitudinal fins, spiral fins, circular fins) was developed and tested experimentally as a waste heat recovery system [189]. In horizontal position, the double tube with longitudinal fins and without fins performed better; in vertical position, the double tube with spiral and circular fins showed an improved performance [189].

Chapter 5

GENERAL OUTLINE OF RESEARCH STUDY

5.1 Research process

Figure 16 shows the research process flow chart.

The first part of the flow chart presents the research process starting with a literature review. The outcome of the first part of the research process is reflected in Chapter 6: Paper I [13], which presents PCM and PCM composites that are available within a phase change temperature range of 15-20°C. It should be noted that the current literature does not report any PCM polymers and PCM electrospun fiber matrices with melting/solidification temperatures within the range of 15-20°C. The first part of the research process involves the selection of PCM candidates.

The second part of the research process flow chart shows the experimental research on PCM and PCM composites. The methods and outcomes of the development and thermal identification of PCM and PCM composites are presented in Chapter 7: Paper II [14], Chapter 8: Paper III [15], Chapter 9: Paper IV [16], and Chapter 11: Additional experimental data.

The third and final part of the research focused on the numerical analysis of LHTES systems. In this part, we have aimed to explore an understudied area and developed a simulation model from scratch in Comsol Multiphysics. Chapter 10: Paper V [17] presents the results of the numerical analysis conducted on the double-pipe LHTES system. Due to limitations and shortcomings in the research study, it was not feasible to construct a small-scale LHTES prototype for further experimental research.

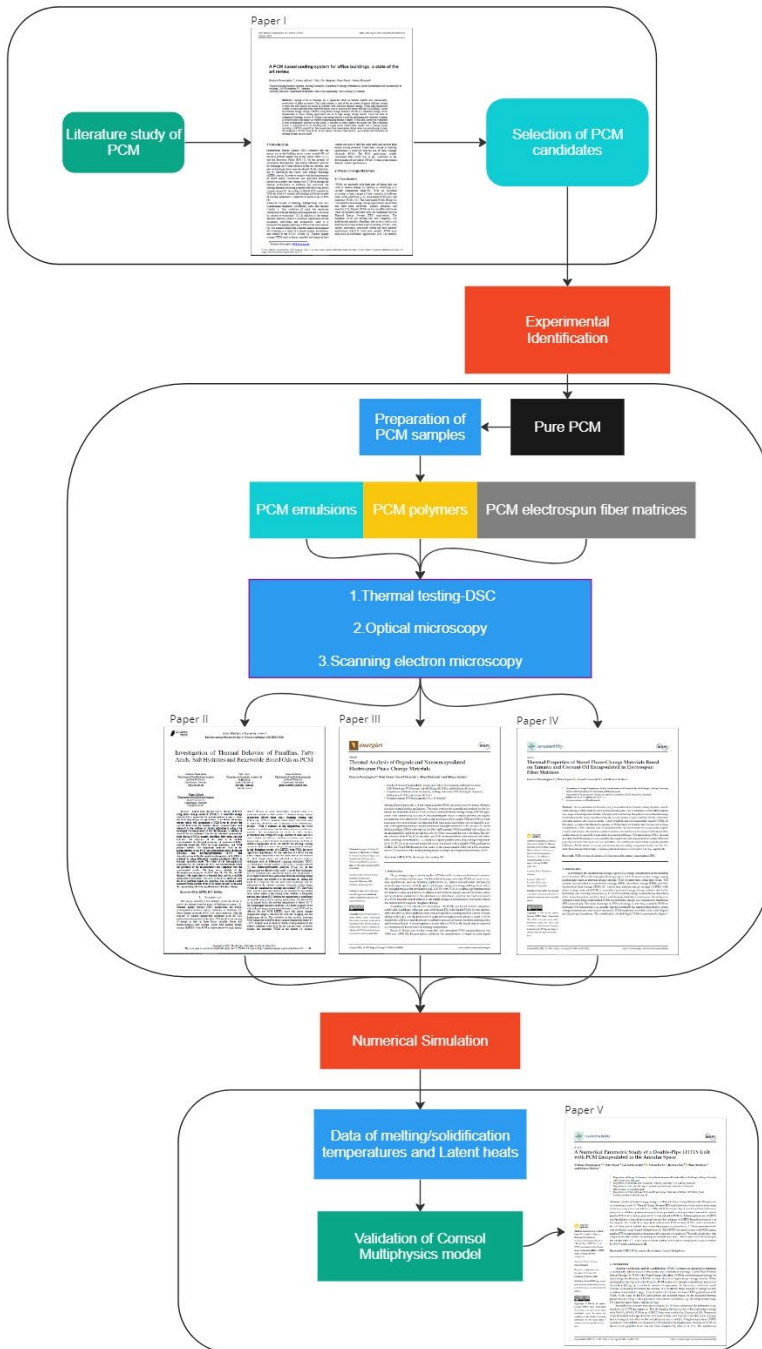


Figure 16: Flow chart of the research process

PART II.
RESEARCH PAPERS

Introduction to research papers

In this chapter, the research papers published throughout the period of the Ph.D. project are presented. The Ph.D. candidate is the main author of the presented papers. All papers are reprinted under the creative commons attribution license.

The first paper is a literature review, which summarizes numerical simulation and experimental studies of PCM materials and their applications for air conditioning chilled water systems [13]. The paper also lists PCMs with the phase change temperature range of 15-20°C [13]. The second paper reports experimental results on seven selected PCMs (paraffins, fatty acids, and salt hydrates) [14]. The thermal properties of the PCMs in pure form, water emulsion, and polymer blends are analyzed, and the long-term stability after 200 thermal cycles is presented [14]. The third paper [15] focuses on the formation and characterization of emulsions and electrospun fibers of organic paraffins and organic non-paraffins. In the fourth paper, tamanu oil and coconut oil in bulk, emulsion, and electrospun fiber form are analyzed [16]. In the third and fourth papers a co-axial electrospinning technique is investigated, and PCM core-shell electrospun microfibers are produced. Polycaprolactone (PCL) 9% w/v and 12% w/v solutions were used to form the fiber shell [15],[16]. PCM emulsified with sodium dodecyl sulfate (SDS) and Polyvinylalcohol 10% w/v (PVA) constituted the core of the fibers [15],[16]. The thermal behavior of the PCM, PCM emulsions, and PCM electrospun fibers were analyzed with differential scanning calorimetry (DSC) [15],[16]. Finally, the fifth paper explores the numerical modeling of a LHTES with PCM [17]. In the fifth paper, different geometries of LHTES are compared, and the use of internal and external fins is studied [17].

All in all, the main objective of the Ph.D. project is the formation and characterization of microencapsulated PCM with a phase change temperature range of 15-20°C and their potential use in LHTES systems for building applications.

Chapter 6

Paper I

A PCM based cooling system for office buildings: a state of the art review

Evdoxia Paroutoglou, Alireza Afshari, Niels Chr. Bergsøe, Peter Fojan and Göran Hultmark

The paper has been published in E3S web of conferences Vol. 111, 01026, 2019

A PCM based cooling system for office buildings: a state of the art review

Evdoxia Paroutoglou^{1}, Alireza Afshari¹, Niels Chr. Bergsøe¹, Peter Fojan², Göran Hultmark¹*

¹Danish Building Research Institute, Aalborg University, Department of Energy Performance, Indoor Environment and Sustainability of buildings, 2450 København SV, Denmark

²Aalborg University, Department of materials science and engineering, 9220 Aalborg Ø, Denmark

Abstract Cooling of air in buildings has a significant effect on thermal comfort and, consequently, productivity of office occupants. This study presents a state of the art review of energy efficient cooling systems that will provide occupants in buildings with satisfying thermal comfort. Using high-temperature cooling systems combined with renewable energy sources increases the energy efficiency in buildings. Latent heat thermal energy storage (LHTES) using Phase Change Materials (PCM) is a renewable energy source implemented in space cooling applications due to its high energy storage density. Since the share of commercial buildings in need of cooling is increasing, there is a need for developing new technical solutions in order to reduce the energy use without compromising thermal comfort. To this end, a proposed ventilation system, preliminarily analyzed in this paper, is expected to reduce further the energy use. The ventilation system is composed of an air handling unit, a 2-pipe active chilled beam system, and a cooling system including a LHTES using PCM. Few researchers have investigated chilled water air-conditioning systems that integrate a LHTES using PCM. In this review, function characteristics, possibilities and limitations of existing systems are discussed.

1 Introduction

International Energy Agency (IEA) estimates that the energy use in the building sector covers around 40% of the total primary energy use in the United States (U.S.) and the European Union (EU) [1]. On the grounds of sustainable development, new energy efficiency policies for buildings have been adopted in the last decades, and new technologies have been developed. In this direction, the EU introduced the Nearly Zero Energy Buildings (nZEB) concept. In order to comply with the requirements of nZEB newly constructed and renovated buildings should reach nearly zero energy use [2]. Even though the thermal performance of buildings has improved, the cooling demands are rising progressively due to the global climate change [3]. According to Global CCS institute by 2020 the share of commercial buildings in Europe in need of cooling equipment is expected to increase up to 60% [4].

American Society of Heating, Refrigerating, and Air-Conditioning Engineers (ASHRAE) states that thermal comfort is “that condition of mind that expresses satisfaction with the thermal environment and is assessed by subjective evaluation” [5]. In addition to the energy demand, thermal comfort is of utmost significance for the occupant's well-being and productivity since it is estimated that people spend up to 90% of the time indoors [6]. It is acknowledged that a healthy indoor environment of a building is a result of a proper design, installation, and control of the HVAC system [7]. Thermal energy storage (TES) such as latent, sensible and chemical heat

storage are used to shift the peak loads and provide high energy saving potential. Latent heat storage in building applications is achieved with the use of Phase Change Materials (PCM). The PCM applications, widely considered after world war II [8], contribute to the development of low energy HVAC systems with optimal thermal comfort performance.

2 Phase Change Materials

2.1 Classification

“PCMs are materials with high heat of fusion that can store or release energy by melting or solidifying at a specific temperature range”[9]. PCM are classified according to their change of state condition in different form: solid-solid PCMs [10], solid-liquid PCMs [11], and liquid-gas PCMs [12]. The solid-liquid PCMs (Figure 1) considered in heat energy storage applications are divided into three main categories: organic, inorganic and eutectics [13]. Organic PCMs such as paraffins which are crude oil products and fatty acids are commonly used in Thermal Energy Storage (TES) applications. The inorganic PCMs are divided into two categories: salt hydrates and metallics. Paraffins, fatty acids as well as salt hydrates have been widely used in building, HVAC, solar energy, electronics, spacecraft, textile and food industry applications [14],[15]. Until now metallic PCMs have been used in electronics applications [15]. The eutectic

* Evdoxia Paroutoglou: EVP@sbi.aau.dk

PCMs are binary or trinary mixtures of chemical compounds that melt and solidify congruently [9].

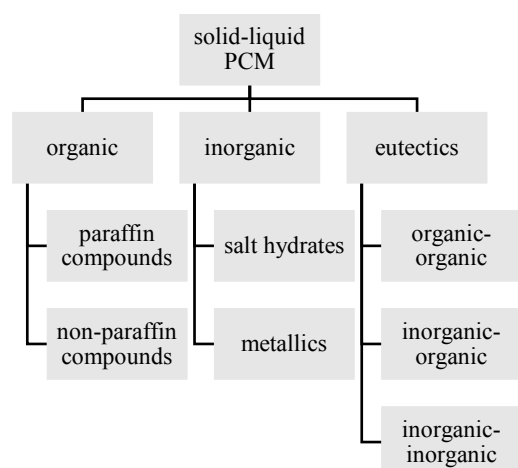


Figure 1: Classification of solid-liquid PCM

2.2 Thermal properties and testing methods

Several studies [16], [17], [18] are focused on the evaluation of the properties of PCMs.

Organic PCMs are regularly used in building envelope applications due to their favorable properties such as chemical and physical stability over repeated thermal cycles, no segregation, no corrosion, compatibility with different materials, no supercooling [19]. Conversely their flammability, low thermal conductivity and volume change are disadvantages of this category [17]. The inorganic PCMs are characterized by high thermal conductivity, small change in their volume, low cost and high heat of fusion, but supercooling and corrosion are effects commonly met in this category [19]. Metallic PCMs were recently attempted to be encapsulated and are proved to have high corrosivity and volume expansion. Eutectic PCMs tend to have a broad range of melting temperatures, high volumetric thermal storage and no segregation is observed throughout the thermal cycles [20]. The thermodynamic properties of PCM can be improved by implementing enhancement techniques such as metal foams, carbon fibers and expanded graphite [19].

Table 1: Testing methods of the thermal properties of PCM

Testing method	Reference
Differential Scanning Calorimetry (DSC)	[13]
Differential Thermal Analysis (DTA)	[21]
T-history method	[16]
Thermogravimetric Analysis (TGA)	[22]

Differential Scanning Calorimetry (DSC) and Differential Thermal Analysis (DTA) are the most commonly used testing methods for the measurement of thermal properties. Both methods are used for the estimation of latent heat and require only a small and homogeneous sample. Another useful testing method of the PCM melting point, heat of fusion, specific heat and thermal conductivity is the T-history method developed by Zhang et al. [16]. Compared to DSC and DTA the T-history method considers a larger sample in a simplified set up. Thermogravimetric analysis (TG/TGA) is a method

where the mass of the sample is measured under different temperatures.

2.3 Incorporation methods

The incorporation methods of PCM in building applications referred in the bibliography are direct incorporation, immersion and encapsulation [8]. In the direct incorporation technique the PCM in liquid or powder form is added in building materials. The immersion technique refers to impregnation of the building materials in melted PCM. The three types of encapsulation depending on the capsule size are macroencapsulation, microencapsulation and nanoencapsulation (Table 2). In macroencapsulation the PCM is encapsulated in a shell such as tubes, spheres or panels [23]. In microencapsulation the PCM particles in solid or liquid form constitute the core and are enclosed in a polymeric film to produce microcapsules [24]. By using the microencapsulation technique, the convective heat transfer coefficient can be increased. Nanoencapsulation is a novel method for encapsulating PCMs in nanoscale. Recent studies [17],[18],[25] indicate that the nanoencapsulation method can optimize the PCMs efficiency. Liu et al. [18] reviewed the preparation methods and application of NanoPCM and suggested further research on molten salt and hydrated salt encapsulation since most studies are focused on organic NanoPCM.

Table 2: Encapsulation methods of PCM

Encapsulation method	Capsule size	Reference
Macroencapsulation	>1000 μm	[26]
Microencapsulation	1–1000 μm	[27]
Nanoencapsulation	1–1000 nm	[18]

3 Latent Heat Thermal Energy Storage (LHTES) by incorporating PCM in the chilled water air conditioning (A/C) system

3.1 Heat exchangers arrangements

PCM are able to store latent heat and several studies have focused on the energy saving potential in building applications. According to Košny [9], PCM applications can reduce the energy use between 5-30% in residential buildings. PCMs inserted in cold storage devices for air-conditioning applications is a method gaining ground in the HVAC technologies. Studies including PCM LHTES systems with water as heat transfer fluid (HTF) are analyzed in this review. The cold storage devices with PCM can be classified according to their construction to flat-plate, double tube, shell and tube, and compact fin and tube heat exchangers [28].

3.1.1 Shell and tube configuration

The factors which play an influential role in the shell and tube heat exchanger configuration were the inlet HTF

temperature, the Prandtl number, the Reynolds number, the length and radius of the tube. Morcos [29] investigated a shell and dimpled finned tube heat exchanger and the PCM used was a mixture of asphalt and paraffin wax. The investigated heat exchanger was efficient for temperature differences between the HTF and the PCM phase transition lower than 16 K. Lacroix [30] investigated the transient behavior of a shell and tube thermal energy storage. The author studied the effect of fins attached to the surface of inner tubes. It was concluded that mass flow rates in the range of 0.0015 kg/s to 0.015 kg/s and inlet temperature at +5 degrees above the PCM melting temperature for the HTF are favorable conditions for heat transfer enhancement [30]. Zhang and Faghri [31] have also studied the effect of fins attached internally in the tube for heat transfer enhancement, and the technique proved to be effective. Anica Trp et al. [32],[33] investigated a shell and tube latent thermal energy storage system and the PCM used was paraffin. The conclusion of this study was that the geometry of the system, as well as the operating conditions, must be based on the required heat transfer rate and the charging or discharging time [33]. Akgün et al. [34] performed an experimental study of a shell and tube latent heat thermal energy storage. Three kinds of paraffins tested as PCM filled the annular space between the tube and the outer shell. The shell surface was set to an inclination angle of 5° in order to enhance the heat transfer, and improve the melting and solidification processes. Hosseini et al. [35] examined a shell and tube LHTES unit. The heat exchanger is comprised of a horizontal cylinder where the HTF flowed and a copper tube placed in the center of the cylinder filled with the paraffinic PCM [35]. The system was externally insulated by glasswool, and it included a charging and a discharging loop with hot and cold water respectively. The study demonstrated that by increasing the inlet HTF temperature the melting time of the PCM decreases and the theoretical efficiency of the heat exchanger increases [35].

3.1.2 Triplex tube configuration

Eslamnezhad and Rahimi investigated a triplex tube heat exchanger including rectangular fins [36]. The authors findings showed that the fins arrangement can increase the heat exchanger efficiency. A triplex tube heat exchanger with PCM for simultaneous charging and discharging was investigated by Joybari et al. [37]. In this study a numerical analysis was conducted. The PCM material was RT31, and different cases were tested depending on the heating mode and the condition of the storage. It was concluded that natural convection is not negligible for the examined configuration. A triplex concentric tube heat exchanger [38] was numerically analyzed and modeled in an experimental apparatus. The PCM filled the cavity of the middle channel. Hot water was the hot heat transfer fluid (HHTF) and cold water was the cold heat transfer fluid (CHTF) flowing outer and inner channel respectively [38]. The results indicated that higher mass flow rate (0.011-0.012 kg/s), lower inlet temperature for charging (23-25°C) and higher inlet temperature (63-

65°C) for discharging led to a shorter solidification/melting time [38].

3.1.3 Fin and tube heat exchangers

A PCM fin and tube heat exchanger was examined by Wen-ju Hu et al. [39], and the study focused on the cooling charging and discharging characteristics of the thermal energy storage exchanger (TESE) using PCM. The heat transfer was enhanced with the addition of fins, and the PCM (RT5) was placed between the fins and the tubes. The thermal conductivity difference between liquid-solid PCM phase led to a higher discharging rate compared to the charging rate. Additionally, the inlet water temperature proved to be a high impact factor on the cooling characteristics of the examined system. Youssef et al. [40] created a physical and a numerical model of a spiral wired tube PCM heat exchanger. The thermal conductivity of the PCM was further increased due to the spiral wired tube arrangement. A 3D CFD model supported the accuracy of the experimental results. The HTF was a mixture of glycol and water. The convection heat transfer and buoyancy led to a faster charging time compared to the discharging time. It was shown that the higher the inlet flow rate the faster the melting and solidification processes.

3.1.4 Double pipe heat exchanger arrangement

Fath [41] investigated numerically and experimentally the performance of a double pipe heat exchanger. The stored energy and the heat transfer rate increased with an increase in the HTF inlet temperature, flow rate and length of storage. Balikowski et al. [42] investigated the charging and discharging characteristics of a double pipe heat exchanger. The authors tested the double pipe heat exchanger under two pipe configurations: a smooth and a spined pipe. The spined fins heat exchanger facilitated the charging and discharging rate through the fins-PCM direct contact. In addition, a higher water flow rate led to greater heat transfer between the HTF and the PCM.

Medrano et al. [43] studied five heat exchangers: three concentric tube heat exchangers, a compact fin-tube heat exchanger, and a plate heat exchanger. The compact fin-tube heat exchanger had by far the highest thermal power for both melting and solidification processes in cases with high-temperature difference between the HTF and the PCM.

The inlet temperature of the HTF, the mass flow rate of the HTF and the fins arrangement are the dominant influencing factors of the heat exchanger efficiency for all the examined heat exchanger configurations.

3.2 Outdoor air for cooling

Outdoor air is a sustainable energy source for free cooling of buildings. According to Maccarini et al. [44], Copenhagen weather condition facilitate the use of free cooling. More specifically for about 93% of the time in a year the temperature is below 18 °C. The ambient temperature is for the greatest part of the year below the

range 15-20°C [44]. In this respect, a PCM with a melting temperature 15-20°C will enable the free cooling process for Copenhagen climate.

3.3 Chilled water A/C systems with PCM

Systems that integrate a Latent Heat Thermal Energy Storage unit with PCM connected to chilled water air-conditioning systems are currently investigated by researchers in the HVAC technologies. This Latent heat storage technology promotes the electrical energy use to the off-peak time.

In the majority of the reviewed studies, the examined LHTES units connected to chilled water A/C systems are PCM storage tanks. Li et al. [45] modeled an A/C system composed by a refrigeration system and a storage tank. The authors looked at the effects of inlet temperature and refrigerant flow on the system. The results showed that the higher the water flow the faster the charging and discharging rate of the PCM in the storage tank. Wu et al. [46] analyzed the mathematical model of a cold thermal energy storage including a packed bed of spherical capsules with n-tetradecane. The simulations' results indicated that the rate of stored and released energy were at a higher level at higher flow rates of the HTF. Lower inlet temperature leads to higher stored energy rate during the charging cycle and lower released energy rate in the discharging cycle.

Parameswaran et al. [47],[48] examined a VAV chilled water air conditioning TES system with spherical PCM encapsulation. The system was tested in a summer and in a winter simulation period for a demand controlled ventilation (DCV) and economizer cycle ventilation (ECV) mode. In the ECV mode outdoor air was provided through the air damper and the chiller was set to 40% of the nominal capacity [47]. A 28% and 47% on peak energy saving was achieved for the DCV and DCV-ECV mode compared with the conventional constant air volume (CAV) air conditioning system. In a later study [48] the authors investigated the effect of a silver nano-based PCM thermal energy storage system incorporated to the DCV and ECV system. The incorporation of silver nanoparticles PCM improved the heat transfer processes through charging and discharging cycles. Falco et al. [49] investigated a chiller-fan coil system integrated with a PCM storage tank. The authors created a 5 kWh prototype consisting of a PET tank with a mixture of RT5HC PCM and distilled water in direct contact. It was concluded that a charging power of 5.7 kW for 54 minutes was capable of charging the storage tank. Moreover, by increasing by 15% the volume of the PCM in the mixture, the stored energy increased by 24%. It was underlined that a small office could reduce the electricity use by 13-16% with the implementation of the developed system. Zhao and Tan [50] performed a numerical analysis and created a model of a PCM shell and tube heat storage integrated with an air-conditioning system. The used PCM was RT22 with a phase change temperature of 19-23°C. The HTF was air during the night-discharging cycle and water during the day-charging circle. Throughout the charging cycle the PCM absorbed heat from the water, flowing through the

inner tube and the PCM liquified. In the discharging cycle outdoor air flowed between outer tube-shell and the PCM solidified. The coefficient of performance (COP) value of the proposed system has shown an increase of about 25% compared to a conventional system.

Experiments, as well as numerical analysis for a TES unit [51] combining three PCMs namely HS-W1, HS-W2 and Paraffin C15, showed that the 1:2:3 proportions combination acquired the largest charging capacity. In the same study, it was validated that the HTF flow rate did not have significant impact on the charging time.

Bruno, Tay, and Belusko [52] performed simulations of a PCM thermal energy storage coupled to a domestic chiller cooling system. The effectiveness-number of transfer units method (ϵ -NTUs) was used in the simulations to calculate the heat transfer. The study targeted the investigation of the off-peak energy saving. The use of a PCM of a melting point at 10°C led to a 13.5% energy saving. The highest impact factors on the energy performance of the system were the thermal conductivity of the PCM as well as the charging time during colder periods. In another study Tay Belusko and Bruno [53] identified the effectiveness of the thermal energy storage connected to a chilled beams system. The storage effectiveness was found to be between 68% and 75%.

4. Thermal energy storage with PCM incorporated into a two-pipe chilled beam system

4.1 Chilled beam systems

The terminal units of the most commonly used air-conditioning systems where water is the medium of heat transfer are fan coils, climatic ceilings and chilled beams [13]. Mechanical ventilation and cooling are combined with the use of chilled beams in office buildings. As stated in REHVA guidebook [54] chilled beams for cooling should be used in buildings when the cooling demand is less than 80 W/ m², the humidity levels are controlled, and the Building Management System (BMS) is adjusted in case of openable windows. Chilled beams have become a preferred solution because they contribute to energy and space savings, satisfactory thermal comfort and they have no need for regular maintenance. It has been demonstrated that chilled beams use less energy than conventional VAV systems to achieve the same level of thermal comfort.

Chilled beam systems can be divided into two categories: passive and active chilled beam systems. Passive or static chilled beam systems operate with natural air convection while active chilled beam systems are connected both to primary air and to chilled and heated water systems [54].

4.2 Innovative two-pipe chilled beam system

Active chilled beam systems can be divided into two configurations: two pipe systems and four pipe systems. The two pipe system configuration is constituted by a supply and a return water pipe which indicates that all the

served zones will receive cold or hot water. The four-pipe configuration includes two supply and two return water pipes. In this way, hot and cold water can be distributed to the building zones simultaneously [55]. Research conducted at Danish Building Research Institute (SBI), Aalborg University, Copenhagen (SBI/AAU) in collaboration with Lindab Comfort A/S has initially set the requirements for the development of a two-pipe system for simultaneous heating and cooling of office buildings. Maccarini [56] designed and developed a novel two-pipe chilled beam system for simultaneous heating and cooling. The analysis was supported by simulations in Dymola. It has been shown that the two-pipe system uses between 12% and 18% less total annual primary energy compared to a conventional four pipes system. In the two-pipe chilled beam system for simultaneous heating and cooling the energy is transferred between warm and cold zones, and thus energy saving is achieved with a high degree of thermal comfort. Additionally, in the two-pipe chilled beam system for simultaneous heating and cooling fewer components are needed compared to a conventional four pipes system. The two-pipe chilled beam system requires only one water pump, fewer pipes, and no control valves.

4.3 Novel LHTES with PCM incorporated into 2 pipes chilled beam system

This state of the art review makes up part of the foundation for an ongoing project. In this project it is aimed to develop- an innovative ventilation system with a cooling system which will integrate active chilled beams as terminal units and use a novel heat exchanger with PCM. The system that is going to be developed will use fewer resources in terms of materials and use significantly less cooling energy compared to a traditional chilled beam system. Calculations performed by Maccarini et al. [44] have shown that an integration of a thermal energy storage with PCM in this system can allow an energy reduction by 67% compared to the initial system. PCMs with a phase change temperature between 15 and 20°C will be preferred since this range is feasible for both charging and discharging phase.

A novel heat exchanger will be designed and constructed which will encapsulate a PCM layer to absorb the rejected heat from the building during occupied hours and release it to the environment during the night. In the charging phase that occurs during night hours, the cold outdoor air cools down the PCM which changes state from liquid to solid. During night operation lamellas open and the fan blows outdoor air towards finned tubes in order to solidify the PCM and store the cooling energy (Figure 2). In the discharging phase which occurs during occupied hours (daytime) the PCM absorbs heat from the return water flow of the system changing state from solid to liquid. The novel heat exchanger will be integrated into a two-pipe chilled beam system. A back-up chiller may be needed in the peak load days.

Table 3 is a list of the PCM with a melting temperature between 15 and 20°C used in experimental and analytical studies consequently.

Table 3: PCM materials with melting temperature 15-20°C

Material	Melting temperature (°C)	Melting enthalpy (kJ/kg)	Ref.
Organic PCM- Paraffins			
Hexadecane	18	236	[57]
RT20	20	142	[58]
PCM-A16	15-17	213	[40]
C16	18.2	238	[59]
RT 15	15	155	[60]
RT 18 HC	18	260	[61]
Organic PCM- Non-Paraffins			
Acetic acid	16.7	184	[62]
Caprylic acid	16.3	148	[63]
Butyl stearate	19,19	140,200	[59], [9]
Propyl palmitate	19	186	[59]
Isopropyl stearate	14-18	142	[9]
Dimethyl-sulfoxide	16.5	86.7	[9]
Glycerin	17.9, 16.85	198.7, 198.5	[64], [65]
A15	15	205	[66]
A16	16	225	[66]
A17	17	235	[66]
A18	18	155	[66]
A19	19	150	[66]
A20	20	160	[66]
Pure Temp15	15	182	[67]
Pure Temp18	18	192	[68]
Pure Temp20	20	171	[69]
Palm oil	17.27	127.3	[70]
Palm oil/xGnPSSPCM	18.33	77.18	[70]
Salt hydrates			
KF4H2O	18.5	231	[59]
K2HPO4 4H2O	18.5	231	[59]
SP15	15-17	180	[71]
S15	15	180	[66]
S17	17	155	[66]
S18	18	145	[66]
S19	19	175	[66]
S20	20	195	[66]
Eutectics			
E19	19	146	[72]
Na2SO4-NaCl-H2O	18		[9]
CaCl2-6H2O-NH4NO3-NH4Br	20	141	[9]
Capric-lauric acid	18	148	[9]
MT17	17.5	77	[73]
Exadecane-octadecane	18.5	121	[74]
Methyl Palmitate- Ethyl Palmitate	20	178	[75]
Methyl Oleate- Methyl Palmitate	19	174	[75]
Emerest2325	20	134	[59]
Emerest2326	20	139	[59]
CaCl26H2O - CaBr26H2O	14.7	140	[14]

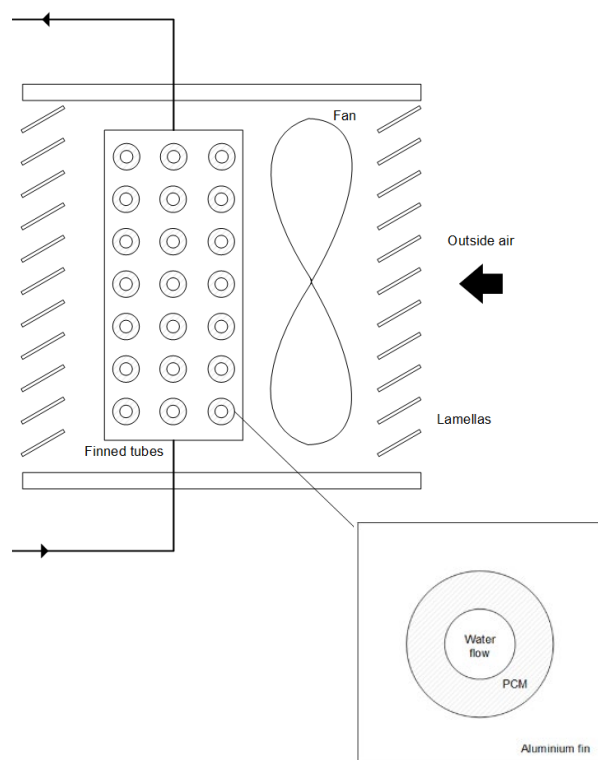


Figure 2: Cooling system assembly

Figure 3 outlines the system. The novelty of the system is depicted in the heat exchange which is achieved in one single phase transition from outdoor air to the two pipe chilled beam system's water circuit.

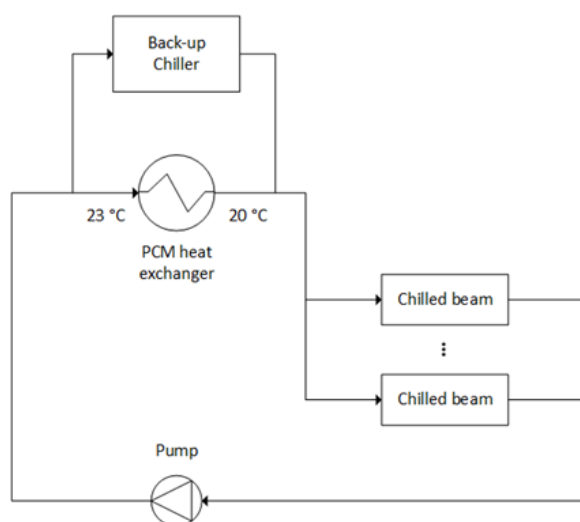


Figure 3: Overall system's assembly

5. Concluding remarks

Studies based on PCM materials and their application for heat exchangers and air conditioning chilled water systems were reviewed in this paper. Numerical-simulation and experimental studies demonstrated that the implementation of PCM in LHTES systems leads to a significant reduction of the peak load. The thermal properties of the selected PCM, the heat exchanger

design, the use of fins or spheres for PCM encapsulation are the most significant considerations for the development of chilled water air conditioning systems with PCM in the existing literature. Paraffins and fatty acids were considered as PCM in the majority of the experimental studies reviewed. Although the implementation of PCMs in cooling systems is a promising technique there is still research to be done. The use of free cooling potential in a PCM-based heat exchanger integrated with a two pipe chilled beam system is expected to bring in remarkable energy savings.

This work is part of an ongoing PhD project at Danish Building Research Institute, Aalborg University in collaboration with Lindab Comfort A/S. The project is financially supported by ELFORSK, a research and development program administrated by Danish Energy.

References

- [1] X. Cao, X. Dai, and J. Liu, *Energy Build.*, **128**, 198-213, (2016)
- [2] G. Paoletti, R. Pascual Pascuas, R. Pernetti, and R. Lollini, *Buildings*, **7**, 43, (2017)
- [3] A. Prieto, U. Knaack, T. Klein, and T. Auer, *Renew. Sustain. Energy Rev.*, **71**, 89–102, (2017)
- [4] B. Sanner, R. Kalf, A. Land, and K. Mutka, P. Papillon, G. Stryi-Hipp, W. Weiss, *European Technology Platform on Renewable Heating & Cooling*, (2011)
- [5] ASHRAE, “Standard 55 -Thermal Environmental Conditions for Human Occupancy,” (2010)
- [6] European Comission, “Indoor air pollution: new EU research reveals higher risks than previously thought,” *Eur. Com.*, (2003)
- [7] R. L. Fehr, *Guid. to Build. Energy Effic. Homes*, 103–130, (2009)
- [8] D. W. Hawes, D. Feldman and D. Banu, *Energy Build.*, **20**, 77-86, (1993)
- [9] J. Košny, *PCM-Enhanced Building Components*, (2015)
- [10] A. Fallahi, G. Guldentops, M. Tao, S. Granados-Focil, and S. Van Dessel, *Appl. Therm. Eng.*, **127**, 1427–1441, (2017)
- [11] W. Su, J. Darkwa, and G. Kokogiannakis, *Renew. Sustain. Energy Rev.*, **48**, 373–391, (2015)
- [12] M. Fatih Demirbas, *Energy Sources, Part B Econ. Plan. Policy*, **1**, 85–95, (2006)
- [13] C. Barreneche, A. Solé, L. Miró, I. Martorell, A. I. Fernández, and L. F. Cabeza, *Thermochim. Acta*, **553**, 23–26, (2013)
- [14] N. Xie, Z. Huang, Z. Luo, X. Gao, Y. Fang, and Z. Zhang, *Appl. Sci.*, **7**, 1317, (2017)
- [15] A. S. Fleischer, *Thermal Energy Storage Using Phase Change Materials Fundamentals and Applications*, (2015)
- [16] Z. Yinping, J. Yi, and J. Yi, *Meas. Sci. Technol.*,

- 10**, 201–205, (1999)
- [17] M. Fuensanta, U. Paiphansiri, M. D. Romero-Sánchez, C. Guillem, Á. M. López-Buendía, and K. Landfester, *Thermochim. Acta*, **565**, 95–101, (2013)
- [18] C. Liu, Z. Rao, J. Zhao, Y. Huo, and Y. Li, *Nano Energy*, 814–826, (2015)
- [19] W. Lu and S. A. Tassou, *Appl. Energy*, **91**, 366–374, (2012)
- [20] M. K. Rathod and J. Banerjee, *Renew. Sustain. Energy Rev.*, **18**, 246–258, (2013)
- [21] R. H. Müller, *Anal. Chem.*, **35**, 103A–105A, (2012)
- [22] S. R. Sandler, W. Karo, J.-A. Bonesteel, and E. M. Pearce, *Polym. Synth. Charact.*, **1**, 108–119, (2007)
- [23] R. Jacob and F. Bruno, *Renew. Sustain. Energy Rev.*, **48**, 79–87, (2015)
- [24] V. V. Tyagi, S. C. Kaushik, S. K. Tyagi, and T. Akiyama, *Renew. Sustain. Energy Rev.*, **15**, 1373–1391, (2011)
- [25] E. M. Shchukina, M. Graham, Z. Zheng, and D. G. Shchukin, *Chem. Soc. Rev.*, **47**, 4156, (2018)
- [26] T. E. Alam, J. S. Dhau, D. Y. Goswami, and E. Stefanakos, *Appl. Energy*, **154**, 92–101, (2015)
- [27] A. Jamekhorshid, S. M. Sadrameli, and M. Farid, *Renew. Sustain. Energy Rev.*, **31**, 531–542, (2014)
- [28] X. Q. Zhai, X. L. Wang, T. Wang, and R. Z. Wang, *Renew. Sustain. Energy Rev.*, **22**, 108–120, (2013)
- [29] V. Morcos, *Sol. Wind Technol.*, **7**, 197–202, (1990)
- [30] M. Lacroix, *Int. J. Heat Mass Transf.*, **36**, 2083–2092, (1993)
- [31] Y. W. Zhang and A. Faghri, *Int. J. Heat Mass Transf.*, **39**, 3165–3173, (1996)
- [32] A. Trp, *Sol. Energy*, **79**, 648–660, (2005)
- [33] A. Trp, K. Lenic, and B. Frankovic, *Appl. Therm. Eng.*, **26**, 1830–1839, (2006)
- [34] M. Akgün, O. Aydin, and K. Kaygusuz, *Appl. Therm. Eng.*, **28**, 405–413, (2008)
- [35] M. J. Hosseini, M. Rahimi, and R. Bahrampoury, *Int. Commun. Heat Mass Transf.*, **50**, 128–136, (2014)
- [36] H. Eslamnezhad and A. B. Rahimi, *Appl. Therm. Eng.*, **113**, 813–821, (2017)
- [37] M. Mastani Joybari, F. Haghighat, and S. Seddegh, *Energy Build.*, **139**, 426–438, (2017)
- [38] L. Jian-you, *Sol. Energy*, **82**, 977–985, (2008)
- [39] W. J. Hu, M. N. Chang, Y. Gao, Q. L. Zhang, L. Y. Yang, and D. Y. Li, *Procedia Eng.*, **205**, 3088–3095, (2017)
- [40] W. Youssef, Y. T. Ge, and S. A. Tassou, *Energy Convers. Manag.*, **157**, 498–510, (2018)
- [41] E. S. Fath, *Energy Convers. Manag.*, **31**, 149–155, (1991)
- [42] J. R. Balikowski and J. C. Mollendorf, *J. Heat Transfer*, **129**, 265, (2007)
- [43] M. Medrano, M. O. Yilmaz, M. Nogués, I. Martorell, J. Roca, and L. F. Cabeza, *Appl. Energy*, **86**, 2047–2055, (2009)
- [44] A. Maccarini, G. Hultmark, N. C. Bergsøe, and A. Afshari, *Sustain. Cities Soc.*, **42**, 384–395, (2018)
- [45] X. Y. Li, Y. Cui, and Y. Y. Wu, *ICIC 2010 - 3rd Int. Conf. Inf. Comput.*, **4**, 23–26, (2010)
- [46] S. Wu, G. Fang, and X. Liu, *Int. J. Therm. Sci.*, **49**, 1752–1762, (2010)
- [47] R. Parameshwaran, S. Harikrishnan, and S. Kalaiselvam, *Energy Build.*, **42**, 1353–1360, (2010)
- [48] R. Parameshwaran and S. Kalaiselvam, *Energy Build.*, **69**, 202–212, (2014)
- [49] M. De Falco, M. Capocelli, and A. Giannattasio, *Energy Build.*, **122**, 1–10, (2016)
- [50] D. Zhao and G. Tan, *Appl. Energy*, **138**, 381–392, (2015)
- [51] X. Y. Li, L. Yang, X. L. Wang, X. Y. Miao, Y. Yao, and Q. Q. Qiang, *Energy*, **150**, 591–600, (2018)
- [52] F. Bruno, N. H. S. Tay, and M. Belusko, *Energy Build.*, **76**, 347–353, (2014)
- [53] N. H. S. Tay, M. Belusko, and F. Bruno, *Energy Build.*, **50**, 234–242, (2012)
- [54] M. Virta D. Butler, J. Gräslund, J. Hogeling, E. Lund Kristiansen, M. Reinikainen, G. Svensson, *Chilled Beams Application Guide Book, Rehva Guidebook no 5*, (2005)
- [55] A. Maccarini, M. Wetter, A. Afshari, G. Hultmark, N. C. Bergsøe, and A. Vorre, *Energy Build.*, **134**, 234–247, (2017)
- [56] A. Maccarini, *A two-pipe system for simultaneous heating and cooling of office buildings*, (2017)
- [57] F. Souayfane, F. Fardoun, and P. H. Biwale, *Energy Build.*, **129**, 396–431, (2016)
- [58] C. Arkar, B. Vidrih, and S. Medved, *Int. J. Refrig.*, **30**, 134–143, (2007)
- [59] H. Akeiber, P. Nejat, M. Z. Abd. Majid, M. A. Wahid, F. Jomehzadeh, I. Z. Famileh, J. K. Calautit, B. R. Hughes, S. A. Zaki, *Renew. Sustain. Energy Rev.*, **60**, 1470–1497, (2016)
- [60] Retrieved from URL: https://www.rubitherm.eu/media/products/datasheets/Techdata_RT15_EN_06082018.PDF
- [61] Retrieved from URL: https://www.rubitherm.eu/media/products/datasheets/Techdata_RT18HC_EN_06082018.PDF
- [62] D. Zhou, C. Y. Zhao, and Y. Tian, *Appl. Energy*, **92**, 593–605, (2012)
- [63] A. Hasan and A. A. Sayigh, *Renew. Energy*, **4**, 69–76, (1994)

- [64] A. Sharma, V. V. Tyagi, C. R. Chen, and D. Buddhi, *Renew. Sustain. Energy Rev.*, **13**, 318–345, (2009)
- [65] S. Kalaiselvam, K. Sureshkumar, and V. Sriram, *Therm. Sci.*, **20**, 1543–1554, (2016)
- [66] Retrieved from URL:
http://www.pcmproducts.net/files/PCM%20Range%202018%20Rev_D%20Compressed.pdf
- [67] Retrieved from URL:
<http://www.puretemp.com/stories/puretemp-15-tds>
- [68] Retrieved from URL:
<http://www.puretemp.com/stories/puretemp-18-tds>
- [69] Retrieved from URL:
<http://www.puretemp.com/stories/puretemp-20-tds>
- [70] S. Wi, J. Seo, S. G. Jeong, S. J. Chang, Y. Kang, and S. Kim, *Sol. Energy Mater. Sol. Cells*, **143**, 168–173, (2015)
- [71] Retrieved from URL:
https://www.rubitherm.eu/media/products/datasheets/Techdata_SP15_EN_15112018.PDF
- [72] U. Stritih and V. Butala, *Int. J. Refrig.*, **33**, 1676–1683, (2010)
- [73] M. Yamaha, S. Misaki, and D. Shinya Misaki, **9669**, (2011)
- [74] K. Nagano, S. Takeda, T. Mochida, K. Shimakura, and T. Nakamura, *Energy Build.*, **38**, 436–446, (2006)
- [75] G. J. Suppes, M. J. Goff, and S. Lopes, *Chem. Eng. Sci.*, **58**, 1751–1763, (2003)

Chapter 7

Paper II

Investigation of Thermal Behavior of Paraffins, Fatty Acids, Salt Hydrates and Renewable Based Oils as PCM

Evdoxia Paroutoglou, Peter Fojan, Göran Hultmark and Alireza Afshari

The paper has been published in Atlantis Highlights in Engineering Vol. 6, 2021.

Investigation of Thermal Behavior of Paraffins, Fatty Acids, Salt Hydrates and Renewable Based Oils as PCM

Evdoxia Paroutoglou
Department of the Built environment
Aalborg University
Copenhagen, Denmark
evp@sbi.aau.dk

Peter Fojan
Department of materials science and
engineering
Aalborg University
Aalborg, Denmark
fp@mp.aau.dk

Göran Hultmark
Department of the Built environment
Aalborg University
Copenhagen, Denmark
goran.hultmark@lindab.com

Alireza Afshari
Department of the Built environment
Aalborg University
Copenhagen, Denmark
ala@sbi.aau.dk

Abstract— Latent heat thermal energy storage (LHTES) using phase change materials (PCM) is a renewable energy solution that is applicable for implementation in space cooling due to its high energy storage density. A novel thermal energy storage which will encapsulate a PCM layer to absorb the rejected heat from the building during occupied hours and release it to the ambient air during night-time is going to be developed. On the grounds of this development, a selection of seven PCMs are examined. The selected materials comprise the basic classes of PCM, namely: paraffins, fatty acids, and salt hydrates. The objective of this study is to identify experimentally the thermal properties of commercial PCM, renewable based oils, PCM in water emulsions, and PCM polymer blends. The supporting materials used in the polymerization of the PCM are polyethylene glycol diacrylate (PEGDA) and polyvinylpyrrolidone (PVP). The characterization of the thermophysical properties of the PCM is achieved by using differential scanning calorimetry (DSC) in dynamic operation mode. The values of the thermophysical properties for the commercial PCM and the renewable based oils provided by the manufacturers are compared with the experimental results. The long term stability of the thermophysical properties of PCM after 50, 100, 150, and 200 thermal cycles equivalent to a 6-month duty cycle in a real-life application is presented. The cases of the PCM emulsions and the PCM polymer blends are analyzed. The obtained results demonstrate the stability of the PCM under thermal cycling and the supercooling effect during the liquid-solid phase change.

Keywords—PCM, LHTES, DSC, Building

I. INTRODUCTION

The energy demand in the building sector has raised to satisfy the thermal comfort needs of building occupants [1]. Thermal energy storage (TES) applications are widely investigated to achieve energy reduction of buildings [2]. Phase change materials (PCM) are smart materials with the capacity to control temperature variations used for TES applications during the last decades. TES involves the storage of energy as heat in three forms: sensible, latent, and

thermochemical heat storage. Latent heat thermal energy storage (LHTES) with PCM is characterized by high energy storage density in small temperature variations and is a preferred solution in TES systems. A thermal energy storage application follows three steps: charging, storing, and discharging. PCM are substances that change state from solid to liquid by absorbing heat (charging) in an endothermic process. With a decrease in the temperature, the PCM solidifies by withdrawing heat (discharging) in an exothermic process. The incorporation of PCM in TES systems accumulates the storage of a large amount of latent heat in a small volume [3]. Energy reduction in heating and cooling applications is achieved with the implementation of PCM in technical equipment. PCM can retrofit the existing cooling system in order to achieve energy saving using free cooling. In the designing process of a LHTES with PCM, the most significant requirements for the selection of a PCM are the phase change temperature and the latent heat of the material [4]. Both characteristics are indicated by thermal analysis techniques such as differential scanning calorimetry (DSC) [5], differential thermal analysis (DTA) [6], T-history method [7] and Thermogravimetric Analysis (TGA) [8]. In the ongoing project related to this study a novel heat exchanger will be designed and constructed which will encapsulate a PCM layer to absorb the rejected heat from the building during occupied hours and release it to the ambient air during the night. It is expected that the novel heat exchanger will be integrated to the already existing “two-pipe chilled beam system for simultaneous heating and cooling” [9]. The PCM layer transfers heat absorbed from the building by the chilled beam water system to the cooling tower, where it is dissipated into the atmosphere [9]. Outdoor air temperature is a preferred sustainable source in free cooling applications. For about 93% on an annual basis, the ambient temperature is below 18 °C for Copenhagen weather conditions [10]. In this respect, PCM with a phase change temperature between 15 and 20°C will be selected for the PCM LHTES since this phase change temperature range is feasible for both the charging and the

discharging phase. The available in the existing literature PCM within the desirable phase change temperature limits 15 - 20°C already used in relevant studies were presented in the author's literature study [11]. In the current study, available organic and inorganic PCMs in the market i.e. organic paraffins, organic non-paraffins and inorganic salts are compared with biobased oils, not known for their phase change properties. Organic PCM are the most commonly used PCM in the current literature [12],[13],[2] due to their phase change temperature range and their heat storage capacity. The two renewable based oils tamanu oil and coconut oil, were found as cosmetic and edible products, respectively, in the market. Recent experimental research is not focused on the long term stability of existing PCM over an extended duty cycle in a real-life application. In the current study, the long term performance and stability of five PCM were investigated.

II. MATERIALS

A. Pure PCM

In total, seven materials and their eutectic mixtures were selected and characterized by DSC. Five commercial PCM with applicability for LHTES systems, and two renewable based PCM not known for their phase change properties were selected. The five commercial PCM belong to the classes of salts, paraffins, and fatty acids. Table 1 illustrates the thermophysical properties provided by the manufacturers. All seven materials namely the two organic paraffins: RT15 and RT18, the two organic non-paraffins PT15 and PT18, the inorganic salt hydrate SP15 and the renewable based oils: tamanu oil and coconut were characterized using DSC in their first thermal cycle.

Table 1: Thermal properties of PCM candidates provided by manufacturers.

Classification	Material	Phase Change Temperature (°C)	Latent heat (J/g)
Organic non-paraffins	PT 15	15	182
	PT 18	18	192
Organic paraffins	RT 15	10-17	155
	RT 18	17-19	260
Inorganic salt hydrate	SP 15	15-17	180
Renewable based oils	Coconut oil	23-26	-
	Tamanu oil	24-26	-

Moreover, the long-term performance of five PCM samples was evaluated by DSC under 200 thermal cycles. The two organic paraffins RT15 and RT18, the two organic non-paraffins PT15 and PT18 and the renewable based tamanu oil were selected for thermal cycling.

B. PCM emulsions and PCM polymers

The organic paraffins RT15 and RT18 were dispersed in water in a ratio of 1:1 to 5:1 with the addition of emulsifiers. Water as PCM has the highest specific heat (4.186 joule/gram °C) compared to other substances, but its use is limited to fixed temperature applications (0 celsius). The emulsions of PCM with water in different ratios were formed and tested using DSC to identify whether the heat capacity of the final solution will be increased or not. Stable oil in water emulsions were formed with the use of Polyethylene glycol sorbitan (Tween 20) and Polyoxyethylensorbitan oleate (Tween 80) as emulsifiers. Tween is non-ionic detergent widely used in

biochemical applications for stabilizing oil in water emulsions. No phase separation was detected in the oil in water emulsions. However, it is complex to determine an emulsion's instability.

Form stable PCM are composed by solid-liquid PCM and supporting materials. The advantage of form-stable PCM is that the material's shape can be maintained when the ambient temperature is higher than the phase change temperature. The PCM polymers of the organic paraffins RT15 and RT18 were synthesized in two different ways. In the first approach, the polymers were formed by the PCM 5% w/v with polyethylene glycol diacrylate (PEGda) 5% w/v as a synthesizer and benzoyl peroxide (BPO) 1% w/v as initiator. In the second solution, the polymers were formed by a PCM emulsion 15% w/v with polyvinylpyrrolidone (PVP) 5% w/v as a synthesizer and ammonium persulfate (APS) 10% w/v as initiator. The PCM emulsion in the second solution was a PCM-Polyvinylalcohol (PVA) emulsion. The PCM-PVA emulsions was formed by mixing 10ml of 30% w/v PCM with 8.4 mmol/L of sodium dodecyl sulfate (SDS) and 100 ml of a 9% w/v polyvinyl alcohol (PVA) solution.

III. TESTING METHODS

A process that releases energy as heat into the surroundings is classified as exothermic and one that absorbs energy as heat from the surroundings is classified as endothermic [14]. The release of heat at constant pressure signifies a decrease in the enthalpy (ΔH) of the system (exothermic process $\Delta H < 0$). The enthalpy changes at constant pressure can be measured as heat transferred from a system. Changes in internal energy are measured experimentally with calorimetry. Enthalpy can be defined by (1) and (2). At constant pressure, the equation of enthalpy is described by (3).

$$H = U + pV \quad (1)$$

$$\Delta H = Q = \int Cp dT \quad (2)$$

$$\Delta H = \Delta U + p\Delta V \quad (3)$$

H=enthalpy, U=internal energy, p=pressure, V=volume

DSC is a versatile technique for thermal analysis introduced in the early 1960s [15], and it measures the energy transferred as heat to or from a sample at constant pressure during physical or chemical change. The dynamic range characterizes the DSC when compared to other calorimetric methods. The sample is compared to a reference material that is not involved in a physical or chemical change, and the temperatures of the sample and reference are scanned during the analysis. The scanning rate is stable in the dynamic operational mode of the DSC. Heat flow rate versus temperature is the outcome of the DSC curve due to the thermal resistance of the sample [16]. The area under the heat flux curve is proportional to the heat of fusion or enthalpy (J/g). The phase change of the PCM is occurring in a specific temperature where a peak is produced in the DSC curve. The DSC tests were performed with the use of a DSC Q2000 instrument with T-zero thermocouples. This DSC equipment offers 50 positions for samples and a temperature range of -180 to 725. A conventional empty crucible was used as a blank for the reference sample. The DSC equipment includes a furnace where a reference sample and the examined sample are heated or cooled under controlled temperature variations. A rate for the temperature fluctuation is defined, and heat is transferred to the samples. The materials response is described in equation (4). The specific heat capacity (C_p) of the

examined PCM can be calculated as a function of temperature (4). Various DSC analysis were performed for the pure materials as well as for their eutectic mixtures. Table 2 depicts the technical features of the DSC equipment. The setup temperature of the DSC was at 40°C, so the material was already melted when it was inserted in the chamber for thermal cycling. For this reason, it was attempted to cycle the materials three times in every test by heating, cooling, and heating the material again with the same scanning rate (°C/min). For industrial applications of PCM, it is essential to evaluate the thermal performance over a simulated lifetime. The samples underwent manual thermal cycling for 200 thermal cycles, which represent 6 months of lifetime in an application. DSC tests were performed for both 50, 100, 150, and 200 thermal cycles.

Table 2: Technical features of TA DSC Q2000 instruments (11)

Series	Q2000
Temperature range	-180 - 725
Calorimetric accuracy	±0.05%
Thermocouple	T-zero

$$q = C_p (dT/dt) + f(T,t) \quad (4)$$

q = heat flow, C_p = specific heat capacity, dT/dt = heating rate, $f(T,t)$ = kinetic response at specific time and temperature

IV. RESULTS AND DISCUSSION

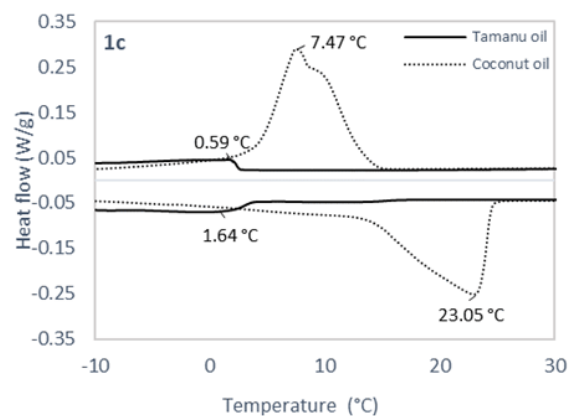
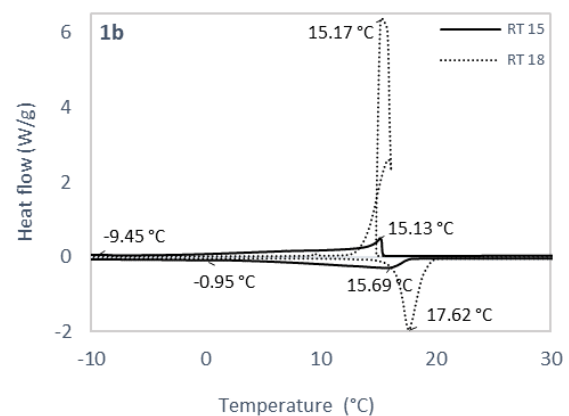
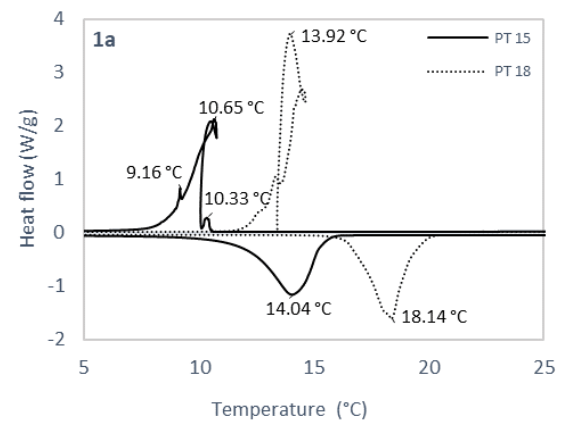
A. Determination of thermal properties of pure PCM

1) Short term thermal performance of PCM

Thermal properties of pure PCM measured with DSC technique are presented in Figure 1. The samples of the pure materials were examined within a temperature range of -30 to 80°C with a scanning rate of 1.5°C / min in a dynamic mode. The mass of each samples was 6 mg. The melting and freezing points are the peak temperatures at the maximum/minimum points in the melting and freezing curve. In every DSC analysis, the melting/freezing point is highly dependent on the scanning rate and the preparation of the sample. The scanning rate has a significant effect on the thermal shifts in the heating and cooling curves. A scanning rate of 1.5°C / min was selected to provide high resolution of the melting and freezing peaks. The DSC thermogram in Figure 1b illustrates a thermal shift of 2.5°C between the melting and freezing curve for the organic paraffin RT18. The same phenomenon is depicted in the DSC thermogram in Figure 1a shown that for the organic non-paraffins the thermal shift reaches 3.5°C for PT15 and 4.5°C for PT18. The DSC thermogram for coconut oil shown in Figure 1c illustrates that the thermal shift is the highest amongst the examined materials reaching 15.5°C. No thermal shift is observed for RT15 (Figure 1b) and tamanu oil (Figure 1c). A vast deviation is applied in the case of the selected salt hydrate, and it may be an outcome of the material's degradation (Figure 1d). The examined thermal properties of the pure materials (Table 3) are compared with the thermal properties provided by the manufacturers (Table 1). The expanded uncertainty for each experimental measurement is ±0.1%. The calculation of the relative error (%) was conducted with the use of equation (5) according to [17].

$$\text{Relative error (\%)} = \frac{|(\text{measured value} - \text{expected value})|}{\text{expected value}} \quad (5)$$

The relative errors calculated for the melting and freezing enthalpies are 40% and 41% for PT 15, 37% and 39% for PT 18, 37% and 36% for RT15, and 45% and 44% for RT18. The relative errors for melting and freezing enthalpies for SP15 reached 99% due to the close to zero experimental melting and freezing enthalpies. No value was provided from the manufacturer of Tamanu oil and coconut oil for the theoretical enthalpy (J/g), and thus the relative errors could not be calculated. The relative errors calculated reflect that the experimental latent heats are in all examined cases lower than the latent heats provided by the manufacturers.



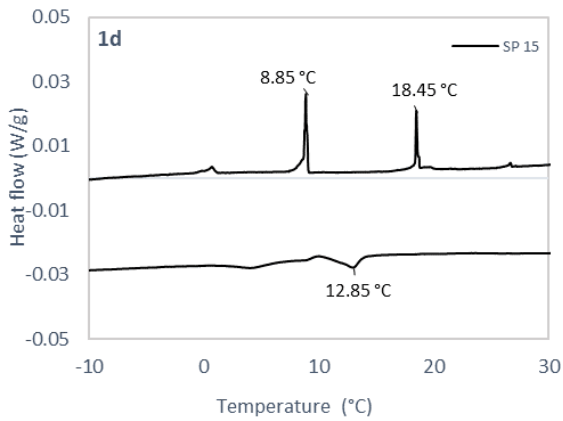


Figure 1: DSC thermogram of a) PT 15, PT 18 b) RT15, RT18, c) tamanu oil and coconut oil d) SP15 in their 1st thermal cycle.

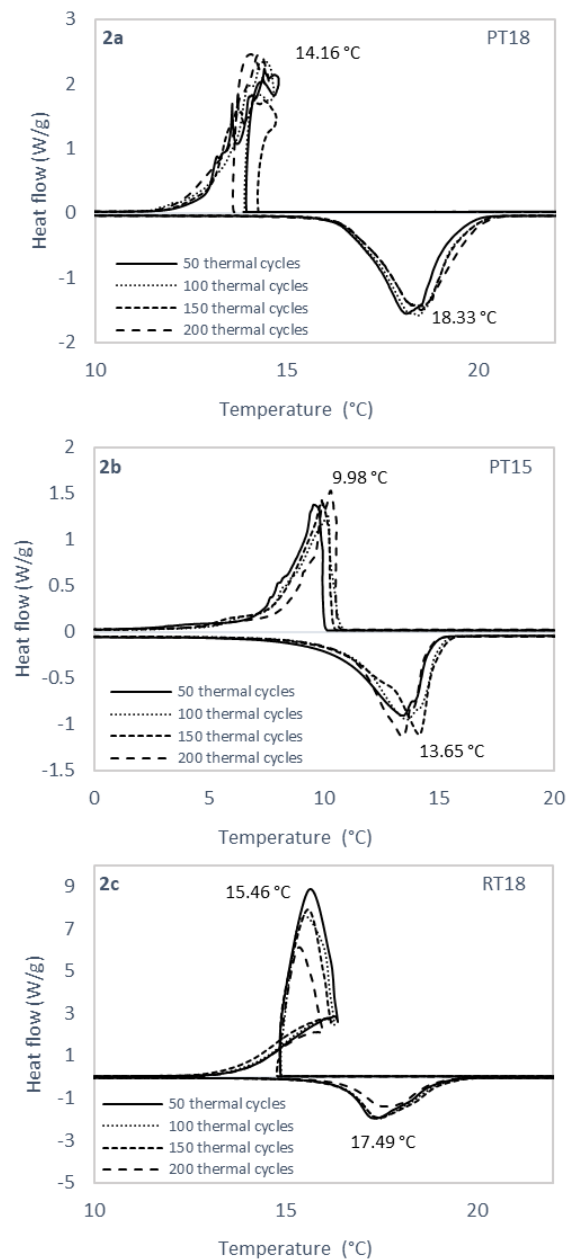
Table 3: Differential scanning calorimetry analyses for PT15, PT18, RT15, RT18, SP15, tamanu oil and coconut oil in their 1st thermal cycle.

Material	Melting Point (°C)	Latent heat (J/g)	Freezing Point (°C)	Latent heat (J/g)
PT 15	14.04	110.00	9.16	107.00
			10.65	
			10.33	
PT 18	18.14	121.50	13.92	117.20
RT15	15.69	97.38	15.13	99.12
	-0.95		-9.45	
RT18	17.62	141.80	15.17	144.00
SP 15	12.85	0.19	18.85	0.13
			8.85	0.31
Coconut oil	23.05	46.94	7.47	57.19
Tamanu oil	0.59	3.98	1.64	4.89

2) Long term thermal performance of PCM

The long-term performance of five PCM samples was evaluated under 200 thermal cycles. The samples of the five selected materials were examined within a temperature range of -30 to 80°C with a scanning rate of 1.5°C / min in a dynamic mode. Figure 2 illustrates the DSC thermogram of the five PCM, which underwent manual thermal cycling for 200 thermal cycles. The obtained data using DSC technique is shown in Table 4. The result indicates a nearly constant latent heat (J/g) throughout the heating and cooling cycles for all the examined materials. The thermal properties indicated by the long term thermal performance DSC analysis (Table 4) are in line with the first thermal cycle's DSC analysis results (Table 3). The experimental results for the melting and freezing points of the organic non-paraffins PT18 (Figure 2a), PT15 (Figure 2b) are outside the temperature range 15-20°C. According to this analysis, it is evident that RT18 is a suitable PCM candidate for a thermal energy storage application that operates in a temperature range within 15-20°C. RT18 (Figure 2c) in all data sets for 50, 100, 150, and 200 thermal cycles performs stably in terms of variation in melting/freezing temperature (°C) and enthalpies (J/g).

More specifically, the melting temperature of RT18 varies between 17.33 to 17.72 °C, and the melting enthalpy varies between 101.7 to 154.5 J/g. Correspondingly the freezing temperature for RT18 varies within 15.3-15.61 °C and the freezing enthalpy 101.7-155.1 J/g. However the melting and freezing latent heat of RT18 for the 200 thermal cycles has been decreased by 33% compared to the 50,100 and 150 thermal cycles. In the cases of PT15, PT18 and RT18, the supercooling effect is detected: the PCM solidifies at a lower temperature. In the melting and freezing curves of RT15 (Figure 2d), two peaks for the phase change temperature are observed for the 50,100, and 150 thermal cycles and three peaks for the 200 thermal cycles. The melting and freezing temperatures for tamanu oil (Figure 2e) are out of the range 15-20°C. The thermal cycling of the pure materials was conducted a period equivalent to 6 months, and this period may not be sufficient for the evaluation of the long term thermal performance.



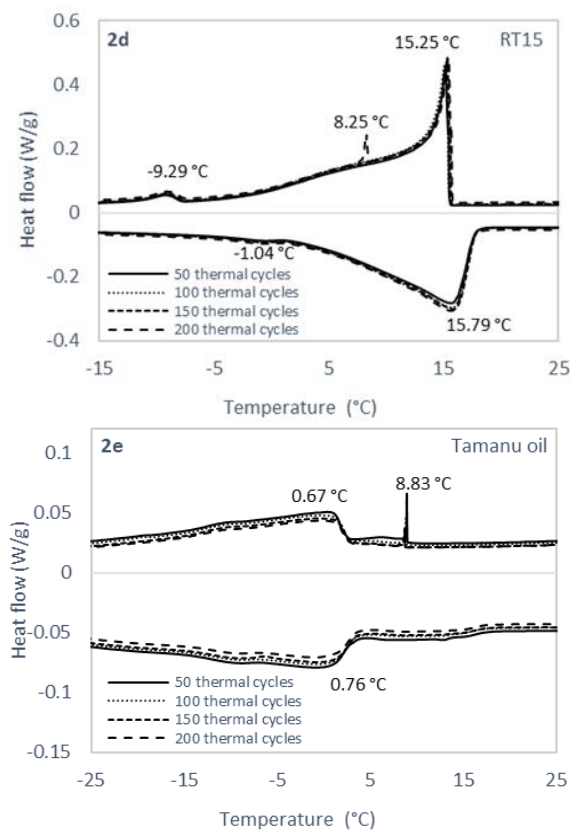


Figure 2: DSC thermogram of a) PT 15 b) PT 18 c) RT15, d) RT18, e) tamanu oil in 50, 100, 150 and 200 thermal cycles.

Table 4: Differential scanning calorimetry analyses for PT15, PT18, RT15, RT18 and tamanu oil in 50, 100, 150 and 200 thermal cycles.

Material	Melting point (°C)	Latent heat (J/g)	Freezing point(°C)	Latent heat (J/g)
50 thermal cycles				
PT 18	18.12	121.80	14.42	117.5
PT 15	13.42	105.50	9.54	105.30
RT18	17.33	144.80	15.61	144.30
RT15	15.76	94.27	15.15	93.14
	-1.00		-9.32	
T.oil	0.67	3.06	0.79	4.65
			8.93	
100 thermal cycles				
PT 18	18.40	129.90	14.41	126.60
PT 15	13.61	103.10	10.15	102.90
RT18	17.44	146.10	15.37	148.30
RT15	15.72	99.15	15.11	98.13
	-0.98		-9.49	
T.oil	0.84	3.49	0.64	4.64
			8.86	
150 thermal cycles				
PT 18	18.30	122.50	13.73	118.40
PT 15	14.15	109.90	9.93	104.9
RT18	17.46	154.50	15.57	155.10

RT15	15.96	98.44	15.32	96.58
	-1.00		-9.20	
T.oil	0.58	3.74	0.70	4.39
			8.69	
200 thermal cycles				
PT 18	18.50	125.00	14.08	120.70
PT 15	13.40	103.40	10.29	101.70
RT18	17.72	101.70	15.30	104.80
RT15	15.71	98.49	15.40	98.30
			8.25	
	-1.18		-9.16	
T.oil	0.96	3.35	0.54	4.71

B. PCM water emulsions and PCM polymers

The results presented in this section are focused on the two organic paraffins water emulsions in a 5:1 ratio with the addition of a 5% v/v Tween 80 in the final solution. Thermal properties of PCM water emulsions measured with DSC technique in a temperature range 5-80°C with a scanning rate of 10°C/min. The paraffins-water emulsions were prepared by mixing water and the PCM (RT15 and RT18) in a ratio of 1:5 followed by addition of 5%v/v of tween 80 in the final solution. The water, paraffins, and tween were then mixed with a T25 digital ULTRA-TURRAX disperser [18] for homogenizing the mixture. The charging and discharging characteristics of the organic paraffins - water emulsions are presented in Figure 3. From Table 5 we can observe that the water emulsion of RT18 can be used for a thermal energy storage application that operates in a temperature range within 15-20°C. The latent heat for this emulsion is around 180 KJ/kg, but the performance of the emulsion is not evaluated under repeated thermal cycles. For this reason, it can not be concluded whether this PCM-water emulsion is suitable for an industrial application. In the case of RT15 - water emulsion, it is evident that there are two peaks for both the melting curve and three peaks in the solidification curve, see Figure 3. The multiple peaks in both the exothermic and endothermic curves of RT15-water emulsion indicate the polymorphic structure of the PCM. In both RT15 and RT18 water emulsions, the solidification is observed at a lower temperature than the melting temperature of the PCM. It is suggested that the materials performance should be further evaluated since the water PCM emulsion may have undergone phase separation.

The combinations for the formation of PCM polymers with the two organic paraffins RT15 and RT18 are illustrated in Figure 4a and Figure 4b. Figure 4a shows the melting curves for the first polymer solutions with PEGda and BPO. The solid liquid crosslinked polymer RT15-PEGda-BPO stores heat at the favorable temperature range and, at the same time, maintains its solid structure. In the case of RT18-PEGda-BPO, the freezing curve contains three freezing points out of the range 15-20 °C. The latent heat for RT15-PEGda-BPO varies between 39-50 J/g and for RT18-PEGda-BPO between 76-63 J/g.

Table 6 depicts the melting temperatures and heat storage capacities of the examined PCM polymers. Figure 4b and Table 6 present as well the thermal properties of the PCM emulsions polymers with PVP as synthesizer and APS as

initiator. A vast difference is indicated in the melting and freezing point for both organic paraffins polymers in this combination. Another point underlined is that the latent heat in this case varies between 0-2 KJ/kg for both organic paraffins. The low latent heat is justified by the percentage of the PCM in the mixture, which is 0.5% w/v in the final polymer solution. The PCM polymers' performance for relevant LHTES applications should be further evaluated under repeated thermal cycles. The encapsulation of a PCM layer in an electrospun PCM fiber matrix followed the current experimental study.

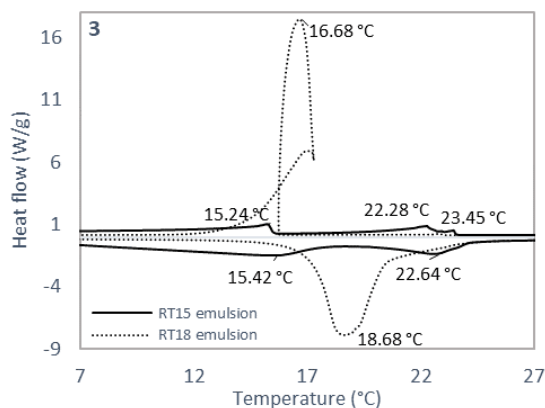


Figure 3: DSC thermogram of RT15, RT18 in water emulsions in their 1st thermal cycle.

Table 5: Differential scanning calorimetry analyses for RT15, RT18 in water emulsions in their 1st thermal cycle.

Material	Water: RT 15 (1:5)	Water: RT 18 (1:5)
Melting point (°C)	15.42	18.68
	22.64	
Latent heat (J/g)	87.70	180.70
Freezing point (°C)	15.24	16.68
	22.28	
	23.45	
Latent heat (J/g)	50.06	180.4
Mass (mg)	8.76	4.38

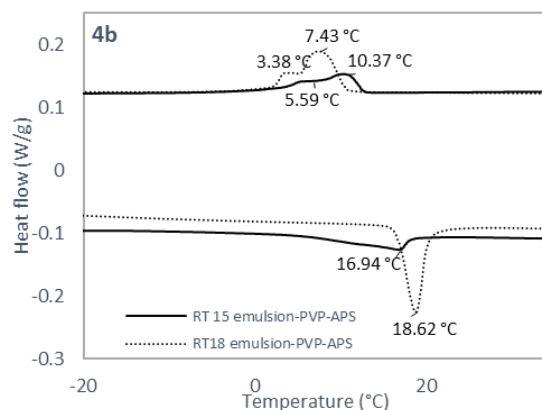
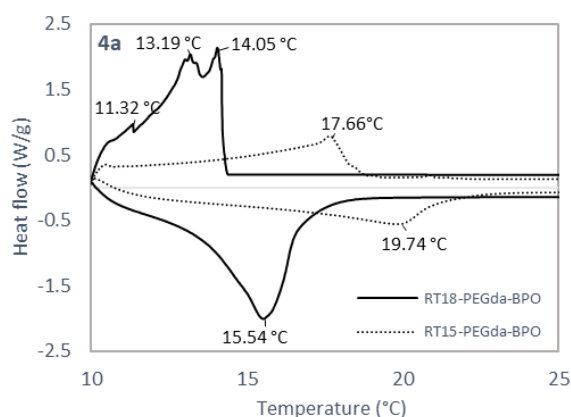


Figure 4: DSC thermogram of RT15-PEGda-BPO, RT18-PEGda-BPO, RT15 emulsion-PVP-APS, RT18 emulsion-PVP-APS in their 1st thermal cycle

Table 6: Differential scanning calorimetry analyses for RT15-PEGda-BPO, RT18-PEGda-BPO, RT15 emulsion-PVP-APS, RT18 emulsion-PVP-APS in their 1st thermal cycle.

Material	RT15-PEGda-BPO	RT18-PEGda-BPO
Melting point (°C)	19.74	15.54
Latent heat (J/g)	50.89	76.20
Freezing point (°C)	17.66	11.32
		13.19
		14.05
Latent heat (J/g)	39.58	63.87
Mass (mg)	7.28	4.00
Material	RT15 emulsion-PVP-APS	RT18 emulsion-PVP-APS
Melting point (°C)	16.94	18.62
Latent heat (J/g)	0.21	2.13
Freezing point (°C)	5.59	3.38
	10.37	7.43
Latent heat (J/g)	1.16	2.17
Mass (mg)	11.83	5.76

V. CONCLUSION

In a phase-change TES, energy is stored and released by a reversible change of state, such as a solid-liquid phase transition. The current study discusses the merits of seven PCM candidates and targets the selection of a suitable PCM for implementation in a LHTES system. It is essential to demonstrate the thermal properties of PCM under repeated thermal cycles, which represents the PCM life in technical implementation. Within the selected PCM, which were analysed with DSC technique in this study, the commercial available organic paraffin based RT18 is a suitable PCM candidate for a thermal energy storage application. RT18 operates in a temperature range within 15-20°C, and the latent heat varied between 101-155 J/g for the 200 thermal cycles. The water emulsion of RT18 proved to be suitable for a thermal energy storage application that operates in a temperature range within 15-20°C. The latent heat for this emulsion is around 180 J/g and the melting and freezing

points 18.68 and 16.68°C, respectively. It is suggested to evaluate the PCM-water emulsion under repeated thermal cycles. The solid liquid crosslinked polymer RT15, in combination with PEGDa and BPO, resulted in a melting point within the desirable temperature limit. Although the thermal properties of the selected PCM candidates are evaluated, it should be underlined that the sample sizes at the range of mg make the analysis insufficient for a large-scale application.

ACKNOWLEDGMENT

This work is part of an ongoing Ph.D. project at the department of the Built environment, Aalborg University, in collaboration with Lindab Comfort A/S. The project is financially supported by ELFORSK, a research, and development program administrated by Danish Energy.

REFERENCES

- [1] L. Yang, H. Yan, and J. C. Lam, "Thermal comfort and building energy consumption implications - A review," *Appl. Energy*, vol. 115, pp. 164–173, 2014.
- [2] D. Zhou, C. Y. Zhao, and Y. Tian, "Review on thermal energy storage with phase change materials (PCMs) in building applications," *Appl. Energy*, vol. 92, pp. 593–605, 2012.
- [3] A. De Gracia and L. F. Cabeza, "Phase change materials and thermal energy storage for buildings," *Energy Build.*, vol. 103, pp. 414–419, 2015.
- [4] A. S. Fleischer, *Thermal Energy Storage Using Phase Change Materials Fundamentals and Applications*. 2015.
- [5] C. Barreneche, A. Solé, L. Miró, I. Martorell, A. I. Fernández, and L. F. Cabeza, "Study on differential scanning calorimetry analysis with two operation modes and organic and inorganic phase change material (PCM)," *Thermochim. Acta*, vol. 553, pp. 23–26, 2013.
- [6] R. H. Müller, "Differential Thermal Analysis," *Anal. Chem.*, vol. 35, no. 4, pp. 103A-105A, 2012.
- [7] Z. Yinping, J. Yi, and J. Yi, "A simple method, the -history method, of determining the heat of fusion, specific heat and thermal conductivity of phase-change materials," *Meas. Sci. Technol.*, vol. 10, no. 3, pp. 201–205, 1999.
- [8] S. R. Sandler, W. Karo, J.-A. Bonesteel, and E. M. Pearce, "Thermogravimetric analysis," *Polym. Synth. Charact.*, vol. 1, no. 906, pp. 108–119, 2007.
- [9] A. Maccarini, *Aalborg Universitet A two-pipe system for simultaneous heating and cooling of office buildings Maccarini , Alessandro*. 2017.
- [10] A. Maccarini, G. Hultmark, N. C. Bergsøe, and A. Afshari, "Free cooling potential of a PCM-based heat exchanger coupled with a novel HVAC system for simultaneous heating and cooling of buildings," *Sustain. Cities Soc.*, vol. 42, no. June 2017, pp. 384–395, 2018.
- [11] E. Paroutoglou, A. Afshari, N. C. Bergsøe, P. Fojan, and G. Hultmark, "A PCM based cooling system for office buildings: a state of the art review," *E3S Web Conf.*, vol. 111, no. 201 9, p. 01026, 2019.
- [12] W. Youssef, Y. T. Ge, and S. A. Tassou, "CFD modelling development and experimental validation of a phase change material (PCM) heat exchanger with spiral-wired tubes," *Energy Convers. Manag.*, vol. 157, no. October 2017, pp. 498–510, 2018.
- [13] H. Akeiber *et al.*, "A review on phase change material (PCM) for sustainable passive cooling in building envelopes," *Renew. Sustain. Energy Rev.*, vol. 60, pp. 1470–1497, 2016.
- [14] R. Rawls, *Physical chemistry*, vol. 58, no. 22. 1980.
- [15] C. Schick, "Differential scanning calorimetry (DSC) of semicrystalline polymers," *Anal. Bioanal. Chem.*, vol. 395, no. 6, pp. 1589–1611, 2009.
- [16] X. Sun, K. O. Lee, M. A. Medina, Y. Chu, and C. Li, "Melting temperature and enthalpy variations of phase change materials (PCMs): a differential scanning calorimetry (DSC) analysis," *Phase Transitions*, vol. 91, no. 6, pp. 667–680, 2018.
- [17] R. A. Fox, R. G. D. Steel, and J. H. Torrie, "Principles and Procedures of Statistics with Special Reference to the Biological Sciences.," *Inc. Stat.*, 1961.
- [18] IKA-Werke GmbH & Co. KG, "Dispersers Dispersers | From Invention to Innovation," 2013.

Chapter 8

Paper III

Thermal analysis of organic and nanoencapsulated electrospun phase change materials

Evdoxia Paroutoglou, Peter Fojan, Leonid Gurevich, Göran Hultmark and Alireza Afshari

The paper has been published in *Energies* Vol. 14, 995, 2021.

Article

Thermal Analysis of Organic and Nanoencapsulated Electrospun Phase Change Materials

Evdoxia Paroutoglou ^{1,*} , Peter Fojan ² , Leonid Gurevich ², Göran Hultmark ¹ and Alireza Afshari ¹

¹ Department of the Built Environment, Division of Sustainability, Energy and Indoor Environment, Aalborg University, 2450 København SV, Denmark; ngh@build.aau.dk (G.H.); aaf@build.aau.dk (A.A.)

² Department of Materials and Production, Aalborg University, 9220 Aalborg Ø, Denmark; fp@mp.aau.dk (P.F.); lg@mp.aau.dk (L.G.)

* Correspondence: EVP@build.aau.dk; Tel.: +45-50210217

Abstract: Latent heat stored in phase change materials (PCM) can greatly improve energy efficiency in indoor heating/cooling applications. This study presents the materials and methods for the formation and characterization of a PCM layer for a latent heat thermal energy storage (LHTES) application. Four commercially available PCMs comprising the classes of organic paraffins and organic non-paraffins were selected for thermal storage application. Pure organic PCM and PCM in water emulsions were experimentally investigated. PCM electrospun microfibers were produced by a co-axial electrospinning technique, where solutions of Polycaprolactone (PCL) 9% *w/v* and 12% *w/v* in dichloromethane (DCM) were used as the fiber shell materials. PCM emulsified with sodium dodecyl sulfate (SDS), and Polyvinylalcohol 10% *w/v* (PVA) constituted the core of the fibers. The thermal behavior of the PCM, PCM emulsions, and PCM electrospun fibers were analyzed with differential scanning calorimetry (DSC). A commercial organic paraffin with a phase change temperature of 18 °C (RT 18) in its pure and emulsified forms was found to be a suitable PCM candidate for LHTES. The PVA-PCM electrospun fiber matrix of the organic paraffin RT18 with a PCL concentration of 12% *w/v* showed the most promising results leading to an encapsulation efficiency of 67%.

Keywords: LHTES; PCM; electrospun fiber matrix; DSC



Citation: Paroutoglou, E.; Fojan, P.; Gurevich, L.; Hultmark, G.; Afshari, A. Thermal Analysis of Organic and Nanoencapsulated Electrospun Phase Change Materials. *Energies* **2021**, *14*, 995. <https://doi.org/10.3390/en14040995>

Academic Editor: Fabrizio Ascione

Received: 7 January 2021

Accepted: 10 February 2021

Published: 14 February 2021

Publisher's Note: MDPI stays neutral with regard to jurisdictional claims in published maps and institutional affiliations.



Copyright: © 2021 by the authors. Licensee MDPI, Basel, Switzerland. This article is an open access article distributed under the terms and conditions of the Creative Commons Attribution (CC BY) license (<https://creativecommons.org/licenses/by/4.0/>).

1. Introduction

The growing energy crisis during the 1970s has led to an increased interest in renewable energy storage technologies. The latent heat storage materials (PCM) are used in various applications such as building applications [1], optical nanophotonic devices [2], phase change memory cells [3], spacecraft design, energy-absorbing clothing, food industry, and pharmaceutical applications [4]. LHTES with PCM is a technology implemented for indoor cooling applications to achieve a reduction in energy use and provide a satisfactory thermal comfort level. Sensible heat and latent heat constitute the total heat stored in a PCM. Sensible heat is related to the initial change in temperature, and latent heat is the heat stored throughout the phase change.

According to their initial and final phase, the PCMs are found in four categories: solid-solid, liquid-gas, solid-gas, and solid-liquid [5]. Solid-liquid PCMs [6] are particularly attractive as their significant heat storage capacity is accompanied by a small volume change (<10%) [7], and the temperature variation throughout each phase is small. A PCM remains in solid form until it absorbs a sufficient amount of heat to reach the melting point and becomes liquid. A reverse process occurs when a PCM in the liquid state is exposed to a temperature lower than the melting temperature.

Barrett K Green was the first researcher who attempted PCM encapsulation in the 1940s and 1950s [8]. Encapsulation facilitates the maintenance of shape in solid-liquid PCM, and at the same time, prevents the PCM from reacting with the surrounding fluids. The

PCM encapsulation can help overcome phase segregation, low thermal conductivity, and volume expansions [9]. Electrospinning or electro-hydrodynamic processing is a low-cost method for the fabrication of ultrafine fibers in the range of micrometers to nanometers by drawing them from a liquid droplet of a polymeric solution or melt using high voltage [9]. The strong electric field produces charged threads of fibers. The significant parameters in the electrospinning process are the flow rate of the feeding solutions, the applied voltage, the collector distance, the capillary tube diameters, the viscosity, and the conductivity emitter of the feeding solutions [4]. Polymers are supporting materials for the encapsulation of the PCM through electrospinning. Numerous studies [5–7,10] demonstrate that the PCM incorporation in polymer matrices is an effective conjugate electrospinning method. An emulsion electrospinning technique was employed by Chalco-Sandoval et al. [11], and the proposed method is investigated in the current study.

The objective of the current work is the experimental evaluation of the thermal properties of commercially available PCMs and their potential use as novel electrospun energy storage materials, able to enhance the thermal storage capacity of LHTES systems [12]. PCMs with a phase change temperature range of 15 to 20 °C are suitable for moderate climate locations, e.g., Denmark, and are explored in the present study.

2. Materials and Methods

2.1. Phase Change Materials

Chemical and physical stability of organic PCMs makes them suitable for LHTES applications. Commercial PCMs for application in the temperature range 15–20 °C have been recently reviewed [13]. In the current study, four commercially available materials and their mixtures are investigated. The examined PCMs belong to the classes of organic paraffins and non-paraffins. Organic paraffins are widely used in LHTES applications at room temperature due to their high latent heat capacity, chemical and physical stability, reliability, and low cost [6]. However, organic paraffins are petroleum-based and not environmentally friendly. On the contrary, organic non-paraffinic PCMs are bio-based and have been recently evaluated for thermal energy storage (TES) applications. Technical grade paraffins RT15 and RT18, Rubitherm Technologies GmbH [14] and organic non-paraffins PT15 and PT18, Pure Temp LLC [15] with phase change temperatures of 15 and 18 °C, as indicated by the names, were selected for this study. RT 15 and RT18 are non-toxic, easy to handle technical grade paraffins that possess high latent heat capacity at constant temperatures [14]. Biodegradable organic non-paraffins PT15 and PT18 are produced by natural sources without the addition of chemical substances [15]. Table 1 shows the thermal properties of the four PCMs as provided by the manufacturers. The four organic PCMs were experimentally studied in their pure form, in water emulsions, and encapsulated in electrospun fiber matrices.

Table 1. Thermal properties of PCM candidates as provided by manufacturers.

Classification	Material	Phase Change Temperature (°C)	Latent Heat (J/g)
Organic non-paraffins	PT 15 15	15	182
	PT 18 15	18	192
Organic paraffins	RT 15 14	10–17	155
	RT 18 14	17–19	260

Furthermore, the long-term performance of the pure materials was evaluated by Differential Scanning Calorimetry (DSC) during 200 thermal cycles, which is equivalent to six months of real-time usage. The thermal performance of pure PCM for both 50, 100, 150, and 200 thermal cycles was evaluated with DSC. In their emulsion form, the organic PCM were mixed with water in ratios between 1:1 and 5:1. Two emulsifiers: Polyethylene glycol sorbitan (Tween 20) and Polyoxyethylensorbitan oleate (Tween 80), were added to a PCM-water mixture as stabilizers of PCM-in-water emulsions. The formation of PCM-in-water

emulsions were observed, and no phase separation was detected. The emulsion images were analyzed with ImageJ software [16].

2.2. PCM Electrospun Fiber Matrix

According to the literature, the most common encapsulation techniques are spherical encapsulation and encapsulation in fiber matrices [17–19]. The innovative encapsulation of PCM in the core of electrospun fibers is achieved through co-axial electrospinning. In co-axial electrospinning or two-fluid electrospinning, two different materials are electrospun simultaneously to form core-shell fibers. The co-axial electrospinning setup consists of two capillary tubes, two syringes connected to the tubes, an inner and an outer needle for the core and shell materials, respectively, a grounded collector, and a high voltage source, as shown in Figure 1. The electrostatic field forces convert the droplets of the feeding materials into charged threads of fibers. The electrospun PCM fiber matrix is an efficient encapsulation technique since no further encapsulation is needed. The high surface to volume ratio of the electrospun PCM fiber leads to an increase in the thermal conductivity.

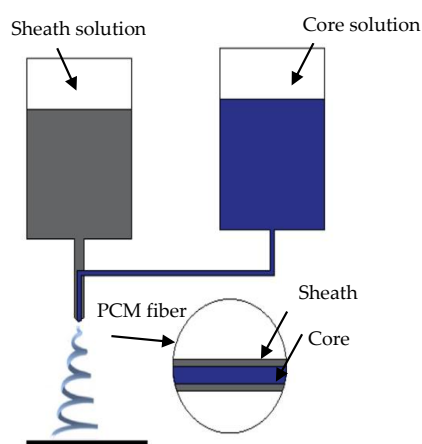


Figure 1. Co-axial electrospinning set up.

Organic paraffins can be efficiently encapsulated using co-axial electrospinning with a solution of polycaprolactone (PCL) [10] in a hydrophobic solvent. Two different solutions with the concentration of PCL in dichloromethane (DCM) of 9% *w/v* and 12% *w/v* were used for the fiber shell. The fiber core contained a PCM-PVA emulsion. PVA is a water-soluble, non-toxic polymer extensively used in electrospinning applications. The PVA emulsion was prepared by dissolving 10% *w/v* of PVA in distilled water and heating up to 100 °C with continuous stirring until fully dissolved [20]. An 80% *v/v* PCM emulsion in water was prepared with 8.4 mmol/L SDS added as a surfactant. The resulting PCM emulsion was homogenized with a T25 digital ULTRA-TURRAX disperser and then mixed with the PVA emulsion in a 1:1 ratio. A non-ionic surfactant Triton X at 0.07% was added to improve the emulsion's spinnability. The core and shell solutions were filled into two plastic 10 mL syringes connected to the capillary tubes.

The obtained PCM emulsion was co-axially electrospun with 9% *w/v* and 12% *w/v* PCL solutions using the setup described above. The voltage threshold for the electrospinning process varied between 10 to 15 kV. Voltages below 10 kV were not sufficient to overcome the surface tension to form a stable Taylor cone. Conversely, voltages higher than 15 kV led to larger fiber diameters, and the PCM was not properly encapsulated. The distance between the needle and the grounded collector plate was 18 cm. The inner diameter of the outer needle was 20 G, and the diameter of the inner needle was 10 G. Three different combinations of shell solution concentrations (% *w/v*) and flow rates of core and shell solutions were studied, as shown in Table 2.

The encapsulation ratio and the encapsulation efficiencies were calculated for the electrospun fiber matrices according to Equations (1) and (2), [21].

$$n = \frac{L_{m,encap,PCM}}{L_{m,PCM}}, n = \text{encapsulation ratio} \quad (1)$$

$$\varepsilon = \frac{L_{m,encap,PCM} + L_{s,encap,PCM}}{L_{m,PCM} + L_{s,PCM}}, \varepsilon = \text{encapsulation efficiency} \quad (2)$$

Thermal properties and morphology of the produced electrospun fiber matrices were characterized with Differential scanning calorimetry (DSC Q2000, TA Instruments, New Castle, DE, USA), scanning electron (Zeiss XB1540), and optical microscopy (Zeiss Axioskop 2 Plus). The images were processed with ImageJ software [16].

Table 2. Cases examined for the construction of PCM electrospun fiber matrices.

Cases	Sheath Solution Concentration (% w/v)	Flow Rate (mL/h) Sheath Solution	Flow Rate (mL/h) Core Solution
1st	9%	0.6	0.3
2nd	9%	0.5	0.5
3rd	12%	0.5	0.5

3. Results

3.1. Experimental Identification of Pure PCM

The long-term performance of technical grade paraffinic and non-paraffinic PCMs was evaluated with 50, 100, 150 and 200 thermal cycles [22]. The samples were manually cycled for up to 200 cycles in a temperature range of -30 to $+80$ °C with a scanning rate of 1.5 °C/min in a dynamic mode. The mass of each sample was ca. 6 mg. Figure 2 shows the obtained melting/solidification temperatures and enthalpies.

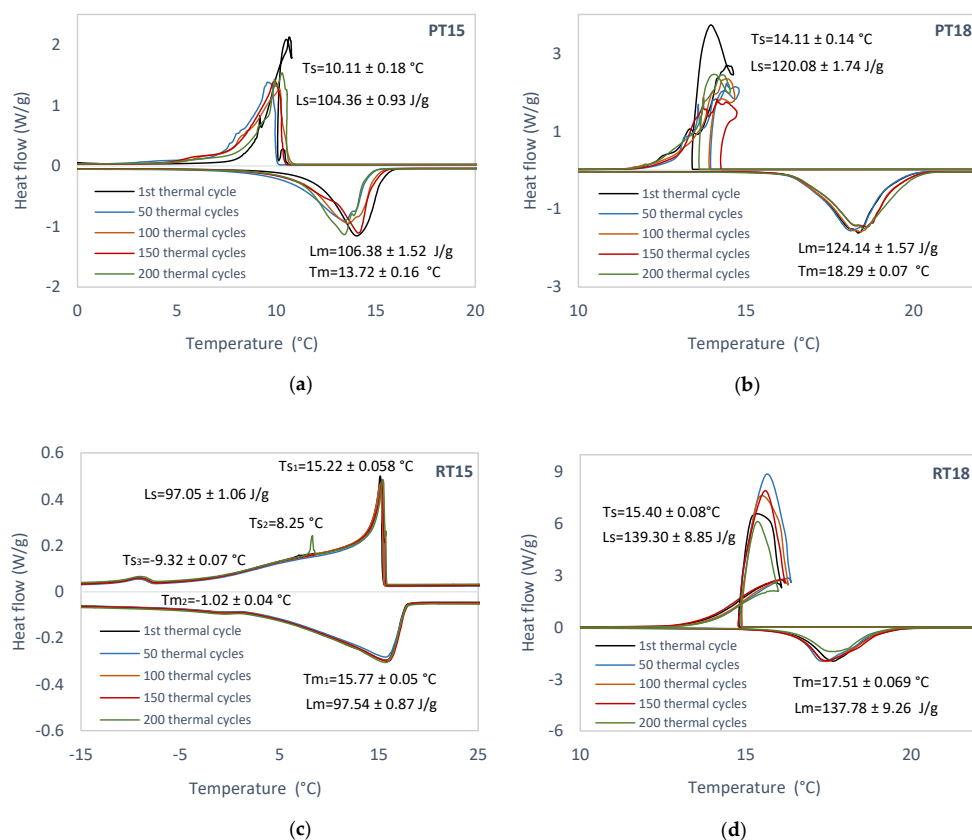


Figure 2. DSC thermogram of (a) PT15, (b) PT18, (c) RT15, (d) RT18 in 1st, 50, 100, 150, 200 thermal cycles. Obtained melting/solidification temperatures and enthalpies are shown.

3.2. Experimental Characterization of PCM Emulsions

Stable oil in water emulsions with 1:1 to 5:1 ratios were formed with Tween 20 and Tween 80 as emulsifiers. The emulsions were formed with an Ultraturrax at 16,000 rpm. The mass of the samples varied between 4 to 8 mg. The expanded uncertainty for each experimental measurement was $\pm 0.1\%$. Figure 3 illustrates the DSC thermograms of the two organic non-paraffins and the two organic paraffins prepared as water emulsions. Moreover, the optical microscopy images and the average emulsion sizes of the four PCM-in-water emulsions are presented in Figure 4 and Table 3, respectively.

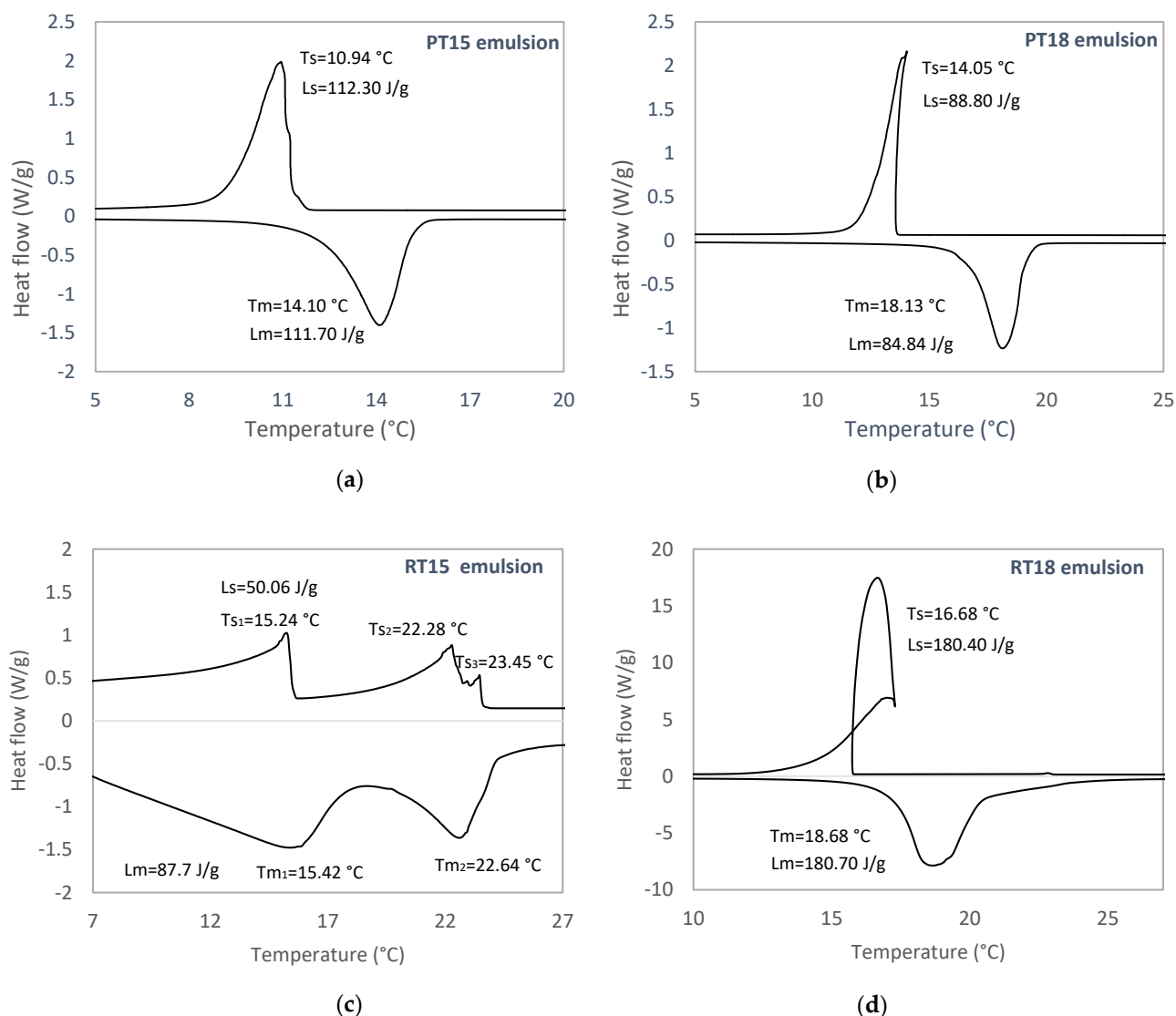
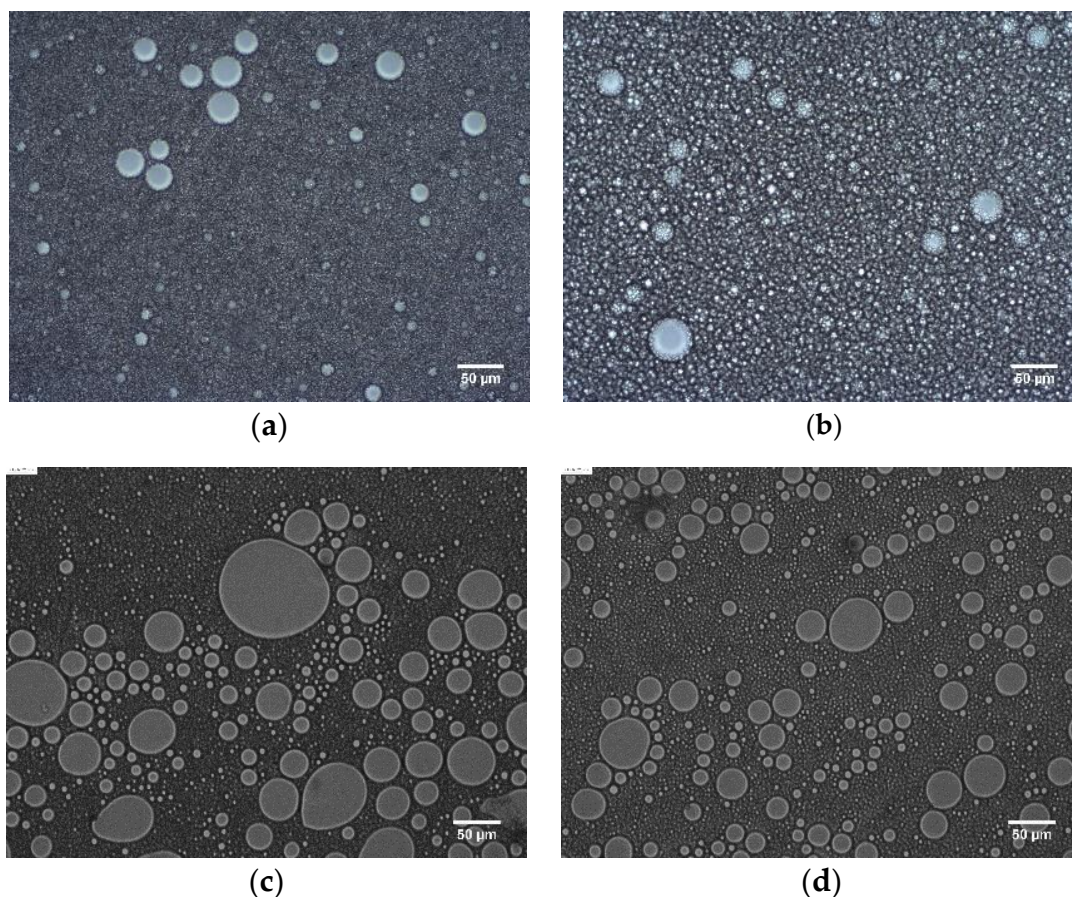


Figure 3. DSC thermogram of (a) PT15 (b) PT18 (c) RT15, (d) RT18 in water emulsions in their 1st thermal cycle. Obtained melting/solidification temperatures and enthalpies are shown.

Table 3. Average droplet size for PT15, PT18, RT15, and RT18 water emulsions.

Emulsions	PT15	PT18	RT15	RT18
Average emulsion size (um)	5.23 ± 0.20	11.00 ± 0.42	8.95 ± 1.33	6.61 ± 0.46

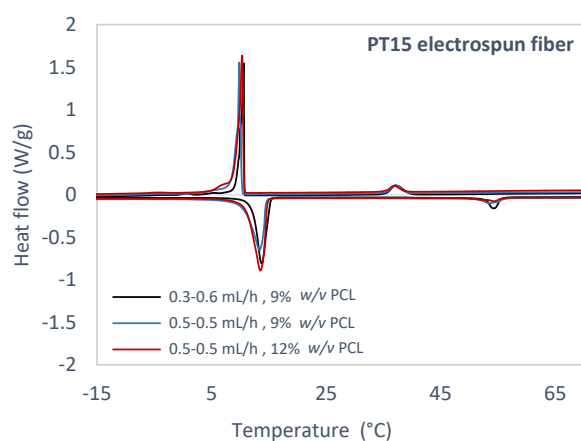
**Figure 4.** Optical microscopy images of (a) PT15, (b) PT18, (c) RT15 and (d) RT18 emulsions.

3.3. Experimental Study of PCM Electrospun Fiber Matrix

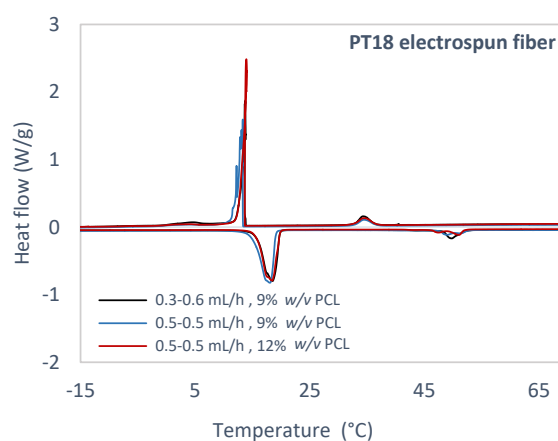
Four PCMs selected for the study were encapsulated as PVA emulsions forming the core of the PCM electrospun fiber matrix, which was encapsulated in a PCL shell. The samples of the electrospun PCM fibers were tested in the temperature range of -30 to 80 °C with a scanning rate of 1.5 °C/min in dynamic mode. The mass of each sample was about 3 mg. The expanded uncertainty for each experimental measurement was $\pm 0.1\%$. Figure 5 and Table 4 show the DSC thermographs and analysis results for electrospun PCM fibers of PT15, PT18, RT15, and RT18 in the 1st thermal cycle. Figures 6–8 depict the morphology of the PCM electrospun fiber matrices. The fiber shell was formed with either 9% w/v or 12% w/v PCL. The encapsulation ratio n is shown in Table 5.

Table 4. DSC results for electrospun PCM fibers of PT15, PT18, RT15, and RT18 in the 1st thermal cycle.

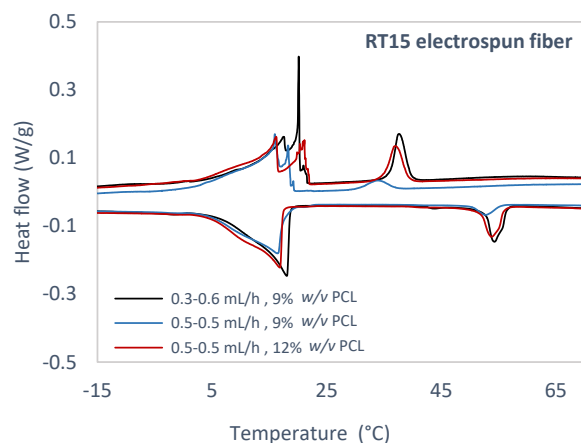
PCM	Case	Melting Temperature (°C)		Enthalpy (J/g)		Solidification Temperature (°C)		Enthalpy (J/g)	
		PCM	PCL	PCM	PCL	PCM		PCM	PCL
						Max Peak	Min Peak		
PT15	1st	13.79	54.32	64.32	10.32	10.67		37.14	55.85
	2nd	13.42	53.42	64.42	6.90	9.83		37.06	61.68
	3rd	13.52	54.38	84.71	4.50	10.36		36.82	81.37
PT18	1st	18.53	49.80	82.41	11.54	13.74		34.29	54.55
	2nd	18.08	49.00	85.30	8.08	13.31		34.47	66.49
	3rd	18.46	51.06	82.24	8.48	13.93		34.47	74.64
RT15	1st	18.04	54.32	49.75	11.40	20.11	17.45	37.62	44.79
	2nd	16.43	52.73	40.08	3.72	15.95	18.25	34	44.21
	3rd	16.82	53.81	47.11	10.68	16.18	21.29	36.95	42.34
RT18	1st	17.19	55.20	80.26	12.07	14.85		37.88	56.24
	2nd	17.40	53.99	109.00	5.67	14.57		37.60	88.12
	3rd	17.33	54.63	102.10	6.11	15.21		37.42	82.21



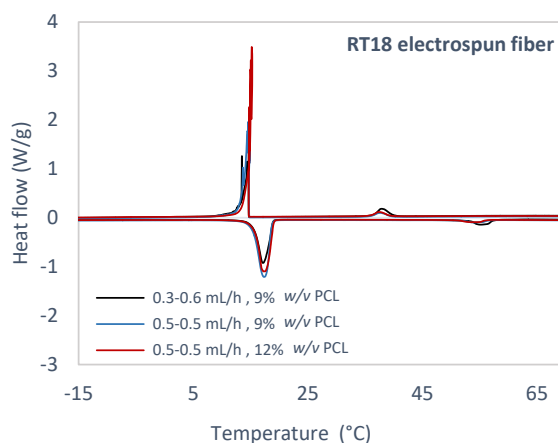
(a)



(b)



(c)



(d)

Figure 5. DSC thermogram of (a) PT15, (b) PT18, (c) RT15, and (d) RT18 in PCL shell electrospun fiber in 1st thermal cycle.

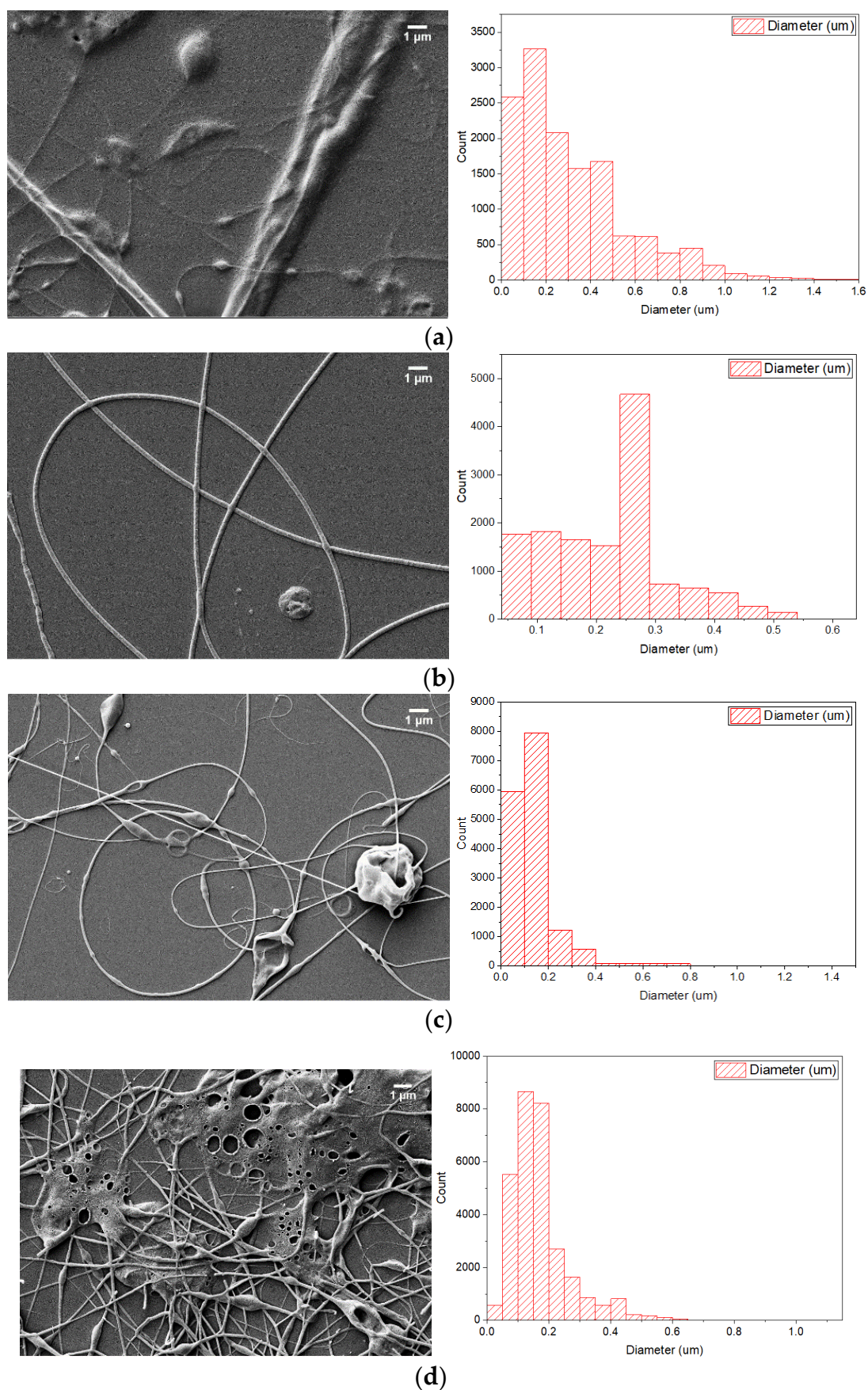


Figure 6. SEM figures of (a) PT15 9%PCL 0.3–0.6 mL/h, (b) PT18 9%PCL 0.3–0.6 mL/h, (c) RT15 9%PCL 0.3–0.6 mL/h, (d) RT18 9%PCL 0.3–0.6 mL/h.

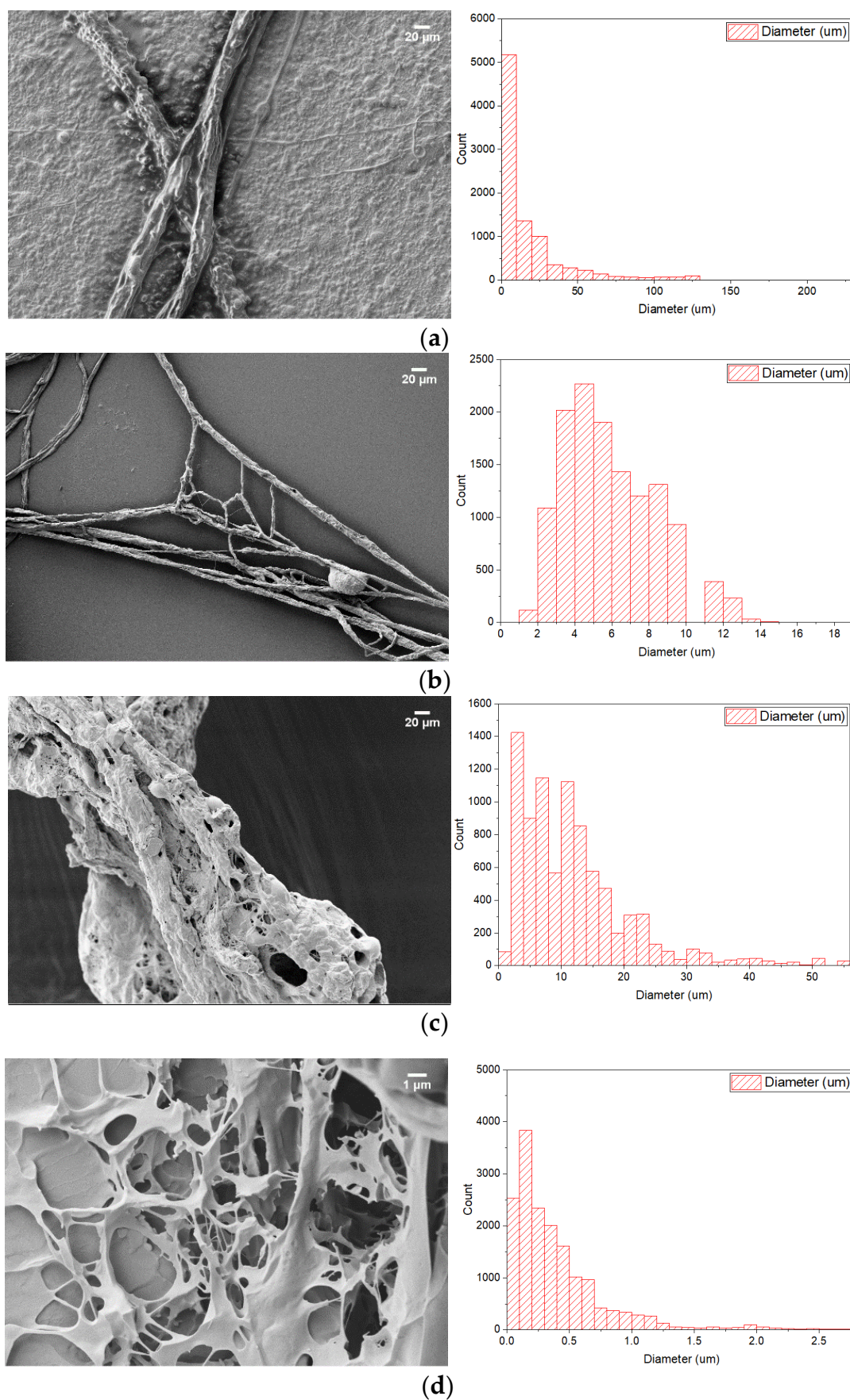


Figure 7. SEM figures of (a) PT15 9%PCL 0.5–0.5 mL/h, (b) PT18 9%PCL 0.5–0.5 mL/h, (c) RT15 9%PCL 0.5–0.5 mL/h, (d) RT18 9%PCL 0.5–0.5 mL/h.

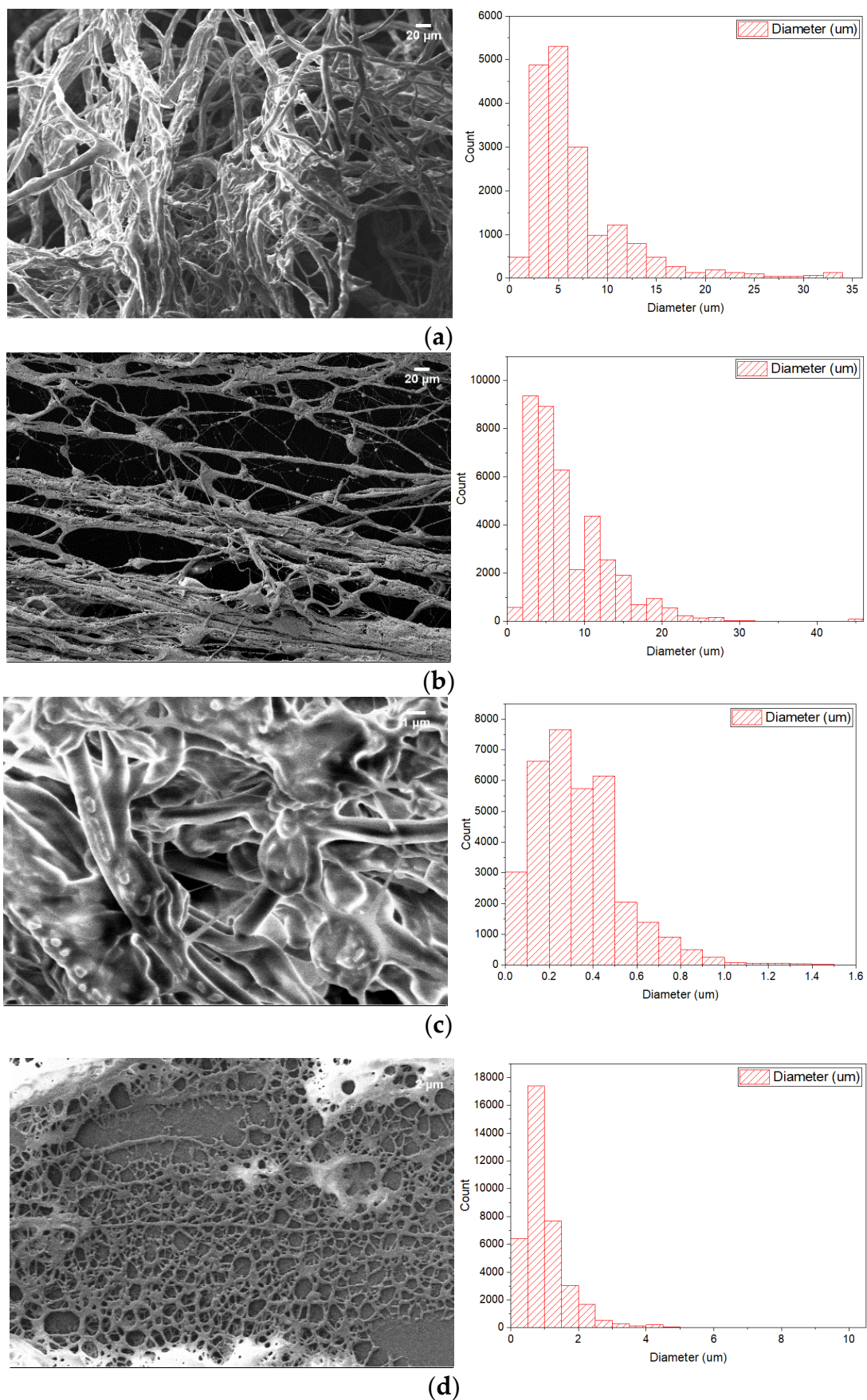


Figure 8. SEM figures of (a) PT15 12%PCL 0.5–0.5 mL/h, (b) PT18 12%PCL 0.5–0.5 mL/h, (c) RT15 12%PCL 0.5–0.5 mL/h, (d) RT18 12%PCL 0.5–0.5 mL/h.

Table 5. Encapsulation ratio, efficiency and mean diameters of encapsulated electrospun PCM.

PCM	PCL	Core Flow Rate (mL/h)	Shell Flow Rate (mL/h)	Encapsulation Ratio η (%)	Encapsulation Efficiency ε (%)	Mean Fiber Diameter (μm)	Fiber Diameter SD (μm)
PT15	9%	0.3	0.6	60.98	57.45	0.1926 ± 0.0016	0.1641
		0.5	0.5	61.08	60.29	2.2934 ± 0.0057	0.5422
	12%	0.5	0.5	80.31	79.40	4.5659 ± 0.0175	2.3694
PT18	9%	0.3	0.6	66.03	55.77	0.2314 ± 0.0008	0.0919
		0.5	0.5	68.35	72.57	5.4409 ± 0.0478	2.8615
	12%	0.5	0.5	65.90	75	5.5630 ± 0.0200	3.9536
RT15	9%	0.3	0.6	50.98	48.70	0.1176 ± 0.0003	0.0401
		0.5	0.5	41.07	43.42	8.1486 ± 0.0764	7.1189
	12%	0.5	0.5	48.28	46.08	0.2714 ± 0.0009	0.1593
RT18	9%	0.3	0.6	58.68	49.65	0.1482 ± 0.0003	0.0521
		0.5	0.5	79.69	71.71	0.2174 ± 0.0013	0.1663
	12%	0.5	0.5	74.65	67.05	0.8022 ± 0.0017	0.3261

4. Discussion

4.1. Experimental Identification of Pure PCM

Several studies [23–27] have addressed the long term stability of PCM over an extended duty cycle in real-life applications. Behzadi and Farid [23] examined commercial organic PCMs and observed a shift in the melting point from 21 to 28 °C and an increase of 36 J/g in the latent heat of fusion over thermal cycles representing 120 days. Sharma et al. [24] concluded that all of the examined organic PCM exhibited a decrease in the melting temperature after being subjected to 500 thermal cycles. Rathod and Banerjee [25] reviewed the thermal stability of PCM in LHTES applications and observed stable performance of organic paraffins under repeated thermal cycles. A. Shukla et al. [26] investigated paraffin waxes, which demonstrated stable thermal performance over 1000 thermal cycles. Hasan and Sayigh [27] examined industrial-grade organic non-paraffins and observed a 10% reduction in the heat of fusion after 450 thermal cycles.

In the current study, the scanning rate of 1.5 °C/min ensures a high resolution of the melting and freezing peaks. The melting/solidification point results acquired from the DSC analysis are highly dependent on the scanning rate and sample preparation laboratory methods. The scanning rate significantly affects the peak thermal shifts in the heating and cooling curves. Table 1 reports that the experimental latent heats in all examined cases were lower than the latent heats provided by the manufacturers. The difference between melting and solidification point arises due to the effect of sub-cooling or incongruent melting. In all cases, except for RT15, a thermal shift between the melting and solidification curve is observed. The thermal shift reaches 3.5 °C for PT15, 4.5 °C for PT18, and 2.5 °C for RT18. The DSC data in Figure 2 indicate a nearly constant latent heat (J/g) and excellent thermal stability and reliability during the thermal cycle tests for the examined materials. No significant changes were observed in the melting and crystallization temperature and enthalpies between 0 and 200 thermal cycles. The stable thermal performance of the examined PCMs is in line with the literature [23–27]. The standard error of mean analysis (Figure 2) demonstrates that the average values for the melting/solidification points and melting/solidification latent heats are in all the examined cases highly reproducible. However, it has been reported that the solidification and melting enthalpy of RT18 for the 200 thermal cycles have been decreased by 33% in comparison with the 50,100 and 150 thermal cycles [22]. The obtained melting and freezing points are 13.72 ± 0.16 °C and 10.11 ± 0.18 °C for the organic non-paraffin PT15 (Figure 2a) and 18.29 ± 0.07 °C and 14.11 ± 0.14 °C for the organic non-paraffin PT18 (Figure 2b). The

organic paraffin RT15 exhibits melting and solidification peaks lower than 15 °C (Figure 2c). The average melting and solidification points for RT18 are 17.51 ± 0.069 °C and 15.40 ± 0.08 °C (Figure 2d). Correspondingly the average latent heats of melting and solidification of RT18 are 137.78 ± 9.26 J/g and 139.30 ± 8.85 J/g. According to this analysis, since RT18 in all data sets for 50, 100, 150, and 200 thermal cycles performed stably in terms of melting/freezing temperature (°C) and enthalpies (J/g), it can be considered as a suitable PCM candidate for thermal energy storage applications in moderate climate conditions.

4.2. Experimental Identification of PCM Emulsions

PCM in water emulsions are novel heat transfer fluids characterized as thermodynamically unstable systems [28]. Zhang et al. [29] developed a water-PCM emulsion, and they concluded that the degree of supercooling increases with a decrease in the droplet size of the emulsion. The result exhibited no phase separation in the oil in water emulsions with Tween 80 as emulsifier.

The emulsions of PCM in water at different ratios were produced and analyzed using the DSC technique to identify and quantify whether the heat capacity of the final solution displays an increase or not. The experimentally found melting and solidification points of the emulsions of PT15 (Figure 3a) and PT18 (Figure 3b) were not in the temperature range 15–20 °C. In all cases, except for the RT15 emulsion (Figure 3c), a thermal hysteresis between the melting and solidification curves was observed. The hysteresis was 3 °C for PT15, 4 °C for PT18, and 2 °C for RT18. According to this analysis, RT18-in-water emulsion exhibited melting and solidification temperatures in the range of 15–20 °C and high melting and solidification enthalpies of ca. 180 J/g.

The PCM emulsion images were captured a few hours after sample preparation. Günther et al. [30] studied n-hexadecane emulsions with a size range of 0.1–20 µm. The average emulsion size given in Table 3 varied between 5 to 11 µm. The average emulsion sizes (Table 3) are over 1 µm, which characterizes them as thermodynamically unstable macro-emulsion systems. In all examined PCM emulsions, the emulsification process was conducted with the same percentage of PCM, water, emulsifier in the solution and the same energy input.

4.3. Experimental Study of PCM Electrospun Fiber Matrix

Several studies [5,6] have demonstrated successful PCM incorporation in polymer matrices by electrospinning. Perez-Masia et al. [10] encapsulated the organic paraffin dodecane in PCL through single fluid electrospinning. The results indicated that the electrospun fiber with encapsulated PCM maintained about 37% of the bulk PCM heat storage capacity. Chalco-Sandoval et al. [11] achieved an encapsulation of PCM/PVA in a PCL shell using co-axial electrospinning. The electrospun fiber matrices were formed using an electrospinning setup, and their thermal properties were analyzed with DSC and SEM.

The DSC thermographs of PT15 (Figure 5a), PT18 (Figure 5b), and RT18 (Figure 5d) fiber matrices displayed two main well-defined peaks at the PCM phase change temperature and the shell material phase change temperature. In connection with RT15 (Figure 5c), two peaks for the PCM phase change temperature and one peak for the shell material are displayed in the solidification curve. Increasing the polymer concentration from 9% w/v to 12% w/v did not significantly change the PCM electrospun fibers' thermal properties, as indicated in Table 4. The experimental results for the melting and freezing points of the electrospun PCM fiber samples of PT15 (Figure 5a), PT18 (Figure 5b), and RT15 (Figure 5c) are outside the temperature range 15–20 °C. The melting and solidification temperatures for PT15 (Figure 5a) varied between 13.4–13.8 °C and 9.8–10.7 °C. Correspondingly the melting and solidification temperatures for PT18 (Figure 5b) were 18.1–18.5 °C and 13.3–13.9 °C. Concerning RT15 (Figure 5c), the melting and solidification temperatures varied between 16.4–18 °C and 16–21.3 °C. The melting and solidification temperatures of RT18 12% w/v 0.5–0.5 mL/h (Figure 5d) were 17.3 °C and 15.2 °C, respectively. The enthalpies of melting and solidification are 102.1 J/g and 82.21 J/g. According to the thermal analyses presented

in Table 4, only the DSC analysis for RT18 12% *w/v* 0.5–0.5 mL/h (3rd case) has shown melting and solidification temperatures within the range of 15–20 °C and appears to have the optimal structure for the LHTES application.

In the examined cases where the PCL solution concentration was below 9% and above 12% *w/v*, the PCM solution's encapsulation could not be achieved. For a PCL solution concentration below 9% *w/v*, the jet broke up into droplets. The electrospun PCM fibers mean diameters in Table 5 indicate that the higher the PCL concentration in the fiber shell, the higher the fiber diameter in all cases except for RT15 in the 3rd case (shell solution concentration of 12% *w/v*). The encapsulation ratio, which varied between 41 and 80% for all fiber matrices, indicates successful encapsulation of the organic PCM compared to relevant literature [10,11]. The highest encapsulation ratios were reached for PT15 12% 0.5–0.5 mL/h, RT18 9% 0.5–0.5 mL/h and RT18 12% 0.5–0.5 mL/h.

5. Conclusions

Four commercially available PCM materials (organic paraffins RT15 and RT18, organic non-paraffins PT15 and PT18) were studied as bulk, emulsion, and encapsulated emulsions in core-shell fibers. All bulk materials demonstrated excellent thermal reliability in DSC analyses after thermal cycling. Bulk RT18 was evaluated as a suitable PCM candidate for thermal energy storage applications in moderate climate conditions. Bulk RT18 exhibited a high average enthalpy of fusion and crystallization of 137–139 J/g throughout the 200 thermal cycles. RT18-in-water emulsion showed higher enthalpies of fusion and crystallization (=180 J/g); its thermal stability should be further investigated. The commercially available organic PCM were encapsulated in the biodegradable polyester PCL and PVA using co-axial electrospinning. The PVA-PCM emulsion was encapsulated in the core of the fibers. The shell of the fibers was constructed of a PCL-DCM solution. The core/shell structure, stably produced at core/shell feed rates of 0.5 mL/h/0.5 mL/h for RT18 with PCL concentration 12% *w/v*, was promising with enthalpies of melting and solidification 102.1 J/g and 82.21 J/g. The PCL matrix encapsulated the PCM in a core to shell ratio of 1:1 and can be potentially used for thermal energy storage applications.

Author Contributions: Conceptualization, E.P. and P.F.; methodology, E.P. and A.A.; software, E.P.; validation, E.P., L.G., and P.F.; formal analysis, E.P.; investigation, E.P., P.F. and A.A.; resources, P.F.; data curation, P.F. and E.P.; writing—original draft preparation, E.P.; writing—review and editing, E.P., L.G., P.F. and A.A.; supervision, E.P., P.F., G.H. and A.A.; project administration, E.P.; funding acquisition, A.A. All authors have read and agreed to the published version of the manuscript.

Funding: The authors acknowledge the support provided by ELFORSK, a research, and development program administrated by Danish Energy.

Informed Consent Statement: Not applicable.

Data Availability Statement: The data that support the findings of this study are available from the corresponding author upon request.

Conflicts of Interest: The authors declare no conflict of interest. The funders had no role in the design of the study; in the collection, analyses, or interpretation of data; in the writing of the manuscript, or in the decision to publish the results.

Abbreviations

Symbol	Definition	Unit
(L) _{m,encap.PCM}	Latent heat of melting for encapsulated PCM	J/g
(L) _{m,PCM}	Latent heat of melting for PCM	J/g
(L) _{s,encap.PCM}	Latent heat of solidification for encapsulated PCM	J/g
(L) _{s,PCM}	Latent heat of solidification for PCM	J/g
n (%)	Encapsulation ratio	-
T _m	Melting temperature	°C
T _s	Solidification temperature	°C

v/v (%)	Volume/Volume	mL/mL
w/v (%)	Weight/Volume	g/mL
ϵ (%)	Encapsulation efficiency	-
Abbreviations		
DSC	Differential scanning calorimetry	
PCL	Polycaprolactone	
PCM	Phase change material	
SDS	Sodium dodecyl sulfate	
TES	Thermal energy storage	

References

- De Gracia, A.; Cabeza, L.F. Phase Change Materials and Thermal Energy Storage for Buildings. *Energy Build.* **2015**, *103*, 414–419. [CrossRef]
- Gerislioglu, B.; Bakan, G.; Ahuja, R.; Adam, J.; Mishra, Y.K.; Ahmadivand, A. The Role of Ge 2 Sb 2 Te 5 in Enhancing the Performance of Functional Plasmonic Devices. *Mater. Today Phys.* **2020**, *12*. [CrossRef]
- Gerislioglu, B.; Dirisaglik, F.; Jurado, Z.; Sullivan, L.; Dana, A. Extracting the Temperature Distribution on a Phase-Change Memory Cell during Crystallization. *J. Appl. Phys.* **2016**, *120*, 164504. [CrossRef]
- Fleischer, A.S. *Thermal Energy Storage Using Phase Change Materials Fundamentals and Applications*; Springer International Publishing AG: New York, NY, USA, 2015. [CrossRef]
- Košný, J. *PCM-Enhanced Building Components*; Springer International Publishing AG: New York, NY, USA, 2015. [CrossRef]
- Su, W.; Darkwa, J.; Kokogiannakis, G. Review of Solid-Liquid Phase Change Materials and Their Encapsulation Technologies. *Renew. Sustain. Energy Rev.* **2015**, *48*, 373–391. [CrossRef]
- Letcher, T.M. Storing Energy: With Special Reference to Renewable Energy Sources. *Chem. Int.* **2016**, *38*. [CrossRef]
- Salunkhe, P.B.; Shembekar, P.S. A Review on Effect of Phase Change Material Encapsulation on the Thermal Performance of a System. *Renew. Sustain. Energy Rev.* **2012**, *16*, 5603–5616. [CrossRef]
- Park, J.S. Electrospinning and Its Applications. *Adv. Nat. Sci. Nanosci. Nanotechnol.* **2010**, *1*. [CrossRef]
- Perez-Masia, R.; Lopez-Rubio, A.; Fabra, M.J.; Lagaron, J.M. Biodegradable Polyester-Based Heat Management Materials of Interest in Refrigeration and Smart Packaging Coatings. *J. Appl. Polym. Sci.* **2013**, *130*, 3251–3262. [CrossRef]
- Chalco-Sandoval, W.; Fabra, M.J.; López-Rubio, A.; Lagaron, J.M. Development of an Encapsulated Phase Change Material via Emulsion and Coaxial Electrospinning. *J. Appl. Polym. Sci.* **2016**, *133*. [CrossRef]
- Maccarini, A.; Hultmark, G.; Bergsøe, N.C.; Afshari, A. Free Cooling Potential of a PCM-Based Heat Exchanger Coupled with a Novel HVAC System for Simultaneous Heating and Cooling of Buildings. *Sustain. Cities Soc.* **2018**, *42*, 384–395. [CrossRef]
- Paroutoglou, E.; Afshari, A.; Bergsøe, N.C.; Fojan, P.; Hultmark, G. A PCM Based Cooling System for Office Buildings: A State of the Art Review. *E3S Web Conf.* **2019**, *111*, 01026. [CrossRef]
- Rubitherm Technologies GmbH. Available online: <https://www.rubitherm.eu/en/about-us.html> (accessed on 12 February 2021).
- Pure Temp LLC. Available online: <https://www.puretemp.com/> (accessed on 12 February 2021).
- ImageJ Image Processing Program. Available online: <http://imagej.nih.gov/ij/> (accessed on 12 February 2021).
- Christiansen, L.; Fojan, P. Solution Electrospinning of Particle-Polymer Composite Fibres. *Manuf. Rev.* **2016**, *3*, 21. [CrossRef]
- Chen, C.; Wang, L.; Huang, Y. A Novel Shape-Stabilized PCM: Electrospun Ultrafine Fibers Based on Lauric Acid/Polyethylene Terephthalate Composite. *Mater. Lett.* **2008**, *62*, 3515–3517. [CrossRef]
- Hu, W.; Yu, X. Encapsulation of Bio-Based PCM with Coaxial Electrospun Ultrafine Fibers. *RSC Adv.* **2012**, *2*, 5580–5584. [CrossRef]
- Zdraveva, E.; Fang, J.; Mijovic, B.; Lin, T. Electrospun Poly(Vinyl Alcohol)/Phase Change Material Fibers: Morphology, Heat Properties, and Stability. *Ind. Eng. Chem. Res.* **2015**, *54*, 8706–8712. [CrossRef]
- Liu, H.; Wang, X.; Wu, D. Innovative Design of Microencapsulated Phase Change Materials for Thermal Energy Storage and Versatile Applications: A Review. *Sustain. Energy Fuels* **2019**, *3*, 1091–1149. [CrossRef]
- Paroutoglou, E.; Fojan, P.; Hultmark, G.; Afshari, A. Investigation of Thermal Behaviour of Paraffins, Fatty Acids, Salt Hydrates and Renewable Based Oils as PCM, Proceedings of International Renewable Energy Storage Conference, Webinar, 2020. In *Atlantis Highlights in Engineering*; Atlantis Press: Paris, France, 2021; p. 7, accepted.
- Behzadi, S.; Farid, M.M. Long Term Thermal Stability of Organic PCMs. *Appl. Energy* **2014**, *122*, 11–16. [CrossRef]
- Sharma, R.K.; Ganesan, P.; Tyagi, V.V. Long-Term Thermal and Chemical Reliability Study of Different Organic Phase Change Materials for Thermal Energy Storage Applications. *J. Therm. Anal. Calorim.* **2016**, *124*, 1357–1366. [CrossRef]
- Rathod, M.K.; Banerjee, J. Thermal Stability of Phase Change Materials Used in Latent Heat Energy Storage Systems: A Review. *Renew. Sustain. Energy Rev.* **2013**, *18*, 246–258. [CrossRef]
- Shukla, A.; Buddhi, D.; Sawhney, R.L. Thermal Cycling Test of Few Selected Inorganic and Organic Phase Change Materials. *Renew. Energy* **2008**, *33*, 2606–2614. [CrossRef]
- Hasan, A.; Sayigh, A. Some Fatty Acids as PCM Energy Storage Materials. *Renew. Energy* **1994**, *4*, 69–76. [CrossRef]

-
28. Zhang, X.; Niu, J.; Wu, J.Y. Development and Characterization of Novel and Stable Silicon Nanoparticles-Embedded PCM-in-Water Emulsions for Thermal Energy Storage. *Appl. Energy* **2019**, *238*, 1407–1416. [[CrossRef](#)]
 29. Zhang, X.; Wu, J.Y.; Niu, J. PCM-in-Water Emulsion for Solar Thermal Applications: The Effects of Emulsifiers and Emulsification Conditions on Thermal Performance, Stability and Rheology Characteristics. *Sol. Energy Mater. Sol. Cells* **2016**, *147*, 211–224. [[CrossRef](#)]
 30. Günther, E.; Schmid, T.; Mehling, H.; Hiebler, S.; Huang, L. Subcooling in Hexadecane Emulsions. *Int. J. Refrig.* **2010**, *33*, 1605–1611. [[CrossRef](#)]

Chapter 9

Paper IV

Thermal properties of novel phase change materials based on tamanu and coconut oil encapsulated in electrospun fiber matrices

Evdoxia Paroutoglou, Peter Fojan, Leonid Gurevich and Alireza Afshari

The paper has been published in Sustainability Vol. 14, 7432, 2022.

Article

Thermal Properties of Novel Phase-Change Materials Based on Tamanu and Coconut Oil Encapsulated in Electrospun Fiber Matrices

Evdoxia Paroutoglou ^{1,*}, Peter Fojan ² , Leonid Gurevich ²  and Alireza Afshari ¹

¹ Department of Energy Performance, Indoor Environment and Sustainability of Buildings, Aalborg University, BUILD, 2450 København SV, Denmark; aaf@build.aau.dk

² Department of Materials and Production, Aalborg University, 9220 Aalborg Øst, Denmark; fp@mp.aau.dk (P.F.); lg@mp.aau.dk (L.G.)

* Correspondence: evp@build.aau.dk

Abstract: The accumulation of thermal energy in construction elements during daytime, and its release during a colder night period is an efficient and green way to maintain a comfortable temperature range in buildings and vehicles. One approach to achieving this goal is to store thermal energy as latent heat of the phase transition using the so-called phase-change materials (PCMs). Vegetable oils came recently into focus as cheap, widely available, and environmentally friendly PCMs. In this study, we report the thermal properties of PCMs based on tamanu and coconut oils in three configurations: pure, emulsion, and encapsulated forms. We demonstrate the encapsulation of pure coconut- and tamanu-oil emulsions, and their mixtures and mixtures with commercial PCM paraffins in fiber matrices produced by a coaxial electrospinning technique. Polycaprolactone (PCL) was used as a shell, the PCM emulsion was formed by the studied oils, and sodium dodecyl sulfate (SDS) and polyvinyl alcohol (PVA) were used as emulsifiers. The addition of commercially available paraffin RT18 into a 70/30 mixture of coconut and tamanu oil, successfully encapsulated in the core of a PCL shell, demonstrated latent heats of melting and solidification of 63.8 and 57.6 kJ/kg, respectively.

Keywords: PCM; coconut oil; tamanu oil; electrospun fiber matrix; encapsulation; DSC



Citation: Paroutoglou, E.; Fojan, P.; Gurevich, L.; Afshari, A. Thermal Properties of Novel Phase-Change Materials Based on Tamanu and Coconut Oil Encapsulated in Electrospun Fiber Matrices. *Sustainability* **2022**, *14*, 7432. <https://doi.org/10.3390/su14127432>

Academic Editor: Constantin Chaliotis

Received: 9 May 2022

Accepted: 16 June 2022

Published: 17 June 2022

Publisher's Note: MDPI stays neutral with regard to jurisdictional claims in published maps and institutional affiliations.



Copyright: © 2022 by the authors. Licensee MDPI, Basel, Switzerland. This article is an open access article distributed under the terms and conditions of the Creative Commons Attribution (CC BY) license (<https://creativecommons.org/licenses/by/4.0/>).

1. Introduction

According to the International Energy Agency [1], energy consumption in the building sector reached 36% of the total global energy use in 2018. In recent years, energy-saving technologies such as thermal energy storage (TES) systems have come into focus. TES systems are classified as sensible heat storage (SHS), latent heat storage (LHS), and thermochemical heat storage (THS) [2]. Latent heat thermal energy storage (LHTES) with phase-change materials (PCM) is currently a preferred energy storage solution due to the increasing cost of energy resources [3]. In LHTES systems, energy is absorbed as latent heat of the phase transition, and then stored and dissipated into the environment. Novel heat exchangers employing encapsulated PCMs can minimize energy use compared to traditional TES solutions [4]. The main challenge in TES technology is selecting a suitable PCM on the basis of its parameters, e.g., density, thermal conductivity, supercooling degree, phase change temperature, and heat of fusion [5]. PCM might rely on solid–solid, solid–liquid, and liquid–gas transitions. The classification of solid–liquid PCMs is presented in Figure 1.

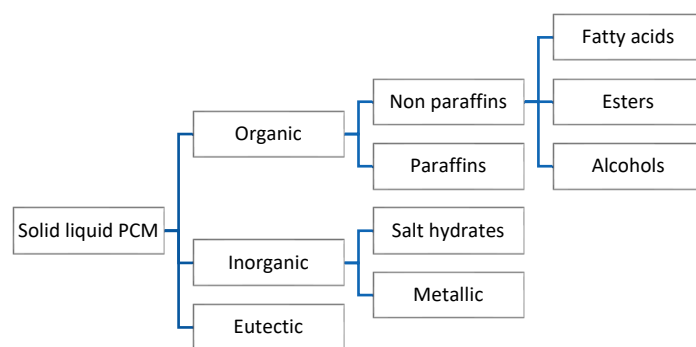


Figure 1. Classification of solid–liquid PCMs [6].

Organic fatty acids are abundant, sustainable, nontoxic, chemically and physically stable PCMs with relatively low cost that exhibit lower melting points than those of organic paraffins [7]. However, ingenious strategies, e.g., additives and flame retardant elements, are applied to eliminate the moderate–high flammability of organic paraffins and fatty acids [8]. Vegetable oils have recently been investigated as a replacement for traditional PCMs, such as organic paraffins and inorganic salt hydrates. Eutectic binary mixtures of fatty acids are suitable for thermal comfort applications due to possibility to adjust the melting temperature to the desired range. Arsana et al. [9] studied corn oil as a PCM applied to the walls of cooling equipment for food storage, and they achieved an energy reduction of 4% and a coefficient of performance (COP) increase of 6%. Rasta et al. [10] investigated a water-based PCM solution with the addition of soya oil ester for low-temperature TES applications. With the addition of 12.5% soya oil ester in tap water, the freezing point was decreased to $-6\text{ }^{\circ}\text{C}$, and the supercooling degree was reduced by 1 K [10]. Djuanda et al. [11] examined virgin coconut oil (VCO) with the addition of 20% soybean oil for TES applications, and a latent heat of fusion of 94.31 kJ/kg was obtained. The addition of 5% to 10% of vegetable oil esters in water with soya oil/corn oil mixtures for cold thermal energy storage (CTES) applications resulted in melting latent heat in the range of $171.72\text{--}230.68\text{ J/g}$ [12]. Kahwaji et al. [13] investigated the thermal properties of edible oils margarine and shortening, refined coconut oil, and virgin coconut oil as PCMs for a TES application. Coconut oil exhibited thermally stable performance with a latent heat of $105 \pm 11\text{ J/g}$ and a phase-change temperature of $24.5 \pm 1.5\text{ }^{\circ}\text{C}$ [13].

Coconut oil is a renewable alternative to traditional PCMs due to its abundance, low cost, and chemical stability. According to the literature, coconut oil exhibits a liquid–solid transition at $24\text{--}27\text{ }^{\circ}\text{C}$ [13], rendering it suitable for application in LHTES systems in a moderate climate. The thermophysical parameters of coconut oil PCMs are within the range of human thermal comfort conditions; their application reduces energy consumption and improved the temperature comfort. Faraj et al. [14] demonstrated a 53.7% increase in the span of charging and discharging processes of an underfloor electric heating system with PCM plates of coconut oil. Coconut oil is utilized in passenger vehicles [15] to reduce the cabin’s average temperature by $15\text{ }^{\circ}\text{C}$ and improve the passengers’ thermal comfort. Irsyad et al. [16] studied a room cooling application with coconut oil as PCM in a container. The experimental solidification phase occurred at $24\text{ }^{\circ}\text{C}$, and the melting phase was reported at $22\text{--}24\text{ }^{\circ}\text{C}$ [16]. Silalahi et al. [17,18] studied coconut oil for potential use in sensible and latent TES for room-temperature conditioning applications in Indonesia, and the latent heat of coconut oil was decreased by adding graphite nanoparticles, CuO, and ZnO. Putri et al. [19] analyzed coconut oil’s thermal performance, and found that the air temperature was decreased by $2\text{ }^{\circ}\text{C}$ for 2 kg of coconut oil in the solid–liquid phase change. In the study by Rahayu et al. [20], coconut oil with 50% lauric acid demonstrated a melting temperature of $26\text{ }^{\circ}\text{C}$ and latent heat of 103 kJ/kg . Sutjahja et al. [21] proved that adding 1 wt.% of graphite, CuO, or ZnO to coconut oil resulted in thermal conductivity enhancement. Wonorahardjo et al. [22,23] proposed the addition of coconut oil in the building envelope to improve the thermal mass effect and air circulation. In [23], Wonorahardjo et al.

showed that 135–170 kg of coconut oil in a 3–4 m² room could decrease the air temperature by 2.0–2.5 K in the afternoon. Alqahtani et al. [24] examined the addition of a 4 cm coconut oil layer in the wall thickness as an optimal solution for improving heat storage capacity. The encapsulation of PCM in solid matrices can drastically simplify their application in construction elements. Several studies reported PCM applications of encapsulated coconut oil [25–30]. The encapsulation of coconut oil in a biochar matrix [25] for thermal insulation resulted in a maximal latent heat of 74.6 kJ/kg. A coaxial electrospinning technique was reported by Ranodhi Udangawa et al., and coconut oil was encapsulated in the core of a cellulose shell [26]. Coconut oil encapsulated by electrospinning can be successfully used for thermoregulation in the temperature range from 7 to 22 °C. Oktay et al. [27] encapsulated coconut oil with two different methods: microencapsulation and UV curing. The melting enthalpy of such microencapsulated oil was 12% higher compared to that of pure coconut oil. Spherical microcapsules with 81.1% encapsulated coconut oil was prepared by Németh et al. [28], and a stable core-shell structure was prepared. Few other studies focused on the development of microcapsules for thermoregulatory textiles [29,30]. Sarac et al. [29] developed organic fabrics with microencapsulated coconut oil in polymer shells and acquired latent heats from 6.7 to 14.9 kJ/kg.

Tamanu oil is a vegetable-based oil extracted from the seeds of *Calophyllum inophyllum* seed oil found in abundance in East Africa, southern coastal India, Malaysia, and Australia, and exhibits liquid–solid transition in the range of 13–14 °C [31]. Tamanu oil's high content in oleic and linoleic fatty acids renders it suitable for biofuel production. Several studies [32–36] addressed tamanu oil (*Calophyllum inophyllum* seed oil) potential for biodiesel production, and its composition [37], but the thermophysical properties of tamanu oil have not been characterized.

In the present paper, we report the thermal properties of coconut and tamanu oils in their pure and emulsion form, and develop a method for their encapsulation into electrospun fiber matrices. The novel fiber matrices of oils mixtures with commercial PCM paraffins produced by a coaxial electrospinning technique were characterized. The current work aims to identify the thermal properties of electrospun nanofibers as an alternative to PCMs in liquid–solid form. In future work, a layer of nanofibers containing PCM could replace traditional PCMs in LHTES applications.

2. Materials and Methods

2.1. Thermophysical Studies

The current study examined coconut oil from coconut palm tree *Cocos nucifera* and tamanu oil from *Calophyllum inophyllum* seeds as novel PCMs, and their thermal properties were analyzed. Tamanu oil and coconut oil are purchased as cosmetic and edible products. The materials' thermal properties were measured using a differential scanning calorimeter (DSC) Q200 (TA Instruments) with T-zero thermocouples. The blank reference sample was a conventional empty aluminum crucible [38]. Nitrogen and air were used as inert purge gases with a 50 mL/min controlled flow rate. The thermal cycles for tamanu oil in its first thermal cycle and coconut oil were set in the range from −30 to 80 °C with a scanning rate of 1.5 °C/min in a dynamic mode. The mass of each sample was 6 mg. The long-term performance of tamanu oil was evaluated under 50, 100, 150 and 200 thermal cycles [38] in the range from −80 to 200 °C with a scanning rate of 10 °C/min in a dynamic mode. The mass of the four samples was in the range from 5.5 to 7.5 mg.

2.2. PCM Emulsions and Mixtures

Two approaches were used to prepare emulsions. In the first approach, coconut oil and tamanu oil were mixed with water in a ratio of 1:1 to 5:1 in the presence of a surfactant. Table 1 shows the oil-in-water emulsions prepared using polyethylene glycol sorbitan (Tween 20) and polyoxyethylensorbitan oleate (Tween 80) as emulsifiers. The high heat capacity of water (335 kJ/kg) further contributes to the latent heat of PCM mixtures. Water

is used in phase-change materials applications for shifting the melting or solidification point [3].

Table 1. Mixture percentage.

PCM	Mixing Ratio Water:(Oil:Emulsifier)	Emulsifier
Coconut oil	1:(1:1)2	5% <i>v/v</i> Tween 20
	1:(1:1)5	
	1:(2:1)3	
	1:(4:1)3	5% <i>v/v</i> Tween 80
	1:(2:1)4	
	1:(3:1)4	
	1:(5:1)4	
	1:(1:1)5	
	1:(2:1)5	
	1:(5:1)3	5% <i>v/v</i> Tween 20
Tamanu oil	1:(5:1)4	
	1:(5:1)5	
	1:(1:1)3	5% <i>v/v</i> Tween 80
	1:(2:1)3	
	1:(3:1)3	
	1:(5:1)3	
	1:(3:1)4	
	1:(4:1)4	
	1:(2:1)5	
	1:(1:1)2	
PCM	Mixing Ratio (PCM:PCM)	Emulsifier
Coconut oil–tamanu oil	90% c.o.–10% t.o.	-
	70% c.o.–30% t.o.	
	50% c.o.–50% t.o.	
	30% c.o.–70% t.o.	
	10% c.o.–90% t.o.	

In the second approach, the two oils were mixed in several ratios (Table 1) without emulsifiers, and the thermal properties of these new solutions were evaluated. The thermal behavior of all mixtures was investigated by DSC using DSC Q2000.

Tamanu and coconut oil/water emulsions in ratios 1:1 to 5:1 were prepared with polyethylene glycol sorbitan (Tween 20) and polyoxyethylensorbitan oleate (Tween 80) as emulsifiers. The structure of emulsions was imaged with an Axioscop plus 2 optical microscope, and analyzed with ImageJ [39]. The mixtures that had not been phase-separated were analyzed using the DSC technique. The thermal cycles for all emulsions were set in the range from -30 to 80 °C with a scanning rate of 1.5 °C/min in a dynamic mode. The mass of each sample was 6 mg. The final expanded uncertainty is 0.1% for each experimental measurement.

2.3. PCM Electrospun Fiber Matrix

Electrospun fibers were produced by coaxial electrospinning using a 2.2.D–500—Yflow electrospinner. The inner diameters of the outer and inner needles were 20 and 10 G, respectively. The voltage threshold for the electrospinning process was in the range from 10 to 15 kV. The process yielded fibers consisting of a PCM in the core encapsulated into solid polymeric shell.

The shell for all the produced fibers was composed of either 9% *w/v* or 12% *w/v* PCL dissolved in dichloromethane (DCM). The combination of studied concentrations and flow rates is shown in Table 2.

Table 2. Cases examined for the construction of PCM electrospun fiber matrices.

Case	Sheath Solution Concentration (%w/v)	Flow Rate (mL/h) Core Solution	Flow Rate (mL/h) Sheath Solution
1st	9%	0.3	0.6
2nd	9%	0.5	0.5
3rd	12%	0.5	0.5

Three different types of core materials were studied: the water emulsions of pure tamanu and coconut oil, a mixture of tamanu and coconut oils, and different mixtures of tamanu and coconut oils with commercial PCM materials, as shown in Table 3.

Table 3. PCM compositions encapsulated in the fiber core.

PCM	Tamanu Oil (t.o.)	Coconut Oil (c.o.)	Tamanu Oil (t.o.) and Coconut Oil (c.o.) and Commercial PCM		
%	100% (t.o.)	100% (c.o.)	30% (t.o.)	70% (c.o.)	15% (t.o.) 35% (c.o.) 50% RT15
					15% (t.o.) 35% (c.o.) 50% RT18
					15% (t.o.) 35% (c.o.) 50% PT15
					15% (t.o.) 35% (c.o.) 50% PT18

Oil/water emulsion samples were prepared by mixing a 10% *w/v* PVA solution with an 80% *v/v* PCM/water emulsion (with 8.4 mmol/L sodium dodecyl sulfate added as a surfactant) in 1:1 ratio. The resulting PCM–PVA emulsion was homogenized using a T25 digital ULTRA-TURRAX disperser with 0.07% of a nonionic surfactant Triton X added to improve emulsion's spinnability.

For the third type of samples, four commercial PCMs (RT15, RT18, PT15, and PT18) were mixed with tamanu and coconut oils in the ratios shown in Table 3, and were encapsulated in a PCL shell by electrospinning. The commercially available PCMs (RT15 and RT18 from Rubitherm Technologies GmbH and PT15 and PT18 from Pure Temp LLC) were analyzed earlier in [38,40].

The obtained electrospun fiber matrices were characterized with DSC and scanning electron microscopy (SEM) using a Zeiss XB1540 field-emission electron microscope. The thermal cycles for all fiber matrices were set in the range from -30 to 80 °C with a scanning rate of 1.5 °C/min in a dynamic mode. The mass of each sample was 3 mg.

3. Results and Discussion

3.1. Thermophysical Characterization of Pure PCMs

The DSC thermograms of tamanu oil for 200 thermal cycles and coconut oil for the first thermal cycle are shown in Figure 2. The obtained melting or solidification temperatures and enthalpies are displayed on the graphs; for each experimental measurement, the expanded uncertainty was $\pm 0.1\%$.

The thermal properties and stability of tamanu oil were characterized with DSC by thermal cycling. As can be seen in Figure 2a, thermograms for the 1st, 50th, 100th, 150th, and 200th thermal cycles perfectly coincided, and no supercooling was observed, indicating no degradation or other changes in material properties. Tamanu oil exhibited average melting and solidification peaks at 0.86 °C, and the average latent heat of melting and solidification were 3.56 and 4.64 kJ/kg.

Several studies [15,18,41,42] identified coconut oil as a suitable PCM candidate. In this work, the thermophysical properties of coconut oil were studied, and Figure 2b depicts the DSC thermograph of coconut oil in its first thermal cycle. According to the

literature [15,18,41,42], the average melting temperature and latent heat of fusion for coconut oil were in the range from 22 to 28 °C and 70 to 255 kJ/kg, respectively. The average melting and solidification peaks were at 23.05 and 7.47 °C, respectively. A thermal hysteresis was observed in coconut oil with a supercooling of 15.58 °C. The average latent heats of melting and solidification of coconut oil are 50.22 kJ/kg and 56.71 kJ/kg.

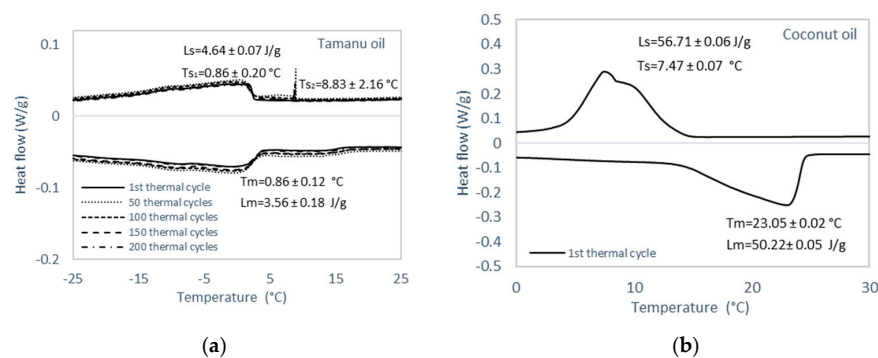


Figure 2. DSC thermogram of (a) tamanu oil in thermal cycles 1, 50, 100, 150, 200; (b) coconut oil in the first thermal cycle.

3.2. Thermophysical Characterization of PCM Emulsions

The DSC thermographs of the two oil emulsions are shown in Figure 3. Figure 3a,b show the thermograph for coconut oil/water emulsions mixed in ratios from 1:1 to 5:1 and with Tween 20 and Tween 80 as surfactants, respectively. Thermographs for similar emulsions produced with tamanu oil are shown in Figure 3c,d. Optical microscopy images of these oil/water emulsions are presented in Figures 4–7. Table 4 summarizes the DSC results and the average emulsion size obtained from optical images.

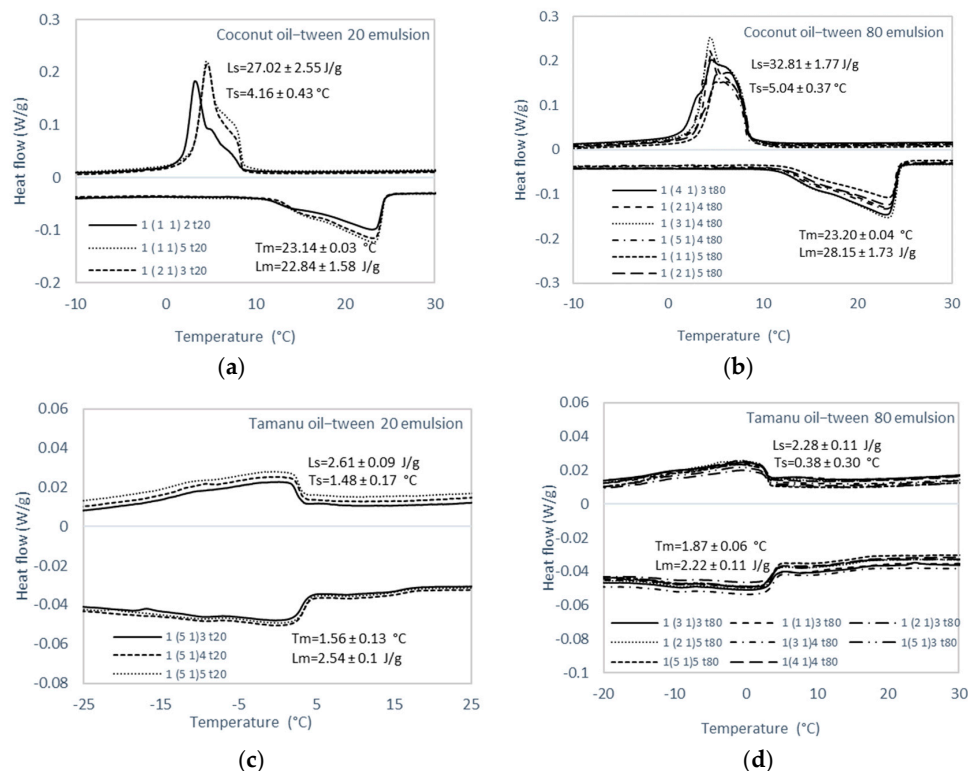


Figure 3. DSC thermograms of (a) coconut oil/water emulsions with Tween 20, (b) coconut oil/water emulsions with Tween 80, (c) tamanu oil/water emulsions with Tween 20, (d) tamanu oil/water emulsions Tween 80 in their first thermal cycle.

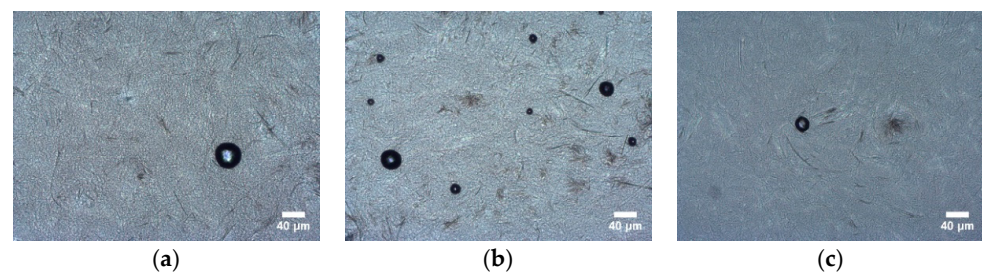


Figure 4. Optical microscopy images of coconut oil/(water emulsion stabilized with Tween 20), water:(oil:emulsifier): (a) 1:(1:1)2, (b) 1:(1:1)5, (c) 1:(2:1)3.

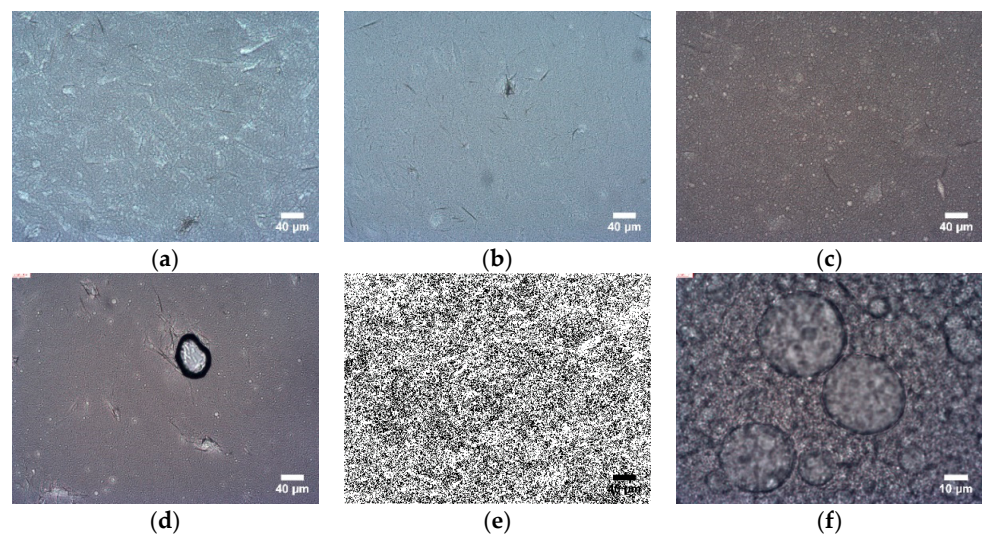


Figure 5. Optical microscopy images of coconut oil/(water emulsion stabilized with Tween 80), water:(oil:emulsifier): (a) 1:(4:1)3, (b) 1:(2:1)4, (c) 1:(3:1)4, (d) 1:(5:1)4, (e) 1:(1:1)5, (f) 1:(2:1)5.

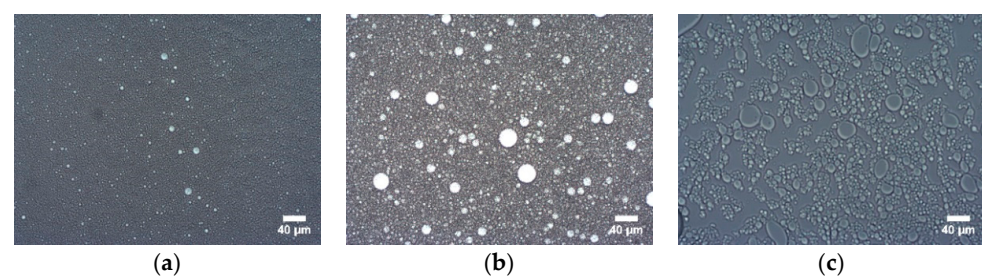


Figure 6. Optical microscopy images of tamanu oil/(water emulsion stabilized with Tween 20), water:(oil:emulsifier): (a) 1:(5:1)3, (b) 1:(5:1)4, (c) 1:(5:1)5.

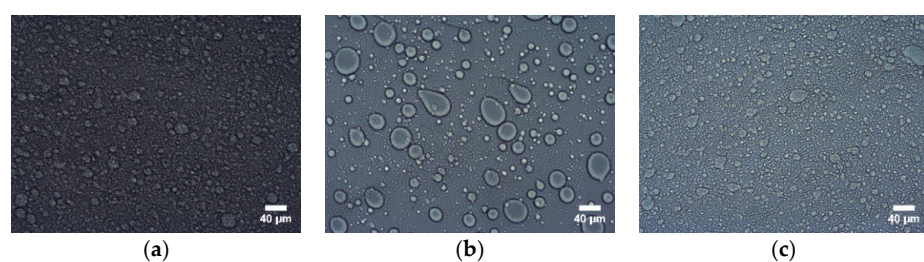


Figure 7. Cont.

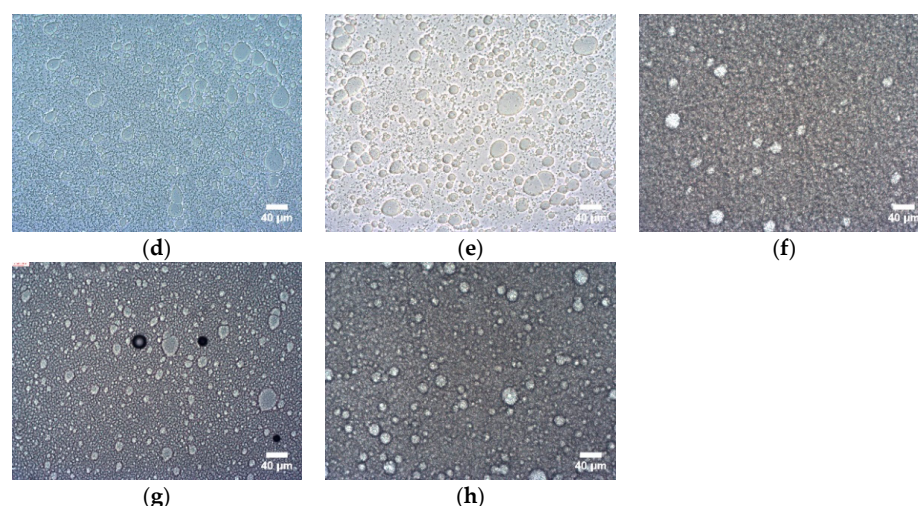


Figure 7. Optical microscopy images of tamanu oil/water emulsion stabilized with Tween 80, water:(oil:emulsifier); (a) 1:(1:1)3, (b) 1:(2:1)3, (c) 1:(3:1)3, (d) 1:(5:1)3, (e) 1:(3:1)4, (f) 1:(4:1)4, (g) 1:(2:1)5, (h) 1:(1:1)2.

Table 4. DSC analyses of coconut oil Tween 20, coconut oil Tween 80, tamanu oil Tween 20, tamanu oil Tween 80 in water emulsions in 1st thermal cycle.

Materials	Mixing Ratio Water:(Oil: Emulsifier)	Melting Temperature (°C)	Melting Enthalpy (kJ/kg)	Solidification Temperature (°C)	Solidification Enthalpy (kJ/kg)	Average Emulsion Size (µm)
Coconut oil Tween 20	1:(1:1)2	23.08	19.69	3.30	22.28	10.5 ± 0.9
	1:(1:1)5	23.19	24.52	4.56	31.04	10.1 ± 0.8
	1:(2:1)3	23.16	24.32	4.63	27.74	10 ± 0.9
Coconut oil Tween 80	1:(4:1)3	23.08	31.92	4.58	37.91	17.4 ± 2.8
	1:(2:1)4	23.31	27.11	4.54	31.54	7.6 ± 0.3
	1:(3:1)4	23.26	33.29	4.43	37.27	12 ± 0.9
	1:(5:1)4	23.04	29.49	4.30	32.65	8.8 ± 0.5
	1:(1:1)5	23.26	22.13	6.16	26.15	4.1 ± 0.1
	1:(2:1)5	23.22	24.95	6.24	31.31	4.8 ± 1.2
Tamanu oil Tween 20	1:(5:1)3	1.31	2.34	1.15	2.46	16.2 ± 0.7
	1:(5:1)4	1.63	2.64	1.69	2.58	5.6 ± 0.2
	1:(5:1)5	1.73	2.64	1.61	2.78	16.2 ± 0.2
Tamanu oil Tween 80	1:(1:1)3	1.95	1.82	0.13	2.14	13.3 ± 0.4
	1:(2:1)3	1.85	1.82	−0.26	1.97	8.4 ± 0.7
	1:(3:1)3	1.76	2.13	0.39	2.02	12.1 ± 0.3
	1:(5:1)3	1.97	2.39	−0.10	2.59	16.6 ± 0.7
	1:(3:1)4	2.20	2.28	0.25	2.35	15.2 ± 0.8
	1:(4:1)4	1.72	2.16	−0.53	2.60	11.5 ± 0.4
	1:(2:1)5	1.69	2.45	1.10	1.94	12.1 ± 0.3
	1:(1:1)2	1.81	2.73	2.06	2.66	9.1 ± 0.3

The DSC thermographs, optical microscopy images, and analytical results of tamanu and coconut oil mixtures in different ratios are shown in Figure 8 and Table 5, respectively. The expanded uncertainty for each experimental measurement was $\pm 0.1\%$.

Maruyama et al. [42] studied the effect of commercial emulsifiers EM1 and EM2 on coconut oil, and observed an increase in melting and solidification enthalpies to 105.5 and 26.7 kJ/g upon the addition of 1% *w/w* of EM1. The peak melting and solidification temperatures [42] were 21.3 and 3.3 °C. The average melting and solidification temperatures, and solidification enthalpy of coconut oil in water emulsions with Tween 20 and Tween 80 (Figure 3a,b) values found in this study coincided with those presented in [42]. However, the melting enthalpies ranged from 19 to 33 kJ/kg (Table 4). In all coconut oil

emulsions thermograms (Figure 3a,b), a thermal shift of 17–20 °C between the melting and solidification curves was observed. Wiyani et al. [43] successfully formulated virgin coconut oil emulsions in a ratio of 80:20 with Tween 80 and Span 80 as emulsifiers. Gulao et al. [44] studied the physicochemical properties of coconut oil in water emulsions with two biopolymers, which resulted in average droplet diameters in the range from 310 to 1200 nm. The average emulsion size, analyzed in Table 4, showed that the coconut oil–Tween 20 (Figure 4) and Tween 80 (Figure 5) emulsion size varied between 9 and 10 µm, and 4 and 17 µm, respectively.

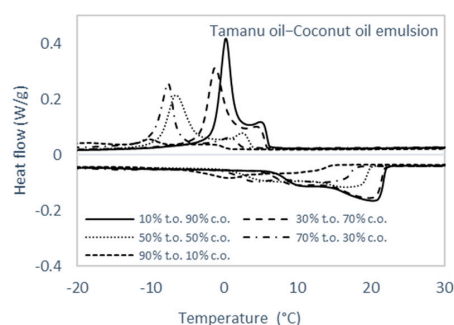


Figure 8. DSC thermograph of different tamanu–coconut oil mixtures in their first thermal cycle.

Table 5. DSC analyses of coconut–tamanu oil mixtures in their first thermal cycle.

Materials	Mixing Ratio	Melting Temperature (°C)		Melting Enthalpy (kJ/kg)	Freezing Temperature (°C)		Solidification Enthalpy (kJ/kg)
		Max	Min		Max	Min	
Coconut oil–tamanu oil mixture	90% c.o. – 10% t.o.	20.28	9.80	45.34	0.23	5.25	44.89
	70% c.o. – 30% t.o.	19.87	9.22	43.60	1.26	4.75	47.86
	50% c.o. – 50% t.o.	16.60	5.27	38.81	−6.66	2.45	38.39
	30% c.o. – 70% t.o.	13.43	3.82	28.90	−7.68	0.71	28.91
	10% c.o. – 90% t.o.	0.75	12.06	24.03	−10.24	−1.33	5.85

In [14], Isryad et al. tested *Calophyllum inophyllum* seed oil (CISO) with water, resulting in peak solidification and melting temperatures of −11.66 and 15.23 °C and latent heat of solidification and melting of 188.31 and 219.74 kJ/kg. In the current study, the melting and solidification temperatures and enthalpies of tamanu oil emulsions with Tween 20 and 80 were in the range from −0.5 to 2.3 °C, and from 2 to 3 kJ/kg. For tamanu oil emulsions (Figure 3c,d), a slight thermal shift in the range of 0.06–2.2 °C between the melting and solidification curves occurred. Urbánková et al. [45] studied tamanu and black cumin oil emulsions with the addition of sodium caseinate, and observed an average emulsion size in the range from 0.3 to 1.5 µm. In the current study, the average emulsion size of tamanu oil with Tween 20 (Figure 6) and Tween 80 (Figure 7) was 5–16 and 8–17 µm, respectively. The examined macroemulsion systems were composed of coconut oil and tamanu oil in water, and formed droplets in the micrometer range. This indicates a microemulsion that is generally thermodynamically unstable. One emulsifier was used to achieve the stability of oil in water emulsion in all different ratios, and the mixing was achieved with the same energy input.

Moreover, tamanu oil was mixed with coconut oil as pure substances without emulsifiers. In the literature, *Jatropha curcas* seed oil (JCSO) mixed with crude palm oil (CPO) [14] resulted in melting and solidification peak temperatures of −1.79 and −14.98 °C, and melting–solidification enthalpies of 8.44 and 21.17 kJ/kg. The DSC thermographs of

tamanu oil and coconut oil mixtures (Figure 8) indicate that, for all examined mixing ratios (Table 5), two peaks for tamanu oil and coconut oil could be identified in the melting and solidification thermal cycles. A hysteresis loop of the latent heat/temperature thermographs is illustrated in tamanu oil mixtures with coconut oil. The higher the percentage of coconut oil in the solution was, the higher the latent heat of fusion in the mixture. More precisely, in the mixture containing 90% coconut oil and 10% tamanu oil, there was an increase of 89% in the latent heat of melting and 667% in the latent heat of solidification compared to the mixture with 10% coconut oil and 90% tamanu oil.

3.3. Thermophysical Characterization of PCM Electrospun Fiber Matrix

Tamanu oil, coconut oil, and their mixtures with commercially available organic PCM (Table 3) were encapsulated in the core of electrospun fiber matrices. The obtained fiber mats were cut to prepare samples of 3 mg each. Figure 9 and Table 6 display the thermographs acquired by DSC and the summary of results, respectively. Figures 10–12 show the optical images of the PCM fiber matrices and the respective histograms of fiber diameters. The encapsulation ratio, efficiency, and mean diameter of the electrospun PCM fiber matrices are summarized in Table 7. Equations (1) and (2) were used for the calculation of the encapsulation ratio and efficiency presented in Table 7.

$$n = \frac{L_{m, \text{encap. PCM}}}{L_{m, \text{PCM}}} \quad (1)$$

$$\varepsilon = \frac{L_{m, \text{encap. PCM}} + L_{s, \text{encap. PCM}}}{L_{m, \text{PCM}} + L_{s, \text{PCM}}} \quad (2)$$

Table 6. DSC analyses of electrospun PCM fiber samples in 1st thermal cycle.

Fibers	PCL	Flow Rate	Melting Temperature (°C)		Enthalpy (J/g)		Freezing Temperature (°C)		Enthalpy (J/g)	
			PCM	PCL	PCM	PCL	PCM	PCL	PCM	PCL
Coconut oil	9%	0.3–0.6 mL/h	56.55	-	34.42	-	34.47	-	39.08	-
		0.5–0.5 mL/h	22.94	54.71	46.91	7.36	8.03	36.49	40.16	8.59
	12%	0.5–0.5 mL/h	22.99	54.80	49.20	6.87	7.41	36.48	46.50	8.10
Tamanu oil	9%	0.3–0.6 mL/h	−0.16	53.60	2.59	14.39	0.11	33.76	3.41	14.62
		0.5–0.5 mL/h	−0.12	50.96	2.35	5.98	−0.05	30.21	3.01	6.64
	12%	0.5–0.5 mL/h	0.26	50.51	2.83	11.03	0.12	31.26	3.32	10.74
Coconut oil 70%–tamanu oil 30%	9%	0.3–0.6 mL/h	20.73	55.43	20.03	19.34	7.75	-	36.52	7.97
		0.5–0.5 mL/h	20.13	54.26	43.93	5.74	3.01	−1.26	34.34	35.32
	12%	0.5–0.5 mL/h	20.32	53.27	31.83	8.94	4.43	-	33.33	27.04
Coconut oil 35%–tamanu oil 15%–RT18 50%	9%	0.3–0.6 mL/h	13.65	53.75	56.69	5.90	8.98	4.48	34.91	37.00
		0.5–0.5 mL/h	13.65	53.78	63.80	7.44	9.02	4.55, 1.48	34.85	57.58
	12%	0.5–0.5 mL/h	13.61	54.20	54.78	8.75	1.68	4.60, 9.27	35.10	46.11
Coconut oil 35%–tamanu oil 15%–RT15 50%	9%	0.3–0.6 mL/h	12.96	54.12	50.79	9.81	9.12	1.67, 13.15	35.03	30.99
		0.5–0.5 mL/h	12.99	53.75	53.01	7.11	9.46	1.63, 12.84	34.92	31.89
	12%	0.5–0.5 mL/h	13.48	53.78	48.55	9.75	12.74	1.52	34.92	31.85
Coconut oil 35%–tamanu oil 15%–PT18 50%	9%	0.3–0.6 mL/h	6.26	50.55	22.45	7.41	−6.37	33.04	30.51	8.66
		0.5–0.5 mL/h	5.89	50.71	23.65	7.75	−6.44	33.71	33.44	8.42
	12%	0.5–0.5 mL/h	5.83	2.69	17.60	8.65	−6.70	33.59	28.59	9.52
Coconut oil 35%–tamanu oil 15%–PT 15 50%	9%	0.3–0.6 mL/h	8.71	53.99	30.03	5.58	−0.83	35.55	46.81	6.99
		0.5–0.5 mL/h	9.06	54.05	33.80	4.89	−0.81	34.70	44.64	5.97
	12%	0.5–0.5 mL/h	10.71	55.59	43	10.43	3.05	0.16	35.96	57.96

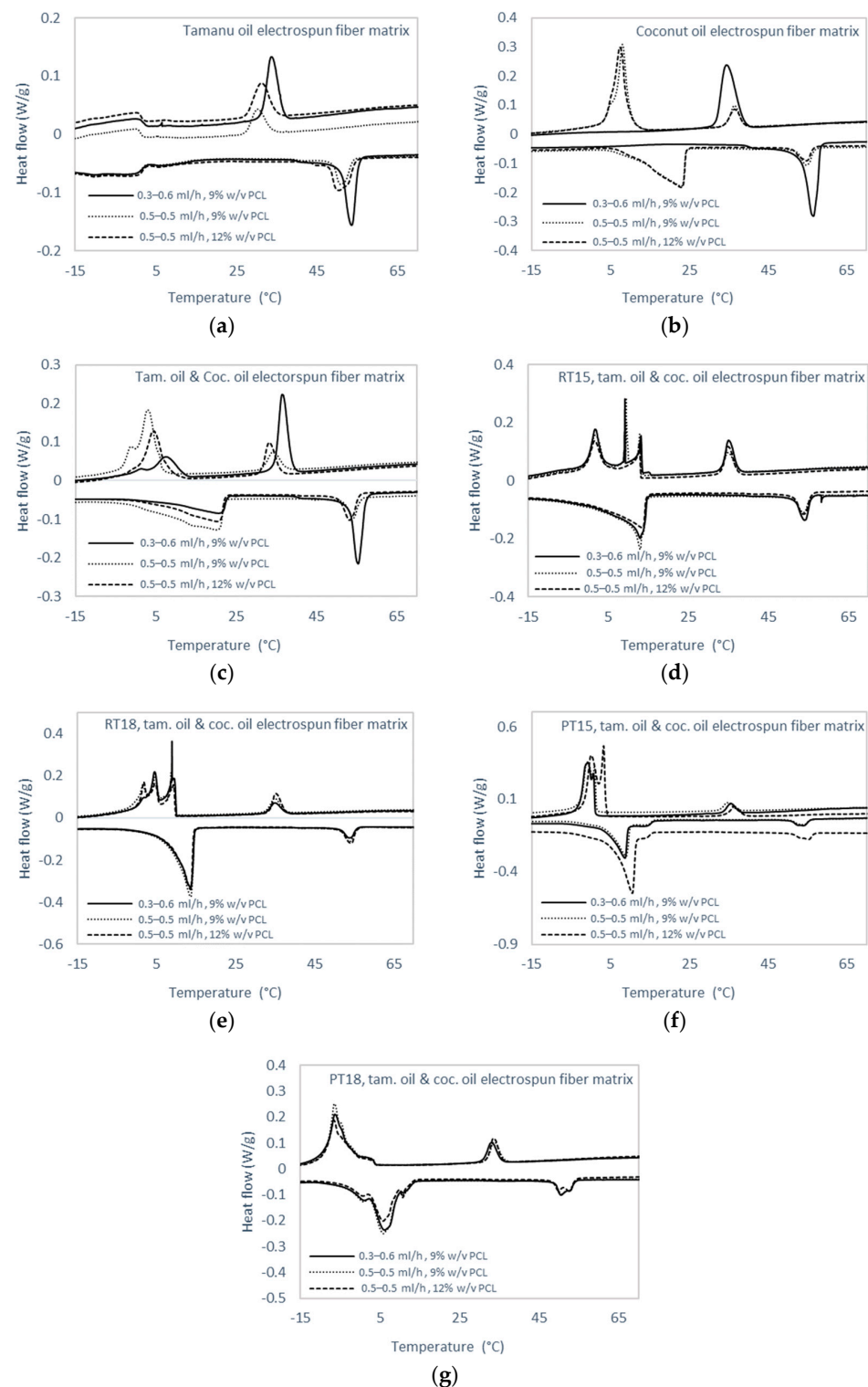


Figure 9. DSC thermograms of PCM encapsulated in the core of electrospun fiber in 1st thermal cycle. Core compositions: (a) tamanu oil emulsion; (b) coconut oil emulsion; (c) mixture of 70% co-conut oil and 30% tamanu oil; (d) mixture of 50% RT15, 15% tamanu oil, and 30% coconut oil; (e) mixture of 50% RT18, 15% tamanu oil, and 35% coconut oil; (f) mixture of 50% PT15, 15% tamanu oil and 35% coconut oil; (g) mixture of 50% PT18, 15% tamanu oil, and 35% coconut oil.

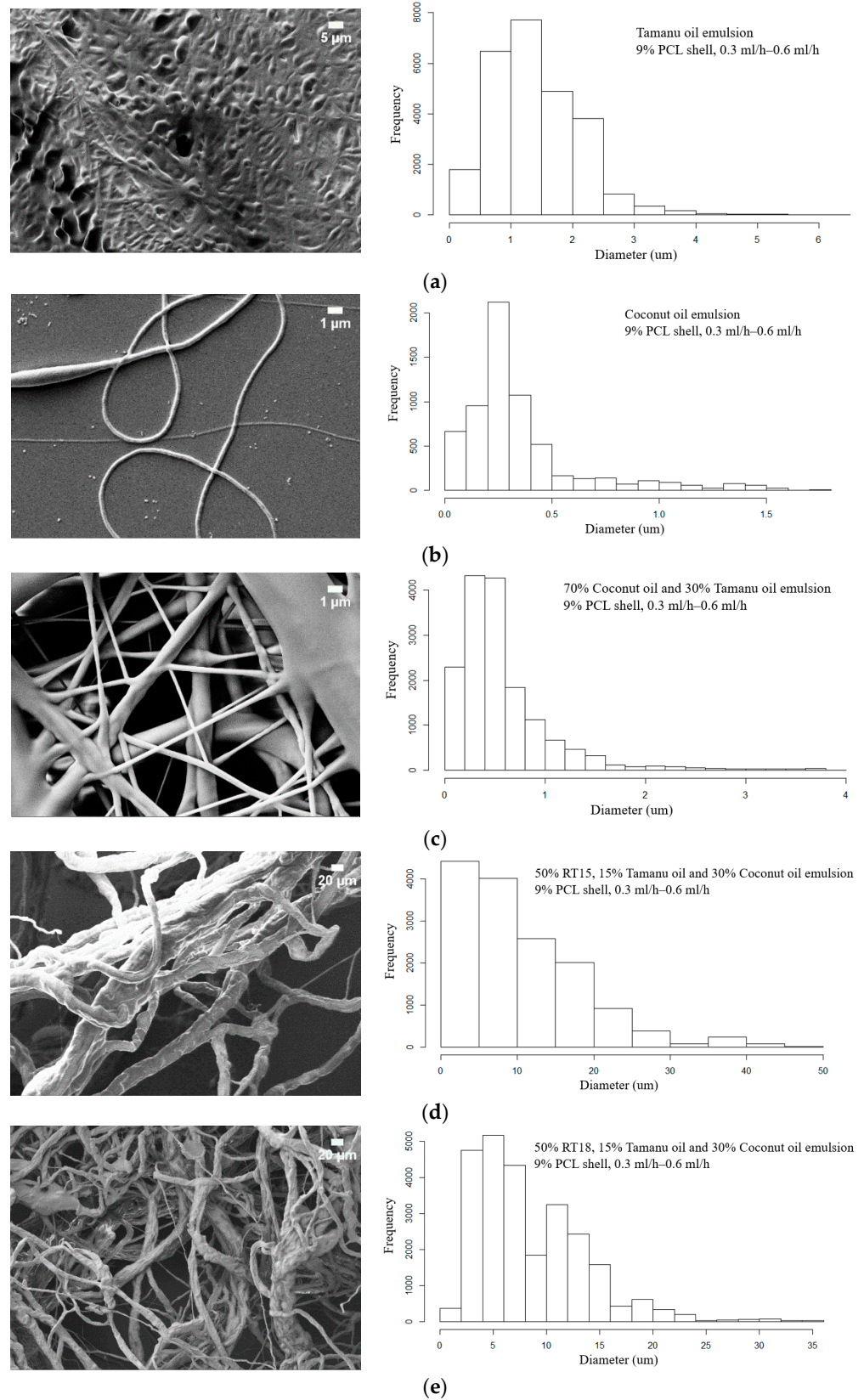


Figure 10. Cont.

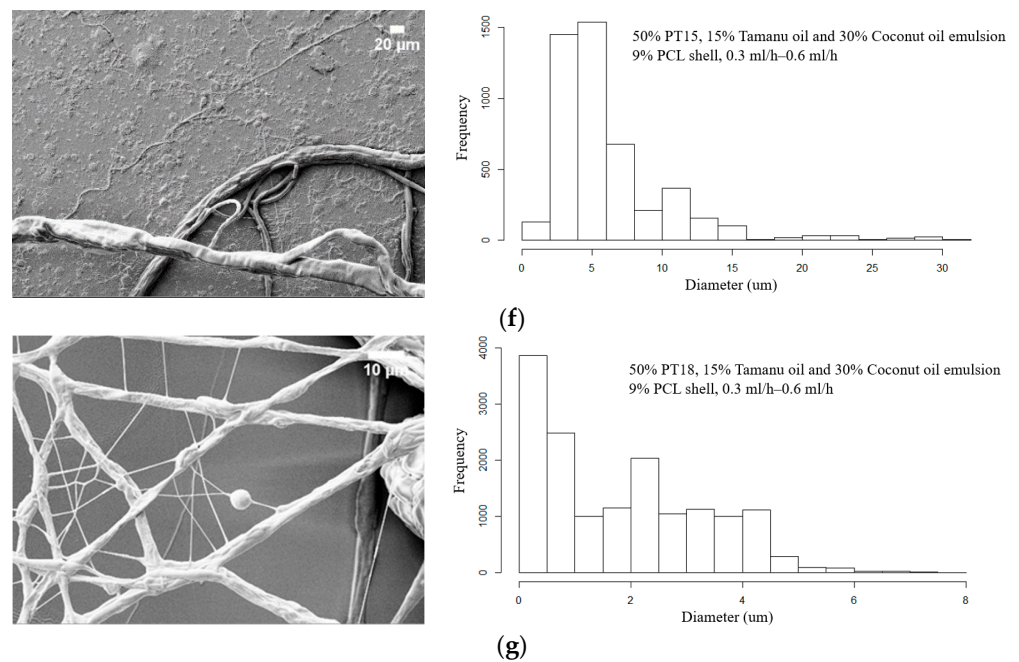


Figure 10. (left) SEM images of core/shell fibers and (right) the respective fiber diameter distributions for electrospun fiber mats produced with 9% PCL shell at flow rates of 0.3 mL/h for the core and 0.6 mL/h for the shell. Core compositions: (a) tamanu oil emulsion; (b) coconut oil emulsion; (c) mixture of 70% coconut oil and 30% tamanu oil; (d) mixture of 50% RT15, 15% tamanu oil, and 30% coconut oil; (e) mixture of 50% RT18, 15% tamanu oil, and 35% coconut oil; (f) mixture of 50% PT15, 15% tamanu oil and 35% coconut oil; (g) mixture of 50% PT18, 15% tamanu oil, and 35% coconut oil.

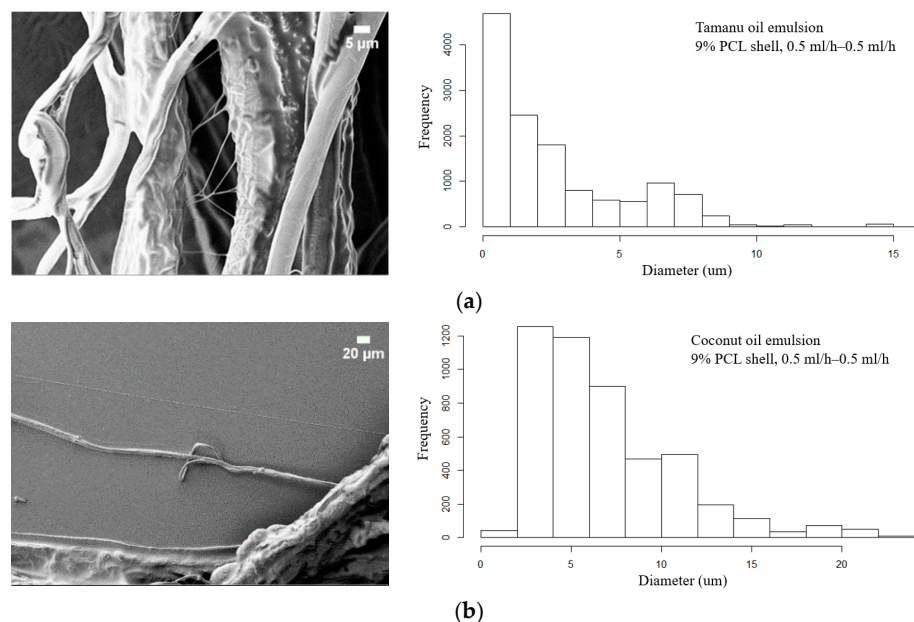


Figure 11. Cont.

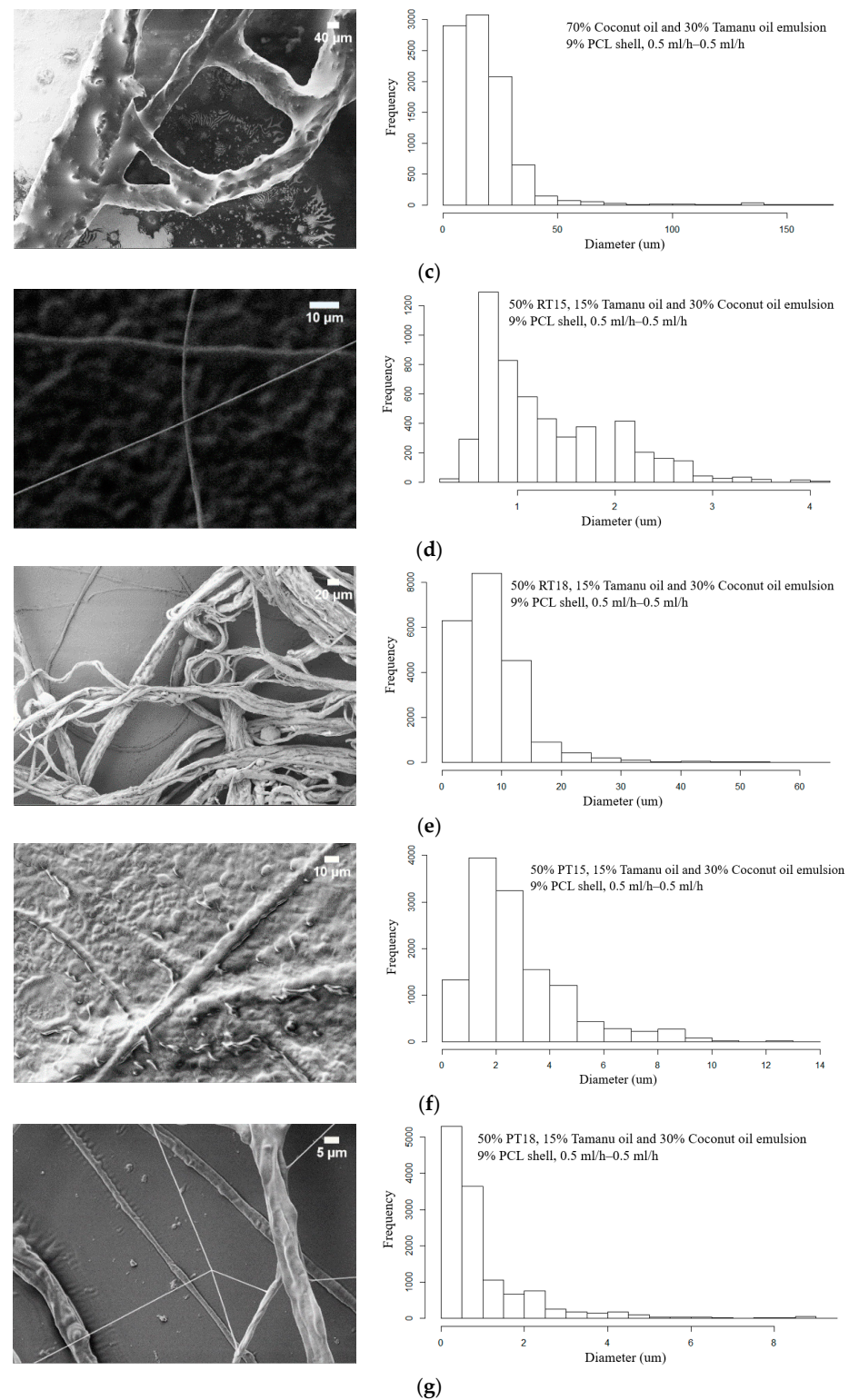


Figure 11. (left) SEM images of core/shell fibers and the (right) respective fiber diameter distributions for electrospun fiber mats produced with 9% PCL shell at flow rates of 0.5 mL/h for the core and 0.5 mL/h for the shell. Core compositions: (a) tamanu oil emulsion; (b) coconut oil emulsion; (c) mixture of 70% coconut oil and 30% tamanu oil; (d) mixture of 50% RT15, 15% tamanu oil, and 30% coconut oil; (e) mixture of 50% RT18, 15% tamanu oil, and 35% coconut oil; (f) mixture of 50% PT15, 15% tamanu oil, and 35% coconut oil; (g) mixture of 50% PT18, 15% tamanu oil, and 35% coconut oil.

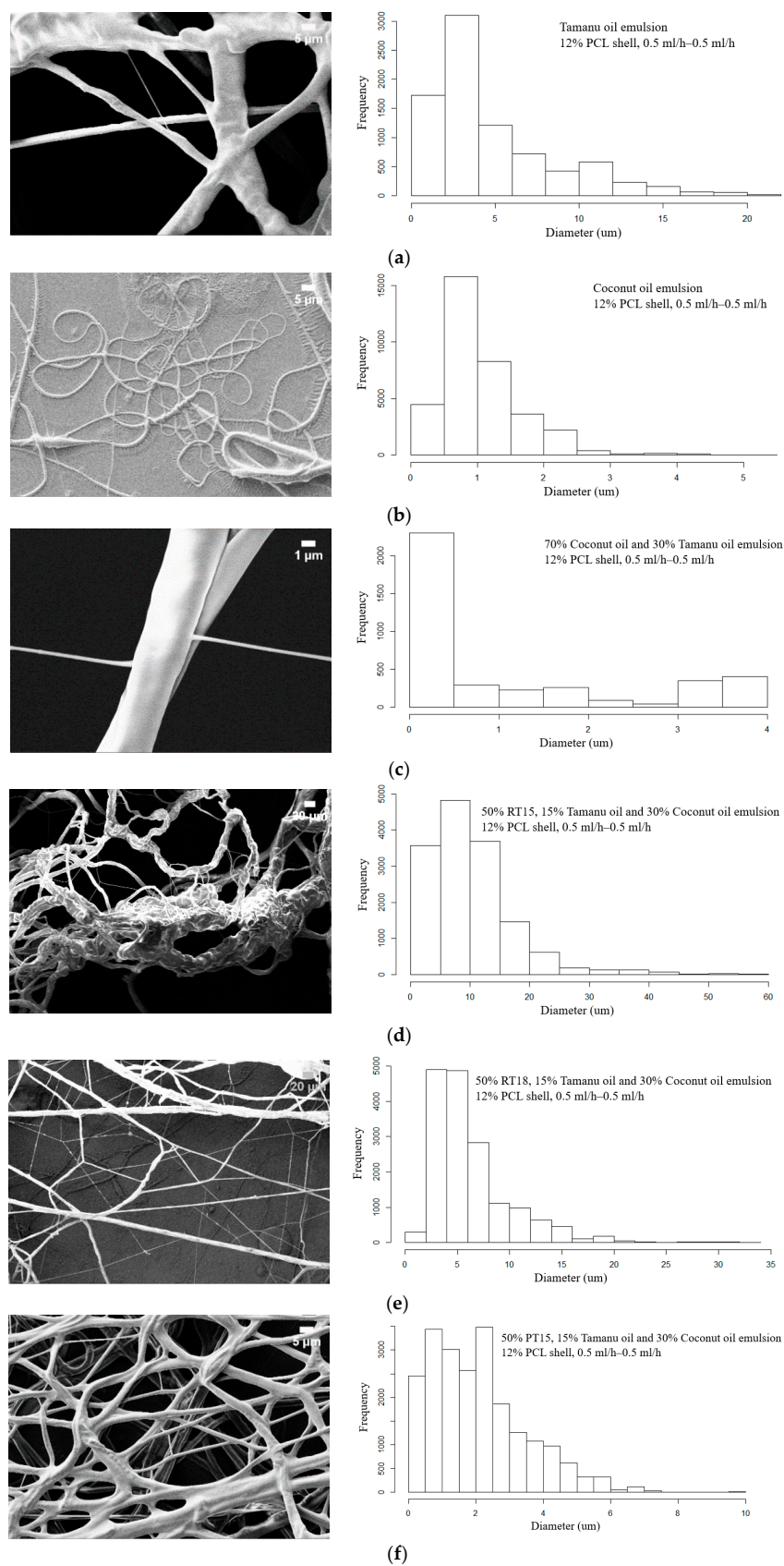


Figure 12. Cont.

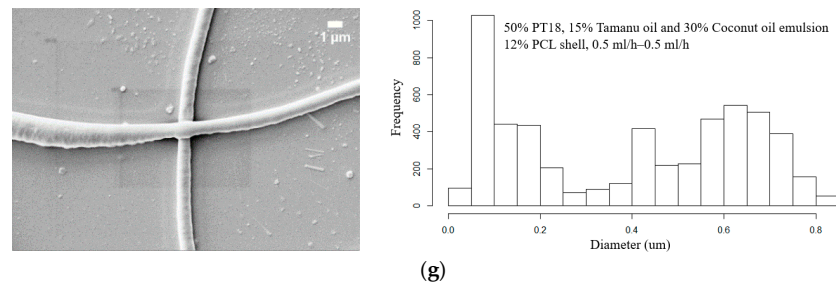


Figure 12. (left) SEM images of core/shell fibers and (right) the respective fiber diameter distributions for electrospun fiber mats produced with 12% PCL shell at flow rates of 0.5 mL/h for the core and 0.5 mL/h for the shell. Core compositions: (a) tamanu oil emulsion; (b) coconut oil emulsion; (c) mixture of 70% coconut oil and 30% tamanu oil; (d) mixture of 50% RT15, 15% tamanu oil, and 30% coconut oil; (e) mixture of 50% RT18, 15% tamanu oil, and 35% coconut oil; (f) mixture of 50% PT15, 15% tamanu oil, and 35% coconut oil; (g) mixture of 50% PT18, 15% tamanu oil, and 35% coconut oil.

Table 7. Encapsulation ratio, efficiency and mean diameter of encapsulated electrospun PCM.

PCM Core Material	PCL	Flow Rate (mL/h)	Encapsulation Ratio n (%)	Encapsulation Efficiency ϵ (%)	Histogram Mean Diameter (μm)
Coconut oil	9%	0.3–0.6	68.5	68.7	0.3 ± 0.001
		0.5–0.5	93.4	81.4	5.6 ± 0.05
	12%	0.5–0.5	98	89.5	0.9 ± 0.002
Tamanu oil	9%	0.3–0.6	72.8	73.2	1.3 ± 0.06
		0.5–0.5	66.1	65.4	0.8 ± 0.004
	12%	0.5–0.5	79.6	75.1	2.7 ± 0.02
Coconut oil 70%–tamanu oil 30%	9%	0.3–0.6	45.9	30.6	0.4 ± 0.002
		0.5–0.5	100	86.6	12.8 ± 0.09
	12%	0.5–0.5	73	64.4	0.2 ± 0.0004
Coconut oil 35%–tamanu oil 15%–PT15 50%	9%	0.3–0.6	39.3	51.2	4.4 ± 0.03
		0.5–0.5	44.2	52.2	2 ± 0.008
	12%	0.5–0.5	56.3	67.2	1.5 ± 0.01
Coconut oil 35%–tamanu oil 15%–PT18 50%	9%	0.3–0.6	28.1	34.4	0.5 ± 0.001
		0.5–0.5	29.6	37.1	0.5 ± 0.001
	12%	0.5–0.5	22	30	0.1 ± 0.0004
Coconut oil 35%–tamanu oil 15%–RT15 50%	9%	0.3–0.6	100	96	6.5 ± 0.06
		0.5–0.5	100	99.6	0.8 ± 0.005
	12%	0.5–0.5	100	94.3	7.5 ± 0.04
Coconut oil 35%–tamanu oil 15%–RT18 50%	9%	0.3–0.6	100	91.9	6.9 ± 0.03
		0.5–0.5	100	100	6.6 ± 0.02
	12%	0.5–0.5	100	99	4.7 ± 0.02

$(L)_{m, \text{encap. PCM}}$ —Latent heat of melting for encapsulated PCM (J/g)

$(L)_{s, \text{encap. PCM}}$ —Latent heat of solidification for encapsulated PCM (J/g)

$(L)_{m, \text{PCM}}$ —Latent heat of melting for PCM (J/g)

$(L)_{s, \text{PCM}}$ —Latent heat of solidification for PCM (J/g)

n —Encapsulation ratio (%)

ϵ —Encapsulation efficiency (%)

Several researchers [26,46,47] attempted the encapsulation of coconut oil in microfibers. In the existing literature [26], biomass microfibers with coconut oil encapsulated in the core resulted in melting and solidification temperatures, and enthalpies for the core material of $T_m = 22\text{ }^{\circ}\text{C}$, $T_{c1} = 14\text{ }^{\circ}\text{C}$, $T_{c2} = 8\text{ }^{\circ}\text{C}$, and $\Delta H_m = 134.9\text{ J/g}$, $\Delta H_c = 64.7\text{ J/g}$. The average fiber diameters were $3 \pm 1\text{ }\mu\text{m}$ for the cylindrical region of the fiber, and $8 \pm 4\text{ }\mu\text{m}$ for the biconical region of the fiber [26]. In another study, coconut oil was successfully encapsulated in PCL gel nanofibers with an efficiency of 60% [46] and 300 to 370 nm mean diameter. Moreover, the melting and crystallization points of the coconut-oil-loaded sample were 25 and $3\text{ }^{\circ}\text{C}$ [46]. Saravana Kumar Jaganathan et al. [47] examined electrospun polyurethane/virgin coconut oil composites, and the fiber's diameter was in the range of $886 \pm 207\text{ nm}$.

A coaxial electrospinning setup was adjusted in the laboratory, core-shell fibers were formed for the oils mixture, and the four commercial PCMs were mixed with the two oils in a PCL shell. The DSC thermographs of tamanu oil (Figure 9a), coconut oil (Figure 9b), and tamanu oil mixed with coconut oil (Figure 9c) in the core of the fiber display two peaks for the PCM and the shell material. The melting or solidification enthalpy (Figure 9a) for tamanu oil was stable (Table 6) for the different flow rates and polymer concentrations. In the case of coconut oil, the electrospun fiber matrix examined in this study (Figure 9b) showed a narrower phase change temperature range ($23\text{ to }8\text{ }^{\circ}\text{C}$) and an increased enthalpy of melting and solidification at 49 to 47 kJ/kg for the case of 12% PCL shell. In the case of tamanu-coconut oil mixture, the electrospun fiber matrix with 9% PCL shell and 0.5/0.5 mL/h core/shell flow rate, enthalpy of 44–35 kJ/kg was observed. In the four cases of commercial PCM materials (RT15 (Figure 9d), RT18 (Figure 9e), Pure Temp 15 (Figure 9f), and Pure Temp 18 (Figure 9g) mixed with the two oils, the melting and solidification curves followed the same trend as that of the curves presented in [40] for electrospun fibers with commercial PCMs alone. Fiber mats with the mixture of RT15 and the two oils in the core (Figure 9d) displayed a phase-change temperature range of $13\text{--}9\text{ }^{\circ}\text{C}$, while the mixture of RT18 with the two oils displayed a $13\text{--}2\text{ }^{\circ}\text{C}$ PCM temperature range. In the two mixtures of the organic paraffins with the renewable oils, a higher enthalpy was observed in the polymer concentration of 9% *w/v* with a 0.5/0.5 mL/h core/shell flow rate. The mixture of organic nonparaffinic PCM PT15 with the two oils (Figure 9f) resulted in the melting or solidification temperature range of $8\text{--}0\text{ }^{\circ}\text{C}$, and the highest enthalpies, in this case, 43 kJ/kg for melting and 58 kJ/kg for solidification observed for the polymer concentration of 12% *w/v* and a 0.5/0.5 mL/h core/shell flow rate. Lastly, organic nonparaffinic PCM PT18 demonstrated a melting solidification temperature range from 6 to $-6\text{ }^{\circ}\text{C}$, and exhibited the highest enthalpies of 24 and 34 kJ/kg for a polymer concentration of 9% *w/v* and a 0.5/0.5 mL/h core/shell flow rate. The highest encapsulation ratio n and encapsulation efficiency ϵ were observed in the cases of polymer concentration of 9% *w/v* and 0.5/0.5 mL/h core/shell flow rate. The equation used to calculate the encapsulation ratio and the efficiency given in [40] indicates that the latent heat of melting for the solution encapsulated in the fiber core for organic paraffins RT15 and RT18 mixed with the two oils is equal to the latent heat of melting the fiber. That being the case, after calculating the encapsulation ratio in organic paraffins RT15 and RT18 with the oil mixture, the outcome was around 100%. This high percentage indicates that the core and fiber materials were melted together in the DSC testing procedure. The average mean diameter of all examined fibers was from 0.1 to $12.8\text{ }\mu\text{m}$. SEM images show that the 12% *w/v* and 0.5–0.5 mL/h flow rate PT15, tamanu oil, and coconut oil fibers were homogeneous and remained stable, with a mean diameter of $1.5\text{ }\mu\text{m}$ and an encapsulation efficiency of 67.2%.

In future work, a uniform layer of electrospun fibers should be fabricated, applied, and tested in the LHTES system to evaluate if the stored energy is sufficient for construction applications.

4. Conclusions

Tamanu oil and coconut oil were studied for potential use as PCM materials in bulk, emulsion, and encapsulated fiber forms. As an outcome of the DSC analysis, bulk coconut oil was classified as a possible new PCM candidate for thermal energy storage applications

with latent heats of 50 and 56 kJ/kg. Tamanu oil and coconut oil emulsions with water and Tween 20 and 80 exhibited lower latent heats than the bulk materials did. The mixture of tamanu oil with coconut oil at a ratio of 70/30 (CO/TO) demonstrated higher latent heats compared to the mixtures with other ratios. The addition of 50% of RT18, a commercially available PCM, to 70/30 mixture of coconut and tamanu oil yielded electrospun fibers with the best latent heat of melting and solidification of 63.8 and 57.6 kJ/kg, respectively. Overall, the developed procedure of coaxial electrospinning with a PCL shell was demonstrated to be suitable for the efficient encapsulation of the PCM in the fibers. In the cases of RT15–tamanu oil–coconut oil and RT18–tamanu oil–coconut oil, the latent heat of the PCM fiber was equal to the latent heat of the encapsulated PCM emulsion. The successful production of electrospun PCM fiber mats with encapsulated oils of biological origin is an important step towards energy-saving and environmentally friendly construction materials.

Author Contributions: Conceptualization, E.P. and P.F.; methodology, E.P. and A.A.; software, E.P.; validation, E.P., L.G. and P.F.; formal analysis, E.P.; investigation, E.P., P.F. and A.A.; resources, P.F.; data curation, P.F. and E.P.; writing—original draft preparation, E.P.; writing—review and editing, E.P., L.G., P.F. and A.A.; supervision, E.P., P.F. and A.A.; project administration, E.P.; funding acquisition, A.A. All authors have read and agreed to the published version of the manuscript.

Funding: The authors acknowledge the support provided by ELFORSK, a research and development program administrated by Danish Energy.

Institutional Review Board Statement: Not applicable.

Informed Consent Statement: Not applicable.

Data Availability Statement: Data are available upon request.

Conflicts of Interest: The authors declare no conflict of interest.

Nomenclature

Parameter	Description	Unit
PCM	Phase change material	-
TES	Thermal energy storage	-
PCL	Polycaprolactone	-
SDS	Sodium dodecyl sulfate	-
DSC	Differential scanning calorimetry	-
(L) _{m,encap,PCM}	Latent heat of melting for encapsulated PCM	(J/g)
(L) _{s,encap,PCM}	Latent heat of solidification for encapsulated PCM	(J/g)
(L) _{m,PCM}	Latent heat of melting for PCM	(J/g)
(L) _{s,PCM}	Latent heat of solidification for PCM	(J/g)
T _m	Melting temperature	(°C)
T _s	Solidification temperature	(°C)
n	Encapsulation ratio	(%)
ε	Encapsulation efficiency	(%)
w/v	Weight/volume	(% g/mL)
v/v	Volume/volume	(% mL/mL)

References

1. IEA. 2019 *Global Status Report for Buildings and Construction*; International Energy Agency: Paris, France, 2019; Volume 224, ISBN 9789280737684.
2. Cabeza, L.F.; Martorell, I.; Miró, L.; Fernández, A.I.; Barreneche, C. Introduction to thermal energy storage (TES) systems. In *Advances in Thermal Energy Storage Systems: Methods and Applications*; Woodhead Publishing: Sawston, UK, 2015; ISBN 9781782420965.
3. Košny, J. *PCM-Enhanced Building Components*; Springer International Publishing: Cham, Switzerland, 2015; ISBN 978-3-319-14285-2.
4. Paroutoglou, E.; Afshari, A.; Bergsøe, N.C.; Fojan, P.; Hultmark, G. A PCM based cooling system for office buildings: A state of the art review. *E3S Web Conf.* **2019**, *111*, 01026. [[CrossRef](#)]

5. Sarbu, I.; Sebarchievici, C. A comprehensive review of thermal energy storage. *Sustainability* **2018**, *10*, 191. [CrossRef]
6. Bruno, F.; Belusko, M.; Liu, M.; Tay, N.H.S. Using solid-liquid phase change materials (PCMs) in thermal energy storage systems. In *Advances in Thermal Energy Storage Systems*; Woodhead Publishing: Sawston, UK, 2015; pp. 201–246. [CrossRef]
7. Casini, M.; Temperature, M.; Heat, L.; Phase, I.; Material, C.; Hydrate, S.; Thermal, L.; Storage, T.E.; Material, P.C.; Conductivity, T. Phase-Change Materials Organic Phase Change Material. Available online: <https://www.sciencedirect.com/science/article/pii/B9780081006351000058> (accessed on 8 May 2022).
8. Png, Z.M.; Soo, X.Y.D.; Chua, M.H.; Ong, P.J.; Suwardi, A.; Tan, C.K.I.; Xu, J.; Zhu, Q. Strategies to reduce the flammability of organic phase change Materials: A review. *Sol. Energy* **2022**, *231*, 115–128. [CrossRef]
9. Arsana, M.E.; Temaja, I.W.; Widiantera, I.B.G.; Sukadana, I.B.P. Corn oil phase change material (PCM) in frozen food cooling machine to improve energy efficiency. *J. Phys. Conf. Ser.* **2020**, *1450*, 012107. [CrossRef]
10. Rasta, I.M.; Wardana, I.N.G.; Hamidi, N.; Sasongko, M.N. The Role of Soya Oil Ester in Water-Based PCM for Low Temperature Cool Energy Storage. *J. Thermodyn.* **2016**, *2016*, 5384640. [CrossRef]
11. Irfan, A.M. Thermophysical Characteristics of VCO-Soybean Oil Mixture as Phase Change Material (PCM) using T-History Method. *J. Phys. Conf. Ser.* **2019**, *1244*, 012033. [CrossRef]
12. Rasta, I.M.; Suamir, I.N. The role of vegetable oil in water based phase change materials for medium temperature refrigeration. *J. Energy Storage* **2018**, *15*, 368–378. [CrossRef]
13. Kahwaji, S.; White, M.A. Edible oils as practical phase change materials for thermal energy storage. *Appl. Sci.* **2019**, *9*, 1627. [CrossRef]
14. Faraj, K.; Faraj, J.; Hachem, F.; Bazzi, H.; Khaled, M.; Castelain, C. Analysis of underfloor electrical heating system integrated with coconut oil-PCM plates. *Appl. Therm. Eng.* **2019**, *158*, 113778. [CrossRef]
15. Saleel, C.A.; Mujeebu, M.A.; Algarni, S. Coconut oil as phase change material to maintain thermal comfort in passenger vehicles: An experimental analysis. *J. Therm. Anal. Calorim.* **2019**, *136*, 629–636. [CrossRef]
16. Irsyad, M.; Harmen. Heat transfer characteristics of coconut oil as phase change material to room cooling application. In Proceedings of the IOP Conference Series: Earth and Environmental Science, Tangerang, Indonesia, 3–5 October 2016.
17. Silalahi, A.O.; Sukmawati, N.; Sutjahja, I.M.; Kurnia, D.; Wonorahardjo, S. Thermophysical Parameters of Organic PCM Coconut Oil from T-History Method and Its Potential as Thermal Energy Storage in Indonesia. *IOP Conf. Ser. Mater. Sci. Eng.* **2017**, *214*, 12034. [CrossRef]
18. Silalahi, A.O.; Sutjahja, I.M.; Kurnia, D.; Wonorahardjo, S. Thermophysical parameters of organic PCM coconut oil from the T-history method and its variation with the chemical dopant. *J. Phys. Conf. Ser.* **2019**, *1204*, 012055. [CrossRef]
19. Putri, W.A.; Fahmi, Z.; Sutjahja, I.M.; Kurnia, D.; Wonorahardjo, S. Thermophysical parameters of coconut oil and its potential application as the thermal energy storage system in Indonesia. *J. Phys. Conf. Ser.* **2016**, *739*, 12065. [CrossRef]
20. Sri Rahayu, A.U.; Putri, W.A.; Sutjahja, I.M.; Kurnia, D.; Wonorahardjo, S. The effectiveness of organic PCM based on lauric acid from coconut oil and inorganic PCM based on salt hydrate $\text{CaCl}_2 \cdot 6\text{H}_2\text{O}$ as latent heat energy storage system in Indonesia. *J. Phys. Conf. Ser.* **2016**, *739*, 012119. [CrossRef]
21. Sutjahja, I.M.; Silalahi, A.O.; Kurnia, D.; Wonorahardjo, S. The role of particle dopant to the thermal conductivities of PCM coconut oil by means of the T-history method. *J. Phys. Conf. Ser.* **2019**, *1204*, 012156. [CrossRef]
22. Wonorahardjo, S.; Sutjahja, I.M.; Kurnia, D. Potential of Coconut Oil for Temperature Regulation in Tropical Houses. *J. Eng. Phys. Thermophys.* **2019**, *92*, 80–88. [CrossRef]
23. Wonorahardjo, S.; Sutjahja, I.M.; Kurnia, D.; Fahmi, Z.; Putri, W.A. Potential of thermal energy storage using coconut oil for air temperature control. *Buildings* **2018**, *8*, 95. [CrossRef]
24. Alqahtani, T.; Mellouli, S.; Bamasag, A.; Askri, F.; Phelan, P.E. Experimental and numerical assessment of using coconut oil as a phase-change material for unconditioned buildings. *Int. J. Energy Res.* **2020**, *44*, 5177–5196. [CrossRef]
25. Jeon, J.; Park, J.H.; Wi, S.; Yang, S.; Ok, Y.S.; Kim, S. Characterization of biocomposite using coconut oil impregnated biochar as latent heat storage insulation. *Chemosphere* **2019**, *236*, 124269. [CrossRef]
26. Udangawa, W.M.R.N.; Willard, C.F.; Mancinelli, C.; Chapman, C.; Linhardt, R.J.; Simmons, T.J. Coconut oil-cellulose beaded microfibers by coaxial electrospinning: An eco-model system to study thermoregulation of confined phase change materials. *Cellulose* **2019**, *26*, 1855–1868. [CrossRef]
27. Oktay, B.; Baştürk, E.; Kahraman, M.V.; Apohan, N.K. Designing Coconut Oil Encapsulated Poly(stearyl methacrylate-co-hydroxyethyl metacrylate) Based Microcapsule for Phase Change Materials. *ChemistrySelect* **2019**, *4*, 5110–5115. [CrossRef]
28. Németh, B.; Németh, Á.S.; Ujhidy, A.; Tóth, J.; Trif, L.; Gyenis, J.; Feczko, T. Fully bio-originated latent heat storing calcium alginate microcapsules with high coconut oil loading. *Sol. Energy* **2018**, *170*, 314–322. [CrossRef]
29. Saraç, E.G.; Öner, E.; Kahraman, M.V. Microencapsulated organic coconut oil as a natural phase change material for thermo-regulating cellulosic fabrics. *Cellulose* **2019**, *26*, 8939–8950. [CrossRef]
30. Uysal, D.; Dilara, Ç.; Eva, B.; Ángeles, B.M.; Jaime, G.; Pablo, D. Annals of the University of Oradea Fascicle of Textiles; Leatherwork Microencapsulation of Bio-Degradable pcm Using Coconut Oil and Ethyl Celulose. pp. 29–32. Available online: <http://textile.webhost.uoradea.ro/Annals/Vol%20XX%20nr.%202-2019/Textile/Art.%20no.%20373%20pag.%2029-32.pdf> (accessed on 8 May 2022).
31. Irsyad, M.; Indartono, Y.S.; Suwono, A.; Pasek, A.D. Thermal characteristics of non-edible oils as phase change materials candidate to application of air conditioning chilled water system. *IOP Conf. Ser. Mater. Sci. Eng.* **2015**, *88*, 012051. [CrossRef]

32. Dinesh, K.; Tamilvanan, A.; Vaishnavi, S.; Gopinath, M.; Mohan, K.S.R. Biodiesel production using *Calophyllum inophyllum* (Tamanu) seed oil and its compatibility test in a CI engine. *Biofuels* **2019**, *10*, 347–353. [CrossRef]
33. Raj, M.T.; Kandasamy, M.K.K. Tamanu oil-an alternative fuel for variable compression ratio engine. *Int. J. Energy Environ. Eng.* **2012**, *3*, 18. [CrossRef]
34. Yarrapragada, K.S.S.R.; Krishna, B.B. Impact of tamanu oil-diesel blend on combustion, performance and emissions of diesel engine and its prediction methodology. *J. Brazil. Soc. Mech. Sci. Eng.* **2017**, *39*, 1797–1811. [CrossRef]
35. Rao, Y.K.; Krishna, B.B. Modeling diesel engine fueled with tamanu oil-Diesel blend by hybridizing neural network with firefly algorithm. *Renew. Energy* **2019**, *134*, 1200–1212. [CrossRef]
36. Mohanraj, T.; Mohan Kumar, K.M. Operating characteristics of a variable compression ratio engine using esterified tamanu oil. *Int. J. Green Energy* **2013**, *10*, 285–301. [CrossRef]
37. Ginigini, J.; Lecellier, G.J.; Nicolas, M.; Nour, M.; Hnawia, E.; Lebouvier, N.; Herbette, G.; Lockhart, P.; Raharivelomanana, P. Chemodiversity of *Calophyllum inophyllum* L. oil bioactive components related to their specific geographical distribution in the South Pacific region. *PeerJ* **2019**, *2019*, e6896. [CrossRef]
38. Paroutoglou, E.; Afshari, A.; Fojan, P.; Hultmark, G. Investigation of Thermal Behavior of Paraffins, Fatty Acids, Salt Hydrates and Renewable Based Oils as PCM. Available online: <https://www.atlantis-pess.com/proceedings/ires-20/125952227> (accessed on 8 May 2022).
39. Rasband, W.S. ImageJ. Available online: <http://imagej.nih.gov/ij/> (accessed on 10 February 2021).
40. Paroutoglou, E.; Fojan, P.; Gurevich, L.; Hultmark, G.; Afshari, A. Thermal Analysis of Organic and Nanoencapsulated Electrospun Phase Change Materials. *Energies* **2021**, *14*, 995. [CrossRef]
41. Tipvarakarnkoon, T.; Blochwitz, R.; Senge, B. Rheological Properties and Phase Change Behaviors of Coconut fats and Oils. 2008. Available online: <https://nordicrheologysociety.org/Content/Transactions/2008/Posters/Tipvarakarnkoon%20et%20al.pdf> (accessed on 8 May 2022).
42. Maruyama, J.M.; Soares, F.A.S.D.M.; D'Agostinho, N.R.; Gonçalves, M.I.A.; Gioielli, L.A.; Da Silva, R.C. Effects of emulsifier addition on the crystallization and melting behavior of palm olein and coconut oil. *J. Agric. Food Chem.* **2014**, *62*, 2253–2263. [CrossRef] [PubMed]
43. Wiyani, L.; Aladin, A.; Yani, S. Rahmawati Stability of virgin coconut oil emulsion with mixed emulsifiers Tween 80 and Span 80. *ARPN J. Eng. Appl. Sci.* **2016**, *11*, 5198–5202.
44. da Silva Gulão, E.; de Souza, C.J.F.; da Costa, A.R.; da Rocha-Leão, M.H.M.; Garcia-Rojas, E.E. Stability and rheological behavior of coconut oil-in-water emulsions formed by biopolymers. *Polimeros* **2018**, *28*, 413–421. [CrossRef]
45. Urbánková, L.; Kašpárková, V.; Egner, P.; Rudolf, O.; Korábková, E. Caseinate-stabilized emulsions of black cumin and tamanu oils: Preparation, characterization and antibacterial activity. *Polymers* **2019**, *11*, 1951. [CrossRef] [PubMed]
46. Mohamadi, P.S.; Hivechi, A.; Bahrami, H.; Hemmatinegad, N.; Milan, P.B. Antibacterial and biological properties of coconut oil loaded poly(ϵ -caprolactone)/gelatin electrospun membranes. *J. Ind. Text.* **2021**, 1528083721991595. [CrossRef]
47. Jaganathan, S.K.; Mohan Prasath, M.; Fauzi Ismail, A.; Manikandan, A.; Gomathi, N. Production and hemocompatibility assessment of novel electrospun polyurethane nanofibers loaded with dietary virgin coconut oil for vascular graft applications. *J. Bioact. Compat. Polym.* **2018**, *33*, 210–223. [CrossRef]

Chapter 10

Paper V

A Numerical Parametric Study of a Double-Pipe LHTES Unit with PCM Encapsulated in the Annular Space

Evdoxia Paroutoglou, Peter Fojan, Leonid Gurevich, Simon Furbo, Jianhua Fan,
Marc Medrano and Alireza Afshari

The paper has been published in Sustainability Vol. 14, 13317, 2022.

Article

A Numerical Parametric Study of a Double-Pipe LHTES Unit with PCM Encapsulated in the Annular Space

Evdoxia Paroutoglou ^{1,*}, Peter Fojan ², Leonid Gurevich ² , Simon Furbo ³, Jianhua Fan ³ , Marc Medrano ⁴ and Alireza Afshari ¹

¹ Department of Energy Performance, Indoor Environment and Sustainability of Buildings, Aalborg University, 2450 København, Denmark

² Department of Materials and Production, Aalborg University, 9220 Aalborg, Denmark

³ Department of Civil and Mechanical Engineering, Technical University of Denmark, 2800 Kongens Lyngby, Denmark

⁴ Department of Computing and Industrial Engineering, University of Lleida, 1300 Lleida, Spain

* Correspondence: evp@build.aau.dk

Abstract: Latent heat thermal energy storage (LHTES) with Phase Change Materials (PCM) represents an interesting option for Thermal Energy Storage (TES) applications in a wide temperature range. A tubular encapsulation model of an LHTES with PCM was developed, and the calculated data were analyzed. In addition, a parametric analysis for the preferable system geometry is presented. Organic paraffin RT18 with a melting point of 18 °C was utilized as PCM for different geometries of LHTES, and the addition of internal and external fins and their influence on LHTES thermal conductivity was investigated. One-step heat exchange from outdoor air to PCM and from PCM to water characterizes the LHTES system in solidification and melting processes, respectively. A 2D axisymmetric model was developed using Comsol Multiphysics 6.0. The LHTES unit performance with PCM organic paraffin RT18 encapsulated in electrospun fiber matrices was analyzed. The study results show that longer internal fins shorten the melting and solidification time. Direct contact of PCM electrospun fiber matrix with 23 °C water showed instant melting, and the phase change process was accelerated by 99.97% in the discharging cycle.

Keywords: LHTES; PCM; numerical simulation; Comsol Multiphysics



Citation: Paroutoglou, E.; Fojan, P.; Gurevich, L.; Furbo, S.; Fan, J.; Medrano, M.; Afshari, A.

A Numerical Parametric Study of a Double-Pipe LHTES Unit with PCM Encapsulated in the Annular Space. *Sustainability* **2022**, *14*, 13317. <https://doi.org/10.3390/su142013317>

Academic Editor: Francesco Riganti Fulginei

Received: 22 September 2022

Accepted: 13 October 2022

Published: 17 October 2022

Publisher's Note: MDPI stays neutral with regard to jurisdictional claims in published maps and institutional affiliations.



Copyright: © 2022 by the authors. Licensee MDPI, Basel, Switzerland. This article is an open access article distributed under the terms and conditions of the Creative Commons Attribution (CC BY) license (<https://creativecommons.org/licenses/by/4.0/>).

1. Introduction

Heating, ventilation, and air-conditioning (HVAC) systems are designed to maintain a satisfactory indoor climate in residential and commercial buildings. Latent Heat Thermal Energy Storage (LHTES) with Phase Change Materials (PCM) is a promising technology for improving the efficiency of HVAC systems due to its high energy-storage density. When undergoing melting and solidification, PCM stores and releases a significant amount of latent heat (kJ/kg) at a relatively constant temperature. In this way, a relatively small volume of material facilitates the storage of a relatively large amount of energy within a narrow temperature range. Several studies [1–8] have reviewed TES applications with PCM. PCMs used in LHTES applications are selected based on the required thermal properties according to the application and climate conditions, e.g., the temperature range (°C) and the latent heat of fusion (kJ/kg).

Several finite element simulation studies [9–18] have addressed the influence of geometries on LHTES performance. The discharging thermal cycles of thermal energy storage with NaNO₃/KNO₃-PCM in an AISI 321 tube were studied by Zhang et al. [9]. Numerical analysis results and experimental data were in line, and inserts of metallic foam/sponge had an insignificant effect on the solidification rate of salt [9]. A high-temperature LHTES system for concentrated solar power (CSP) plants with magnesium chloride as PCM enhanced with graphite foam has also been analyzed by Zhao et al. [10]. The addition of

graphite foam in the PCM increased the exergy efficiency and improved the heat transfer processes [10]. Aadmi et al. [11] studied experimentally and numerically (with Comsol Multiphysics) a hot plate apparatus with PCM composites of epoxy resin paraffin wax. It was discovered that the container geometry affected the melting of PCM and a higher PCM content improved the LHTES capacity. $\text{KNO}_3\text{--NaNO}_3$ was encapsulated in a spherical shell, and no cracking was observed in the shell in an experimental and numerical investigation [12]. In another study by Arena et al. [13], the mushy zone of a finned double-pipe LHTES with paraffin RT35 was examined in three cases of heat transfer by convection and two cases for laminar and turbulent flow. Larger values for the mushy zone constant, representing the mushy area, led to a reduction of natural convection in the charging and discharging thermal cycles. A TES system with composite epoxy resin spherical shape paraffin wax RT27 was studied by Moulahi et al. [14], and the mushy zone proved to have an impact on the melting range. A numerical study of a PCM-air heat exchanger with dodecanoic acid was conducted by Herbingier et al. [15], and a higher heat transfer rate was observed for smaller heat exchanger channels and a higher air temperature. LHTES system performance under partial load in both charging and discharging cycles has also been studied by Arena et al. [16]. At a melting fraction of 0.75 and 0.90, the duration of the thermal cycles decreased up to 50% and the stored energy up to 30% [16]. The thermal properties of a PU-PCM composite were experimentally and numerically examined by Purohit and Sistla [17], and the study output indicated nucleation and crystallization domination of salt hydrate. Afsharpanah et al. [18–20] focused on several enhancement methods, such as porous foams, fins, and nanomaterials. A copper foam enhancement technique [18] increased the phase change rate by 92.5%.

In other studies [19,21–24], various thermal conductivity enhancement methods (e.g., examination of various geometries and addition of fins) have been analyzed for double-pipe LHTES systems. The effect of sinusoidal wavy fins has been studied by Shahsavari et al. [21,22] and achieved a melting/solidification time reduction of 43.49% and 17.81% with a wavy fin with amplitude and wavelength of 2 and 1 mm, respectively. The heat transfer enhancement with six configurations of different fin numbers and orientations of a double-pipe LHTES has been studied by Boulaktout [23], and it was shown that fewer fins with a proper orientation could be an effective geometry solution. The impact of fin type and orientation of a double pipe heat exchanger with N-eicosane as a PCM has been numerically analyzed by Nicholls et al. [24], and the transversal corrugated fin design exhibited shorter charging and discharging time. Anchor-type longitudinal fins [19] in shell and tube storage lead to a melting process slower up to 201.5% than the solidification process.

In experimental and analytical studies, PCM with a phase change temperature range of 15 to 20 °C has been reviewed in the author's previous work [8]. Several materials comprising the classes of salt hydrates, organic paraffins, organic fatty acids, and renewable-based oils in the phase change temperature range of 15 to 20 °C have been experimentally identified for their thermal properties in the author's previous studies [25–27]. Among the examined PCM, organic paraffin RT18 exhibited the most stable performance and the highest latent heat (J/g) after being subjected to 200 thermal cycles, equivalent to a six-month lifetime. PCM in emulsion, polymer, and electrospun fiber matrix have been analyzed experimentally [25–27]. The thermal properties of the electrospun fiber matrix of organic paraffin RT18 have also been reported [25].

Several studies have focused on the finite element design of LHTES systems, while the addition of fins has also been analyzed [21–24]. The present study examines the potential use of organic paraffin RT18 in pure and fiber form as a PCM in an LHTES system with different geometry configurations in both charging and discharging thermal cycles. The LHTES system is characterized by a one-step heat exchange from outdoor air to the PCM and from the PCM to the water. The project's overall aim is to develop a heat exchanger for night cooling applications in office buildings.

2. Materials and Methods

2.1. LHTES System Design

The aim of this project was to exploit the latent heat of fusion in an LHTES by using materials with a melting point around room temperature, so energy reduction for cooling can be achieved. In the current study, the encapsulated PCM layer in the LHTES facilitates the absorption of rejected heat during occupied hours and the release of heat to the environment at night. In the charging phase that occurs during night hours, cold outdoor air cools down the PCM, which changes state from liquid to solid. In the discharging phase during occupied hours, the PCM absorbs heat from the return water flow changing state from solid to liquid. The charging (solidification) and discharging (melting) diagrams of LHTES are presented in Figure 1. In the discharging phase, water is circulated through the inner copper pipe with a constant mass flow rate of 0.038 kg/s in a turbulent flow. The HTF (water) temperature was set to 23 °C at the inlet of the LHTES unit for discharge. In the charging phase, solidification was achieved through the air to the tube wall and PCM heat transfer; thus, the water flow was neglected. Steady conditions for air temperature are set at 10 °C in the charging/solidification case. The cold night air is circulated through fans when lamellas are open during the night, and the solidification of PCM progresses. In that way, natural and forced convection are assumed in the charging phase, and the water pump stops during the night, not circulating the water. The current analysis focuses on the most significant parameters for the LHTES unit characterization, such as charge and discharge cycle duration and energy stored and released. Thus, eleven different charging and discharging processes were simulated for different geometries and LHTES unit configurations, as shown in Table 1. In this numerical study, a double-pipe LHTES unit was analyzed. The unit includes an inner copper pipe with water flowing through it, surrounded by a PCM layer and an external copper pipe. In the charging phase, heat exchange is achieved from outdoor air to PCM, and in the discharging phase, from water to PCM.

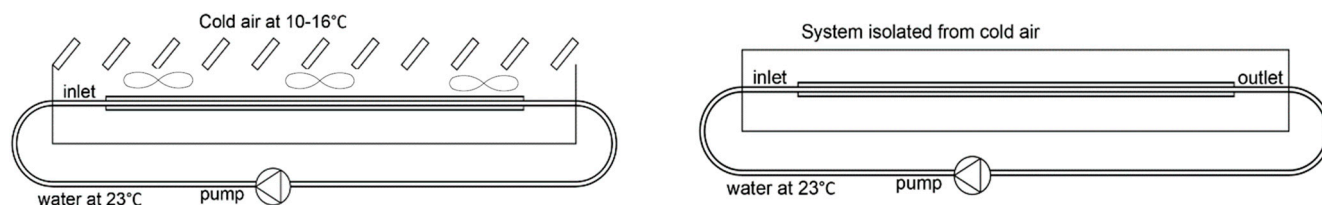


Figure 1. Charging (left) and discharging (right) diagram of LHTES.

Table 1. Geometry of models studied in cases 1–6.

Case	Copper PCM Pipe Inner Diameter (m)	Thickness of PCM Pipe (m)	PCM Mass (kg)	Internal Fins	External Fins	Fins Width (m)		Fins Height (m)	Distance between Fins (m)
1	0.026797 m	0.000889 m	0.158			-	-	-	-
2	0.0327914 m	0.0010668 m	0.257			-	-	-	-
3	0.0387858 m	0.0012446 m	0.376			-	-	-	-
4	0.0387858 m	0.0012446 m	0.362	x		0.0065 m	0.0004 m	0.0021 m	
5	0.0387858 m	0.0012446 m	0.352	x		0.00975 m	0.0004 m	0.0021 m	
6	0.0387858 m	0.0012446 m	0.364	x		0.00975 m	0.0004 m	0.0046 m	
7	0.0387858 m	0.0012446 m	0.376		x	0.0065 m	0.0004 m	0.0021 m	
8	0.0387858 m	0.0012446 m	0.376		x	0.00975 m	0.0004 m	0.0021 m	
9	0.0387858 m	0.0012446 m	0.376		x	0.00975 m	0.0004 m	0.0046 m	
10	0.0387858 m	0.0012446 m	0.352	x	x	Int. fins 0.00975 m	Ext. fins 0.0065 m	0.0004 m	0.0021 m
11	0.0387858 m	0.0012446 m	0.198			-	-	-	-

The double-pipe LHTES unit configuration with and without fins analyzed in this study are presented in Figures 2–4. A parametric analysis was conducted for the system's geometry. The studied geometry of the model replicated a tubular double-pipe LHTES. Type M copper tubes with a length of 0.4 m were used for both pipes. The water pipe's

inner diameter (m) is 11.43 mm with a thickness of 0.635 mm. The double-pipe model's geometry is presented in Table 1. A novel LHTES unit consisting of a water pipe with encapsulated PCM electrospun fiber matrix has also been studied (Figure 5).

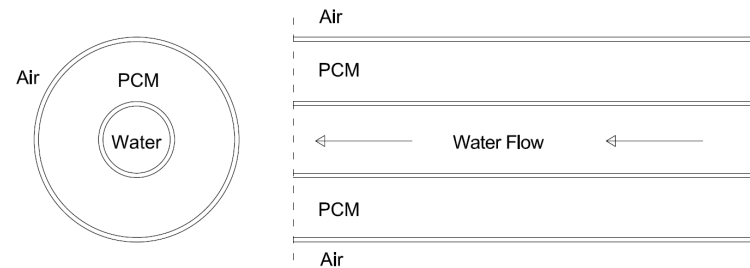


Figure 2. Configuration of double-pipe LHTES unit without fins.

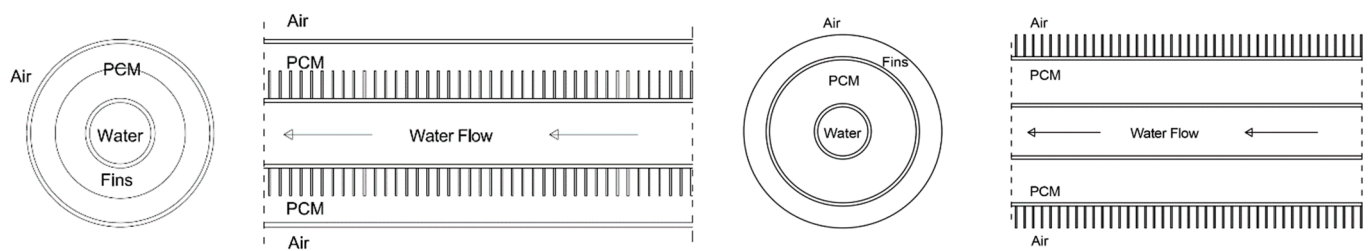


Figure 3. Configuration of double-pipe LHTES unit with fins on the internal pipe (left), LHTES unit with fins on the external pipe (right).

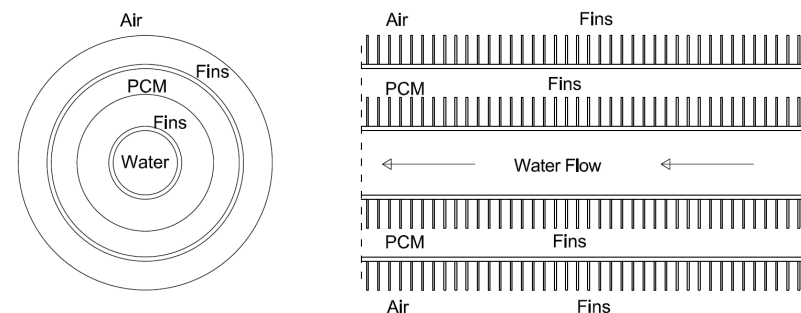


Figure 4. Configuration of double-pipe LHTES unit with fins on the internal and external pipes of the LHTES unit.

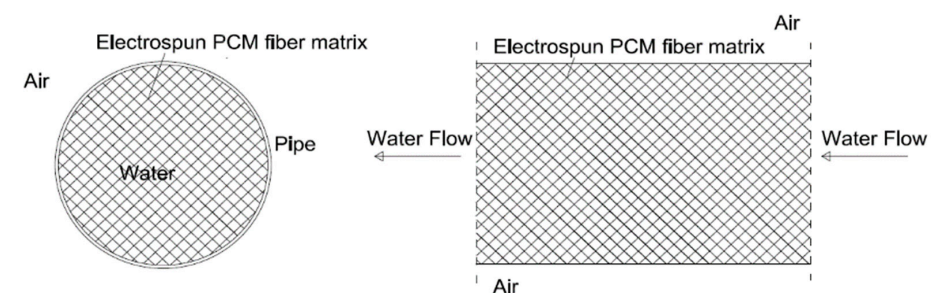


Figure 5. Configuration of the LHTES unit with RT18 electrospun fiber matrix as PCM.

The thermophysical properties provided by the manufacturers and the experimental thermal properties of organic paraffin RT18 in pure and electrospun fiber form are presented in Table 2. The PCM experimental properties have been previously analyzed [25,26], and the results were acquired in the laboratory of materials and production at Aalborg University. In the discharging phase, water was considered the heat transfer fluid (HTF), flowing with a turbulent flow and mass flow rate of 0.038 kg/s. The inlet water temperature for both charge and discharge was set to 23 °C. During the charging process, forced convection is

utilized with a convective heat flux of a heat transfer coefficient of 100 W/m²K and air temperature of 10 °C (the fan is blowing air over the LHTES). The LHTES system was isolated from air during discharging. Type M Copper pipes were selected for both unit's pipes with a better heat transfer rate than aluminum pipes.

Table 2. Thermophysical properties of organic paraffin RT18.

Theoretical Properties	
Density (Solid)	0.88 kg/L
Density (Liquid)	0.77 kg/L
Heat Capacity (Solid)	2 kJ/kg·K
Heat Capacity (Liquid)	2 kJ/kg·K
Latent Heat of Fusion	260 kJ/kg
Thermal Conductivity	0.2 W/m·K
Melting Point	18 °C
Experimental Properties (Pure RT18)	
Melting temperature	17.5 °C
Solidification temperature	15.4 °C
Latent heat of melting	137.8 kJ/kg
Latent heat of solidification	139.3 kJ/kg
Experimental Properties (RT18 Electrospun Fiber Matrix)	
Melting temperature	17.3 °C
Solidification temperature	15.2 °C
Latent heat of melting	102.1 kJ/kg
Latent heat of solidification	82.2 kJ/kg
Porosity of fiber matrix	0.474

2.2. Numerical Model

The model was developed with Comsol Multiphysics 6.0 using different geometrical configurations in a two-dimensional axisymmetric interface. The finite element method and linear shape functions were used for all physics interfaces. The implicit backward differentiation formula (BDF) was the used stepping method with a time step of 10 s. The interval of $\Delta T_{1 \rightarrow 2}$ around the phase change temperature was investigated experimentally and set to 5K in melting and 2.5 K in solidification processes. Within the interval $\Delta T_{1 \rightarrow 2}$, there is a “mushy zone” with mixed material properties. Cases 1–3 use a double pipe unit with no fins, while cases 4–6 and 7–9 involve double pipe with internal and external fins, respectively. Case 10 addresses a double pipe with internal and external fins. Case 11 examines a single pipe encapsulating a PCM electrospun fiber matrix. An extra fine mesh was used in the Comsol model for a minimum error range, and the average element quality in all geometries was 0.81–0.89. In the discharging phase, we decided to couple together, in a time-dependent study, the two single-physics codes of turbulent flow and heat transfer in solids and liquids in a multiphysics system. This method transfers information between each module during the solution process. In the charging phase, a time-dependent study of heat transfer in solids and liquids was used. A $k-\epsilon$ model using the RANS (Reynolds-Averaged Navier–Stokes) equation was selected for the simulation of turbulent flow (Equation (1)). For the heat transfer in solids and liquids, the energy Equation (2) was used. The heat transfer process's effective density, heat capacity, mass fraction, and thermal conductivity in the phase change module are described by Equation (3)–(6).

$$\rho \frac{\partial u}{\partial t} + \rho(u \nabla) u = \nabla[-Pl + K] + F, \quad \rho \nabla u = 0 \quad (1)$$

$$\rho C_P \frac{\partial T}{\partial t} + \rho C_P u \nabla_T + \nabla_q = Q, \quad q = -k \nabla_T \quad (2)$$

$$\rho = \theta_1 \rho_{ph1} + \theta_2 \rho_{ph2}, \quad \theta_1 + \theta_2 = 1, \quad (3)$$

$$C_P = \frac{1}{\rho} \left(\theta_1 \rho_{ph1} C_{P,1} + \theta_2 \rho_{ph2} C_{P,2} \right) + L_{1 \rightarrow 2} \frac{\partial a_m}{\partial T}, \quad (4)$$

$$a_m = \frac{1}{2} \frac{\theta_2 \rho_{ph2} - \theta_1 \rho_{ph1}}{\theta_1 \rho_{ph1} + \theta_2 \rho_{ph2}}, \quad (5)$$

$$k = \theta_1 k_1 + \theta_2 k_2 \quad (6)$$

3. Results and Discussion

3.1. Validation Model Analysis

Medrano et al. have studied different configurations of LHTES systems [28]. The parameters of two experiments with a turbulent flow of 0.38 m³/h and 0.35 m³/h were presented in Table 3. The double-pipe heat exchanger with encapsulated PCM in the annular space configuration previously presented [28] is the same configuration as the one analyzed in the current study. For this reason, the model created in Comsol Multiphysics was adjusted to have the same geometry and was validated with previous experimental data [24]. The parameters studied for the validation were the inlet and outlet temperature of the water, the temperature of the PCM-copper pipe wall, as well as the melting time of the PCM. The melting time of the PCM was calculated through the solid-to-liquid phase indicator for average surface in the numerical simulation. In the experimental process, an uncertainty of 30 s for the time interval was calculated. The percentage difference between the experimental and calculated melting time for the validation case is shown in Table 4. The percentage difference is calculated according to Equation (7). The percentage differences for the melting time are below 5% and 8.3%, which is considered a positive outcome.

$$\% \text{ difference} = \frac{|\text{Experimental value} - \text{Numerical value}|}{\text{Experimental value}} \quad (7)$$

Table 3. Parameters of experiments.

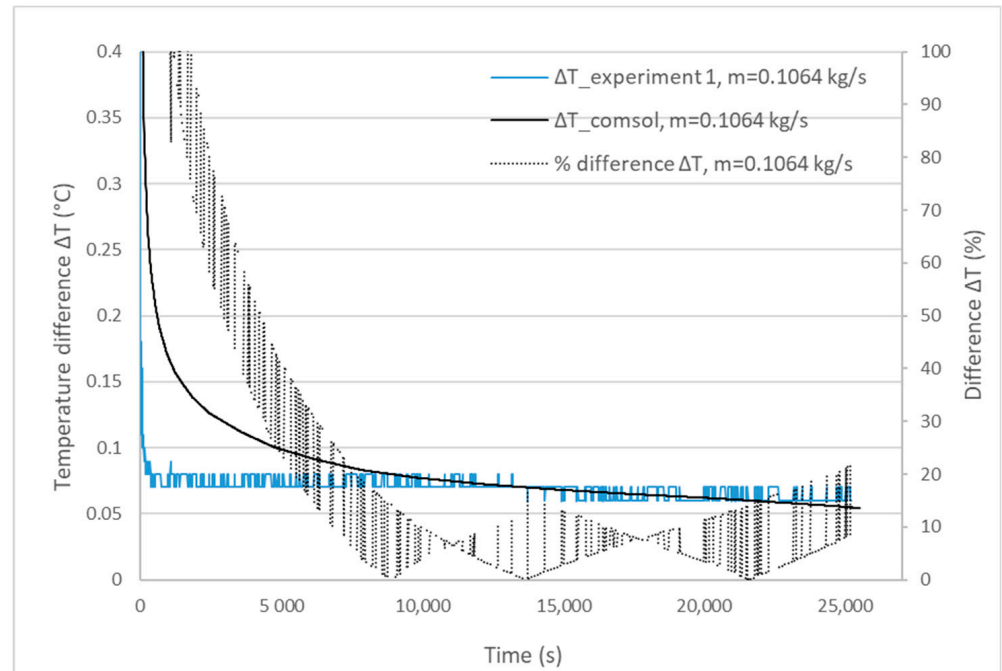
Experiment	Process	Temperature Conditions		Turbulent Flow	PCM Properties		Air Temperature (°C)
		Water Inlet (°C)	PCM at Start (°C)	Volumetric Flow Rate (m ³ /h)	Latent Heat (J/g)	Phase Change Temp. (°C)	
1	Charge (Melting)	50	24	0.38	157	35	22–24
2	Charge (Melting)	50	24	0.35	157	35	22–24

Table 4. Experimental/Numerical melting time.

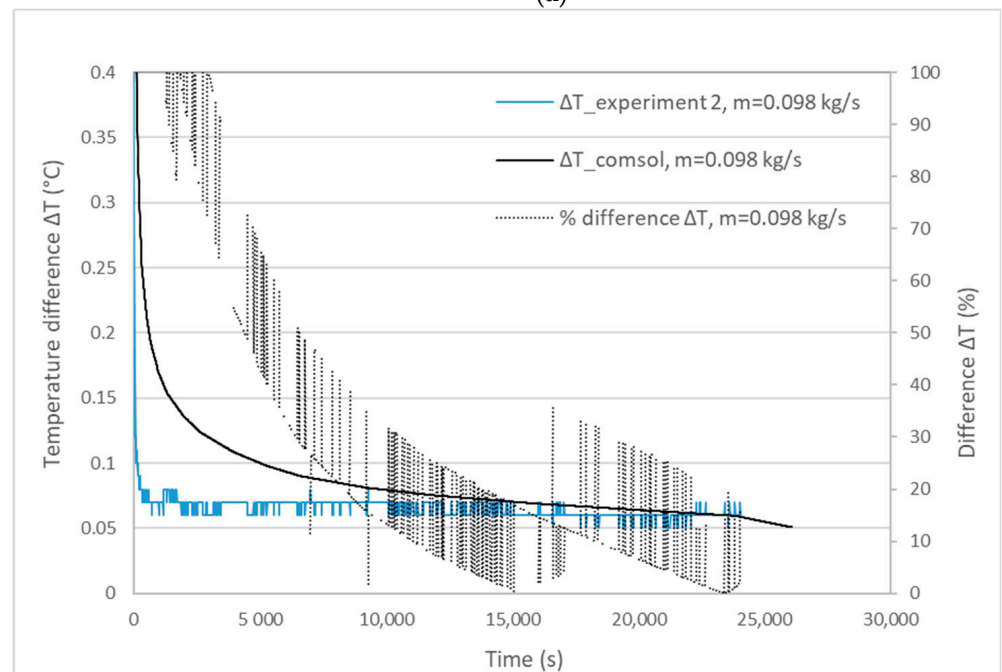
Experiment	Mass Flow Rate (kg/s)	Experimental Melting Time	Calculated Melting Time	Percentage Difference
1	0.1064	25,200 s	26,470 s	5% < 10%
2	0.0980	24,060 s	26,060 s	8.3% < 10%

In Figure 6a,b, the temperature difference between inlet and outlet water temperatures, as well as the % differences of ΔT for the two mass flow rates of 0.1064 kg/s and 0.098 kg/s in the experiment and the simulation, are presented. ΔT water temperature difference % for different mass flow rates was calculated with Equation (7). In the experimental measurement, the inlet temperature at the beginning of the testing process fluctuates. As can be observed in Figure 6, the temperature difference between the inlet and outlet water

temperature graphs did not converge at the start of the experimental/simulation time. The temperature in the PCM-copper wall boundary and the temperature difference (ΔT) between the experiment and the simulation for the two mass flow rates of 0.1064 kg/s and 0.098 kg/s are depicted in Figures 7a and 7b, respectively. The numerical simulation output is in good agreement with the experimental data. An error of 0.1 K was estimated for the calibrated temperature sensors in the experimental analysis.



(a)



(b)

Figure 6. Inlet and outlet water temperature in experiments/numerical simulation for mass flow rate (a) $m = 0.1064$ kg/s, (b) $m = 0.098$ kg/s.

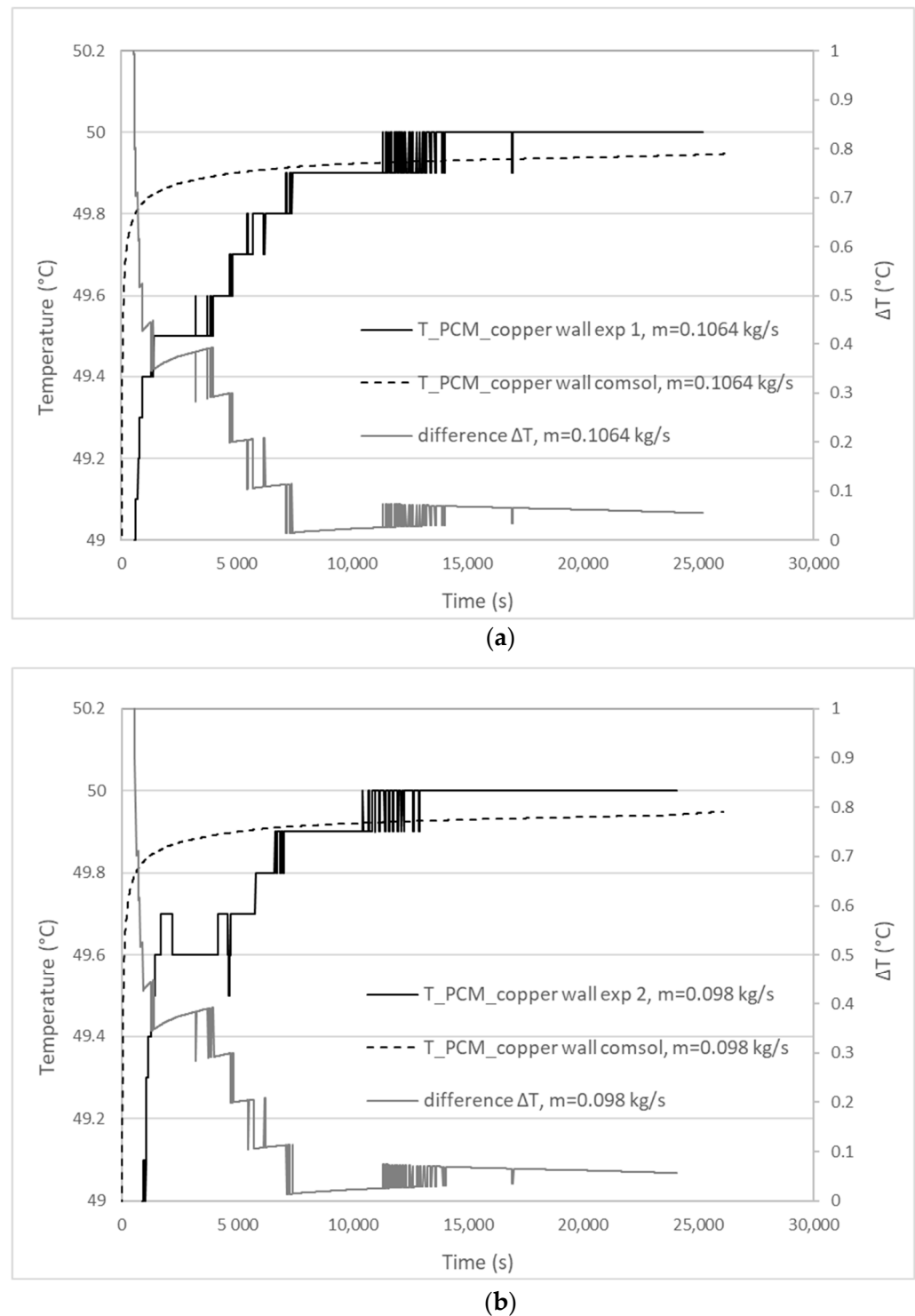


Figure 7. Temperature of PCM-copper wall in experiments/numerical simulation for mass flow rate (a) $m = 0.1064$ kg/s, (b) $m = 0.098$ kg/s.

3.2. Charging and Discharging Thermal Cycles

During the charging (solidification) process, the heat transfer mechanisms are conduction, forced convection (mechanical means-fans), and natural convection. In the discharging cycle (melting), conduction and natural convection occur in the phase change process. Natural convection plays a significant role at the beginning of the solidification process and when the melting fraction is increased in the melting process. The numerical simulation of solidification (charging) and melting (discharging) time is presented in Table 5. In cases 1,

2, and 3 (without fins), the discharging process lasts longer than the charging process. As expected, the duration of the charging and discharging processes gets longer with a higher PCM volume in the system. The PCM mass (kg) is reduced in the internal fins cases 4, 5, and 6 compared to base case 3 by 3.7%, 6.4%, and 3.2%, respectively. Due to PCM mass reduction, the charging and discharging time (cases 4–6 with internal fins) is significantly decreased compared to case 3. Longer internal fins reduce the charging and discharging time, while the melting/solidification time is increased with a longer distance between fins. The volumes of PCM in the cases of external fins are equal to the volume of PCM in case 3. In cases 7, 8, and 9 (with external fins), longer external fins decrease the melting and solidification time. When the distance between fins gets longer, the solidification time decreases, but the melting time increases (compared to case 8). The PCM mass reduction for case 10 with internal and external fins is estimated at 6.4%. As anticipated, the addition of internal and external fins (case 10) shows a reduction in time for both charging and discharging. The PCM mass in case 11 of the fiber matrix is reduced by 47.3% compared to base case 3. In case 11, the solidification time is shorter compared to case 3. The last case examined (analyzing the electrospun fiber matrix) exhibits a concise melting time of 4 s, which is expected due to the direct contact of the fiber matrix with the encapsulated PCM and water at 23 °C.

Table 5. Numerical simulation melting and solidification time.

Case	Charging (Solidification) Time	Discharging (Melting) Time
1	3310 s	3420 s
2	4090 s	7070 s
3	6940 s	13,620 s
4	5500 s	3220 s
5	4060 s	1230 s
6	4500 s	1530 s
7	5830 s	14,590 s
8	5710 s	14,070 s
9	4520 s	14,510 s
10	3040 s	1040 s
11	4780 s	4 s

The phase evolution at MF (melting fraction) equal to 0.75, 0.5, and 0.25 in charging and discharging processes for the eleven different geometries tested are presented in Figure 8. The blue-colored region represents the solid fraction in the phase evolution, and the red region represents the liquid fraction.

In the melting phase (discharging), the inner water tube wall is at a higher temperature, and the melted PCM is heated and moving due to buoyancy currents.

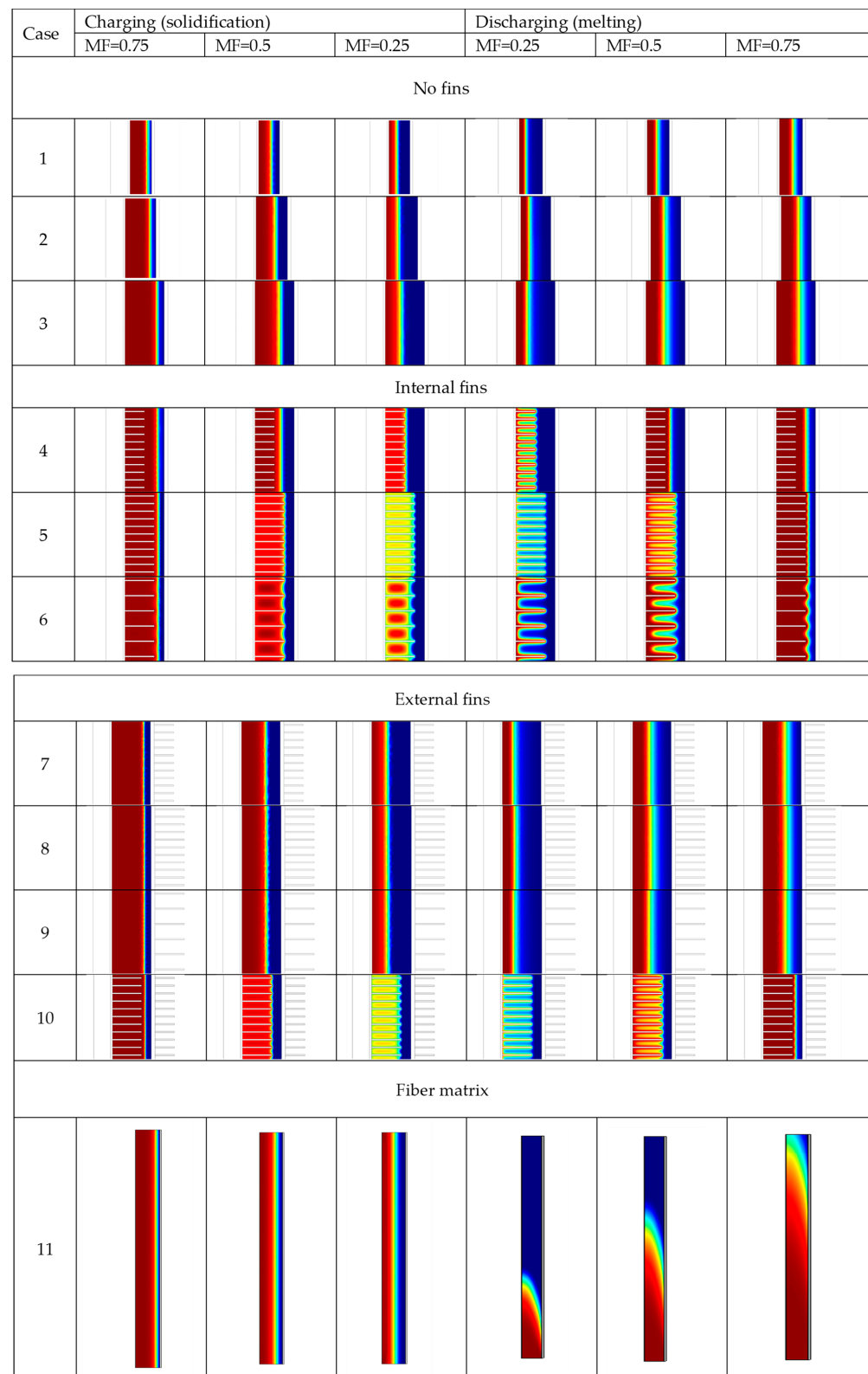


Figure 8. Phase evolution at MF = 0.75, 0.5 and 0.25.

The charge and discharge percentage during the thermal cycle duration are represented by the melting fraction (MF) graphs. The melting fraction is the ratio between the liquid/solid phase PCM volume and the total PCM volume. The MF graphs representing the variation between the solid-liquid phase of PCM and the melting front during the charging and discharging processes are depicted in Figure 9. The melting fraction is always 0 initially

for the discharging process (PCM is solid) and 1 for the charging process (PCM is liquid). In case 3, the MF curve (Figure 9a) represents a slower melting fraction evolution during the charging process than in all other cases. The external fins in cases 7, 8, and 9 MF curves (Figure 9c) converge in the charging and discharging process. In the discharging process, the MF evolution of internal fins in cases (4–6) (Figure 9b) is evidently faster than the MF evolution of the external fins in cases (7–9) (Figure 9c). Case 1 (Figure 9a) and case 10 (Figure 9d) follow the same trend during charging. Case 10 (Figure 9d), during the discharging, exhibits a faster MF evolution than case 1 (Figure 9a). Case 1 (Figure 9a) and case 11 (Figure 9e) converge during charging, while case 11 represents a swift MF evolution in the discharging phase.

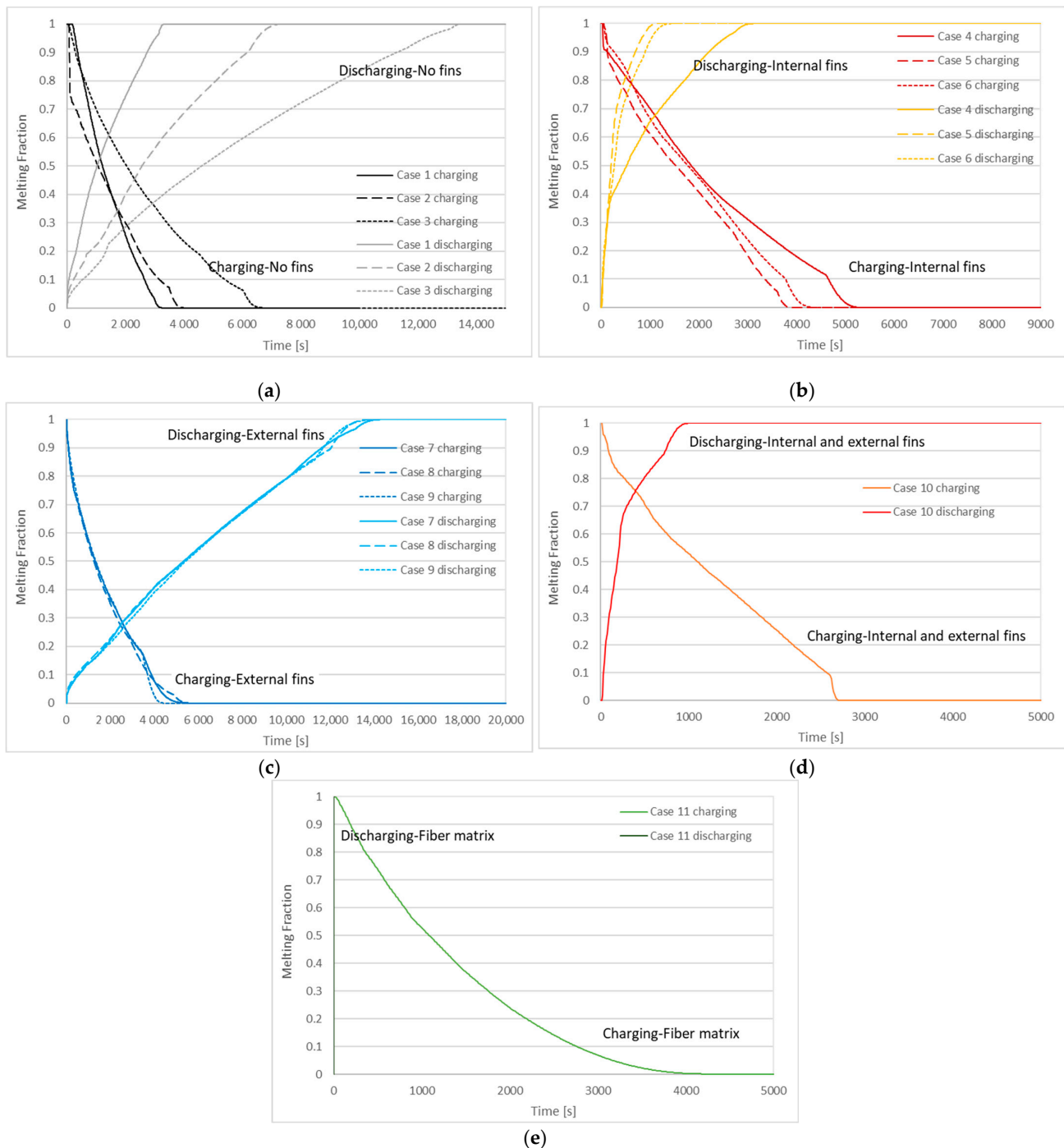


Figure 9. Melting fraction during charging and discharging processes (a) cases 1–3, (b) cases 4–6, (c) cases 7–9, (d) case 10, (e) case 11.

The surface average PCM temperature profile during the charging and discharging processes are depicted in Figure 10. In the charging phase, the temperature difference between the cold air (10 °C) and PCM drives the heat transfer rate inside the storage system. The decrease (charging) and increase in temperature versus time are analyzed in Figure 9. The solidification process is initiated at 15.4 °C for cases 1–10 (Figure 10a–d) and at 15.21 °C for case 11 (Figure 10e). The melting process starts at 17.51 °C for cases 1–10 (Figure 10a–d) and 17.33 °C for case 11 (Figure 10e). Throughout the melting process (discharging), sensible heat from the inner water tube is initially absorbed by PCM in a solid state. Then the PCM temperature increases, and natural convection is initiated when the melting process progresses.

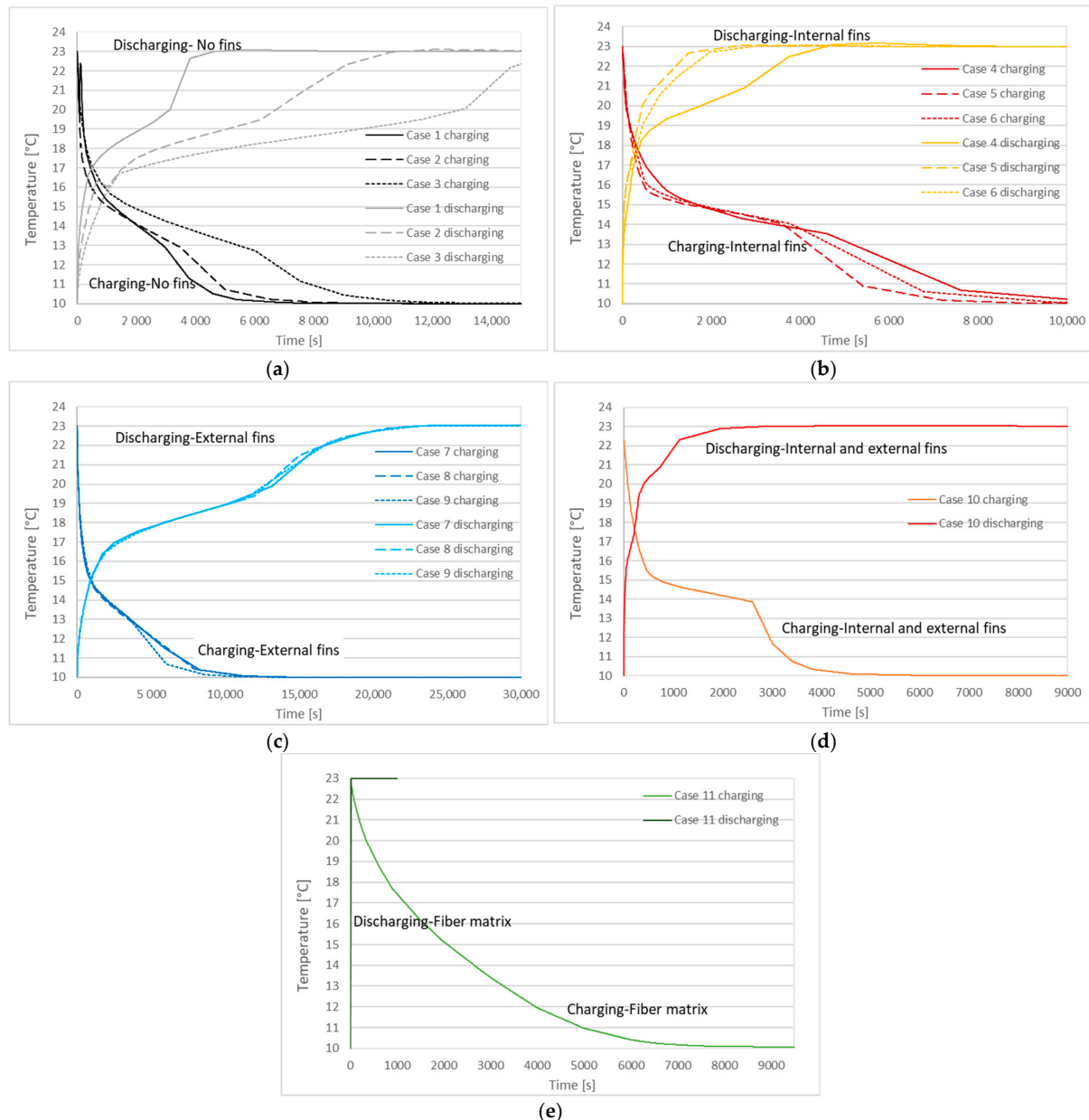


Figure 10. PCM temperature during charging and discharging processes (a) cases 1–3, (b) cases 4–6, (c) cases 7–9, (d) case 10, (e) case 11.

The evolution of total energy fluxes (W/m^2) during the charging and discharging phases is depicted in Figure 11. The linear average energy flux for the charging (solidification) process for the right boundary PCM-wall-air is analyzed in Figure 11. For the discharging (melting) phase, the total energy flux (W/m^2) of the left boundary PCM-wall-water is presented in

Figure 11. The heat flux flow (W/m^2) evolves quickly in the simulation's beginning and then approaches zero. The simulated energy fluxes during charging and discharging display little variations. In the charging phase for cases 1–3 (Figure 11a), the smaller diameter LHTES (case 1) presented a lower heat flux and approached 0 more quickly at 3 h. Additionally, in cases 5 and 6 with internal fins (Figure 11b), longer fins displayed lower energy flux and approached 0 at 3.3–3.6 h. the energy flux curves of cases 7–9 (Figure 11c) with external fins converge and present three times higher energy flux at the beginning of the simulation compared to other cases and reach 0 at around 4 h. Case 10 (Figure 11d) follows the same trend as cases 4–6. The energy flux of case 11 fiber matrix (Figure 11e) started at a higher value than cases with no fins and internal fins and reached 0 at 2.5 h. The discharging curves of energy flux cases 1–10 follow the same trend as the charging curves. However, the energy flux of case 11 with the electrospun fiber matrix approaches 0 at 10 s. This is explained due to direct-contact heat transfer of the water-electrospun fiber matrix. In both charging and discharging thermal cycles, external fins (cases 7–9) enhance the heat transfer of the LHTES system.

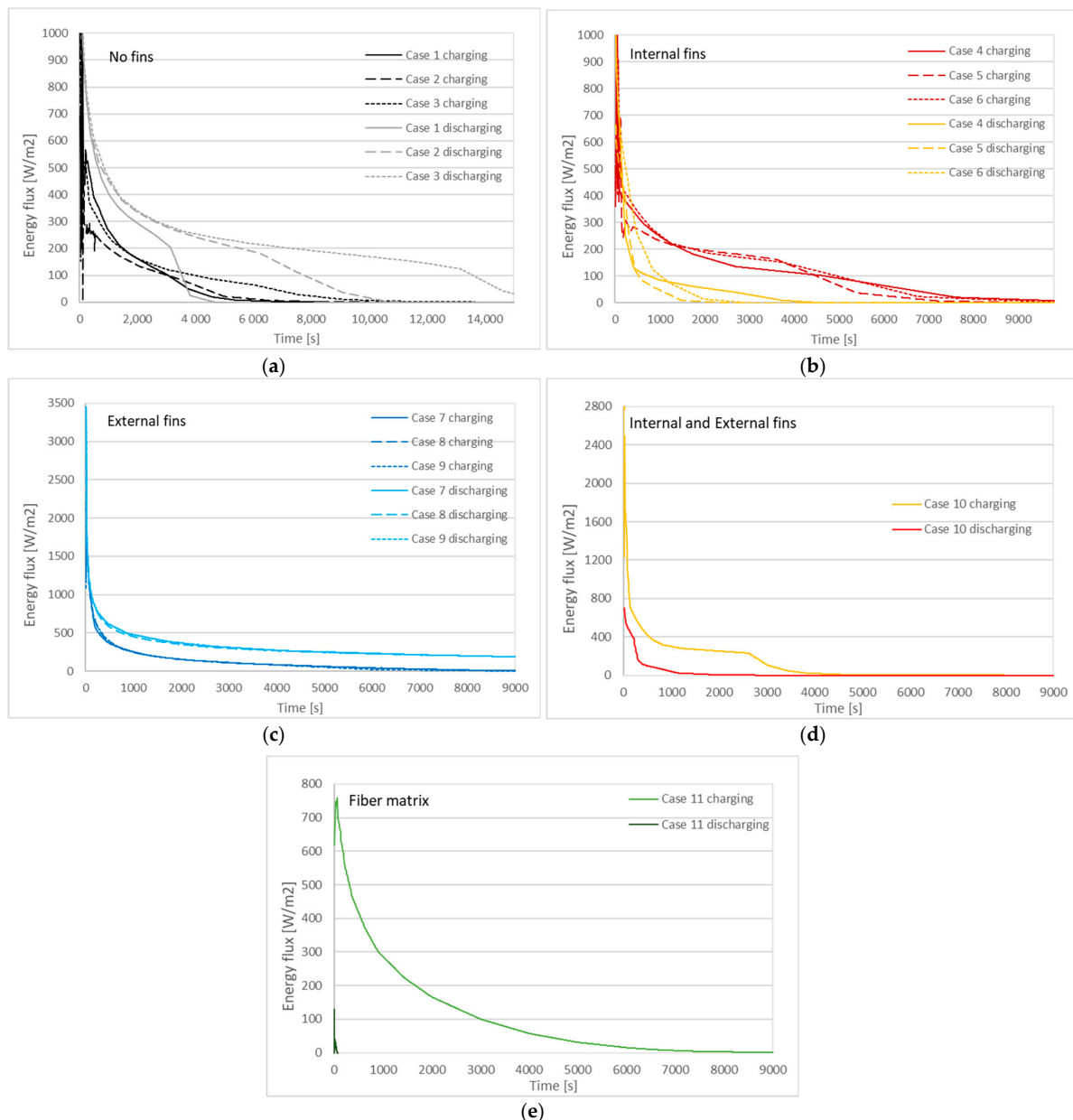


Figure 11. Energy flux (W/m^2) during charging and discharging processes (a) cases 1–3, (b) cases 4–6, (c) cases 7–9, (d) case 10, (e) case 11.

The total enthalpy for the LHTES system during the charging and discharging processes are presented in Figure 12. The time required to store and release the energy (kJ/kg) corresponds to the solidification and melting time. As observed in Figure 12, the duration needed for storing and releasing the total latent heat is affected by the length and number of internal and external fins. More specifically, during charging and discharging in cases 1–3 with no fins (Figure 12a), the bigger the diameter of the PCM annular tube, the higher the stored enthalpy. In solidification (charging) in cases 4–6 with internal fins (Figure 12b), case 5 with longer fins exhibits lower total enthalpy than the other two cases. Total enthalpy curves of cases 7–9 (Figure 12c) follow the same trend as cases 4–6 during solidification. Throughout melting, the total enthalpy curves of cases 7, 8, and 9 converge, and case 9 presents the higher total enthalpy at the beginning of the discharging. In all cases with fins, the higher total enthalpy when the LHTES is charged is observed for the case with longer internal fins in a decreased number of fins. The total enthalpy of case 11 (Figure 12e) at the start of the charging phase and the end of the discharging phase is 64.6 kJ/kg.

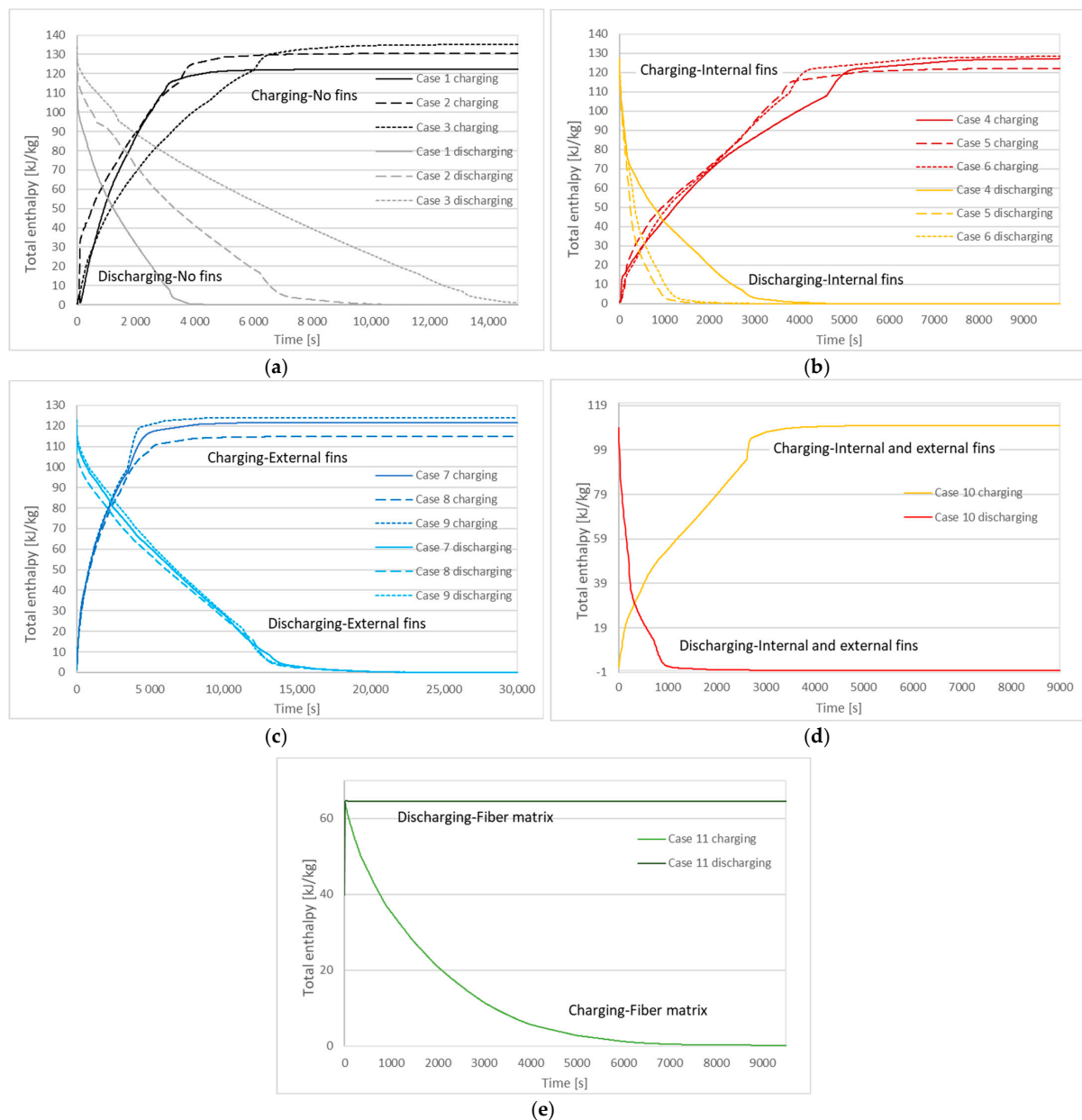


Figure 12. Total enthalpy of LHTES during charging and discharging processes (a) cases 1–3, (b) cases 4–6, (c) cases 7–9, (d) case 10, (e) case 11.

4. Conclusions

A numerical model of an LHTES unit was developed using Comsol Multiphysics 6.0, and a parametric analysis based on the geometry characteristics was conducted. The influence of external and internal fins was studied by examining ten cases of a double-tube heat exchanger and one single-tube LHTES. RT18, as a PCM, filled the annular space of the double tube, and its experimental melting/solidification latent heats (kJ/kg) and melting/solidification temperatures ($^{\circ}\text{C}$) were used as input. RT18 electrospun fiber matrix, as a PCM, filled the LHTES tube in case 11. The impact of the number and length of fins on the LHTES system performance is observed using the results of liquid fraction, PCM temperature, energy flux, and total enthalpy. As the length of internal and external fins increases, the melting and solidification are accelerated. The highest energy fluxes (W/m^2) are displayed in cases with external fins. Case 1, with the lowest PCM volume, and case 10, with internal and external fins, exhibit the fastest solidification time of 0.92 h and 0.84 h, respectively. The numerical simulation's shortest discharging time is displayed for the electrospun fiber matrix case at 4 s due to the direct contact heat transfer of PCM matrix water. The phase change process was accelerated by 99.97% in the discharging cycle and by 31.12% in the charging cycle compared to the case with no fins of the same external tube diameter (case 3). A small-scale LHTES shall be constructed in future work, and an experimental evaluation should be conducted as additional research.

Author Contributions: Conceptualization, E.P. and P.F.; methodology, E.P. and A.A.; software, E.P.; validation, E.P., L.G. and P.F.; formal analysis, E.P.; investigation, E.P., P.F. and A.A.; resources, P.F.; data curation, P.F. and E.P.; writing—original draft preparation, E.P.; writing—review and editing, E.P., L.G., P.F., M.M., S.F., J.F. and A.A.; supervision, E.P., P.F. and A.A.; project administration, E.P.; funding acquisition, A.A. All authors have read and agreed to the published version of the manuscript.

Funding: The authors acknowledge the support provided by ELFORSK, a research and development program administrated by Danish Energy.

Institutional Review Board Statement: Not applicable.

Informed Consent Statement: Not applicable.

Data Availability Statement: Data are available upon request.

Conflicts of Interest: The authors declare no conflict of interest.

Nomenclature

Parameter	Description	Unit
ρ	Density	kg/m^3
P	Pressure	Pa
u	Velocity	m/s
θ	Fraction/Indicator of phase transition	-
C_p	Specific heat	J/kgK
a_m	Mass fraction	-
k	Thermal conductivity	W/mK
HTF	Heat Transfer Fluid	-
LHTES	Latent Heat Thermal Energy Storage	-
PCM	Phase Change Material	-

References

1. Souayfane, F.; Fardoun, F.; Biwole, H.P. Phase change materials (PCM) for cooling applications in buildings: A review. *Energy Build.* **2016**, *129*, 396–431. [[CrossRef](#)]
2. Osterman, E.; Tyagi, V.V.; Butala, V.; Rahim, N.A.; Stritih, U. Review of PCM based cooling technologies for buildings. *Energy Build.* **2012**, *49*, 37–49. [[CrossRef](#)]
3. Al-Abidi, A.A.; Bin Mat, S.; Sopian, K.; Sulaiman, M.Y.; Lim, C.H. The Review of thermal energy storage for air conditioning systems. *Renew. Sustain. Energy Rev.* **2012**, *16*, 5802–5819. [[CrossRef](#)]

4. Zhai, X.Q.; Wang, X.L.; Wang, T.; Wang, R.Z. A review on phase change cold storage in air-conditioning system: Materials and applications. *Renew. Sustain. Energy Rev.* **2013**, *22*, 108–120. [\[CrossRef\]](#)
5. Lin, Y.; Jia, Y.; Alva, G.; Fang, G. Review on thermal conductivity enhancement, thermal properties and applications of phase change materials in thermal energy storage. *Renew. Sustain. Energy Rev.* **2018**, *82*, 2730–2742. [\[CrossRef\]](#)
6. Rathod, M.K.; Banerjee, J. Thermal stability of phase change materials used in latent heat energy storage systems: A review. *Renew. Sustain. Energy Rev.* **2013**, *18*, 246–258. [\[CrossRef\]](#)
7. Sharma, A.; Tyagi, V.V.; Chen, C.R.; Buddhi, D. Review on thermal energy storage with phase change materials and applications. *Renew. Sustain. Energy Rev.* **2009**, *13*, 318–345. [\[CrossRef\]](#)
8. Paroutoglou, E.; Afshari, A.; Bergsøe, N.C.; Fojan, P.; Hultmark, G. A PCM based cooling system for office buildings: A state of the art review. *E3S Web Conf.* **2019**, *111*, 01026. [\[CrossRef\]](#)
9. Zhang, H.L.; Baeyens, J.; Degreè, J.; Cáceres, G.; Segal, R.; Pitié, F. Latent heat storage with tubular-encapsulated phase change materials (PCMs). *Energy* **2014**, *76*, 66–72. [\[CrossRef\]](#)
10. Zhao, W.; France, D.M.; Yu, W.; Kim, T.; Singh, D. Phase change material with graphite foam for applications in high-temperature latent heat storage systems of concentrated solar power plants. *Renew. Energy* **2014**, *69*, 134–146. [\[CrossRef\]](#)
11. Aadmi, M.; Karkri, M.; El Hammouti, M. Heat transfer characteristics of thermal energy storage for PCM (phase change material) melting in horizontal tube: Numerical and experimental investigations. *Energy* **2015**, *85*, 339–352. [\[CrossRef\]](#)
12. Parrado, C.; Cáceres, G.; Bize, F.; Bubnovich, V.; Baeyens, J.; Degreè, J.; Zhang, H.L. Thermo-mechanical analysis of copper-encapsulated NaNO₃-KNO₃. *Chem. Eng. Res. Des.* **2015**, *93*, 224–231. [\[CrossRef\]](#)
13. Arena, S.; Casti, E.; Gasia, J.; Cabeza, L.F.; Cau, G. Numerical simulation of a finned-tube LHTES system: Influence of the mushy zone constant on the phase change behaviour. *Energy Procedia* **2017**, *126*, 517–524. [\[CrossRef\]](#)
14. Moulahi, C.; Trigui, A.; Boudaya, C.; Karkri, M. Smart macroencapsulated resin/wax composite for energy conservation in the built environment. *J. Thermoplast. Compos. Mater.* **2017**, *30*, 887–914. [\[CrossRef\]](#)
15. Herbinger, F.; Bhouri, M.; Groulx, D. Investigation of heat transfer inside a PCM-air heat exchanger: A numerical parametric study. *Heat Mass Transf. Stoffuebertragung* **2018**, *54*, 2433–2442. [\[CrossRef\]](#)
16. Arena, S.; Casti, E.; Gasia, J.; Cabeza, L.F.; Cau, G. Numerical analysis of a latent heat thermal energy storage system under partial load operating conditions. *Renew. Energy* **2018**, *128*, 350–361. [\[CrossRef\]](#)
17. Purohit, B.K.; Sistla, V.S. Studies on solution crystallization of Na₂SO₄·10H₂O embedded in porous polyurethane foam for thermal energy storage application. *Thermochim. Acta* **2018**, *668*, 9–18. [\[CrossRef\]](#)
18. Afsharpanah, F.; Izadi, M.; Hamedani, F.A.; Mousavi Ajarostaghi, S.S.; Yaici, W. Solidification of nano-enhanced PCM-porous composites in a cylindrical cold thermal energy storage enclosure. *Case Stud. Therm. Eng.* **2022**, *39*, 1DUMMY. [\[CrossRef\]](#)
19. Afsharpanah, F.; Mousavi Ajarostaghi, S.S.; Arıcı, M. Parametric study of phase change time reduction in a shell-and-tube ice storage system with anchor-type fin design. *Int. Commun. Heat Mass Transf.* **2022**, *137*, 106281. [\[CrossRef\]](#)
20. Afsharpanah, F.; Pakzad, K.; Mousavi Ajarostaghi, S.S.; Arıcı, M. Assessment of the charging performance in a cold thermal energy storage container with two rows of serpentine tubes and extended surfaces. *J. Energy Storage* **2022**, *51*, 104464. [\[CrossRef\]](#)
21. Shahsavari, A.; Goodarzi, A.; Mohammed, H.I.; Shirneshan, A.; Talebizadehsardari, P. Thermal performance evaluation of non-uniform fin array in a finned double-pipe latent heat storage system. *Energy* **2020**, *193*, 116800. [\[CrossRef\]](#)
22. Shahsavari, A.; Goodarzi, A.; Talebizadehsardari, P.; Arıcı, M. Numerical investigation of a double-pipe latent heat thermal energy storage with sinusoidal wavy fins during melting and solidification. *Int. J. Energy Res.* **2021**, *45*, 20934–20948. [\[CrossRef\]](#)
23. Boulaktout, N.; Mezaache, E.H.; Teggat, M.; Arıcı, M.; Ismail, K.A.R.; Yildiz, Ç. Effect of Fin Orientation on Melting Process in Horizontal Double Pipe Thermal Energy Storage Systems. *J. Energy Resour. Technol. Trans. ASME* **2021**, *143*, 1–14. [\[CrossRef\]](#)
24. Nicholls, R.A.; Moghimi, M.A.; Griffiths, A.L. Impact of fin type and orientation on performance of phase change material-based double pipe thermal energy storage. *J. Energy Storage* **2022**, *50*, 104671. [\[CrossRef\]](#)
25. Paroutoglou, E.; Fojan, P.; Gurevich, L.; Hultmark, G.; Afshari, A. Thermal Analysis of Organic and Nanoencapsulated Electrospun Phase Change Materials. *Energies* **2021**, *14*, 995. [\[CrossRef\]](#)
26. Paroutoglou, E.; Afshari, A.; Fojan, P.; Hultmark, G. Investigation of Thermal Behavior of Paraffins, Fatty Acids, Salt Hydrates and Renewable Based Oils as PCM. In Proceedings of the International Renewable Energy Storage Conference 2020 (IRES 2020), Düsseldorf, Germany, 10–12 March 2020; Volume 6, pp. 34–40. [\[CrossRef\]](#)
27. Paroutoglou, E.; Fojan, P.; Gurevich, L. Thermal Properties of Novel Phase-Change Materials Based on Tamanu and Coconut Oil Encapsulated in Electrospun Fiber Matrices. *Sustainability* **2022**, *14*, 7432. [\[CrossRef\]](#)
28. Medrano, M.; Yilmaz, M.O.; Nogués, M.; Martorell, I.; Roca, J.; Cabeza, L.F. Experimental evaluation of commercial heat exchangers for use as PCM thermal storage systems. *Appl. Energy* **2009**, *86*, 2047–2055. [\[CrossRef\]](#)

Chapter 11

THERMAL TESTS OF BULK PCM AND PCM FORMULATIONS

11.1 Introduction

Unpublished experimental data gathered throughout the Ph.D. study that have not been included in the scientific papers (Chapters 6-10) is presented thoroughly in the current chapter. This chapter presents the experimental output of water bath tests and DSC in dynamic mode. Figure 17 presents the experimental research process milestones. As shown in Figure 17, the water bath test precedes the DSC tests of PCM.

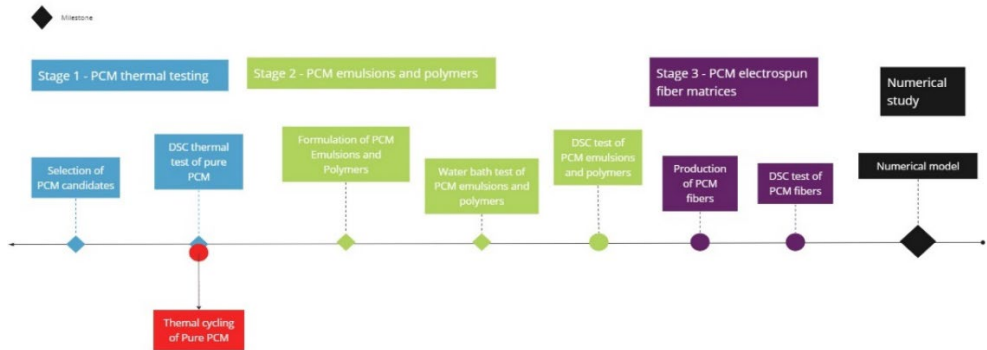


Figure 17: Flow chart of the research process

The water bath test is a simple and rapid method of incubating the samples, and their melting/solidification phase evolution and thermal storage capacity can be examined in a specific temperature range [191]. Figure 18 depicts an example of a water bath setup. In the water bath test, the sample's behavior is monitored manually, and in the case of the PCM water bath test, we can observe the time until the melting process is initiated and the melting time. This data is considered helpful for the DSC testing process and was used as a guideline for the DSC testing method conditions.

In several studies [192]–[194], water bath setups have been used to analyze LHTES systems. The melting temperatures of a mixture of n-octadecane and n-heptadecane in ratios 1:9 to 9:1 were observed with the water bath tube method and were found in the range of 22 to 23°C [192]. Metals Al1100 and Al6061 in contact with salt hydrates $\text{Na}_2\text{HPO}_4 \cdot 12\text{H}_2\text{O}$ and $\text{Zn}(\text{NO}_3)_2 \cdot 6\text{H}_2\text{O}$ were investigated using a water bath in temperatures 55–60°C, and the corrosion rates were in the range 68.71–103.07 mpy [193]. Heat storage with RT44HC as PCM was coupled with a water bath setup

as photovoltaic and was tested in the range of 25-49°C for three different volume flow rates 0.5, 1, and 2 L/min [194]. The results indicated that the lowest flow rate of 0.5 L/min resulted in the highest heat capacity [194].

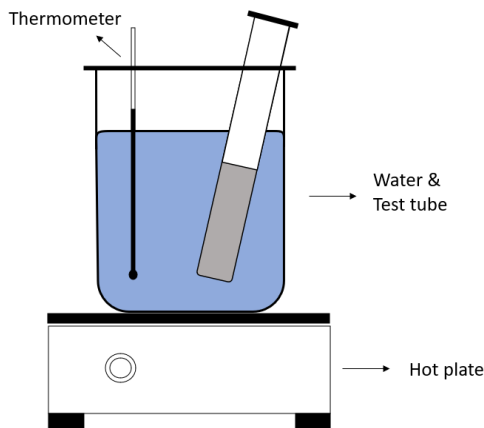


Figure 18: Water bath set up

11.2 Method and Materials

11.2.1 PCM emulsions and polymers

PCM in the form of a water emulsion with Pure Temp-15™, Pure Temp-18™, RT15™, RT18™, coconut oil, and tamanu oil were subjected manually to water bath tests, and the melting temperatures were monitored.

PCM polymers were prepared with PVP (Polyvinylpyrrolidone) as a synthesizer and APS (Ammonium Persulfate) as an initiator mixed with PCM in pure form (Pure Temp-15™, Pure Temp-18™, RT15™, RT18™, coconut oil, and tamanu oil). PCM polymers with 15%w/v of PCM, 5%w/v of PVP and 1%w/v of APS were prepared. Additionally, PCM polymers with 5%w/v of PCM emulsion, 5%w/v of PVP and 1%w/v of APS for the organic paraffins, organic non-paraffins, and renewable oils were prepared and tested with DSC. PCM polymers of PCM 5%w/v with PEGDa 2%w/v as synthesizer and BPO 1%w/v as polymerization initiator were prepared. Lastly PCM polymers of organic non-paraffins 5%w/v with PEGDa 5%w/v as synthesizer and BPO 1%w/v as polymerization initiator were prepared.

11.2.2 PCM fiber matrices

A solution of 10ml of water with 3.488 ml PCM (30%w/v) and 0.0242ml SDS (8.4 mmol/L) was mixed with 100ml of water 9% PVA w/v solution. 0.0072 ml of Triton

was added to the final solution and fibers were produced in a single fluid electrospinning setup. Co-axial electrospinning was used for the fabrication of PCM fibers in the core of polyvinylalcohol (PVA) shell. The external fiber is constituted by a 10% PVA solution. The fiber's core comprises 30% PCM encapsulated and 4% w/v Polyethylene Glycol.

11.3 Results and Discussion

11.3.1 PCM emulsions and polymers

Table 7, Table 8 and Table 9 depict the melting temperatures monitored for all examined PCM emulsions.

Table 7: Water bath test of organic paraffins and non-paraffins in water emulsions

PCM	Ratio (water: PCM)	Melting Temp. (°C)	Stable emulsion
Pure Temp-15 TM	1:1	18	-
Pure Temp-15 TM	1:2	18.5	-
Pure Temp-15 TM	1:3	18.5	-
Pure Temp-15 TM	1:4	18.5	-
Pure Temp-15 TM	1:5	18.5	+
Pure Temp-18 TM	1:1	21.5	-
Pure Temp-18 TM	1:2	21.5	-
Pure Temp-18 TM	1:3	21.7	-
Pure Temp-18 TM	1:4	21.7	-
Pure Temp-18 TM	1:5	21.7	+
RT15 TM	1:1	18.5	-
RT15 TM	1:2	18.5	-
RT15 TM	1:3	18.7	-
RT15 TM	1:4	18.7	-
RT15 TM	1:5	18.3	+
RT18 TM	1:1	22.7	-
RT18 TM	1:2	22	-
RT18 TM	1:3	22.8	-
RT18 TM	1:4	23	-
RT18 TM	1:5	23.2	+

Table 8: Water bath test of coconut oil in water emulsions

Ratio water:(coconut oil: tween)	Melting Temp. (°C)	Stable emulsion
1:(1:1)1 tween 20	25.8	-
1:(1:1)2 tween 20	26	+
1:(1:1)3 tween 20	26	-
1:(1:1)4 tween 20	26.3	-
1:(1:1)5 tween 20	26.8	+
1:(1:1)1 tween 80	25	-
1:(1:1)2 tween 80	27	-
1:(1:1)3 tween 80	26.8	-
1:(1:1)4 tween 80	26.3	-
1:(1:1)5 tween 80	28.2	+

Table 9: Water bath test of tamanu oil in water emulsions with tween 80 emulsifier

Ratio Water: (tamanu oil:tween 80)	Melting temperature (°C)	Stable emulsion	Ratio Water: (tamanu oil:tween 20)	Melting temperature (°C)	Stable emulsion
1:(1:1)2	21.9	+	1:(1:1)2	17	-
1:(2:1)2	24	-	1:(2:1)2	16.5	-
1:(3:1)2	17.5	-	1:(3:1)2	16	-
1:(4:1)2	18.5	-	1:(4:1)2	15	-
1:(5:1)2	13.5	-	1:(5:1)2	15	-
1:(1:1)3	28.7	+	1:(1:1)3	15	-
1:(2:1)3	29.5	+	1:(2:1)3	15	-
1:(3:1)3	29.5	+	1:(3:1)3	15	-
1:(4:1)3	29	-	1:(4:1)3	15	-
1:(5:1)3	30.5	+	1:(5:1)3	15	+
1:(1:1)4	32	-	1:(1:1)4	17	-
1:(2:1)4	30.7	-	1:(2:1)4	19.5	-
1:(3:1)4	28	+	1:(3:1)4	21	-
1:(4:1)4	20	+	1:(4:1)4	19.5	-
1:(5:1)4	26.5	-	1:(5:1)4	17	+
1:(1:1)5	25.2	-	1:(1:1)5	16	-
1:(2:1)5	27.5	+	1:(2:1)5	16	-
1:(3:1)5	27.9	-	1:(3:1)5	16	-
1:(4:1)5	29	-	1:(4:1)5	16	-
1:(5:1)5	32	-	1:(5:1)5	16	+

This simple setup for water bath test was used in order to observe whether the PCM-water emulsions were phase separated or not. All the emulsions marked as stable in Table 7, Table 8 and Table 9 were not phase separated and the melting temperatures were noted. For a detailed identification of the thermal properties DSC tests were conducted for all stable emulsions and the analysis results are presented in [14],[15],[16].

The DSC thermograms of PCM polymers with PVP and APS of organic paraffins, organic non-paraffins, and renewable oils were analyzed and the results are given in Table 10. The polymer testing conditions are given as well in Table 10. As can be observed in Table 10 RT15TM-PVP-APS showed melting/solidification temperatures in the range 15-20°C. Nonetheless, all polymers with PVP and APS presented latent heats of melting and solidification lower than 10 kJ/kg.

Table 10: PCM-PVP-APS polymers testing conditions and thermal analysis results

PCM-PVP-APS	Mass (mg)	DSC temp. range (°C)	Scanning rate (°C/min)	Melting Temp. (°C)	ΔH (kJ/kg)	Freezing Temp. (°C)	ΔH (kJ/kg)
Coconut oil-PVP-APS	12.61	10 to 80°C	5°C/min	24.65	3.198	-	-
Tamanu oil-PVP-APS	6.22	10 to 80°C	5°C/min	79.74	2.815	10.2	2.727
Pure Temp-15 TM -PVP-APS	6.1	10 to 80°C	5°C/min	13.59	9.555	-	-
Pure Temp-18 TM -PVP-APS	13.5	5 to 80°C	3°C/min	17.98	6.721	11.47	7.046
RT15 TM -PVP-APS	5.3	5 to 80°C	3°C/min	20.61	2.449	18.88	3.298
RT18 TM -PVP-APS	13.22	10 to 80°C	5°C/min	16.52	9.302	-	-

The thermograms of PCM polymers of PCM emulsions with PVP and APS of organic paraffins, organic non-paraffins, and renewable oils were analyzed. The

polymer testing conditions and thermal analysis results are given in Table 11. There was a failure in the DSC tests of the polymers of RT15TM, coconut oil and tamanu oil emulsions. The rest of PCM polymers presented low latent heats of melting/solidification (< 4 kJ/kg).

Table 11: PCM emulsion-PVP-APS polymers testing conditions and thermal analysis results

PCM emulsion -PVP-APS	Mass (mg)	DSC Temp. range (°C)	Scanning rate (°C/min)	Melting Temp. (°C)	ΔH (kJ/kg)	Freezing Temp. (°C)	ΔH (kJ/kg)
Pure Temp-15 TM emulsion -PVP-APS	7.95	-80 to 200°C	10°C/min	14.82	1.323	1.07	1.327
Pure Temp-18 TM emulsion -PVP-APS	10.01	-80 to 200°C	10°C/min	20.22	4.04	-3.49	3.836
RT18 TM emulsion -PVP-APS	5.76	-80 to 200°C	10°C/min	18.62	2.134	7.43	2.152

Organic non-paraffins polymers were prepared, and the DSC thermograms were analyzed. The testing conditions and thermal analysis results of the polymers PCM 5%w/v-PEGDa 2%w/v-BPO 1%w/v are provided in Table 12. The melting temperature of Pure Temp-18TM with PEGDa 2%w/v and BPO 1%w/v was in the range of 15-20°C. The latent heats of melting/solidification for Pure Temp-15TM and Pure Temp-18TM with PEGDa 2%w/v and BPO 1%w/v were 101.3/85.32 kJ/kg and 83.26/84.33 kJ/kg.

Table 12: PCM -PEGDa-BPO polymers testing conditions and thermal analysis results

PCM-PEGDa-BPO	Mass (mg)	DSC Temp. range (°C)	Scanning rate (°C/min)	Melting Temp. (°C)	ΔH (kJ/kg)	Freezing Temp. (°C)	ΔH (kJ/kg)
Pure Temp-15™-PEGDa-BPO	7.60 mg	5 to 80°C	3°C/min	14.21°C	101.3 kJ/kg	9.76°C	85.32 kJ/kg
Pure Temp-18™-PEGDa-BPO	10.70 mg	5 to 80°C	3°C/min	17.83°C	83.26 kJ/kg	13.18°C	84.33 kJ/kg

Table 13: PCM-PEGDa-BPO polymers testing conditions and thermal analysis results

PCM-PEGDa-BPO	Mass (mg)	DSC Temp. range(°C)	Scanning rate (°C/min)	Melting Temp. (°C)	ΔH (kJ/kg)	Freezing Temp. (°C)	ΔH (kJ/kg)
Pure Temp-15™-PEGDa-BPO	8.5 mg	5 to 80°C	3°C/min	14.51	144.9	10.52	103.6
Pure Temp-18™-PEGDa-BPO	4.53 mg	10 to 80°C	5°C/min	17.81	88.69	-	-
RT15™-PEGDa-BPO	7.28 mg	10 to 80°C	5°C/min	19.74	51.50	17.66	39.62
RT18™-PEGDa-BPO	4 mg	10 to 80°C	5°C/min	15.54	77.98	14.05	66.66
Coconut oil-PEGDa-BPO	9.34 mg	10 to 80°C	5°C/min	24.45	40.95	-	-

The testing conditions and thermal analysis results of the polymers PCM 5%w/v-PEGDa 5%w/v-BPO 1%w/v are provided in Table 13. A fail occurred in the DSC

test of tamanu oil for both melting/solidification thermal cycle. Additionally, a fail occurred in the DSC test of Pure Temp-18™ and Coconut oil with PEGDa 5%w/v-BPO 1%w/v in their cooling cycle. RT15™ polymer with PEGDa 5%w/v-BPO 1%w/v showed melting/solidification temperatures in the range 15-20°C with latent heats of melting/solidification of 51.50/39.62 kJ/kg which are reduced by 47.2% and 59.18%.

11.3.2 PCM fiber matrices

PCM fibers containing 30%w/v PCM mixed with 9% PVA w/v solution were produced with a single fiber electrospinning set up. The DSC thermogram and the thermal analysis results are presented in Table 14.

Table 14: Testing conditions and thermal properties of single PCM-PVA fiber

Single fiber	Mass (mg)	DSC Temp. range (°C)	Scanning rate (°C/min)	Melting Temp. (°C)	ΔH (kJ/kg)	Freezing Temp. (°C)	ΔH (kJ/kg)
Pure Temp-18™	1.96	10 to 80°C	5°C/min	15.87	15.93	10.71	12.58
Tamanu oil	1.93	10 to 80°C	5°C/min	51.45	3.871	-	-

The DSC thermograms of PVA-PCM co-axial electrospun fibers and the thermal analysis results are analyzed and the results were presented in Table 15. All co-axial electrospun fibers of commercial organic PCM with PVA showed low latent heats of melting/solidification (<17 kJ/kg). Tamanu oil co-axial electrospun fiber in a PVA shell showed latent heats of melting/solidification of 37.6/24.14 kJ/kg which are higher than the latent heats of melting/solidification of bulk tamanu oil (3.56/4.64 kJ/kg). Figure 19 and Figure 20 depict the SEM images of organic paraffins and non-paraffins. The average diameters of organic paraffins RT15™ and RT18™ PVA electrospun fibers showed average diameters of $0.3469 \pm 0.0808 \mu\text{m}$ and $0.4907 \pm 0.0665 \mu\text{m}$. Moreover, the average diameters of organic non-paraffins Pure Temp-15™ and Pure Temp-18™ with PVA were $0.5211 \pm 0.0889 \mu\text{m}$ and $0.3094 \pm 0.0703 \mu\text{m}$.

Table 15: Testing conditions and thermal properties of PCM emulsion encapsulated in PVA shell

Fiber in fiber	Mass (mg)	DSC Temp. range (°C)	Scanning rate (°C/min)	Melting Temp. (°C)	ΔH (kJ/kg)	Freezing Temp. (°C)	ΔH (kJ/kg)
Pure Temp-15 TM	1.58	0 to 80°C	1.5°C/min	13.46	5.734	8.41	11.88
Pure Temp-18 TM	2.42	0 to 80°C	1.5°C/min	19.76	5.029	7.45	4.851
RT15 TM	3.48	0 to 80°C	1.5°C/min	-	-	-	-
RT18 TM	1.63	0 to 80°C	1.5°C/min	19.99	17.36	7.43	16.82
Coconut oil	0.66	0 to 80°C	1.5°C/min	19.92	9.23	7.38	10.98
Tamanu oil	2.54	-80 to 200°C	10°C/min	156.36	37.6	161.05	24.14

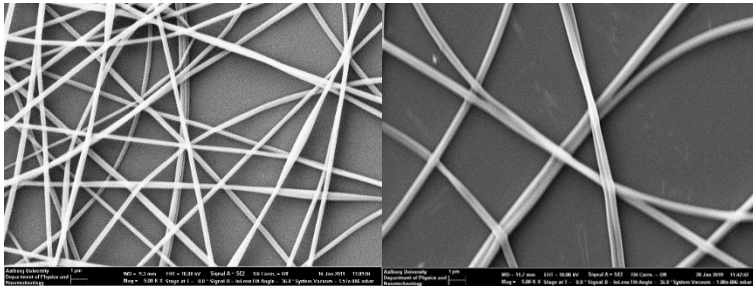


Figure 19: SEM figures of Pure Temp-18TM (left) and Pure Temp-15TM (right) fiber matrices

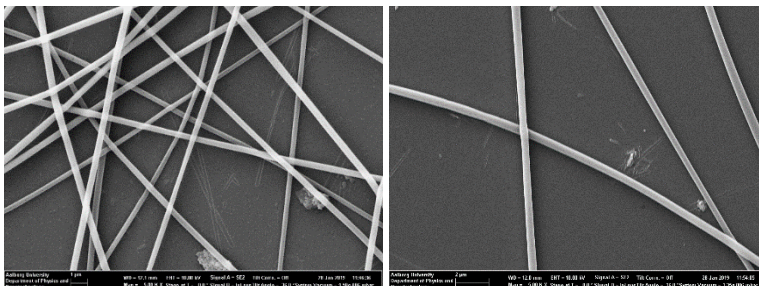


Figure 20: SEM figures of RT15TM (left) and RT18TM (right) fiber matrices

11.4 Conclusions

Pure Temp-15TM and Pure Temp-18TM with PEGDa 2%w/v and BPO 1%w/v showed high latent heats of melting/solidification for were 101.3/85.32 kJ/kg and 83.26/84.33 kJ/kg but their melting/solidification temperatures were not in the range 15-20°C. Among all polymers examined, RT15TM polymer with the addition of PEGDa 5%w/v and BPO 1%w/v had melting/solidification temperatures of 19.74/17.66 and latent heats of melting/solidification of 51.50/39.62 kJ/kg. In the DSC tests it was shown that tamanu oil co-axial electrospun fibers in a PVA shell acquired latent heats of melting/solidification 10 and 5 times higher than the latent heats of bulk tamanu oil which indicates an improvement of thermal properties.

PART III.

**DISCUSSION, CONCLUSION AND
FUTURE RESEARCH**

Chapter 12

DISCUSSION

12.1 Thermal performance of PCM

The selected PCMs comprising the classes of organic paraffins (RT 15, RT 18), organic non-paraffins (PT15, PT18), and renewable-based oils (tamanu oil, coconut oil) were the PCMs presenting higher theoretical latent heats (J/g) [14]–[16]. Tamanu oil and Coconut oil are derived from *Calophyllum inophyllum* seeds and *Cocos nucifera* fruits, respectively, and are classified as solid-liquid PCMs. In the case of Coconut oil, it is a renewable resource, abundant at low prices on the market, and no additional agricultural area needs to be sacrificed for its production. A tree with non-edible fruits producing tamanu oil is already used in cosmetic products. All selected PCMs have been examined in their pure form, as well as in emulsion, polymer- and fiber-encapsulated forms [14]–[16]. The PCMs were characterized based on melting/solidification temperatures and latent heat of melting/solidification. Comparing PCMs in different forms has been based on these two critical thermal characteristics. The range of phase change temperatures of 15-20°C has been targeted to meet occupants' thermal comfort requirements and utilize the cooling potential of PCMs in HVAC applications.

12.1.1 Long-Term Stability of PCM in pure form

The long-term stability study is essential for using PCMs in HVAC systems because they must operate for an extended period of time without replacing the working media.

The PCMs in this study underwent testing over 200 thermal cycles, representing 6-months of lifetime [14]–[16]. All commercial PCMs exhibited highly reproducible melting/solidification temperatures and latent heat, with a relative standard deviation (RSD) ranging from 1% to 4% and 2% to 15%, respectively. However, tamanu oil demonstrated melting/solidification temperatures and latent heats with a wider range of relative standard deviation, at 30%-50% RSD and 3%-12%RSD, respectively.

Thermal cycling tests of pure PCM indicated that only the organic paraffins RT15™ and RT18™ exhibited melting solidification temperatures in the desired range of 15 to 20°C.

Several literature studies [150], [195]–[198] have addressed long-term stability, with a particular focus on organic paraffins. In the case of, RT21 [195], a melting point shift of 7°C (21 to 28 °C) and an increase in the latent heat of 36 J/g (from 134 to 170 J/g) were observed during a long-term stability analysis conducted over 120

days. Others [197] have reported a melting point shift of 1-3°C and a latent heat decrease of 21-48 J/g (first to last thermal cycle) for paraffins. Similarly, another examined paraffin [196] showed a variation of melting temperature and latent heat in the ranges of 1 to 3 and -10 to 14 J/g, respectively.

In the present study, the organic paraffin RT15™ demonstrated a stable performance compared to other organic paraffins [195]–[197], maintaining consistent melting/solidification temperatures and enthalpies with relatively small shifts (<1°C and <1 J/g) from 1st to 200th thermal cycle. On the other hand, the organic paraffin RT18™ presented a negligible change in melting/solidification temperature (<1°C) but showed a 33% reduction in latent heat from 150 to 200 thermal cycles, with a total decrease of 39 to 40 J/g between 1st and 200th thermal cycle. However, it should be underlined that no macroscopic degradation was observed after 150 thermal cycles. Myristic, palmitic, and stearic acids, as presented in [196] and [199] showed almost stable melting temperatures. In terms of latent heats, myristic palmitic and stearic acids showed a reduction of 17 J/g to 26 J/g after 450 thermal cycles. In [196], myristic and palmitic acids showed a reduction of 1 J/g and 38 J/g respectively after 1500 thermal cycles. In the present study, the organic non-paraffins Pure Temp-15™ and Pure Temp-18™ displayed negligible thermal shifts (<1°C) in their melting temperatures. When analyzing the latent heats of melting/solidification Pure Temp-15™ showed a slight decrease of 5 to 7 J/g, while Pure Temp-18™, on the other hand, a slight increase of 3 J/g indicating stable performance in terms of thermal storage capacity.

Tamanu oil showed phase change temperatures around 0°C and relatively low latent heat (<10 kJ/kg), but no supercooling was observed during thermal cycling. Tamanu oil presented poor storage performance (4 J/g) and melting/solidification temperatures below the application requirements. However, it has been used in this study due to its more environmentally friendly nature compared to coconut oil. The latent heats acquired from the DSC test of coconut oil were 50-56 kJ/kg, but the supercooling degree reached 15°C, and therefore it was not subjected to thermal cycling. Palm oil examined in the literature [34] presented a melting temperature of 17°C and a 2.5 times higher latent heat (127 kJ/kg) compared to the experimental results of coconut oil analyzed in the current study. Both coconut and palm oil have environmental impacts, including deforestation, soil degradation, water pollution, and carbon emissions due to transportation. Additionally, when comparing Coconut oil with Tamanu oil, it is evident that coconut oil has higher melting but lower solidification temperatures, whereas tamanu oil shows both melting and solidification temperatures lower than the targeted.

Although performance-wise non-sustainable PCMs perform better than sustainable PCMs, the non-sustainable ones are based on a fossil resource.

12.1.2 Formulation and Thermal identification of PCM composites

PCM emulsions/polymers were formulated to investigate the potential shift in the melting-solidification temperatures and the impact of large heat capacity of water-immiscible systems. Thermal properties of PCM emulsions with water and PCM mixtures were studied in [14]–[16]. PCM emulsions in the phase change temperature range of 15-20°C were addressed in [63], [68], [70], [73], [76], [78], [80]. The PCM emulsions of organic paraffin n-hexadecane with a phase change temperature range of 15-20°C showed latent heats of melting/solidification 43-80 kJ/kg. The latent heat of melting [80] of n-alkane emulsions with linear alcohol ethoxylates were 53-61 kJ/kg. The PCM water emulsions of organic paraffins RT15™ and RT18™ were prepared at a ratio of PCM: water of 1:5 with the addition of 5%v/v Tween 80 as emulsifiers. RT18™ in water emulsion is a good option for the temperature range of 15-20°C with a thermal hysteresis of 2°C and latent heat of around 180 kJ/kg, which is higher than the latent heats of n-alkane emulsions [63], [68], [70], [73], [76], [78], [80] analyzed in Chapter 2. The latent heat of RT18™ in water emulsion was increased by 43 kJ/kg and 41 kJ/kg compared to RT18™ in bulk for melting and solidification processes, respectively. RT15™ in water emulsion presents almost no supercooling (0.2°C thermal hysteresis) with two peaks in melting and three peaks in the solidification process following the same pattern as RT15™ in bulk with a supercooling of 0.5°C. However, the latent heats of melting and solidification of RT15™ in water emulsion were decreased compared to RT15™ in bulk by 10 kJ/kg and 48 kJ/kg in melting and solidification processes, respectively. The average emulsion size of RT15™ and RT18™ water emulsions were 9 and 7 µm. The n-hexadecane [63], [68], [70], [73], [76], [78], [80] emulsion size reported in literature shows a wide range of distributions from 20nm to 20µm, and the average n-alkane emulsion size was above 1 µm.

The latent heats of emulsions of organic non-paraffins Pure Temp-15™ and Pure Temp-18™ with a water ratio of 1:5 and 5%v/v Tween 80 are 111-112 kJ/kg and 84-88 kJ/kg. The latent heats of an emulsion of Pure Temp-15™ were increased by 5 and 8 kJ/kg compared to Pure Temp-15™ in bulk for melting and solidification processes, respectively. On the contrary, the latent heats of the emulsion of Pure Temp-18™ were decreased by 39 and 31 kJ/kg compared to Pure Temp-18™ in bulk for melting and solidification processes. However, Pure Temp-15™ and Pure Temp-18™ in water emulsions present a thermal hysteresis of 3°C and 4°C respectively, and melting/solidification temperatures of 14°C /11°C and 18°C/14°C, respectively. The average emulsion size of organic paraffins and non-paraffins were in the range of 5-11µm.

When examining coconut oil in water emulsions with Tween 20 and Tween 80, the melting/solidification latent heats were lower (19 to 38 kJ/kg) compared to the latent heats of bulk material (50-56 kJ/kg) and presented a high thermal hysteresis of 17-

20°C. Tamanu oil in water emulsions depicted very low latent heats (2-3 kJ/kg) and did not present any improvement in terms of melting/solidification temperatures and latent heats compared to bulk tamanu oil. In water emulsions, the average emulsion size of coconut oil and tamanu oil were 4-17 μm and 5-17 μm , respectively. Moreover, the mixtures of coconut oil tamanu oil without emulsifiers presented in the mixture of 90% coconut oil and 10% tamanu oil latent heats of melting/solidification of around 45 kJ/kg decreased by 5 and 12 kJ/kg when compared to the latent heats of bulk coconut oil [16].

PCM polymers investigated in this project were analyzed in Chapter 7 and Chapter 11. Based on PCM polymers presented in the current literature, it was decided to formulate and thermally identify the PCM polymers with polyvinylpyrrolidone (PVP)-ammonium persulfate (APS) and polyethylene glycol diacrylate (PEGDa)-benzoyl peroxide (BPO). All polymers prepared with polyvinylpyrrolidone (PVP) and ammonium persulfate (APS) (Chapter 7 and Chapter 11) [14] presented latent heats <10 kJ/kg, and for this reason, the PCM polymers with PVP and APS were not further investigated. Among all the polymer solutions prepared and tested thermally, only RT15TM polymer with polyethylene glycol diacrylate and benzoyl peroxide showed melting/solidification temperatures in the range of 15-20°C.

RT15TM-PEGDa-BPO polymer showed melting/solidification peaks of 20/18 °C and latent heats of 51/40 kJ/kg. Nonetheless, in this case, the latent heats of RT15TM in polymer form were decreased by 48% and 59% compared to bulk RT15TM. (Calculated per total weight and normalized, related to the reduction of PCM in polymer form) RT18TM-PEGda-BPO showed a melting temperature of 16°C and solidification temperatures of 11/13/14°C with latent heats of melting/solidification 76/64 kJ/kg. In the case of RT18TM-PEGDa-BPO, the melting/solidification temperatures in the polymer solution were decreased in comparison with bulk PCM and PCM emulsion. The latent heats measured on RT18TM-PEGda-BPO were decreased by 45% and 54% compared to the latent heats of bulk RT18TM. The two polymers showed lower latent heats compared to bulk material, and their melting/solidification temperatures were shifted. In [49], n-hexadecane was encapsulated in polymethyl methacrylate, and melamine formaldehyde shell showed latent heats of 95-130 kJ/kg and 150 kJ/kg, respectively. Additionally, n-octadecane in a polystyrene shell shows latent heat of 124 kJ/kg [86]. PRS paraffin wax encapsulated in polystyrene [85] and paraffin RT80 in styrene-butyl acrylate [199] show latent heats of 154 kJ/kg and 5-25 kJ/kg. The two polymers presented higher latent heats than RT80 in styrene-butyl acrylate [199] but lower latent heats than n-hexadecane in polymethyl methacrylate, melamine formaldehyde shell [49], PRS paraffin wax in polystyrene [85] and n-octadecane in polystyrene shell [86].

12.1.3 Formulation and Thermal identification of PCM fiber matrices

Electrospun core-shell fibers containing polymer and PCM and fiber in fiber formulations were examined. What is interesting about PCM fiber matrices, is that they are acting as heat reservoirs and enabling effective heat management. In all examined electrospun fibers, the phase transition of the shell was maintained, and the shape stabilization was not lost.

Fibers produced with a single fluid electrospinning setup encapsulated 30%w/v PCM as a core in 9% w/v PVA polyvinyl alcohol (PVA) shell. Pure Temp-18™ was successfully encapsulated in this way, but the latent heats were in the range of 13-16 kJ/kg, which is low compared to other formulations studied (bulk and emulsion). The single-fluid PCM fibers of organic non-paraffins examined in the current study compared to single-fluid PCM fibers reported in the literature [123]–[132] exhibited very low latent heats indicating degradation of thermal properties.

In several studies [133]–[139], co-axial electrospun fibers of different organic PCM were reported. Low latent heats were observed for co-axial electrospun fibers with PCM encapsulated in the core of the PVA shell presented in Chapter 11. However, tamanu oil encapsulated in a PVA shell showed enthalpies of melting/solidification of 38/24 kJ/kg, which are 9.5 and 4.2 times higher than the melting/solidification enthalpies of bulk tamanu oil.

PCM core-shell fibers were produced with three different combinations of core-shell flow rates (0.3-0.6 ml/h and 0.5-0.5 ml/h and polycaprolactone (PCL) concentration (9% w/v and 12% w/v) for the shell material [16],[15].

Co-axial electrospun fibers with Pure Temp-15™, Pure Temp-18™, and RT18™ showed two peaks in melting and solidification for the core and shell materials. In the case of RT15™ co-axial electrospun fibers, two peaks were observed in the solidification range of PCM material. Figure 21 and Figure 22 depict RT15, RT18, and composites of the two paraffins in a melting/solidification temperature range of 15-20°C. RT15™, 0.5-0.5 ml/h in a 9%w/v shell and RT18™, 0.5-0.5 ml/h in a 12%w/v shell depicted melting/solidification points in the range 15-20°C.

RT18™ co-axial fibers in all combinations presented the highest latent heats among all the materials. RT18™ (0.5-0.5 ml/h, 12%w/v PCL) showed melting/solidification temperatures and latent heats of 17/15°C and 102/82 kJ/kg with an encapsulation efficiency of about 67% [15]. Figure 21 shows that RT18™ (0.5-0.5 ml/h, 12%w/v PCL) presented lower latent heat than RT18 in pure form and lower latent heat than RT18 in water emulsion [15]. RT15™ (0.5-0.5 ml/h, 9%w/v PCL) showed lower latent heat than RT15™ in pure form for both melting and solidification processes (Figure 22) [15]. However, compared with RT15 PEGDa BPO polymer, it showed lower melting enthalpy but higher solidification enthalpy (Figure 22).

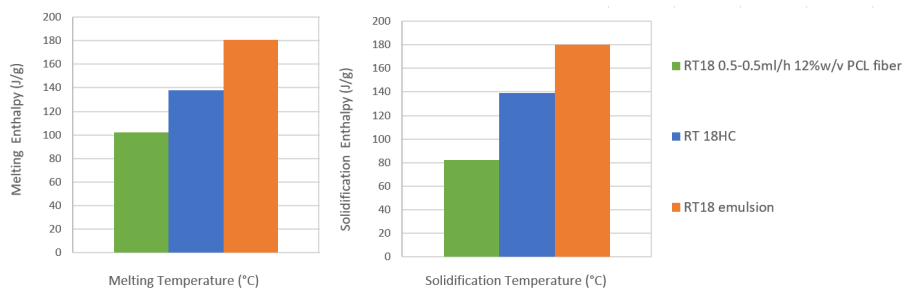


Figure 21: RT18 and RT18 composites in melting/solidification temperature range 15-20°C

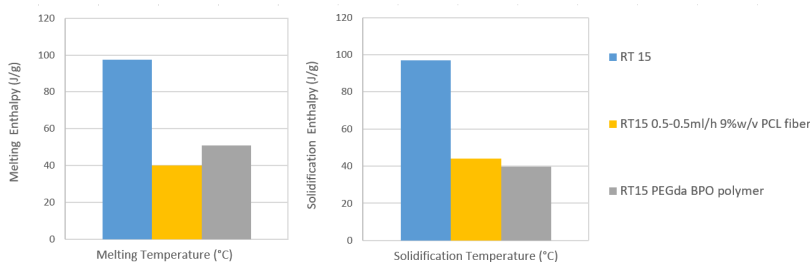


Figure 22: RT15 and RT15 composites in melting/solidification temperature range 15-20°C

The calculated encapsulation ratio of organic paraffins (RT15TM, RT18TM) and non-paraffins (Pure Temp-15TM, Pure Temp-18TM) was in the range of 41-80%, and the average diameters were 0.2-8 μ m. Another study reported that 82% of an RT5TM organic paraffin emulsion was encapsulated in a polycaprolactone matrix [136]. Additionally, the four commercial organic paraffins and non-paraffins, tamanu oil and coconut oil, and mixtures of commercial PCMs with the two oils were encapsulated in the core of PCL fibers. The reason for testing ternary mixtures of commercial PCMs with the two oils is to examine how the melting/solidification temperatures shift. Coconut oil electrospun fibers showed 34-49 kJ/kg latent heats with 68-89% encapsulation efficiencies. On the other hand, co-axial fibers with tamanu oil encapsulated in the core presented low latent heats of 2-3 kJ/kg. All fibers, including oils and mixtures of oils with commercial materials, present melting/solidification temperatures outside the desired temperature range of 15-20°C. The highest enthalpies of 64/58 kJ/kg were presented in the case of Coconut oil 35%-tamanu oil 15%-RT18TM 50% in a 9% w/v PCL shell with 0.5-0.5 ml/h flow rate. In this case, the encapsulation ratio and efficiency reached 100%, which indicated that the latent heat of the mixture was preserved when the mixture was encapsulated in the core of the PCL shell. In a relevant study in literature, the specific heat capacity of coconut oil encapsulated in a cellulose shell was increased

by 98% compared to pure material [137]. The mean diameters of PCM fibers with the oils and the mixtures in the core of the PCL shell were in the range of 0.2-13 μm .

12.2 Numerical analysis of a LHTES system

The numerical analysis of an LHTES system containing encapsulated PCMs addressed the performance, optimal geometry to be used, and the potential benefits of fins for thermal performance.

A double tube LHTES was analyzed with Comsol Multiphysics 6.0. Different cases with internal and external fins of different lengths and distances between fins were studied. The geometry without fins was compared to other geometries with different fin arrangements. The effect of fins has been previously analyzed [185]–[188]. Sinusoidal wavy fins [185], [186] led to a reduction of melting/solidification time by 43.5%/17.8%. Different fin densities (2,4,8) and orientations were studied in [187], and the case of 2 vertical fins showed the shortest charging time. Transversal corrugated fins yielded an 88% reduction in melting time compared to the simplest geometry [188]. In this thesis, the geometry including internal and external fins (Case 10) yielded PCM's fastest solidification and melting time at 0.84 h and 0.3 h [17]. The charging/discharging time was reduced by 56%/92% compared to the finless geometry (case 3) [17]. Additionally, a single tube LHTES with PCM fibers (case 11) was presented in Figure 5 of Chapter 10: Paper V, The novelty of the system, is subjected to direct contact of the PCM electrospun fiber matrix with, causing instant melting of the PCM encapsulated in the core of the fiber matrix with conservation of the matrix [17]. Here, the solidification time was decreased by 31% compared to the finless geometry [17]. The bar chart of Figure 23 presents the charging and discharging time of cases 1 to 11 analyzed in Chapter 10: Paper V.

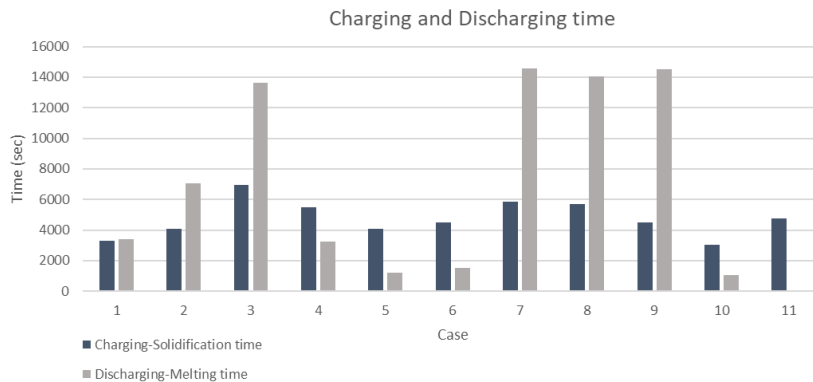


Figure 23: Charging and Discharging time (case 1-3: double-pipe LHTES without fins, case 4-6: double-pipe LHTES with internal fins, case 7-9: double-pipe LHTES

with external fins, case 10: double-pipe LHTES with internal and external fins and case 11: LHTES unit with PCM fiber matrix [17])

Chapter 13

CONCLUSIONS

Phase change materials store and release thermal energy and have great potential in thermal energy storage applications. PCMs comprising the classes of organic paraffins (RT15TM and RT18TM), organic non-paraffins (Pure Temp-15TM and Pure Temp-18TM), organic, renewable oils (coconut oil and tamanu oil), and an inorganic salt hydrate (SP15TM) were characterized for their thermal performance. The selected PCMs were studied as bulk, emulsion, as well as encapsulated in electrospun fiber matrices. The commercial organic paraffins and non-paraffins exhibited exceptional thermal stability in DSC tests after being subjected to 200 thermal cycles. Organic paraffin RT18TM in its pure form possessed the highest average enthalpy of melting and solidification in the range of 137-139 kJ/kg after 200 thermal cycles. The average melting and solidification temperatures of RT18TM in pure form were 18°C and 15°C. Coconut oil is a renewable alternative with latent heats of 50 and 56 kJ/kg and is a promising candidate for LHTES applications.

RT18TM in water emulsion exhibited melting/solidification temperatures within the desired range and high latent heat of melting and solidification (180 kJ/kg).

PCM and PCM emulsions with PVA were encapsulated in the core of a co-axial electrospun fiber matrix with PCL as the shell. Co-axial fibers with organic paraffin RT18TM (0.5-0.5ml/h, 12%w/v PCL) presented melting/solidification temperatures in the temperature range 15-20°C, along with high latent heats and encapsulation efficiency of about 67%. Fibers with a PCM mixture of 15% tamanu oil, 35% coconut oil, and 50% RT18TM encapsulated in a 9% w/v PCL shell exhibited an encapsulation efficiency close to 100%.

The parametric analysis of eleven different geometries of LHTES systems was carried out using Comsol Multiphysics 6.0. It was found that the melting and solidification processes accelerated with an increase in the length of internal and external fins. Additionally, a single tube containing PCM electrospun fiber matrix in direct contact with water was also examined. It was found that the melting was immediate in this case.

The experimental and numerical results lay the foundation for the development of a large-scale LHTES system. The integration of PCM materials and PCM composites in HVAC systems were studied on both macro and micro-scale, with a specific focus on a phase change temperature range (15-20°C) to satisfy occupant thermal comfort.

Chapter 14

FUTURE RESEARCH

Laboratory scale LHTES experiments are required to validate the numerical analysis, and an upscale of the experimental laboratory results should be done as a next step. A possible assembly for a laboratory-scale LHTES system is envisioned in Figure 24 and Figure 25. The cooling system assembly consists of a fan, tubes, and lamellas. During the charging phase of the LHTES, there is no water circulation in the water pipes. In the discharging phase during daytime, the PCM is melted by absorbing heat from the return water flow. The set up for the discharging phase involves a pump for water circulation through the water pipe at a stable temperature of 23°C representing the return water temperature [13]. In the discharging phase, lamellas are closed, and the LHTES is isolated from the outdoor air [13]. The melting and solidification temperatures and the PCM's melting and solidification time will be identified with temperature sensors. The water (HTF) temperatures (inlet and outlet) difference and the mass flow rates will be measured during the discharging phase with an energy and flow meter. The rate of heat transfer will be calculated based on the measurements. The long-term performance of the LHTES shall be evaluated in the next step after the system is established in an office building.

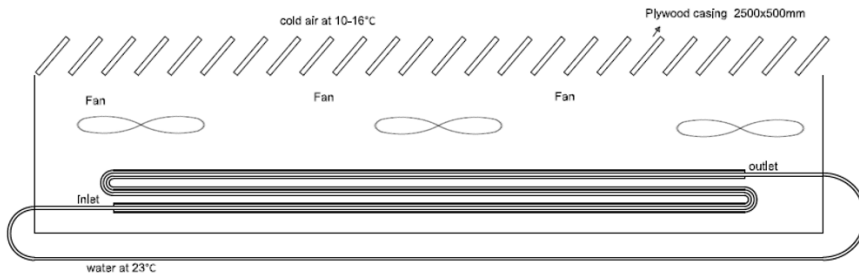


Figure 26: Experimental setup of the charging phase for the LHTES

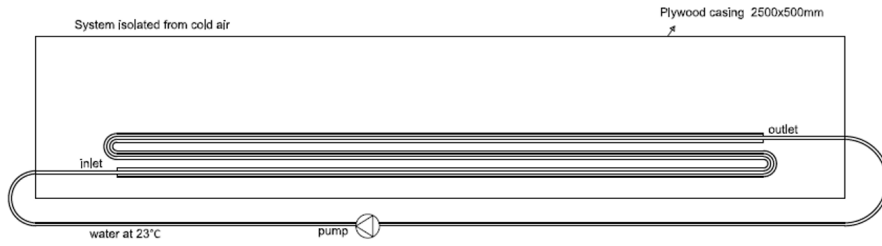


Figure 27: Experimental setup of the discharging phase for the LHTES

Literature List

- [1] International Energy Agency (IEA), “The Future of Cooling Opportunities for energy- efficient air conditioning,” p. 92, 2018, [Online]. Available: https://iea.blob.core.windows.net/assets/0bb45525-277f-4c9c-8d0c9c0cb5e7d525/The_Future_of_Cooling.pdf. (Accessed 7 May 2022).
- [2] “Cooling,” Paris, 2021. [Online]. Available: <https://www.iea.org/reports/cooling>. (Accessed 7 October 2022).
- [3] G. Alva, Y. Lin, and G. Fang, “An overview of thermal energy storage systems,” *Energy*, vol. 144, pp. 341–378, 2018, doi: 10.1016/j.energy.2017.12.037.
- [4] L. F. Cabeza, I. Martorell, L. Miró, A. I. Fernández, and C. Barreneche, “Introduction to thermal energy storage (TES) systems,” in *Advances in Thermal Energy Storage Systems: Methods and Applications*, 2015, doi: 10.1533/9781782420965.1.
- [5] M. Medrano, A. Gil, I. Martorell, X. Potau, and L. F. Cabeza, “State of the art on high-temperature thermal energy storage for power generation. Part 2-Case studies,” *Renew. Sustain. Energy Rev.*, vol. 14, no. 1, pp. 56–72, 2010, doi: 10.1016/j.rser.2009.07.036.
- [6] M. Felderhoff, R. Urbanczyk, and S. Peil, “Thermochemical heat storage for high temperature applications-A review,” *Green*, vol. 3, no. 2, pp. 113–123, 2013, doi: 10.1515/green-2013-0011.
- [7] A. S. Fleischer, *Thermal Energy Storage Using Phase Change Materials Fundamentals and Applications, Springer Briefs in Applied Sciences and Technology Thermal Engineering and Applied Science*, 2015.
- [8] A. Sharma, V. V. Tyagi, C. R. Chen, and D. Buddhi, “Review on thermal energy storage with phase change materials and applications,” *Renew. Sustain. Energy Rev.*, vol. 13, no. 2, pp. 318–345, 2009, doi: 10.1016/j.rser.2007.10.005.
- [9] D. Zhou, C. Y. Zhao, and Y. Tian, “Review on thermal energy storage with phase change materials (PCMs) in building applications,” *Appl. Energy*, vol. 92, pp. 593–605, 2012, doi: 10.1016/j.apenergy.2011.08.025.
- [10] V. V. Tyagi and D. Buddhi, “PCM thermal storage in buildings: A state of art,” *Renew. Sustain. Energy Rev.*, vol. 11, no. 6, pp. 1146–1166, 2007, doi: 10.1016/j.rser.2005.10.002.

- [11] N. Soares, J. J. Costa, A. R. Gaspar, and P. Santos, "Review of passive PCM latent heat thermal energy storage systems towards buildings' energy efficiency," *Energy Build.*, vol. 59, pp. 82–103, 2013, doi: 10.1016/j.enbuild.2012.12.042.
- [12] X. Q. Zhai, X. L. Wang, T. Wang, and R. Z. Wang, "A review on phase change cold storage in air-conditioning system: Materials and applications," *Renew. Sustain. Energy Rev.*, 2013, doi: 10.1016/j.rser.2013.02.013.
- [13] E. Paroutoglou, A. Afshari, N. C. Bergsøe, P. Fojan, and G. Hultmark, "A PCM based cooling system for office buildings: a state of the art review," *E3S Web Conf.*, vol. 111, no. 201 9, p. 01026, 2019, doi: 10.1051/e3sconf/201911101026.
- [14] E. Paroutoglou, A. Afshari, P. Fojan, and G. Hultmark, "Investigation of Thermal Behavior of Paraffins, Fatty Acids, Salt Hydrates and Renewable Based Oils as PCM," *Proc. 14th Int. Renew. Energy Storage Conf. 2020 (IRES 2020)*, vol. 6, 2021, doi: 10.2991/ahe.k.210202.006.
- [15] E. Paroutoglou, P. Fojan, L. Gurevich, G. Hultmark, and A. Afshari, "Thermal Analysis of Organic and Nanoencapsulated Electrospun Phase Change Materials," *Energies*, vol. 14, no. 4, p. 995, 2021, doi: 10.3390/en14040995.
- [16] E. Paroutoglou, P. Fojan, and L. Gurevich, and A. Afshari, "Thermal Properties of Novel Phase-Change Materials Based on Tamanu and Coconut Oil Encapsulated in Electrospun Fiber Matrices," *Sustainability*, vol 14, no. 12, p. 7432, 2022, doi:10.3390/su14127432.
- [17] E. Paroutoglou *et al.*, "A Numerical Parametric Study of a Double-Pipe LHTES Unit with PCM Encapsulated in the Annular Space," *Sustainability*, vol 14, no. 20, p. 13317, 2022, doi: 10.3390/su142013317.
- [18] A. T. Waterman, "Positive ionisation of certain hot salts, together with some observations on the electrical properties of molybdenite at high temperatures.," *London, Edinburgh, Dublin Philos. Mag. J. Sci.*, vol. 33, no. 195, pp. 225–247, 1917, doi: 10.1080/14786440308635634.
- [19] A. Fallahi, G. Guldentops, M. Tao, S. Granados-Focil, and S. Van Dessel, "Review on solid-solid phase change materials for thermal energy storage: Molecular structure and thermal properties," *Appl. Therm. Eng.*, vol. 127, no. September, pp. 1427–1441, 2017, doi: 10.1016/j.applthermaleng.2017.08.161.

- [20] K. Faraj, M. Khaled, J. Faraj, F. Hachem, and C. Castelain, "A review on phase change materials for thermal energy storage in buildings: Heating and hybrid applications," *J. Energy Storage*, vol. 33, 2021, doi: 10.1016/j.est.2020.101913.
- [21] Ma, Xiaoli, Zhao, Xudong, "Advanced Energy Efficiency Technologies for Solar Heating, Cooling and Power Generation" Springer International Publishing, 2019.
- [22] J. M. P. Q. Delgado, J. C. Martinho, A. Vaz Sá, A. S. Guimarães, and V. Abrantes, *Thermal Energy Storage with Phase Change Materials: A Literature Review of Applications for Buildings Materials*. 2019.
- [23] Y. Yuan, N. Zhang, W. Tao, X. Cao, and Y. He, "Fatty acids as phase change materials: A review," *Renew. Sustain. Energy Rev.*, vol. 29, pp. 482–498, 2014, doi: 10.1016/j.rser.2013.08.107.
- [24] Sharma, R. K., et al. "Developments in Organic Solid–liquid Phase Change Materials and Their Applications in Thermal Energy Storage." *Energy Conversion and Management*, vol. 95, 2015, pp. 193–228, doi:10.1016/j.enconman.2015.01.084.
- [25] S. D. Sharma, D. Buddhi, and R. L. Sawhney, "Accelerated thermal cycle test of latent heat-storage materials," *Sol. Energy*, vol. 66, no. 6, pp. 483–490, 1999, doi: 10.1016/S0038-092X(99)00045-6.
- [26] I. Dincer and M. A. Ezan, *Heat Storage: A Unique Solution For Energy Systems*. 2018.
- [27] M. Koschenz and B. Lehmann, "Development of a thermally activated ceiling panel with PCM for application in lightweight and retrofitted buildings," *Energy Build.*, vol. 36, no. 6, pp. 567–578, 2004, doi: 10.1016/j.enbuild.2004.01.029.
- [28] C. Arkar, B. Vidrih, and S. Medved, "Efficiency of free cooling using latent heat storage integrated into the ventilation system of a low energy building," *Int. J. Refrig.*, vol. 30, no. 1, pp. 134–143, 2007, doi: 10.1016/j.ijrefrig.2006.03.009.
- [29] W. Youssef, Y. T. Ge, and S. A. Tassou, "CFD modelling development and experimental validation of a phase change material (PCM) heat exchanger with spiral-wired tubes," *Energy Convers. Manag.*, vol. 157, no. October 2017, pp. 498–510, 2018, doi: 10.1016/j.enconman.2017.12.036.

- [30] H. Akeiber *et al.*, “A review on phase change material (PCM) for sustainable passive cooling in building envelopes,” *Renew. Sustain. Energy Rev.*, vol. 60, pp. 1470–1497, 2016, doi: 10.1016/j.rser.2016.03.036.
- [31] J. Kośny, *PCM-Enhanced Building Components*. 2015.
- [32] A. E. Bailey, “Melting and Solidification of fats,” *Wiley Interscience*. 1950.
- [33] M. M. Farid, F. A. Hamad, and M. Abu-Arabi, “Phase change cool storage using dimethyl-sulfoxide,” *Energy Convers. Manag.*, vol. 39, no. 8, pp. 819–826, 1998, doi: 10.1016/S0196-8904(97)00037-X
- [34] S. Wi, J. Seo, S. G. Jeong, S. J. Chang, Y. Kang, and S. Kim, “Thermal properties of shape-stabilized phase change materials using fatty acid ester and exfoliated graphite nanoplatelets for saving energy in buildings,” *Sol. Energy Mater. Sol. Cells*, vol. 143, pp. 168–173, 2015, doi: 10.1016/j.solmat.2015.06.040.
- [35] A. Abhat, “Low temperature latent heat thermal energy storage: Heat storage materials,” *Sol. Energy*, vol. 30, no. 4, pp. 313–332, 1983, doi: 10.1016/0038-092X(83)90186-X.
- [36] R. Naumann and H. H. Emons, “Results of thermal analysis for investigation of salt hydrates as latent heat-storage materials,” *J. Therm. Anal.*, vol. 35, no. 3, pp. 1009–1031, 1989, doi: 10.1007/BF02057256.
- [37] D. Feldman, M. M. Shapiro, D. Banu, and C. J. Fuks, “Fatty acids and their mixtures as phase-change materials for thermal energy storage,” *Sol. Energy Mater.*, vol. 18, no. 3, pp. 201–216, 1989, doi: 10.1016/0165-1633(89)90054-3.
- [38] K. Peippo, P. Kauranen, and P. D. Lund, “A multicomponent PCM wall optimized for passive solar heating,” *Energy Build.*, 1991, doi: 10.1016/0378-7788(91)90009-R.
- [39] M. N. Roxas-Dimaano and T. Watanabe, “The capric and lauric acid mixture with chemical additives as latent heat storage materials for cooling application,” *Energy*, vol. 27, no. 9, pp. 869–888, 2002, doi: 10.1016/S0360-5442(02)00024-5.
- [40] U. Stritih and V. Butala, “Experimental investigation of energy saving in buildings with PCM cold storage,” *Int. J. Refrig.*, vol. 33, no. 8, pp. 1676–1683, 2010, doi: 10.1016/j.ijrefrig.2010.07.017.

- [41] M. Yamaha, S. Misaki, and D. Shinya Misaki, "The Evaluation of Peak Shaving by a Thermal Storage System Using Phase-Change Materials in Air Distribution Systems," *HVAC & R Research*, vol. 9669, 2011, doi: 10.1080/10789669.2006.10391213.
- [42] K. Nagano, S. Takeda, T. Mochida, K. Shimakura, and T. Nakamura, "Study of a floor supply air conditioning system using granular phase change material to augment building mass thermal storage - Heat response in small scale experiments," *Energy Build.*, vol. 38, no. 5, pp. 436–446, 2006, doi: 10.1016/j.enbuild.2005.07.010.
- [43] G. J. Suppes, M. J. Goff, and S. Lopes, "Latent heat characteristics of fatty acid derivatives pursuant phase change material applications," *Chem. Eng. Sci.*, vol. 58, no. 9, pp. 1751–1763, 2003, doi: 10.1016/S0009-2509(03)00006-X.
- [44] M. Kenisarin and K. Mahkamov, "Solar energy storage using phase change materials," *Renew. Sustain. Energy Rev.*, vol. 11, no. 9, pp. 1913–1965, 2007, doi: 10.1016/j.rser.2006.05.005.
- [45] Rubitherm [Online]. Available: "Rubitherm GmbH." <https://www.rubitherm.eu/en/>. (Accessed 7 October 2018).
- [46] Pure Temp [Online]. Available: "Pure Temp." <https://puretemp.com/>. (Accessed 7 October 2018).
- [47] W. Main and S. Suite, "Safety Data sheet for Tiki Tamanu oil 100 % natural," [Online]. Available: <https://www.monoitiki.pf/>. (Accessed 12 February 2019).
- [48] S. Clarke, "Composition of essential oils and other materials," *Essent. Chem. Aromather.*, pp. 123–229, 2008, doi: 10.1016/b978-0-443-10403-9.00007-8.
- [49] A. R. Shirin-Abadi, A. R. Mahdavian, and S. Khoee, "New approach for the elucidation of PCM nanocapsules through miniemulsion polymerization with an acrylic shell," *Macromolecules*, vol. 44, no. 18, pp. 7405–7414, 2011, doi: 10.1021/ma201509d.
- [50] C. Liu, Z. Rao, J. Zhao, Y. Huo, and Y. Li, "Review on nanoencapsulated phase change materials: Preparation, characterization and heat transfer enhancement," *Nano Energy*. 2015, doi: 10.1016/j.nanoen.2015.02.016.
- [51] R. Jacob and F. Bruno, "Review on shell materials used in the encapsulation of phase change materials for high temperature thermal energy storage,"

- Renew. Sustain. Energy Rev.*, vol. 48, pp. 79–87, 2015, doi: 10.1016/j.rser.2015.03.038.
- [52] P. B. Salunkhe and P. S. Shembekar, “A review on effect of phase change material encapsulation on the thermal performance of a system,” *Renew. Sustain. Energy Rev.*, vol. 16, no. 8, pp. 5603–5616, 2012, doi: 10.1016/j.rser.2012.05.037.
- [53] A. Jamekhorshid, S. M. Sadrameli, and M. Farid, “A review of microencapsulation methods of phase change materials (PCMs) as a thermal energy storage (TES) medium,” *Renew. Sustain. Energy Rev.*, vol. 31, pp. 531–542, 2014, doi: 10.1016/j.rser.2013.12.033.
- [54] H. Zhang, C. Xu, and G. Fang, “Encapsulation of inorganic phase change thermal storage materials and its effect on thermophysical properties: A review,” *Sol. Energy Mater. Sol. Cells*, vol. 241, no. April, p. 111747, 2022, doi: 10.1016/j.solmat.2022.111747.
- [55] S. Valdivia-Rivera, T. Ayora-Talavera, M. A. Lizardi-Jiménez, U. García-Cruz, J. C. Cuevas-Bernardino, and N. Pacheco, “Encapsulation of microorganisms for bioremediation: Techniques and carriers,” *Rev. Environ. Sci. Biotechnol.*, vol. 20, no. 3, pp. 815–838, 2021, doi: 10.1007/s11157-021-09577-x.
- [56] C. V. Podara, I. A. Kartsonakis, and C. A. Charitidis, “Towards phase change materials for thermal energy storage: classification, improvements and applications in the building sector,” *Appl. Sci.*, vol. 11, no. 4, pp. 1–26, 2021, doi: 10.3390/app11041490.
- [57] A. Taha *et al.*, “Ultrasonic emulsification: An overview on the preparation of different emulsifiers-stabilized emulsions,” *Trends Food Sci. Technol.*, vol. 105, pp. 363–377, 2020, doi: 10.1016/j.tifs.2020.09.024.
- [58] S. Akbari and A. H. Nour, “Emulsion types, stability mechanisms and rheology: A review,” *Int. J. Innov. Res. Sci. Stud.*, vol. 1, no. 1, pp. 11–17, 2018, doi: 10.53894/ijirss.v1i1.4.
- [59] T. Sheth, S. Seshadri, T. Prileszky, and M. E. Helgeson, “Multiple nanoemulsions,” *Nat. Rev. Mater.*, vol. 5, no. 3, pp. 214–228, 2020, doi: 10.1038/s41578-019-0161-9.
- [60] O. Ansl, “Study on Demulsification of Water-in-Oil Emulsions Via Microwave Heating Technology,” 2005, [Online]. Available: https://www.academia.edu/6668249/Lufenuron_Impair_the_Chitin_Synthesi

s_and_Development_of_Spodoptera_littoralis_Bosid_Lepidoptera_Noctuidae_. (accessed 10 November 2022).

- [61] C. A. Buckner *et al.*, “Microemulsions: Thermodynamic and Dynamic Properties,” *Thermodynamics*, vol. 11, p. 13, 2016, [Online]. Available: <https://www.intechopen.com/books/advancedbiometricstechnologies/liveness-detection-in-biometrics>. (accessed 2 November 2022).
- [62] Y. T. Hu, Y. Ting, J. Y. Hu, and S. C. Hsieh, “Techniques and methods to study functional characteristics of emulsion systems,” *J. Food Drug Anal.*, vol. 25, no. 1, pp. 16–26, 2017, doi: 10.1016/j.jfda.2016.10.021.
- [63] X. Zhang, J. Niu, and J. Y. Wu, “Development and characterization of novel and stable silicon nanoparticles-embedded PCM-in-water emulsions for thermal energy storage,” *Appl. Energy*, vol. 238, no. April 2018, pp. 1407–1416, 2019, doi: 10.1016/j.apenergy.2019.01.159.
- [64] T. Kousksou, T. El Rhafiki, A. Jamil, P. Bruel, and Y. Zeraouli, “PCMs inside emulsions: Some specific aspects related to DSC (differential scanning calorimeter)-like configurations,” *Energy*, vol. 56, pp. 175–183, 2013, doi: 10.1016/j.energy.2013.04.040.
- [65] C. J. Ho, S. T. Hsu, T. F. Yang, B. L. Chen, S. Rashidi, and W. M. Yan, “Cooling performance of mini-channel heat sink with water-based nano-PCM emulsion-An experimental study,” *Int. J. Therm. Sci.*, vol. 164, no. February, 2021, doi: 10.1016/j.ijthermalsci.2021.106903.
- [66] C. J. Ho, S. T. Hsu, S. Rashidi, and W. M. Yan, “Water-based nano-PCM emulsion flow and heat transfer in divergent mini-channel heat sink—An experimental investigation,” *Int. J. Heat Mass Transf.*, vol. 148, 2020, doi: 10.1016/j.ijheatmasstransfer.2019.119086.
- [67] M. Delgado, A. Lázaro, J. Mazo, C. Peñalosa, J. M. Marín, and B. Zalba, “Experimental analysis of a coiled stirred tank containing a low cost PCM emulsion as a thermal energy storage system,” *Energy*, vol. 138, pp. 590–601, 2017, doi: 10.1016/j.energy.2017.07.044.
- [68] L. Liu, J. Li, J. Niu, and J. Y. Wu, “Evaluation of the energy storage performance of PCM nano-emulsion in a small tubular heat exchanger,” *Case Stud. Therm. Eng.*, vol. 26, no. June, p. 101156, 2021, doi: 10.1016/j.csite.2021.101156.
- [69] X. Zhang, J. Niu, S. Zhang, and J. Y. Wu, “PCM in water emulsions: Supercooling reduction effects of nano-additives, viscosity effects of

- surfactants and stability,” *Adv. Eng. Mater.*, vol. 17, no. 2, pp. 181–188, 2015, doi: 10.1002/adem.201300575.
- [70] X. Zhang, J. Y. Wu, and J. Niu, “PCM-in-water emulsion for solar thermal applications: The effects of emulsifiers and emulsification conditions on thermal performance, stability and rheology characteristics,” *Sol. Energy Mater. Sol. Cells*, vol. 147, pp. 211–224, 2016, doi: 10.1016/j.solmat.2015.12.022.
- [71] L. Sapei, I. G. Y. H. Sandy, I. M. K. D. Suputra, and M. Ray, “The effect of different concentrations of tween-20 combined with rice husk silica on the stability of o/w emulsion: A kinetic study,” *IOP Conf. Ser. Mater. Sci. Eng.*, vol. 273, p. 012023, 2017, doi: 10.1088/1757-899x/273/1/012023.
- [72] X. Zhang, J. Niu, and J. yong Wu, “Evaluation and manipulation of the key emulsification factors toward highly stable PCM-water nano-emulsions for thermal energy storage,” *Sol. Energy Mater. Sol. Cells*, vol. 219, no. March 2020, p. 110820, 2021, doi: 10.1016/j.solmat.2020.110820.
- [73] T. El Rhafiki, T. Kousksou, A. Jamil, S. Jegadheeswaran, S. D. Pohekar, and Y. Zeraouli, “Crystallization of PCMs inside an emulsion: Supercooling phenomenon,” *Sol. Energy Mater. Sol. Cells*, vol. 95, no. 9, pp. 2588–2597, 2011, doi: 10.1016/j.solmat.2011.03.027.
- [74] T. Kousksou, T. El Rhafiki, M. Mahdaoui, P. Bruel, and Y. Zeraouli, “Crystallization of supercooled PCMs inside emulsions: DSC applications,” *Sol. Energy Mater. Sol. Cells*, vol. 107, pp. 28–36, 2012, doi: 10.1016/j.solmat.2012.07.023.
- [75] E. Günther, T. Schmid, H. Mehling, S. Hiebler, and L. Huang, “Subcooling in hexadecane emulsions,” *Int. J. Refrig.*, vol. 33, no. 8, pp. 1605–1611, 2010, doi: 10.1016/j.ijrefrig.2010.07.022.
- [76] L. Liu, J. Niu, and J. Y. Wu, “Formulation of highly stable PCM nano-emulsions with reduced supercooling for thermal energy storage using surfactant mixtures,” *Sol. Energy Mater. Sol. Cells*, vol. 223, no. December 2020, p. 110983, 2021, doi: 10.1016/j.solmat.2021.110983.
- [77] F. Agresti *et al.*, “Nano-encapsulated PCM emulsions prepared by a solvent-assisted method for solar applications,” *Sol. Energy Mater. Sol. Cells*, vol. 194, no. July 2018, pp. 268–275, 2019, doi: 10.1016/j.solmat.2019.02.021.
- [78] L. Huang, E. Günther, C. Doetsch, and H. Mehling, “Subcooling in PCM emulsions-Part 1: Experimental,” *Thermochim. Acta*, vol. 509, no. 1–2, pp.

93–99, 2010, doi: 10.1016/j.tca.2010.06.006.

- [79] E. Günther, L. Huang, H. Mehling, and C. Dötsch, “Subcooling in PCM emulsions - Part 2: Interpretation in terms of nucleation theory,” *Thermochim. Acta*, vol. 522, no. 1–2, pp. 199–204, 2011, doi: 10.1016/j.tca.2011.04.027.
- [80] S. Gschwander, S. Niedermaier, S. Gamisch, M. Kick, F. Klünder, and T. Haussmann, “Storage capacity in dependency of supercooling and cycle stability of different pcm emulsions,” *Appl. Sci.*, vol. 11, no. 8, 2021, doi: 10.3390/app11083612.
- [81] W. H. Carothers, “Polymerization,” *Chem. Rev.*, vol. 8, no. 3, pp. 353–426, 1931, doi: 10.1021/cr60031a001.
- [82] W. Su, J. Darkwa, and G. Kokogiannakis, “Review of solid-liquid phase change materials and their encapsulation technologies,” *Renew. Sustain. Energy Rev.*, vol. 48, pp. 373–391, 2015, doi: 10.1016/j.rser.2015.04.044.
- [83] B. Srinivasaraonaik, L. P. Singh, I. Tyagi, A. Rawat, and S. Sinha, “Microencapsulation of a eutectic PCM using in situ polymerization technique for thermal energy storage,” *Int. J. Energy Res.*, vol. 44, no. 5, pp. 3854–3864, 2020, doi: 10.1002/er.5182.
- [84] F. Khakzad, Z. Alinejad, A. R. Shirin-Abadi, M. Ghasemi, and A. R. Mahdavian, “Optimization of parameters in preparation of PCM microcapsules based on melamine formaldehyde through dispersion polymerization,” *Colloid Polym. Sci.*, vol. 292, no. 2, pp. 355–368, 2014, doi: 10.1007/s00396-013-3076-9.
- [85] L. Sánchez, P. Sánchez, M. Carmona, A. de Lucas, and J. F. Rodríguez, “Influence of operation conditions on the microencapsulation of PCMs by means of suspension-like polymerization,” *Colloid Polym. Sci.*, vol. 286, no. 8–9, pp. 1019–1027, 2008, doi: 10.1007/s00396-008-1864-4.
- [86] Y. Fang, S. Kuang, X. Gao, and Z. Zhang, “Preparation of nanoencapsulated phase change material as latent functionally thermal fluid,” *J. Phys. D. Appl. Phys.*, vol. 42, no. 3, 2009, doi: 10.1088/0022-3727/42/3/035407.
- [87] A. M. Borreguero, M. Carmona, M. L. Sanchez, J. L. Valverde, and J. F. Rodriguez, “Improvement of the thermal behaviour of gypsum blocks by the incorporation of microcapsules containing PCMS obtained by suspension polymerization with an optimal core/coating mass ratio,” *Appl. Therm. Eng.*, vol. 30, no. 10, pp. 1164–1169, 2010, doi:

- 10.1016/j.applthermaleng.2010.01.032.
- [88] L. Sánchez-Silva, J. F. Rodríguez, A. Romero, A. M. Borreguero, M. Carmona, and P. Sánchez, “Microencapsulation of PCMs with a styrene-methyl methacrylate copolymer shell by suspension-like polymerisation,” *Chem. Eng. J.*, vol. 157, no. 1, pp. 216–222, 2010, doi: 10.1016/j.cej.2009.12.013.
 - [89] M. Fuensanta, U. Paiphansiri, M. D. Romero-Sánchez, C. Guillem, Á. M. López-Buendía, and K. Landfester, “Thermal properties of a novel nanoencapsulated phase change material for thermal energy storage,” *Thermochim. Acta*, vol. 565, pp. 95–101, 2013, doi: 10.1016/j.tca.2013.04.028.
 - [90] T. Qian, J. Li, W. Feng, and H. Nian, “Enhanced thermal conductivity of form-stable phase change composite with single-walled carbon nanotubes for thermal energy storage,” *Sci. Rep.*, vol. 7, no. November 2016, pp. 1–10, 2017, doi: 10.1038/srep44710.
 - [91] C. Wang *et al.*, “Graphene oxide stabilized polyethylene glycol for heat storage,” *Phys. Chem. Chem. Phys.*, vol. 14, no. 38, pp. 13233–13238, 2012, doi: 10.1039/c2cp41988b.
 - [92] M. Li, Z. Wu, and H. Kao, “Study on preparation and thermal properties of binary fatty acid/diatomite shape-stabilized phase change materials,” *Sol. Energy Mater. Sol. Cells*, vol. 95, no. 8, pp. 2412–2416, 2011, doi: 10.1016/j.solmat.2011.04.017.
 - [93] K. A. Eckert, S. Dasgupta, B. Selge, and P. Ay, “Solid liquid phase diagrams of binary fatty acid mixtures - Palmitic/stearic with oleic/linoleic/linolenic acid mixture,” *Thermochim. Acta*, vol. 630, pp. 50–63, 2016, doi: 10.1016/j.tca.2016.02.008.
 - [94] A. N. Mustapha, Y. Zhang, Z. Zhang, Y. Ding, and Y. Li, “A systematic study on the reaction mechanisms for the microencapsulation of a volatile phase change material (PCM) via one-step in situ polymerisation,” *Chem. Eng. Sci.*, vol. 252, p. 117497, 2022, doi: 10.1016/j.ces.2022.117497.
 - [95] Y. Taguchi, R. Morita, N. Saito, and M. Tanaka, “Formation of Pickering emulsion by use of PCM and SiC and application to preparation of hybrid microcapsules with interfacial polycondensation reaction,” *Polym. Adv. Technol.*, vol. 27, no. 4, pp. 422–428, 2016, doi: 10.1002/pat.3687.
 - [96] L. Liu *et al.*, “Shape-stabilized phase change materials based on

- poly(ethylene-graft-maleic anhydride)-g-alkyl alcohol comb-like polymers,” *Sol. Energy Mater. Sol. Cells*, vol. 143, pp. 21–28, 2015, doi: 10.1016/j.solmat.2015.06.038.
- [97] D. Rafiei, S.; Hamrang, Abbas ; Balkose, Devrim ; Hamrang, A ; Balkose, “No Title,” in *Applied Methodologies in Polymer Research and Technology*, 2014.
- [98] F. K. Ko, Y. Wan., *Introduction to Nanofiber Materials*. Cambridge university press, 2014.
- [99] Rui L. Reis, *Encyclopedia of Tissue Engineering and Regenerative Medicine*. Elsevier, 2019.
- [100] Y. Imura, R. M. C. Hogan, and M. Jaffe, “Dry spinning of synthetic polymer fibers,” *Adv. Filam. Yarn Spinn. Text. Polym.*, pp. 187–202, 2014, doi: 10.1533/9780857099174.2.187.
- [101] N. Tucker, J. J. Stanger, M. P. Staiger, H. Razzaq, and K. Hofman, “The history of the science and technology of electrospinning from 1600 to 1995,” *J. Eng. Fiber. Fabr.*, vol. 7, no. 3, pp. 63–73, 2012, doi: 10.1177/155892501200702s10.
- [102] R. Amna, K. Ali, M. I. Malik, and S. I. Shamsah, “A brief review of electrospinning of polymer nanofibers: History and main applications,” *J. New Mater. Electrochem. Syst.*, vol. 23, no. 3, pp. 151–163, 2020, doi: 10.14447/jnmes.v23i3.a01.
- [103] W. E. Teo and S. Ramakrishna, “A review on electrospinning design and nanofibre assemblies,” *Nanotechnology*, vol. 17, no. 14, 2006, doi: 10.1088/0957-4484/17/14/R01.
- [104] N. R, “Fabrication and characterisation of polypropylene nanofibres by melt electrospinning and meltblowing.,” RMIT University, Melbourne, 2012.
- [105] Moustafa M. Zagho and Ahmed Elzatahry, “Recent Trends in Electrospinning of Polymer Nanofibers and their Applications as Templates for Metal Oxide Nanofibers Preparation,” in *Intech*, 2012, p. 13.
- [106] L. D. Tijjing, Y. C. Woo, M. Yao, J. Ren, and H. K. Shon, *Electrospinning for Membrane Fabrication: Strategies and Applications*, July. 2017.
- [107] C. Zhang, Y. Li, P. Wang, and H. Zhang, “Electrospinning of nanofibers: Potentials and perspectives for active food packaging,” *Compr. Rev. Food*

- Sci. Food Saf.*, vol. 19, no. 2, pp. 479–502, 2020, doi: 10.1111/1541-4337.12536.
- [108] J. He and Y. Zhou, “Chapter 6 - Multineedle Electrospinning,” in *Electrospinning: Nanofabrication and Applications*, B. Ding, X. Wang, and J. Yu, Eds. William Andrew Publishing, 2019, pp. 201–218.
- [109] M. Wang *et al.*, “Electrospinning of silica nanochannels for single molecule detection,” *Appl. Phys. Lett.*, vol. 88, no. 3, pp. 1–3, 2006, doi: 10.1063/1.2165277.
- [110] D. Li and Y. Xia, “Direct fabrication of composite and ceramic hollow nanofibers by electrospinning,” *Nano Lett.*, vol. 4, no. 5, pp. 933–938, 2004, doi: 10.1021/nl049590f.
- [111] D. Han and A. J. Steckl, “Triaxial electrospun nanofiber membranes for controlled dual release of functional molecules,” *ACS Appl. Mater. Interfaces*, vol. 5, no. 16, pp. 8241–8245, 2013, doi: 10.1021/am402376c.
- [112] I. Partheniadis, I. Nikolakakis, I. Laidmäe, and J. Heinämäki, “A mini-review: Needleless electrospinning of nanofibers for pharmaceutical and biomedical applications,” *Processes*, vol. 8, no. 6, 2020, doi: 10.3390/PR8060673.
- [113] Taylor, Geoffrey Ingram. “Disintegration of Water Drops in an Electric Field.” *Proceedings of the Royal Society of London. Series A, Mathematical and Physical Sciences*, vol. 280, no. 1382, 1964, pp. 383–97, doi:10.1098/rspa.1964.0151.
- [114] C. Chen, L. Wang, and Y. Huang, “Electrospinning of thermo-regulating ultrafine fibers based on polyethylene glycol/cellulose acetate composite,” *Polymer (Guildf.)*, vol. 48, no. 18, pp. 5202–5207, 2007, doi: 10.1016/j.polymer.2007.06.069.
- [115] C. Chen, L. Wang, and Y. Huang, “Crosslinking of the electrospun polyethylene glycol/cellulose acetate composite fibers as shape-stabilized phase change materials,” *Mater. Lett.*, vol. 63, no. 5, pp. 569–571, 2009, doi: 10.1016/j.matlet.2008.11.033.
- [116] Q. Shi, Z. Liu, X. Jin, Y. Shen, and Y. Liu, “Electrospun fibers based on polyvinyl pyrrolidone/Eu-polyethylene glycol as phase change luminescence materials,” *Mater. Lett.*, vol. 147, pp. 113–115, 2015, doi: 10.1016/j.matlet.2015.02.040.

- [117] C. Chen, K. Liu, H. Wang, W. Liu, and H. Zhang, "Morphology and performances of electrospun polyethylene glycol / poly (dl-lactide) phase change ultra fine fibers for thermal energy storage," *Sol. Energy Mater. Sol. Cells*, vol. 117, pp. 372–381, 2013, doi: 10.1016/j.solmat.2013.07.001.
- [118] W. Zhu *et al.*, "Environmental-friendly electrospun phase change fiber with exceptional thermal energy storage performance," *Sol. Energy Mater. Sol. Cells*, vol. 222, no. July 2020, p. 110939, 2021, doi: 10.1016/j.solmat.2020.110939.
- [119] E. Zdraveva, J. Fang, B. Mijovic, and T. Lin, "Electrospun Poly(vinyl alcohol)/Phase Change Material Fibers: Morphology, Heat Properties, and Stability," *Ind. Eng. Chem. Res.*, vol. 54, no. 35, pp. 8706–8712, 2015, doi: 10.1021/acs.iecr.5b01822.
- [120] C. Chen, S. Liu, W. Liu, Y. Zhao, and Y. Lu, "Synthesis of novel solidliquid phase change materials and electrospinning of ultrafine phase change fibers," *Sol. Energy Mater. Sol. Cells*, vol. 96, no. 1, pp. 202–209, 2012, doi: 10.1016/j.solmat.2011.09.057.
- [121] R. Perez-Masia, A. Lopez-Rubio, M. J. Fabra, and J. M. Lagaron, "Biodegradable polyester-based heat management materials of interest in refrigeration and smart packaging coatings," *J. Appl. Polym. Sci.*, vol. 130, no. 5, pp. 3251–3262, 2013, doi: 10.1002/app.39555.
- [122] L. Zhao, "Emulsion-electrospinning n -octadecane / silk composite fiber as environmental-friendly form-stable phase change materials," vol. 45538, pp. 1–10, 2017, doi: 10.1002/app.45538.
- [123] C. Chen, L. Wang, and Y. Huang, "A novel shape-stabilized PCM: Electrospun ultrafine fibers based on lauric acid/polyethylene terephthalate composite," *Mater. Lett.*, vol. 62, no. 20, pp. 3515–3517, 2008, doi: 10.1016/j.matlet.2008.03.034.
- [124] Y. Cai *et al.*, "Effects of nano-SiO₂ on morphology, thermal energy storage, thermal stability, and combustion properties of electrospun lauric acid/PET ultrafine composite fibers as form-stable phase change materials," *Appl. Energy*, vol. 88, no. 6, pp. 2106–2112, 2011, doi: 10.1016/j.apenergy.2010.12.071.
- [125] Huizhen Ke, Yibing Cai, Qufu Wei, Yao Xiao, Ju Dong, Yuan Hu, Lei Song, Guangfei He, Yong Zhao, Hao Fong, "Electrospun ultrafine composite fibers of binary fatty acid eutectics and polyethylene terephthalate as innovative form-stable phase change materials for storage and retrieval of

- thermal energy,” *Int. J. ENERGY Res.*, vol. 37, pp. 657–664, 2012, doi: 10.1002/er.2888.
- [126] C. Chen, L. Wang, and Y. Huang, “Morphology and thermal properties of electrospun fatty acids / polyethylene terephthalate composite fibers as novel form-stable phase change materials,” *Sol. Energy Mater. Sol. Cells*, vol. 92, pp. 1382–1387, 2008, doi: 10.1016/j.solmat.2008.05.013.
- [127] Y. Cai *et al.*, “Electrospun ultrafine composite fibers consisting of lauric acid and polyamide 6 as form-stable phase change materials for storage and retrieval of solar thermal energy,” *Sol. Energy Mater. Sol. Cells*, vol. 103, pp. 53–61, 2012, doi: 10.1016/j.solmat.2012.04.031.
- [128] Y. Cai *et al.*, “The improvement of thermal stability and conductivity via incorporation of carbon nanofibers into electrospun ultrafine composite fibers of lauric acid/polyamide 6 phase change materials for thermal energy storage,” *Int. J. Green Energy*, vol. 11, no. 8, pp. 861–875, 2014, doi: 10.1080/15435075.2013.829068.
- [129] H. Ke, Y. Li, J. Wang, B. Peng, Y. Cai, and Q. Wei, “Ag-coated polyurethane fibers membranes absorbed with quinary fatty acid eutectics solid-liquid phase change materials for storage and retrieval of thermal energy,” vol. 99, pp. 1–9, 2016, doi: 10.1016/j.renene.2016.06.033.
- [130] C. Lin *et al.*, “Ultrafine electrospun fiber based on ionic liquid/AlN/copolyamide composite as novel form-stable phase change material for thermal energy storage,” *Sol. Energy Mater. Sol. Cells*, vol. 223, no. December 2020, p. 110953, 2021, doi: 10.1016/j.solmat.2020.110953.
- [131] C. Chen, L. Wang, and Y. Huang, “Ultrafine electrospun fibers based on stearyl stearate / polyethylene terephthalate composite as form stable phase change materials,” vol. 150, pp. 269–274, 2009, doi: 10.1016/j.cej.2009.03.007.
- [132] P. S. Mohamadi, A. Hivechi, H. Bahrami, N. hemmatinegad, and P. B. Milan, “Antibacterial and biological properties of coconut oil loaded poly(ϵ -caprolactone)/gelatin electrospun membranes,” *J. Ind. Text.*, pp. 1–25, 2021, doi: 10.1177/1528083721991595.
- [133] J. T. McCann, M. Marquez, and Y. Xia, “Melt coaxial electrospinning: A versatile method for the encapsulation of solid materials and fabrication of phase change nanofibers,” *Nano Lett.*, vol. 6, no. 12, pp. 2868–2872, 2006, doi: 10.1021/nl0620839.

- [134] W. Hu and X. Yu, "Encapsulation of bio-based PCM with coaxial electrospun ultrafine fibers," *RSC Adv.*, vol. 2, no. 13, pp. 5580–5584, 2012, doi: 10.1039/c2ra20532g.
- [135] Y. S. Fengyu Li, Yong Zhao, Sen Wang, Dong Han, Lei Jiang, "Thermochromic Core–Shell Nanofibers Fabricated by Melt Coaxial Electrospinning," *Inc. J Appl Polym Sci*, vol. 112, pp. 269–274, 2008, doi: 10.1002/app.29384.
- [136] W. Chalco-Sandoval, M. J. Fabra, A. López-Rubio, and J. M. Lagaron, "Development of an encapsulated phase change material via emulsion and coaxial electrospinning," *J. Appl. Polym. Sci.*, vol. 133, no. 36, 2016, doi: 10.1002/app.43903.
- [137] W. M. R. N. Udangawa, C. F. Willard, C. Mancinelli, C. Chapman, R. J. Linhardt, and T. J. Simmons, "Coconut oil-cellulose beaded microfibers by coaxial electrospinning: An eco-model system to study thermoregulation of confined phase change materials," *Cellulose*, vol. 26, no. 3, pp. 1855–1868, 2019, doi: 10.1007/s10570-018-2151-2.
- [138] S. Li, H. Wang, H. Mao, J. Li, and H. Shi, "Light-to-Thermal Conversion and Thermoregulated Capability of Coaxial Fibers with a Combined Influence from Comb-like Polymeric Phase Change Material and Carbon Nanotube," *ACS Appl. Mater. Interfaces*, vol. 11, no. 15, pp. 14150–14158, 2019, doi: 10.1021/acsami.9b02387.
- [139] Y. Wan, P. Zhou, Y. Liu, and H. Chen, "Novel wearable polyacrylonitrile/phase-change material sheath/core nano-fibers fabricated by coaxial electro-spinning," *RSC Adv.*, pp. 21204–21209, 2016, doi: 10.1039/c6ra00281a.
- [140] W. Chalco-Sandoval, M. J. Fabra, A. López-Rubio, and J. M. Lagaron, "Electrospun heat management polymeric materials of interest in food refrigeration and packaging," *J. Appl. Polym. Sci.*, vol. 131, no. 16, 2014, doi: 10.1002/app.40661.
- [141] Wilson Chalco-Sandoval, María José Fabra, Amparo López-Rubio, Jose M. Lagaron, "Use of Phase Change Materials to develop Electrospun Coatings of interest in Food Packaging Applications," *J. M. J. Food Eng.*, vol. 192, pp. 122–128, 2017, doi: 10.1016/j.jfoodeng.2015.01.019.
- [142] M. E. Darzi, S. I. Golestaneh, M. Kamali, and G. Karimi, "Thermal and electrical performance analysis of co-electrospun-electrosprayed PCM nanofiber composites in the presence of graphene and carbon fiber powder,"

- Renew. Energy*, vol. 135, pp. 719–728, 2019, doi: 10.1016/j.renene.2018.12.028.
- [143] J. Xue, C. Zhu, J. Li, H. Li, and Y. Xia, “Integration of Phase-Change Materials with Electrospun Fibers for Promoting Neurite Outgrowth under Controlled Release,” *Adv. Funct. Mater.*, vol. 28, no. 15, pp. 1–11, 2018, doi: 10.1002/adfm.201705563.
- [144] S. I. Golestaneh, A. Mosallanejad, G. Karimi, M. Khorram, and M. Khashi, “Fabrication and characterization of phase change material composite fibers with wide phase-transition temperature range by co-electrospinning method,” *Appl. Energy*, vol. 182, pp. 409–417, 2016, doi: 10.1016/j.apenergy.2016.08.136.
- [145] S. K. Jaganathan, M. Mohan Prasath, A. Fauzi Ismail, A. Manikandan, and N. Gomathi, “Production and hemocompatibility assessment of novel electrospun polyurethane nanofibers loaded with dietary virgin coconut oil for vascular graft applications,” *J. Bioact. Compat. Polym.*, vol. 33, no. 2, pp. 210–223, 2018, doi: 10.1177/0883911517720815.
- [146] G. Chen *et al.*, “Polyacrylonitrile/polyethylene glycol phase-change material fibres prepared with hybrid polymer blends and nano-SiC fillers via centrifugal spinning,” *Polymer (Guildf)*, vol. 186, no. October 2019, p. 122012, 2020, doi: 10.1016/j.polymer.2019.122012.
- [147] X. Zhang *et al.*, “Preparation and performance of novel polyvinylpyrrolidone/polyethylene glycol phase change materials composite fibers by centrifugal spinning,” *Chem. Phys. Lett.*, vol. 691, pp. 314–318, 2018, doi: 10.1016/j.cplett.2017.11.041.
- [148] G. Chen *et al.*, “Preparation and properties of polyacrylonitrile / polyethylene glycol composite fibers phase change materials by centrifugal spinning,” *Mater. Res. Express*, Volume 6, Number 9, doi: 10.1088/2053-1591/ab2d0a
- [149] A. Safari, R. Saidur, F. A. Sulaiman, Y. Xu, and J. Dong, “A review on supercooling of Phase Change Materials in thermal energy storage systems,” *Renew. Sustain. Energy Rev.*, vol. 70, no. December 2016, pp. 905–919, 2017, doi: 10.1016/j.rser.2016.11.272.
- [150] M. K. Rathod and J. Banerjee, “Thermal stability of phase change materials used in latent heat energy storage systems: A review,” *Renew. Sustain. Energy Rev.*, vol. 18, pp. 246–258, 2013, doi: 10.1016/j.rser.2012.10.022.

- [151] Q. Peng, X. Wei, J. Ding, J. Yang, X. Yang , “High-temperature thermal stability of molten salt materials,” *Int. J. ENERGY Res.*, vol. 33, pp. 1164–1174, 2008, doi: 10.1002/er.1453.
- [152] K. R. Rajisha, B. Deepa, L. A. Pothan, and S. Thomas, “9 - Thermomechanical and spectroscopic characterization of natural fibre composites,” in *Interface Engineering of Natural Fibre Composites for Maximum Performance*, N. E. Zafeiropoulos, Ed. Woodhead Publishing, 2011, pp. 241–274.
- [153] K. H. J. Buschow, *The Encyclopedia of Materials : Science and Technology*. Pergamon Imprint, 2001.
- [154] S. A. Memon, “Phase change materials integrated in building walls: A state of the art review,” *Renew. Sustain. Energy Rev.*, vol. 31, pp. 870–906, 2014, doi: 10.1016/j.rser.2013.12.042.
- [155] T. Mokhena, M. Mochane, M. Tshwafo, L. Linganis, O. Thekiso, and S. Songca, *Isothermal Calorimetry: Molecular Interactions between Small Molecules in Organic Solvents*. 2016.
- [156] J. D. Menczel, L. Judovits, R. B. Prime, H. E. Bair, M. Reading, and S. Swier, “Differential Scanning Calorimetry (DSC),” *Therm. Anal. Polym. Fundam. Appl.*, pp. 7–239, 2008, doi: 10.1002/9780470423837.ch2.
- [157] Mackenzie RC, “Differential Thermal Analysis,” pp. 207–213, 1970.
- [158] C. De Blasio, “Fundamentals of biofuels engineering and technology: Thermogravimetric Analysis (TGA),” *Green Energy Technol.*, pp. 91–102, 2019, doi: 10.1007/978-3-030-11599-9.
- [159] A. Solé, L. Miró, C. Barreneche, I. Martorell, and L. F. Cabeza, “Review of the T-history method to determine thermophysical properties of phase change materials (PCM),” *Renew. Sustain. Energy Rev.*, vol. 26, pp. 425–436, 2013, doi: 10.1016/j.rser.2013.05.066.
- [160] KV Kodre, SR Attarde, PR Yendhe, RY Patil, “Differential scanning calorimetry: A Review,” *J. Pharm. Anal.*, vol. 5, no. 7, p. 60, 2014.
- [161] P. M. V Raja and A. R. Barron, “Physical methods in chemistry,” *Nature*, vol. 134, no. 3384, pp. 366–367, 1934, doi: 10.1002/jctb.5000533702.
- [162] C. Barreneche, A. Solé, L. Miró, I. Martorell, A. I. Fernández, and L. F. Cabeza, “Study on differential scanning calorimetry analysis with two

- operation modes and organic and inorganic phase change material (PCM)," *Thermochim. Acta*, vol. 553, pp. 23–26, 2013, doi: 10.1016/j.tca.2012.11.027.
- [163] C. M. C. Huang, S. F. Su, K. J. Lin, W. C. Chang, C. F. Yang, and Y. C. M. Li, "Metrology based on transient heat transfer theory for evaluating phase change materials with differential scanning calorimetry," *Thermochim. Acta*, vol. 707, no. November 2021, p. 179111, 2022, doi: 10.1016/j.tca.2021.179111.
- [164] X. Sun, K. O. Lee, M. A. Medina, Y. Chu, and C. Li, "Melting temperature and enthalpy variations of phase change materials (PCMs): a differential scanning calorimetry (DSC) analysis," *Phase Transitions*, vol. 91, no. 6, pp. 667–680, 2018, doi: 10.1080/01411594.2018.1469019.
- [165] D. Gaona, E. Urresta, J. Marínez, and G. Guerrón, "Medium-temperature phase-change materials thermal characterization by the T-History method and differential scanning calorimetry," *Exp. Heat Transf.*, vol. 30, no. 5, pp. 463–474, 2017, doi: 10.1080/08916152.2017.1286413.
- [166] P. K. Pandis, S. Papaioannou, M. K. Koukou, M. G. Vrachopoulos, and V. N. Stathopoulos, "Differential scanning calorimetry based evaluation of 3D printed PLA for phase change materials encapsulation or as container material of heat storage tanks," *Energy Procedia*, vol. 161, pp. 429–437, 2019, doi: 10.1016/j.egypro.2019.02.088.
- [167] S. Gibout, E. Franquet, D. Haillot, J. P. Bédécarrats, and J. P. Dumas, "Challenges of the usual graphical methods used to characterize Phase Change Materials by Differential Scanning Calorimetry," *Appl. Sci.*, vol. 8, no. 1, pp. 1–41, 2018, doi: 10.3390/app8010066.
- [168] D. Banu, D. Feldman, and D. Hawes, "Evaluation of thermal storage as latent heat in phase change material wallboard by differential scanning calorimetry and large scale thermal testing," *Thermochim. Acta*, vol. 317, no. 1, pp. 39–45, 1998, doi: 10.1016/S0040-6031(98)00368-2.
- [169] A. K. Rai, S. Raju, B. Jeyaganesh, E. Mohandas, R. Sudha, and V. Ganesan, "Effect of heating and cooling rate on the kinetics of allotropic phase changes in uranium: A differential scanning calorimetry study," *J. Nucl. Mater.*, vol. 383, no. 3, pp. 215–225, 2009, doi: 10.1016/j.jnucmat.2008.09.012.
- [170] W. Su, L. Gao, L. Wang, and H. Zhi, "Calibration of differential scanning calorimeter (DSC) for thermal properties analysis of phase change material,"

- J. Therm. Anal. Calorim.*, vol. 143, no. 4, pp. 2995–3002, 2021, doi: 10.1007/s10973-020-09470-9.
- [171] C. Barreneche, A. Solé, L. Miró, I. Martorell, A. I. Fernández, and L. F. Cabeza, “New methodology developed for the differential scanning calorimetry analysis of polymeric matrixes incorporating phase change materials,” *Meas. Sci. Technol.*, vol. 23, no. 8, 2012, doi: 10.1088/0957-0233/23/8/085606.
 - [172] O. Levenspiel, *Engineering flow and heat exchange, third edition*, Springer, 2014.
 - [173] Karwa and Rajendra, *Laws of thermal radiation. Heat and Mass Transfer*, pp. 733-765, 2020.
 - [174] C. Ezgi, “Basic Design Methods of Heat Exchanger,” *Heat Exchangers–Design, Experiment and Simulation*, pp. 9-35, 2017.
 - [175] R. K. Shah, “Classification of heat exchangers.,” Washington, U.S.A., *Hemisphere Publishing Corp.*, pp.9-14., 1983, doi: 10.1201/9780429469862-1.
 - [176] A. Motevali, M. H. Rostami, G. Najafi, and W. M. Yan, “Evaluation and improvement of pcm melting in double tube heat exchangers using different combinations of nanoparticles and pcm (The case of renewable energy systems),” *Sustain.*, vol. 13, no. 19, 2021, doi: 10.3390/su131910675.
 - [177] C. J. Ho, S. H. Huang, and C. M. Lai, “Enhancing laminar forced convection heat transfer by using Al₂O₃/PCM nanofluids in a concentric double-tube duct,” *Case Stud. Therm. Eng.*, vol. 35, no. March, 2022, doi: 10.1016/j.csite.2022.102147.
 - [178] E. M. Salilih, N. H. Abu-Hamdeh, A. Khoshaim, R. A. Almasri, S. M. Sajadi, and A. Karimipour, “Thermal systems energy optimization employing two independent circuits of double vertical ground U-tube with PCM as the backfill material for building,” *J. Build. Eng.*, vol. 56, no. May, p. 104752, 2022, doi: 10.1016/j.jobte.2022.104752.
 - [179] M. S. Mahdi, H. B. Mahood, J. M. Mahdi, A. A. Khadom, and A. N. Campbell, “Improved PCM melting in a thermal energy storage system of double-pipe helical-coil tube,” *Energy Convers. Manag.*, vol. 203, no. September 2019, p. 112238, 2020, doi: 10.1016/j.enconman.2019.112238.
 - [180] Y. Pahamli, M. J. Hosseini, A. A. Ranjbar, and R. Bahrampoury, “Inner pipe

- downward movement effect on melting of PCM in a double pipe heat exchanger,” *Appl. Math. Comput.*, vol. 316, pp. 30–42, 2018, doi: 10.1016/j.amc.2017.07.066.
- [181] M.R. Kadivar, M.A. Moghimi, P. Sapin, and C.N. Markides, “Annulus eccentricity optimisation of a phase-change material (PCM) horizontal double-pipe thermal energy store,” *Journal of Energy Storage*, vol. 26, pp. 0–4, 2019, doi: 10.1016/j.est.2019.101030
- [182] Fajar Anggara et al., “Simulation and validation of PCM melting in concentric double pipe heat exchanger,” *AIP Conf. Proc.*, vol. 2001, doi: 10.1063/1.5049968.
- [183] S. Arena, E. Casti, J. Gasia, L. F. Cabeza, and G. Cau, “Numerical simulation of a finned-tube LHTES system: Influence of the mushy zone constant on the phase change behaviour,” *Energy Procedia*, vol. 126, pp. 517–524, 2017, doi: 10.1016/j.egypro.2017.08.237.
- [184] S. Arena, E. Casti, J. Gasia, L. F. Cabeza, and G. Cau, “Numerical analysis of a latent heat thermal energy storage system under partial load operating conditions,” *Renew. Energy*, vol. 128, pp. 350–361, 2018, doi: 10.1016/j.renene.2018.05.072.
- [185] A. Shahsavari, A. Goodarzi, H. I. Mohammed, A. Shirmeshan, and P. Talebizadehsardari, “Thermal performance evaluation of non-uniform fin array in a finned double-pipe latent heat storage system,” *Energy*, vol. 193, p. 116800, 2020, doi: 10.1016/j.energy.2019.116800.
- [186] A. Shahsavari, A. Goodarzi, P. Talebizadehsardari, and M. Arıcı, “Numerical investigation of a double-pipe latent heat thermal energy storage with sinusoidal wavy fins during melting and solidification,” *Int. J. Energy Res.*, vol. 45, no. 15, pp. 20934–20948, 2021, doi: 10.1002/er.7152.
- [187] N. Boulaktout, E. H. Mezaache, M. Teggari, M. Arici, K. A. R. Ismail, and Ç. Yildiz, “Effect of Fin Orientation on Melting Process in Horizontal Double Pipe Thermal Energy Storage Systems,” *J. Energy Resour. Technol. Trans. ASME*, vol. 143, no. 7, pp. 1–14, 2021, doi: 10.1115/1.4050904.
- [188] R. A. Nicholls, M. A. Moghimi, and A. L. Griffiths, “Impact of fin type and orientation on performance of phase change material-based double pipe thermal energy storage,” *J. Energy Storage*, vol. 50, no. April, p. 104671, 2022, doi: 10.1016/j.est.2022.104671.
- [189] M. H. Alhamdo, M. A. Theeb, and A. S. Golam, “Finned double-tube PCM

- system as a waste heat storage,” *IOP Conf. Ser. Mater. Sci. Eng.*, vol. 95, no. 1, 2015, doi: 10.1088/1757-899X/95/1/012033.
- [190] M. Azad, D. Groulx, and A. Donaldson, “Natural convection onset during melting of phase change materials: Part II – Effects of Fourier, Grashof, and Rayleigh numbers,” *Int. J. Therm. Sci.*, vol. 170, no. May, 2021, doi: 10.1016/j.ijthermalsci.2021.107062.
- [191] J. Xie, Y. Li, W. Wang, S. Pan, N. Cui, and J. Liu, “Comments on thermal physical properties testing methods of phase change materials,” *Adv. Mech. Eng.*, vol. 2013, 2013, doi: 10.1155/2013/695762.
- [192] J. Hun Park, S. Wi, J. Lee, B. Yeol Yun, S. Yang, and S. Kim, “Manufacture of optimized PCM within thermal comfort range to improve building energy performance,” *IOP Conf. Ser. Mater. Sci. Eng.*, vol. 609, no. 4, 2019, doi: 10.1088/1757-899X/609/4/042019.
- [193] M. M. Taherian, M. Yousefpour, and E. Borhani, “The effect of ARB process on corrosion behavior of nanostructured aluminum alloys in $\text{Na}_2\text{HPO}_4 \cdot 12\text{H}_2\text{O}$ and $\text{Zn}(\text{NO}_3)_2 \cdot 6\text{H}_2\text{O}$ PCMs,” *Eng. Fail. Anal.*, vol. 107, no. April 2019, p. 104222, 2020, doi: 10.1016/j.engfailanal.2019.104222.
- [194] H. A. Nasef, H. Hassan, S. Mori, and S. A. Nada, “Experimental investigation on the performance of parallel and staggered arrays of PCM energy storage system for PV thermal regulation,” *Energy Convers. Manag.*, vol. 254, no. December 2021, p. 115143, 2022, doi: 10.1016/j.enconman.2021.115143.
- [195] S. Behzadi and M. M. Farid, “Long term thermal stability of organic PCMs,” *Appl. Energy*, vol. 122, pp. 11–16, 2014, doi: 10.1016/j.apenergy.2014.01.032.
- [196] R. K. Sharma, P. Ganesan, and V. V. Tyagi, “Long-term thermal and chemical reliability study of different organic phase change materials for thermal energy storage applications,” *J. Therm. Anal. Calorim.*, vol. 124, no. 3, pp. 1357–1366, 2016, doi: 10.1007/s10973-016-5281-5.
- [197] A. Shukla, D. Buddhi, and R. L. Sawhney, “Thermal cycling test of few selected inorganic and organic phase change materials,” *Renew. Energy*, vol. 33, no. 12, pp. 2606–2614, 2008, doi: 10.1016/j.renene.2008.02.026.
- [198] A. Hasan and A. A. Sayigh, “Some fatty acids as phase-change thermal energy storage materials,” *Renew. Energy*, vol. 4, no. I, pp. 69–76, 1994, doi: 10.1016/0960-1481(94)90066-3.

- [199] M. Fuensanta, U. Paiphansiri, M. D. Romero-Sánchez, C. Guillem, Á. M. López-Buendía, K. Landfester, “Thermal properties of a novel nanoencapsulated phase change material for thermal energy storage,” *Thermochim. Acta*, vol. 565, pp. 95-101, 2013, doi: 10.1016/j.tca.2013.04.028.

ISSN (online): 2446-1636
ISBN (online): 978-87-7573-773-4

AALBORG UNIVERSITY PRESS